UNIVERSITY OF SÃO PAULO
INSTITUTE OF GEOSCIENCES

Hydrogeological Conceptual Model of Sete Lagoas (MG) and Associated Implications of Urban Development in Karst Region

Paulo Henrique Ferreira Galvão

Supervisor: Dr. Ricardo Hirata

DOCTORAL THESIS

Mineral Resources and Hydrogeology Graduate Program

SÃO PAULO
2015

UNIVERSIDADE DE SÃO PAULO
INSTITUTO DE GEOCIÊNCIAS

Modelo Hidrogeológico Conceitual de Sete Lagoas (MG) e Implicações Associadas ao Desenvolvimento Urbano em Regiões Cársticas

Paulo Henrique Ferreira Galvão

Orientador: Dr. Ricardo Hirata

TESE DE DOUTORAMENTO

Programa de Pós-graduação em Recursos Minerais e Hidrogeologia

SÃO PAULO
2015

Ficha catalográfica preparada pelo Serviço de Biblioteca e Documentação do Instituto de Geociências da Universidade de São Paulo

Galvão, Paulo Henrique Ferreira
Modelo hidrogeológico conceitual de Sete Lagoas (MG) e implicações associadas ao desenvolvimento urbano em regiões cársticas / Paulo Henrique Ferreira Galvão. – São Paulo, 2015.
124 p. : il.

Tese (Doutorado) : IGc/USP
Orient.: Hirata, Ricardo

1. Hidrogeologia 2. Carste 3. Risco geotécnico 4. Geoquímica 5. Isótopos estáveis I. Título

This thesis is dedicated exclusively to my mom Odete Ferreira Galvão, an example of dignity, dedication, devotion and love. To this woman, my safe haven, I thank all her values and principles that were transferred and that formed the basis of what I am today.

Essa tese é dedicada exclusivamente à minha mãe Odete Ferreira Galvão, exemplo de dignidade, dedicação, entrega e amor. A essa mulher, meu porto seguro, agradeço todos os valores e princípios que me foram repassados e que formaram as bases do que sou hoje.

"Try not to become a man of success, but rather try to become a man of value."

Albert Einstein

"Não sei, só sei que foi assim!"

Chicó, in the book "O Auto da Compadecida"

ACKNOWLEDGMENTS

The development of this doctoral thesis has been, along this 4 years journey, a rewarding experience. It would not have come to fruition without the contributors listed below, who spent directly or indirectly their busy time supporting and helping me in the best way it could be.

First, I would like to thank deeply my mom Odete Ferreira Galvão for dedication and patience. You were and are the key of my success in the past, present and in the future. I would also like to thank my family for supporting me, specially my aunts Irene Ferreira Galvão and Ruth Ferreira Galvão for helping me in the worst times.

A special thanks to Dr. Ricardo Hirata, my supervisor, for his excellent support and patience throughout these four years. Without his supervision and devices, this thesis would be more difficult. A special thanks to Dr. Todd Halihan, my co-supervisor, for his great support during my exchange period at Oklahoma State University (Go Pokes!), in Stillwater, USA. It was a privilege to have had both of them as supervisors, which I could enjoy their experiences and wisdoms. The discussions and observations we had during all this work period were immensely important for my formation as a researcher and as a person

I gratefully acknowledge Servmar Environmental & Engineering and São Paulo Research Foundation (FAPESP) [*FAPESP - Fundação de Amparo à Pesquisa do Estado de São Paulo*] for supporting and funding my Doctoral studies. To Water Supply and Sewage Service (SAAE) [*SAAE - Serviço de Abastecimento de Água e Esgoto*] for providing me with the necessary data, as well as for treating me in a very friendly way, specially to Fátima L'Abbate and Tereza Cristina Luppi Miranda.

My sincere thanks for such a fruitful collaboration to the Servmar's project partners: Arnaldo Cordeiro, Daniela Barbati, Gilcélia Cristina Barboza, and Saulo Bertolino for being a good friends and helping me in fieldworks and giving me indispensable advices. Their great contributions were essentials, as well as the great time we had together in numerous meetings, fieldworks, hangouts and pubs. We started as good co-workers to become great friends. A very special thanks to Jorge Peñaranda (Miguelito) for coordinating the project, and especially for becoming my friend, helping me and giving me good advices in a very important moments.

I would also like to thank my colleagues at the Laboratory of Physical Models (LAMO) [*Laboratório de Modelos Físicos*] Bruno Pirilo, Glaucia Santos, Jonathan

Batista, Marcus Ucci, Marcos Barbosa, and Sandra Guerra for the support, several "hydrotalks" and the great time together hanging out. A special thank to Rafael Terada, for the support in the fieldworks and the several chats about our theses and future plans, and also for being part of the Tia Darcy band, a genuine "hydroband", as the base guitar player and vocalist with Lucas Andreata (drummer) and Ricardo Saito (bass player), all of them also from LAMO. All of you guys became great friends of mine.

To all USP graduate colleagues, in which I had the pleasure to enjoy the excellent companies and great friendships. A special thanks to Dr. Geane Carolina Cavalcante, for the great contributions in the chapter about structural geology and for the essential tips, and to Prof. Dr. Renato Paes de Almeida for providing the TinyPerm II portable hand-held permeameter.

To my American friends Kyle Spears (The Survivor Man!) and Kaitlyn Beard (KB) for correcting my English grammar mistakes and helped me a lot when I arrived in Stillwater, but the most important thing, for becoming my friends. You both are part of a select group of special people, which I will never forget, such as Jordan McCall, Britney Temple, Jon Fields, and my American rock band integrants Jared Oxford (bass player), Nick Richards (base guitar player), Noel Treatwell (drummer), and Nick Nease (vocalist). To my Egyptian friends, for the great time together playing soccer every Friday night, even in negative Celsius temperatures, and especially to Ibrahim Sabri, for have been a good roommate for one year and for showing me how beautiful is his religion. My time in Stillwater with all those people was unforgettable.

To my close friends Neto Camarinha, Victor Camarinha, Ely Costa, and Glauco Oliveira for being part of my life since I was a child. I would also like to thank Mauricio Rodrigues and Raquel Pistilli, for treating me as part of their house in São Paulo in a very receptive and friendly way for almost four years. For those who I eventually did not mention here, my sincerely acknowledge for everything.

Finally, I am also very grateful to the members of the thesis committee, for providing great input to this work.

ABSTRACT

This research integrated geological, hydrogeological, geochemical, and stable isotope studies conducted in the municipality of Sete Lagoas (MG), Brazil, in order to understand the water circulation in a karst terrain and to propose alternatives for a better water use, aiming to avoid geotechnical problems. The area is constituted by Neoproterozoic limestones from the Sete Lagoas Formation, where karst conduits were developed, giving origin to the homonymous aquifer, which is covered by Cenozoic unconsolidated sediments and, occasionally, by Neoproterozoic metasedimentary rocks from the Serra de Santa Helena Formation. It was observed that in this aquifer the primary porosity is very low and the secondary porosity (micro-fractures) is also reduced, due to the filling by calcite. The great volume of groundwater migrates through the tertiary porosity characterized by two dominant solutionally enlarged bedding planes and, to a lesser extent, by sub-vertical enlarged fractures. The recharge, related to rainfall occurring from October to December, takes place through sinkholes, caves entrances, and where the limestones are under the Cenozoic sediments. A detailed study evaluating the scale effects also allowed the establishment of permeability distributions of the Sete Lagoas Aquifer. Other results obtained also established that the groundwater extractions are associated to karst geotechnical events located in the urbanized area of the municipality. The high groundwater extractions make the shallowest solutionally enlarged bedding plane, in some points, entirely in the unsaturated zone, causing geotechnical events. A geotechnical map identifies five levels of risk, based on the lithology and the groundwater level interaction. This type of mapping should guide the groundwater extractions and caring the urban land occupation in Sete Lagoas, preventing or delaying the occurrence of new subsidences or collapses.

Keywords: hydrogeology, karst, geotechnical risk, geochemistry, stable isotopes.

RESUMO

Esta pesquisa integrou estudos geológicos, hidrogeológicos, geoquímicos e de isótopos estáveis no município de Sete Lagoas (MG), Brasil, com o objetivo de entender a circulação da água em terreno cárstico e propor alternativas para o seu melhor uso, a fim de se evitar problemas geotécnicos. A área é constituída por calcários neoproterozoicos da Formação Sete Lagoas, onde se desenvolveram condutos cársticos, dando origem ao aquífero homônimo, o qual está coberto por sedimentos cenozoicos inconsolidados e, ocasionalmente, por rochas metasedimentares neoproterozoicas da Formação Serra de Santa Helena. Foi observado que neste aquífero a porosidade primária é muito baixa e a secundária (micro-fraturas) é igualmente reduzida, devido ao preenchimento por calcita. O grande volume de água subterrânea migra através da porosidade terciária caracterizada dominantemente por dois planos de acamamentos carstificados e, em menor grau, por fraturas sub-verticais carstificadas. A recarga, relacionada às chuvas que ocorrem no período de outubro a dezembro, se dá através de sumidouros, entradas de cavernas e onde o calcário está sob os sedimentos cenozoicos. Um detalhado estudo avaliando os efeitos de escala permitiu também o estabelecimento da distribuição das permeabilidades do Aquífero Sete Lagoas. Outros resultados obtidos também estabeleceram que as extrações de águas subterrâneas estão associadas aos eventos geotécnicos cársticos localizados na área urbana do município. A elevada extração das águas subterrâneas faz com que o plano de acamamento carstificado mais raso, em algumas áreas, esteja inteiramente na zona não saturada, provocando os eventos geotécnicos. Um mapa de risco geotécnico identifica, a partir da litologia e do nível de água subterrânea, cinco níveis. Este tipo de mapeamento deveria orientar as extrações e os cuidados na ocupação do terreno urbano em Sete Lagoas, prevenindo ou retardando a ocorrência de novas subsidências ou colapsos.

Palavras-chave: hidrogeologia, carste, risco geotécnico, geoquímica, isótopos estáveis.

SUMMARY

ACKNOWLEDGMENTS iii

ABSTRACT v

RESUMO vi

SUMMARY vii

CHAPTER 1: INTRODUCTION 1

1.1 Presentation 1

1.2 Objectives and justifications 1

1.3 Structure of this thesis 2

CHAPTER 2: SITE DESCRIPTION 4

CHAPTER 3: MATERIALS AND METHODS 9

3.1 Geological approaches 9

3.1.1 Geologic mapping 9

3.1.2 Subsurface lithologic contact 10

3.2 Hydrogeological approaches 10

3.2.1 Pumping tests 10

3.2.2 Stable isotopes samples 12

3.2.3 Geochemistry analysis 13

3.3 Georeferencing data and software 13

CHAPTER 4: KARST HYDROGEOLOGY: ORIGINS AND CONCEPTS 16

4.1 The origin of karst 17

4.2 Features and controls on the development of karst system 18

4.2.1 Recharge of karst aquifer (input control) 19

4.2.2 Hydraulic parameters (throughput control) 19

4.2.3 Discharge of karst aquifer (output control) 23

4.3 Karst landform 24

4.3.1 Sinkholes (Dolines) 24

4.3.2 Caves 24

4.3.3 Springs 25

4.3.4 Poljes 25

4.3.5 Karst valleys 25

4.3.6 Sinking streams 26

4.4 Human impacts on karst system 26

4.4.1 Groundwater contamination in karst aquifer 26

4.4.2 Induced subsidences 27

4.5 Isotopes and significance to karst hydrology 28

CHAPTER 5: GEOLOGIC CONCEPTUAL MODEL OF THE MUNICIPALITY OF SETE LAGOAS (MG, BRAZIL) AND THE SURROUNDINGS **32**

1. Introduction **32**

2. Site description **33**

3. Methods **34**

4. Results and discussions **36**

4.1. Geologic mapping 36

4.2. Structural geology 40

4.3. Spatial distribution of the geologic formations 42

4.4. Geologic conceptual model 46

5. Conclusion **49**

CHAPTER 6: EVALUATING KARST GEOTECHNICAL RISK IN THE URBANIZED AREA OF SETE LAGOAS, MINAS GERAIS, BRAZIL **52**

1. Introduction **52**

2. Site description **54**

3. Methods **54**

4. Results **57**

4.1. Geology 57

4.2. Lithostructural contacts and spatial distribution 57

4.3. Locations of the subsidence/collapse events and hydrogeological correlation 59

4.4. Karst geotechnical risk evaluation 62

5. Discussion **62**

6. Conclusion **64**

CHAPTER 7: THE KARST PERMEABILITY SCALE EFFECT OF SETE LAGOAS, MG, BRAZIL **69**

1. Introduction **69**

2. Site description **72**

3. Methods **74**

3.1. Permeability database 74

3.2. Permeability component data 76

3.3. Permeability combination models 78

4. Results **78**

4.1. Sete Lagoas permeability database 78

4.2. Permeability feature sizes from inversion 83

4.3. Permeability combination model 84

5. Discussion **87**

6. Conclusion **90**

CHAPTER 8: STABLE ISOTOPES AND GEOCHEMICAL STUDIES TO EVALUATE FLOWPATHS AND RECHARGE AREAS IN AN URBAN KARST AQUIFER OF SETE LAGOAS, MG, BRAZIL **97**

1. Introduction **97**

2. Site description **99**

3. Methods **100**

3.1 Stable isotopes 100

3.2 Geochemistry analysis 102

4. Results **102**

4.1 Stable isotopes 102

4.2 Geochemistry 105

5. Discussion **110**

5.1 Stable isotopes 110

5.2 Geochemistry 111

5.3 Water evolution and sources of recharge 113

6. Conclusion **116**

CHAPTER 9: CONCLUSIONS **120**

9.1 Geological features of Sete Lagoas and surroundings **120**

9.2 Hydrogeological features of the city of Sete Lagoas **121**

9.3 Groundwater evolution and source of recharges **123**

9.4 Urban groundwater extraction and karst geotechnical risks **123**

9.5 General recommendations **124**

CHAPTER 1: INTRODUCTION

1.1 Presentation

The doctoral thesis was a result of a research that integrated geological, hydrogeological, geochemical, and stable isotope studies conducted in the municipality of Sete Lagoas, Minas Gerais state, Brazil. This region has a population greater than 200,000, over an area of 538 km^2, where the urban development was more intense in the central portion of this municipality. Geologically, the area is located in the São Francisco Craton, where carbonate argillo-arenaceous sediments are emplaced giving origin to the Bambuí Group. In this group, karst conduits in the limestones from the Sete Lagoas Formation were developed, which are storing a large amount of groundwater. Because of this, the current water supply is almost entirely groundwater from the Sete Lagoas karst aquifer. As it is common in developing countries like Brazil, mostly cities has rapid urban growth having not always been guided by planning, reflecting sometimes in water supply problems for local populations. These features also take place in Sete Lagoas, with an aggravating factor: the location of this city in a karst region, which problems related to geotechnical issues caused by groundwater exploitation, as well as problems in water supply during dry season, are common. The results obtained in this multidisciplinary research, where some methodologies used in this thesis were never applied for karst regions, especially in Brazil, were used to understand the water circulation in this karst terrain and its behaviors with others geological formations, and then giving alternative responses for a better use of water, mitigating problems related to that.

1.2 Objectives and justifications

The main goal of this thesis was to characterize quantitatively and qualitatively the Sete Lagoas karst aquifer and its relationship with other rock formations in order to understand: (1) the underlying mechanisms that control the water circulation; (2) the possible origin of groundwater recharge and its flowpaths; (3) the multi-scale permeability structure evaluation (in small-, well-, and regional-scale); and (4) the physical mechanisms of subsidence and collapse development. Investigating all

these mechanisms is important because of the increasing demands on this karst aquifer, which require users to have a better understanding of how it functions, so that it can be properly utilized and protected, avoiding water resource degradations, as well as facilitating stakeholder decision making in urban planning.

1.3 Structure of this thesis

This doctoral thesis is organized in the form of scientific papers, which were published, accepted and submitted to international journals. Thus, each chapter can be read relatively independently to the others. After the Chapter 1 "Introduction", it is presented the Chapter 2 containing the site descriptions and its hydrogeological features.

The Chapter 3 is about the main methods used in the research to understand the circulation of groundwater and its relationships in karst terrains, while the Chapter 4 is the state of art "Karst hydrogeology: origins and concepts".

The Chapter 5 contains the paper "Geologic conceptual model of the municipality of Sete Lagoas (MG, Brazil) and the surroundings", accepted in the Anais da Academia Brasileira de Ciências [*Annals of the Brazilian Academy of Sciences*] (Galvão et al. in press). This paper was important to understand, firstly, the spatial distribution and the structural framework geometry to establish a new geologic perspective of the region before developing the other papers.

The Chapter 6 presents the paper "Evaluating karst geotechnical risk in the urbanized area of Sete Lagoas, MG, Brazil", already published in the Hydrogeology Journal (Galvão et al. 2015). The primary goal of this paper was to evaluate and identify the potential subsidence or collapse risk zones. Aerial photographs, lithologic well profiles, optical well logs, and geologic mapping were utilized to categorize risk factors influencing karst subsidence and collapse, using an index system. The results showed that the majority of the urbanized area overlies mantled limestone from the Sete Lagoas Formation covered with unconsolidated sediments contained within a graben, resulting in barrier boundaries for groundwater. Five risks zones in the municipality were identified (negligible, low, moderate, considerable, and high) related to geologic and hydrologic risk factors. The urbanized area is located largely in the high-risk zone where the majority of the collapse features are located.

The Chapter 7 contains the paper "The karst permeability scale effect of Sete Lagoas, MG, Brazil", submitted in the Journal of Hydrology (Galvão et al. in review). The Sete Lagoas karst aquifer was used to evaluate the permeability structure across a range of scales in order to develop a quantitative model of permeable features that is consistent across all scales of measurement, from matrix properties to regional-scale flow. This aquifer has some wells that do not have measurable drawdown during pumping due to high permeability. Based on bulk permeability measurements, inverted estimate of the size of hydraulic features, and the permeability combination forward modeling, the results indicated an increase in permeabilities from the matrix- to well-scale, but a decrease of these parameters from well- to regional-scale due to the localized development of karst bedding plane dissolution in one structurally controlled region of the aquifer. The physical sizes of permeable features of the aquifer are consistent across the scales of data collection and their geometry provides a quantitative understanding of the scale effects of permeability measurements.

The Chapter 8 presents the paper "Stable isotopes and geochemical studies to evaluate flowpaths and recharge areas in an urban karst aquifer in Sete Lagoas, MG, Brazil", to be submitted in the Annals of the Brazilian Academy of Sciences. The main goal was identify indirectly the various sources and areas of recharge in the karst area, its flowpaths, and surface-ground water interaction, which is important for proper water resource management, avoiding eventual contaminations and other future water quality problems. Analyzing data of stable isotopes ^{18}O and ^{2}H and major ions measurements, it was possible to understand that the origin of groundwater is directly from precipitation, having a limited period of recharge. In the central urbanized area, where the karst aquifer is in contact with Cenozoic unconsolidated sediments, there may be punctual superficial water infiltration. The major ions concentrations presented the highest values at the same region, where the most developed karstic structure was found in the Sete Lagoas Formation. These data could suggest larger water reservoir indicating more mineralization, which are in concordance with the geologic information.

Chapter 9 consists in a synthesis of the overall conclusions acquired from all the results and discussions from the papers and general recommendations for future works.

CHAPTER 2: SITE DESCRIPTION

The municipality of Sete Lagoas is located in the state of Minas Gerais, Brazil, 70 km northwest of Belo Horizonte, the state capital. This region has a population greater than 200,000 over an area of 538 km^2 (IBGE 2010). The urban development was more intense in the northern and northeastern sectors, in comparison to the initial settlement (Fig. 1). There is a considerable industrial activity located mainly along the main federal highway, which is a corridor of significant growth. Rapid urban development has not always been guided by planning, especially in relation to environmental and geotechnical issues, reflected by 17 documented occurrences of subsidence or/and collapse since 1988 (Peñaranda J and Cordeiro A. Hydrogeologists, Servmar Environmental & Engineering, unpublished data, 2013). The majority of these occurrences are clustered in the central portion of the urbanized area, which the most important event happened in 1988 (Silva 1988), when a collapse having around a 20 meters in diameter was registered.

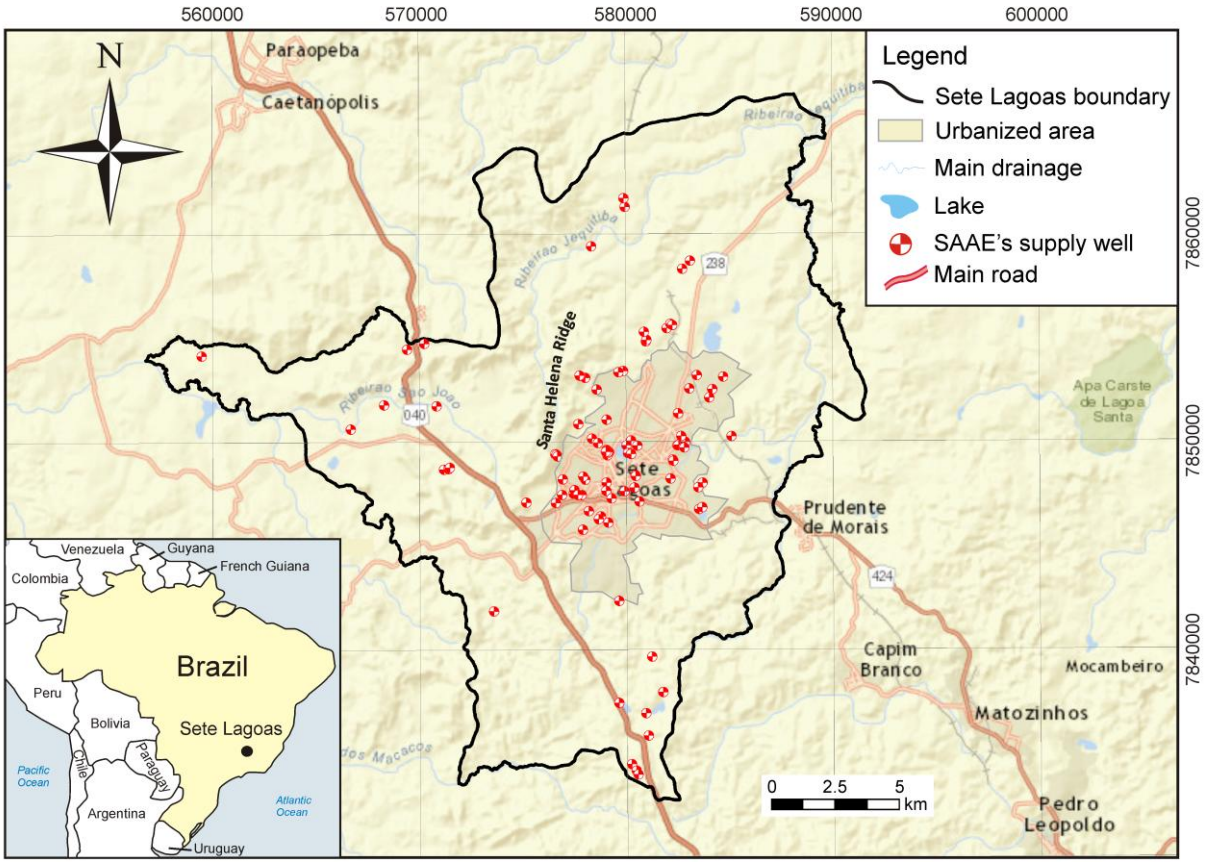

Fig. 1. Location map of Sete Lagoas, in UTM coordinates, showing the urbanized area limits located in the central portion of the municipality. Is also showed the location of the SAAE's public supply wells, where the majority of them are located in the urban area, where it is possible to obtain the highest discharge rates in well.

Geologically, the area is located in the São Francisco Craton, where Neoproterozoic carbonate argillo-arenaceous sediments are emplaced giving origin to the Bambuí Group (Branco and Costa 1961, Oliveira 1967, Schöll and Fogaça 1973, Dardene 1978, Schobbenhaus 1984, Ribeiro et al. 2003, Tuller et al. 2010). The statigraphy of the region can be seen in the Fig. 2.

The Archaean basement is represented by the Belo Horizonte Complex, which is generally characterized by a set of gneissic rocks and migmatite zones, with polymetamorphic features, belonging to the geotectonic unit corresponding to the São Francisco Craton (Ribeiro et al. 2003). Epigenic and igneous metamorphic/migmatite rocks with plutonic features mark this occurrence. Mafic intrusions may also occur, which preferentially fills in the fracture planes. The contacts between different lithotypes are generally transitional, mainly between gneiss, migmatites and/or granitoids. The granitoids are light gray to white, with granulation varying from gross to medium, sometimes with sparse porphyroblasts of tabular feldspars, xenoliths from other rocks or restites from partial fusion (Tuller et al. 2010). This complex was intensely affected by basic injections, provoking the appearance of a group of basic rock dikes (Ribeiro et al. 2003).

Overlying the basement, the Bambuí Group is represented by the lower Sete Lagoas Formation (Dardenne 1978) and the upper Serra de Santa Helena Formation (Branco and Costa 1961) (Fig. 2). The Sete Lagoas Formation is divided and characterized by two members (Ribeiro et al. 2003): Pedro Leopoldo, at the base, composed of fine limestones, dolomites, marlstones and pelites; and Lagoa Santa, on the top, composed of medium-grained black limestones. In general, the lower contact of this formation with rocks from the basement is abrupt, discordant and tectonic, with faults. The upper contact with the Serra de Santa Helena Formation is most commonly abrupt as well. The Serra de Santa Helena Formation is composed of slate, marble, siltstone and argillite. This formation overlies the Sete Lagoas Formation with abrupt, tectonic, or occasionally, gradational contacts. With the basement, the contacts are abrupt and discordant (angular discordance), tectonic, by thrust belt faults, easily seen on the basin border (Tuller et al. 2010). Three stratigraphic members constitute this formation (Grossi et al. 1998): (1) lower, represented by silt-clay rhythmites, generally carbonaceous, and dark shales; (2) middle, by marble and shales; and (3) upper, constituted by shales, siltstones, slate cleavage, and cross bedding.

The Bambuí Group is covered by the Cenozoic unconsolidated sediments, divided into (1) detritus coverage, (2) alluvial terraces, and (3) alluvium (Ribeiro et al. 2003). The detritus coverage is composed of sediments with a predominant red color, sand to silt with varying levels of gravel, which occur indistinctly on all units, but mainly over the Serra de Santa Helena Formation. The alluvial terraces occur along drainages and are mainly constituted of semi-consolidated sand to silt material, with whitish to yellowish and reddish color. The alluvium occurs along the meanders of the large watercourses. They are composed of fine to coarse sand, with discontinuous amounts of quartz pebbles, siltstone and sandstone (Tuller et al. 2010).

Geomorphologically, the area is in a karst setting, which provides the presence of lakes (located mainly in the central area), caves, sinkholes, and closed drainage basins (Pessoa 1996, Ribeiro et al. 2003, Tuller et al. 2010). Areas that have denser drainage are related to the Santa Helena Ridge foothills in the center, basement outcrops in the south, and metasediments in the north. The elevation of the area ranges from around 750 to 1000 m, declining from southwest to northeast, where the highest elevations are located in the Santa Helena Ridge (Fig. 2).

Regarding the hydrogeology, the Sete Lagoas karst aquifer consists of Neoproterozoic limestones, which the groundwater is predominantly classified as a calcium-bicarbonate type, with pH values between 6.5 and 7.5, being slightly basic. Regarding the electrical conductivity, this groundwater has an average of 333 μmhos/cm, combining with the high levels of dissolved salts (calcium and bicarbonate). This water, stored in karst conduits, offers good quality for human consumption, only presenting a light level of water hardness, sometimes causing an unpleasant taste and problems of encrustation in pipes with smaller diameter (Pessoa 1996). These limestones dip and become thicker and completely covered by competent rocks from the Serra de Santa Helena Formation to the northeast, considered as the local aquiclude. The Belo Horizonte basement works as a fissure aquifer, where the groundwater is stored in the fractures/faults, which is an alternative source of groundwater for the municipality.

Because of these hydrogeological features, the current municipal water supply is almost entirely groundwater from the Sete Lagoas karst aquifer, with less contribution from the basement, which is managed by the Water Supply and Sewage Service (SAAE) [*SAAE - Serviço Autônomo de Água e Esgoto*]. For these, this

company has more than 100 public wells located especially in the urbanized area, where it is possible to obtain the highest discharge rates (Fig. 1).

The mean total monthly precipitation is 106 mm, while the total annual is 1271.8 mm. The rainy season occurs from October to March, with total rainfall of 1132 mm, accounting for 89% of annual precipitation. The period with less precipitation occurs from April to September, with 139 mm. The average annual temperature is 20.9 ºC, with July having the lowest monthly mean value (17.5 °C), and February the highest one (22.9 °C). The annual variation is around 5°C. According to Pessoa (1996), the water balance in Sete Lagoas is divided, monthly, in: (1) water excess from January to March; (2) water deficit from April to September; and (3) water replacement between October and December, the period of recharging.

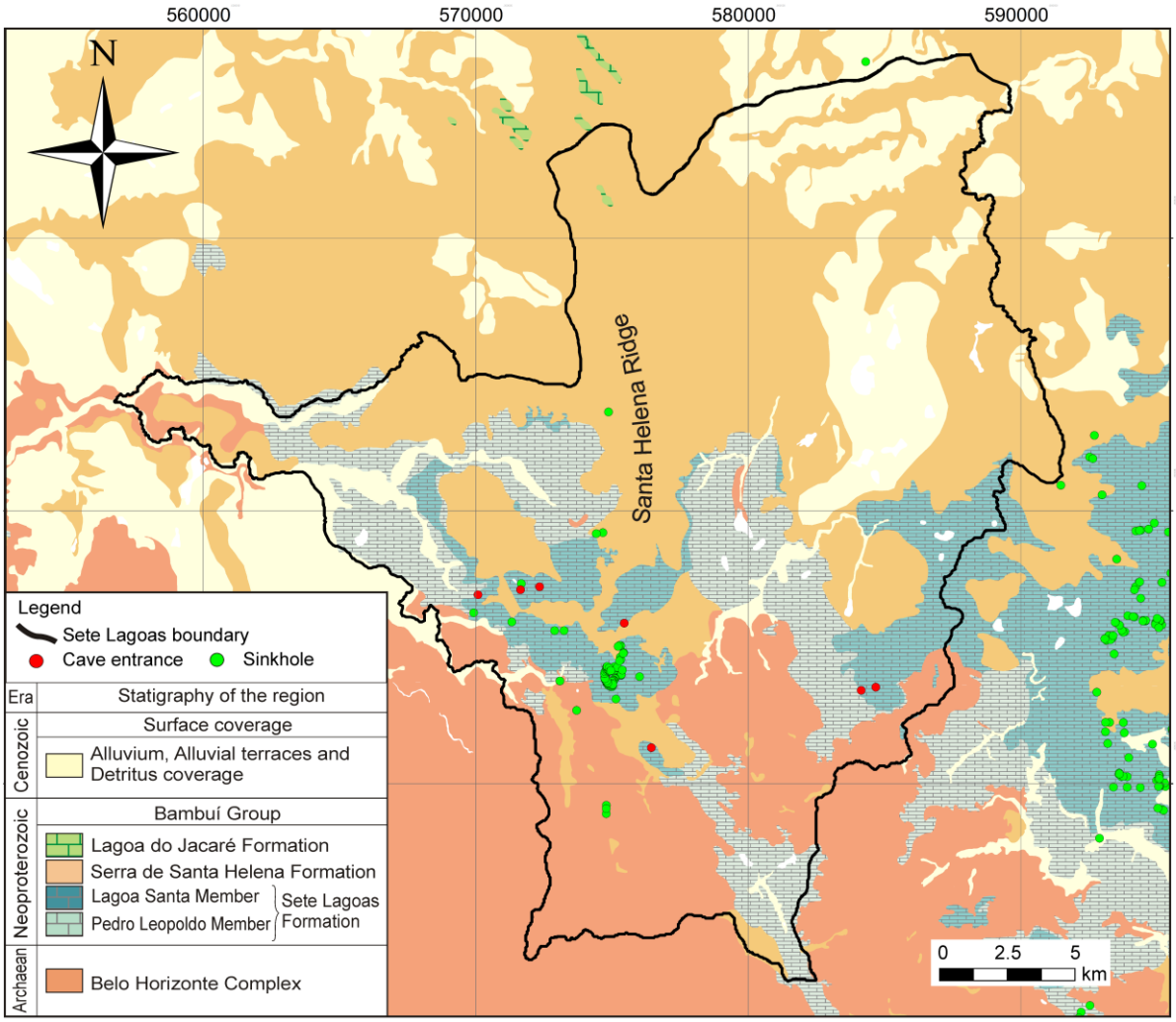

Fig. 2. Geologic map and the stratigraphic column showing the lithologies found in the study area (modified from Tuller et al. 2010), as well as the location of cave entrances and sinkholes (CECAV 2009).

REFERENCES

Branco Jr, Costa MT (1961) Belo Horizonte-Brasilia roadmap tour. In: Brazilian Congress of Geology, Brasilia. Radioactive Research Institute, Federal University of Minas Gerais (UFMG), Publication 15, Belo Horizonte, p 25.

CECAV (2009) Centro Nacional de Pesquisa e Conservação de Cavernas [National Center for Research and Conservation of Cave]. Available: http://www.icmbio.gov.br/cecav/downloads Accessed on March 2014.

Dardenne MA (1978) Synthesis on the stratigraphy of Bambuí Group in Central Brazil. In: Brazilian Congress of Geology, 30, Recife. Annals Recife: Brazilian Society of Geology, 1978 v.2, p.597-610.

Grossi Sad JH, Chiodi Filho C, Chiodi DK (1998) Overview of slates at Minas Gerais State, Brazil. Belo Horizonte: COMIG. CD- ROM.

IBGE - Brazilian Institute of Geography and Statistics (2010). Basic Municipal Information. Avaliable: http://www.ibge.gov.br/cidadesat/topwindow.htm?1 Accessed on March 2014.

Oliveira LM (1997) The management of urban geological risks in karst areas. Undergraduate thesis. Pontifícia Universidade Católica do Paraná (PUC-PR). 46 p.

Pessoa P (1996) Hydrogeological characterization of the region of Sete Lagoas - MG: Potentials and Risks. Master Thesis. Department of Geosciences, University of São Paulo. São Paulo

Ribeiro JH, Tuller MP, Danderfer Filho A (2003) Geological mapping of the region of Sete Lagoas, Pedro Leopoldo, Matozinhos, Lagoa Santa, Vespasiano, Capim Branco, Prudente de Morais, Confins and Funilândia, Minas Gerais State, Brazil (scale 1:50,000). 2nd edn. Belo Horizonte. 54 p.

Schobbenhaus C (1984) Geology of Brazil. National Department of Mineral Production, p 275-277

Schöll WU, Fogaça ACC (1973) Stratigraphy of the Espinhaço in the Diamantina region. In: Symposium on Geology of Minas Gerais State, Brazil, 1. Acts. Belo Horizonte: Brazilian Geology Society p 55-73 [Bulletin. 1].

Silva AB (1988) Soil subsidence in the city of Sete Lagoas, Minas Gerais State, Brazil. Brazilian Groundwater Journal, n.12

Tuller MP, Ribeiro JH, Signorelli N, Féboli WL, Pinho JMM (2010) Sete Lagoas - Abaeté Project, Minas Gerais State, Brazil. 6 geological maps, scale 1:100,000 (Geology Program of Brazil), 160p.

CHAPTER 3: MATERIALS AND METHODS

To achieve the objectives of the thesis, several different methods were utilized and developed. For better understanding, these methodologies will be separated by geological and hydrogeological approaches. For geological issues, geologic mapping, aerial photography interpretation, lithologic well profiles, and optical well log analysis were made. For hydrogeological issues, pumping tests were run, and water table measurements were made. Groundwater samples, superficial water and rainwater were collected for stable isotopes analysis and just groundwater samples were used for chemical analysis of major ions. These sets of data were integrated to be evaluated analytically and empirically to understand the mechanisms of the water circulation in the local karst aquifer and its relationships between other geological formations. These methods are presented sequentially followed by the approach to data integration.

3.1 Geological approaches

3.1.1 Geologic mapping

Geologic mapping of the Sete Lagoas was carried out in a scale of 1:25,000. The classification of the sedimentary rocks followed the definitions of Folk (1980) and the microscopic classification of the carbonate rocks followed the definitions of Folk (1959) and Dunham (1962). For the metamorphic and igneous rocks, the classification followed the definitions of Winter (2001). All the data were recorded on paper topographic maps and converted to digital format. Later, integration of the field data and the sheet geologic maps Baldim (SE.23-Z-C-III), Sete Lagoas (SE.23-Z-C-II), Contagem (SE.23-Z-C-V), and Belo Horizonte (SE.23-Z-C-VI), scale 1:100,000, was performed. These maps were acquired from the CPRM database, available on: http://geobank.sa.cprm.gov.br/.

Aerial photography interpretation (scale 1:40,000, dated 1977) and the SRTM image (Shuttle Radar Topography Mission), Sheet SE-23-Z-C, acquired from the EMBRAPA's website (EMBRAPA 2006) were evaluated to define the map view lithologic contacts (http://www.relevobr.cnpm.embrapa.br).

The locations of karst features (caves and sinkholes) were acquired from the National Center for Research and Conservation of Cave's website [*CECAV - Centro*

Nacional de Pesquisa e Conservação de Cavernas], as a GIS file, available on: http://www.icmbio.gov.br/cecav/downloads (CECAV 2009).

3.1.2 Subsurface lithologic contact

In order to obtain information on subsurface about lithologic contacts and karst features, lithologic well profiles were analyzed and optical well logs were run.

For lithologic well profiles, a series of 218 profiles located in the municipalities of Baldim, Caetanópolis, Capim Branco, Cordisburgo, Esmeralda, Fortuna de Minas, Funilândia, Inhaúma, Inimutaba, Lagoa Santa, Maravilhas, Matozinhos, Papagaio, Paraobepa, Pedro Leopoldo, Prudente de Morais, São José da Lapa, and Sete Lagoas were acquired from the SIAGAS database, at the website: http://siagasweb.cprm.gov.br/layout/. In addition, 52 public well profiles located in Sete Lagoas were analyzed, provided by Water Supply and Sewage Service database (SAAE) [*SAAE -Serviço de Abastecimento de Água e Esgoto*]. Out of the 270 profiles that were analyzed, the best and the most reliable were chosen.

Optical well analysis yielded 30 vertical image profiles collected with R-Cam 1000 Camera (Laval Underground Surveys). In addition to the standard downhole view, this camera offered a 360 degrees side-view perspective, capable of capturing a comprehensive survey of water wells. The camera had a maximum depth of 300 meters and was connected to a receiver with monitor that enabled real time imaging. Therefore, it was possible to register the depths of dissolution zones, fractures and lithologic contacts. The location of these optical well logs can be seen in the Fig. 3.

3.2 Hydrogeological approaches

3.2.1 Pumping tests

To obtain information about hydrogeological parameters, long transient pumping tests and drawdown tests were run in the SAAE's public supply wells (Fig. 3). Nine long duration transient pumping tests (48 hours) were made to calculate well-scale transmissivity and hydraulic conductivity using the Thiem (1906) and Theis (1935) methods. These tests involved pumping a well at a constant rate and measuring the drawdown in water level in some observation wells.

Twenty-seven time-drawdown or step-drawdown tests to estimate specific capacity were made, consisting of a measure of the productivity pumping in a well at

a constant rate and measuring the resulting drawdown in water level. In mathematical terms, the specific capacity is defined as the pumping rate in the well, divided by the observed decline in hydraulic head in the well, from a time-drawdown test. For the step-drawdown tests, every discharge value was divided by its respective drawdowns observed in each step and, then, the mean specific capacity was calculated.

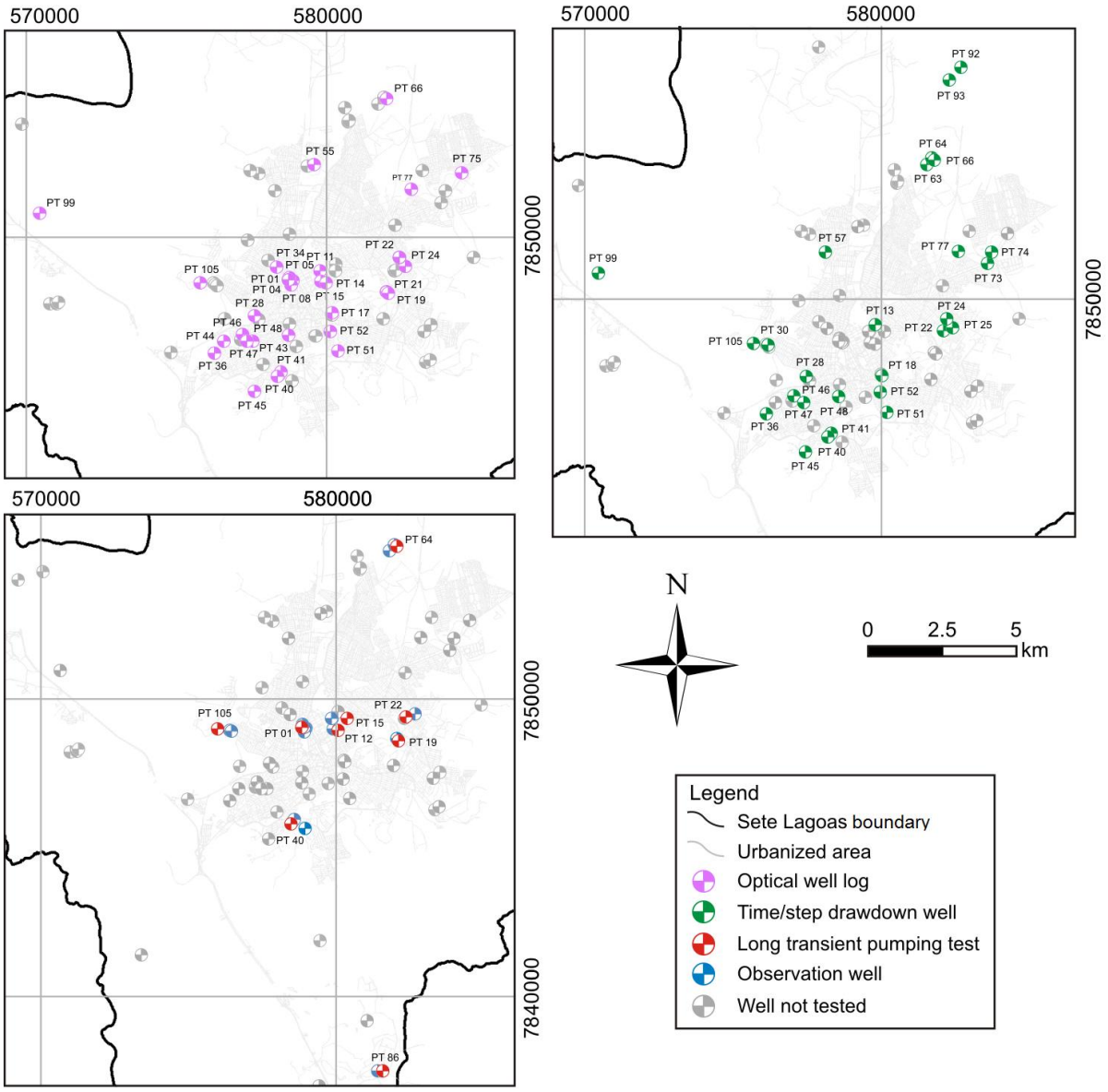

Fig. 3. Location map of the thirty optical well logs (pink color, top/left figure); and the pumping tests, divide by twenty-seven time-drawdown or step-drawdown tests (green color, top/right figure), and nine long duration transient pumping tests (red color, bottom/right figure).

3.2.2 Stable isotopes samples

Groundwater samples were taken during August 2011 and November 2012 in 30 SAAE's public supply wells (25 samples from Sete Lagoas karst aquifer and 5 samples from the basement) (Fig. 4). The wells located in the central area are pumping waters from the conduits in the karst aquifer. These samples were taken after removing several well volumes of water, using pumps installed in these wells. This was done to purge the aquifer of stagnant water and to acquire fresh aquifer samples for analysis. After sampling, physicochemical parameters (pH, temperature - T, electrical conductivity - EC, and oxidation-reduction potential - ORP) using the HI 9828 portable multiparameter meter were measured.

The surface water samples were collected in June 2013 in seven lakes: Brejão, Grande, José Felix, Paulino, Pedras, Piranhas, and Fazenda da Morada (Fig. 4). For this, samples were taken in the center of each lake using a peristaltic pump (brand Geopump). This method followed the low flow principle, avoiding sediment from the lake's substrate (Puls and Barcelona 1996).

Eleven cumulative monthly rain isotope samples were also collected representing a hydrological year, from April 2012 to April 2013 (no samples in July 2012 due to lack of rain). For this, a polypropylene bottle (10 L) with an also polypropylene funnel connected in that bottle were used and placed in a cooler to keep the temperature and prevent sunlight penetration. A silicone hose with 6 m long was also attached on the bottle to balance the pressure and prevent exchanges with atmospheric air. This method followed the GNIP (Global Network of Isotopes in Precipitation) instruction, where evaporation and loss of lighter isotopes are negligible (IAEA/WMO 2004).

The main concern with these samples was to avoid the post-sampling fractionation. For this, pre-cleaned polypropylene vials (30 ml) were used. These vials were completely filled with samples, avoiding air bubbles inside and stored in coolers maintaining the temperature. All samples were analyzed for ^{18}O and ^{2}H at the Groundwater Research Center (CEPAS) [*CEPAS - Centro de Pesquisas de Águas Subterrâneas*], Institute of Geosciences, University of São Paulo. The samples were run on PICARRO L2130i, processed by Laboratory Information Management System (LIMS) for Lasers software, and were normalized to internal laboratory water standards that were previously calibrated relative to the Vienna Standard Mean Ocean Water (VSMOW). The results were expressed as $\delta^{18}O$ and $\delta^{2}H$, where δ_{sample}

(‰) = ((R_{sample} /$R_{standard}$) − 1) × 1000, where R is D/H, $^{18}O/^{16}O$. The analytical precisions were ±0.09‰ for $\delta^{18}O$ and ±0.9‰ for $\delta^{2}H$.

After all of these analyzes, the samples were compared with the latest Global Meteoric Water Line (GMWL) reported by Rozansky (1993), available at IAEA website: http://isohis.iaea.org. This meteoric water line is linearly related by the equation $\delta^{2}H = 8.17\delta^{18}O + 11.27$, and it is an enhancement to the first meteoric water line proposed by Craig (1961), related by the equation $\delta^{2}H = 8\ \delta^{18}O + 10$. This high correlation coefficient reflects the fact that the oxygen and hydrogen stable isotopes in water molecules are intimately associated.

3.2.3 Geochemistry analysis

The same supply wells used to collect groundwater samples for isotopic analysis were also used for geochemistry evaluation (Fig. 4). Samples for major cations (Na^{+}, K^{+}, Ca^{2+}, Mg^{2+}), major anions (HCO^{-}_{3}, CO^{-2}_{3}, SO^{2-}_{4}, Cl^{-}, NO^{-}_{3}), total dissolved solids (TDS), and total water hardness (WH) were collected in pre-cleaned 1 L plastic polyethylene bottles, and then stored in coolers at 4°C, according to the Sampling and Water Samples Preservation Guide (CETESB 1998). For some analyzes, samples were filtered through a 0.45 µm filter, while for major cations were acidified with nitric acid to a pH of less than 2. All these samples were analyzed at the Analytical Solution Company's laboratory, in São Paulo.

3.3 Georeferencing data and software

All the information was entered in a GIS database and georeferenced in ArcGIS 10.1 software. The coordinate system was the Universal Transverse Mercator (UTM) projection, Zone 23, datum SAD 69, with units in meters.

A four-step process was used to convert all the maps data to digital form: (1) automation: a scanned image of the original field map was vectorized, edited, and processed into arc, polygon, and point formats; (2) projection: digital files were transformed from digitizer coordinates to real-world coordinates and converted to a cartographic projection; (3) tables: tables were created to hold label information for polygons, arcs, and points; and (4) symbology: symbols were added for each different layers to indicate different information on the map plots.

To address areas with low data, and to help understand the spatial distribution of subsurface lithological contacts, as well as to understand the spatial concentration of some parameters, such as major ions or potentiometric surface, kriging interpolations of the data were carried out in Surfer 8 software, drawing isopleths maps. After that, these maps were visually improved in CorelDraw X3 software.

For geochemical samples, all the measurements were checked for accuracy by calculating the mass balance, and then the water types were classified using the Piper's diagram of water (Piper 1944) at the AquaChem 4.0 software. For saturation index of calcite and dolomite calculations, PHREEQCI software was used.

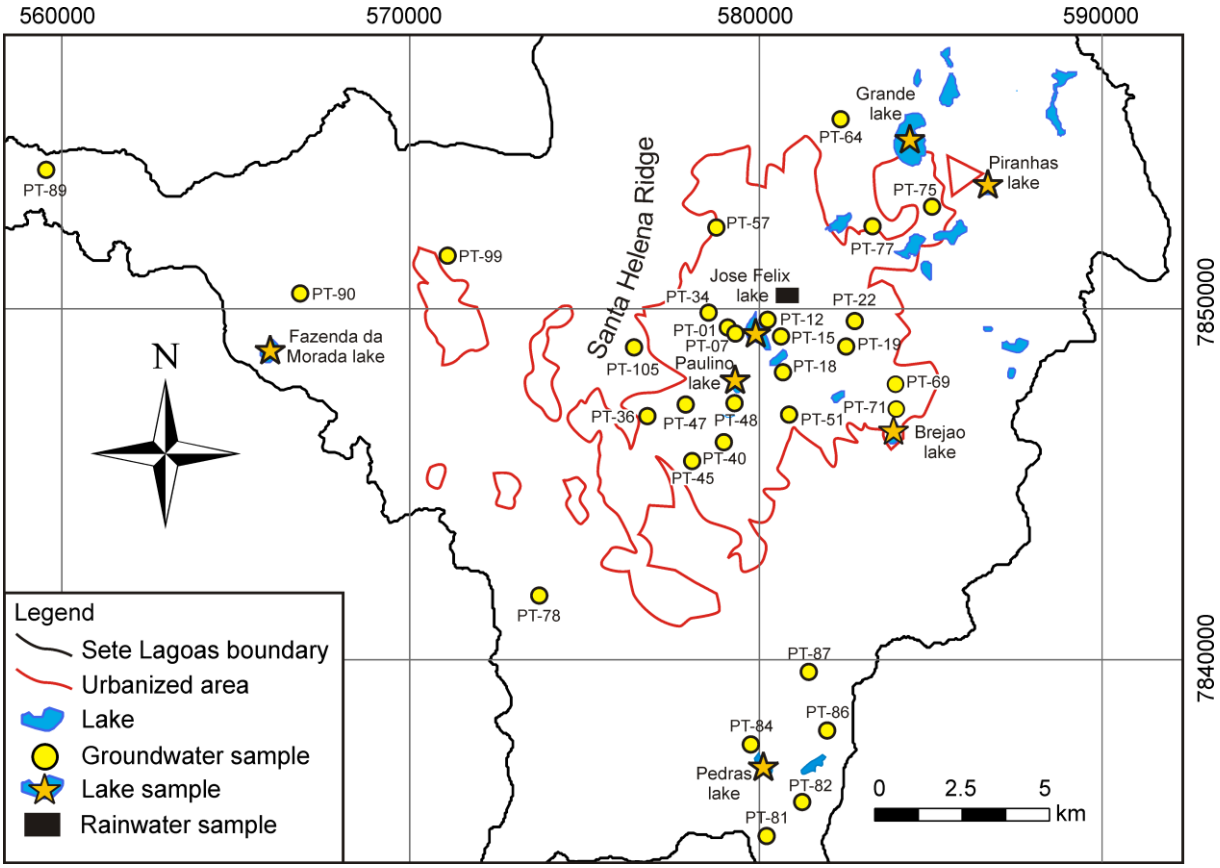

Fig. 4. Location map of sampling points: groundwater in supply wells (yellow dots), rainwater collector (central black rectangle), and surface water in seven lakes (orange star).

REFERENCES

CECAV (2009) Centro Nacional de Pesquisa e Conservação de Cavernas [National Center for Research and Conservation of Cave]. Available: http://www.icmbio.gov.br/cecav/downloads Accessed on March 2014.

CETESB (1998) Sampling and Water Samples Preservation Guide. São Paulo, 150 p.

Craig H (1961) Standard for reporting concentration of deuterium and oxygen-18 in natural waters. Science 133, 1702–1703.

Dunham R J (1962) Classification of carbonate rocks according to depositional texture. In: W.E.HAM (ed): Classification of carbonate rocks. Am. Assoc. Petrol. Geol., Mem.1, Tulsa, Oklahoma, p. 108-121.

EMBRAPA (2006) Empresa Brasileira de Pesquisa Agropecuária [Brazilian Agricultural Research Corporation]. Available: http://www.relevobr.cnpm.embrapa.br/download/mg/mg.htm. Accessed on March 2013.

Folk RL (1959) Practical petrographic classification of limestones: American Association of Petroleum, Geologists Bulletin, v. 43, p 1-38

Folk RL (1980) Petrology of Sedimentary Rocks. Hemphill Publishing, Austin, TX, 184p.

IAEA/WHO (2004) Global Network of Isotopes in Precipitation. The GNIP Database. Available at: http://isohis.iaea.org.

Piper AM (1944) A graphical procedure in the geochemical interpretation of water-analysis. Transactions American Geophysical union. v. 25, p. 914-928.

Puls RW, Barcelona MJ (1996) Low flow (minimal drawndown) groundwater sampling procedures. United States Environmental Protection Agency, Office of Research and Development, Office of Solid Waste and Emergency Response, EPA/540/S-95/504, April, 12p.

Rozanski K, Araguás-Araguás L, Gonfiantini R (1993) Isotopic patters in modern global precipitation, in *Climate Change in Continental Isotopic Records,* Geophys. Monogr. Ser., 78, ed. by P.K. Swart, et al, pp. 1-36, AGU, Washington, DC.

Theis CV (1935) The relation between the lowering of the piezometric surface and the rate and duration of discharge of a well using groundwater storage. Transactions of the American Geophysical Union. v. 16, pp.519-524.

Thiem G (1906) Hydrologische Methoden; Gebhardt, Leipzig.

Winter JD (2001) An Introduction to Igneous and Metamorphic Petrology. Prentice Hall Inc., Upper Saddle River, 697.

CHAPTER 4: KARST HYDROGEOLOGY: ORIGINS AND CONCEPTS

The term "karst", meaning stony ground, originates in the Dinaric Plateau in the Balkans region of Eastern Europe. This is also where the field of karst science began (Van Beynen 2011). Jovan Cvijić (1865-1927) helped lay down the foundation for the modern understanding of geomorphic processes in the late nineteenth century, where the karst science has expanded to include other types of karst, such as relict, paleokarst, fluviokarst, thermokarst, etc. (Ford and Williams 2007). Now in the twenty-first century, the science of karst has greatly advanced, incorporating an improved understanding of karst environments, their fragility, and their value to human development.

Rocks types potentially containing karst cover about 20% of the Earth's land surface, especially those developed in carbonate rocks, such as limestone, dolomite, or gypsum (Fig. 5), where 20-25% of the global population depends largely, or entirely, on groundwater obtained from them (Ford and Williams 2007). In Brazil, it is estimated that between 5 - 7% of the total surface of the country is composed by karst rocks (Karmann 1994), with the most extensive karst regions occurring in central Brazil, developed on Proterozoic and Lower Cambriam limestones and dolomites (Auler and Farrant 1996). Karst aquifers are extremely heterogeneous with a distribution of permeability that spans many orders of magnitude. They often contain open conduit flowpaths with hydraulic characteristics more like surface streams than groundwater (White 2003).

These resources are coming under increasing pressure and have great need of rehabilitation and sustainable management, so the knowledge of their properties is increasingly important. The sections that follow will provide brief comments about the most relevant concepts related to karst hydrogeological systems that were useful to the development of this research and that may be useful for who will read this thesis as a reference for future works.

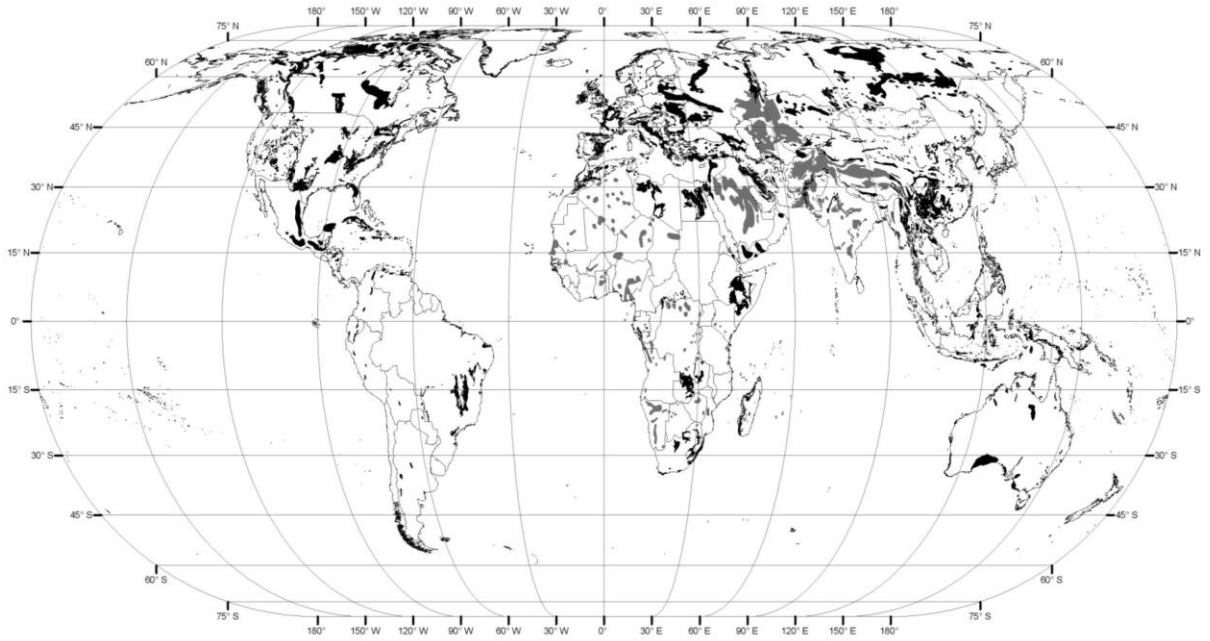

Fig. 5. Global distribution of major outcrops of carbonate rocks, where the black areas are pure carbonates and the grey areas are impure carbonates (from Ford and Williams 2007). The resulting karst terrain tends to have high numbers of caves and sinkholes.

4.1 The origin of karst

Karst is commonly considered as the result of the solution process of carbonate rocks, named “karstification”. It occurs by chemical and, sometimes, mechanical action of water in a region generally of limestone, dolomite, or gypsum bedrock (Karamouz et al. 2011). The chemical composition of groundwater from these bedrocks is usually dominated by products from dissolution of carbonate minerals including calcite, aragonite and dolomite. The carbonate solution occurs because the water is acidic when it contains dissolved CO_2, according to the following stoichiometric equations (Goldscheider and Drew 2007):

$$CO_2 + H_2O \leftrightarrow H_2CO_3 \quad (1)$$

$$H_2CO_3 \leftrightarrow HCO^-_3 + H^+ \quad (2)$$

$$CaCO_3 \leftrightarrow Ca^{2+} + CO_3^{2-} \quad (3)$$

$$CO_3^{2-} + H^+ \leftrightarrow HCO^-_3 \quad (4)$$

The solubility product corresponding to reaction 3 is quite small. However, because the carbonate ion is “removed” by protonation (equation 4), dissolution of carbonate minerals can proceed to a significant extent, depending on the quantity of

carbonic acid that is available and delivers protons (equation 2). Equations 1 - 4 can be summarized by equation 5:

$$2H_2O + CaCO_3 + CO_2 \leftrightarrow H_2O + Ca^{2+} + 2HCO^-_3 \quad (5)$$

Because the concentration of dissolved CO_2 is driven by both the temperature and the CO_2 partial pressure of the atmosphere related to (ground) water, climate is generally considered as driving karst processes (Smith and Atkinson 1976, Bakalowicz 1992). Presently, and for late geologic time, CO_2 was only abundant in the subsurface where it was produced either in soils by biological activity, or at depth by geological processes. Consequently, karst develops mainly with groundwater solution of the carbonate rocks.

In fact, the solution of carbonate rocks proceeds only if groundwater flows, which export the products of dissolution creating underground voids. These voids progressively organize into a hierarchical structure (the conduit system or karst network) in the vadose and the phreatic zone. In it, pipe flow conditions prevail, either under pressure or at atmospheric pressure. Therefore, groundwater flow determines the hydrogeological structure of karst media, which in return creates an important feedback effect modifying the flow conditions (White 2003). The orientation and extension of the flow system and conduit network may change with time, where conduits may collapse, or be filled with sediments, or saturated conduits may transform into unsaturated conduits, or vice-versa (Goldscheider and Drew 2007).

For this, karst develops only if the following conditions occur: (1) the possibility of dissolving carbonate rock, i.e. the existence of a solvent; and (2) a groundwater flow, determined by a hydraulic gradient and geological discontinuities, such as joints and bedding planes, folds, or faults/fractures. These conditions result in aquifers in which there may be unexpected groundwater flow paths and drainage outlet points, which cannot be predicted on the basis of the present topographic and hydrologic setting (White 2003, Goldscheider and Drew 2007).

4.2 Features and controls on the development of karst system

A karst region is usually formed by a set of phenomena, grouped into systems that are formed because of the existence of smaller structures dominated by tectonic,

stratigraphic, and lithologic factors. These elements are divided into three groups: (1) the epigenetic forms of absorption, where the infiltration of water in karst carves the karst morphology; (2) the hypogenic forms, where the water circulates through underground caves and other underground conduits; and (3) where the hypogenic circulation returns to normal epigenetic way through surges. All karst system, in local or regional scale, could have these three types of karst forms characterizing the "hydrogeological model", with recharge, water circulation (and its heterogeneities) and discharge area (White 2003).

Király (2002) pointed out that groundwater flow depends on hydraulic parameters and on boundary conditions and, consequently, that other factor, such as geology, geomorphology, and climate, exert their influence on groundwater movement solely through hydraulic parameter fields and boundary conditions. These essential components inside of a karst aquifer flow system will be discussed as following.

4.2.1 Recharge of karst aquifer (input control)

A karst aquifer can be envisaged as an open system with a boundary defined by the catchment limits and with input, throughput and output flows, mechanisms and controls (Ford and Williams 2007). In the simplest case, there are different categories for karst aquifer recharge. If the karst area recharges itself, it is called autogenic recharge. Allogenic recharge occurs when the adjacent non-karst areas recharge the karst aquifer (Goldscheider and Drew 2007).

Whereas autogenic recharge is often quite diffuse, down many fissures across the karst outcrop, allogenic recharge normally occurs as concentrated point-inputs of sinking streams. Both the water chemistry and the recharge volume per unit area are different in these two styles of recharge, with considerable consequences for the scale and distribution of the development of secondary permeability (Ford and Williams 2007).

4.2.2 Hydraulic parameters (throughput control)

4.2.2.1 Permeability of karst aquifer

Formation bulk permeability depends on the shape, amount, distribution and interconnectivity of void spaces, or permeability structure. The "karstification" of an aquifer is in large part measured by its permeability distribution. For many years, this

has been discussed in terms of the "triple permeability" model (White 2003), consisting of: (1) matrix permeability of the bedrock itself (or primary porosity); (2) fracture permeability (or secondary porosity); and (3) conduit permeability (or tertiary porosity).

The matrix permeability of many Paleozoic limestones and dolomites is very low and can often be ignored. Mezosoic limestones, such as those of Florida and the Caribbean islands may have very high matrix permeabilities. Fracture permeability requires two parameters: the fracture aperture and the fracture spacing. Both are statistical and have a range of values within the same aquifer. Fracture permeability is modified by solution so that fracture apertures range from tens or hundreds of micrometers in unmodified limestone up to 10 millimeters. The latter is the aperture at which non-linear effects begin to appear in the flow field and marks a useful boundary between large fractures and very small conduits. Conduits can range in size from 10 mm to tens (sometimes hundreds) of meters. Hydrologically, they behave much as storm drains. In map view, conduits take on many different patterns depending on local geology and various characteristics of the flow field itself. To understand the dynamics of a karst aquifer, then, it is necessary to understand the rate of recharge into the various components of the permeability and the exchange of water between these components (White 2003, Ford and Williams 2007).

Because of this triple permeability, karst limestones can lead to well-known permeability scale effects, which are generally defined as continual increases in permeability magnitude from small- to regional-scale estimates, which is probably caused by fractures on the small-scale, and that the largest permeabilities on the regional-scale were caused by karstic conduits (Ratz 1967, Király 1975, Maclay and Land 1988, Halihan et al. 1999). According to Halihan et al. (2000), this increment in permeability can reach nine orders of magnitude variability.

4.2.2.2 Transmissivity and hydraulic conductivity

In practical terms, the transmissivity equals the horizontal groundwater flow rate through a vertical strip of aquifer one unit wide. Transmissivity is directly proportional to aquifer thickness and hydraulic conductivity. However, the concept of transmissivity in karst aquifers is not straight-forward: it is obvious that the transmissive properties of conduits and channels, where the groundwater preferentially flows, are much higher than in the surrounding aquifer matrix. At the

same time, the hydraulic conductivity has no real physical meaning in the case of conduit and channel flow; it is proportionality constant in Darcy's law, which was derived for intergranular porous media, and has the dimension of velocity. Although the hydraulic conductivity has been used to calculate flow in all aquifer types, it should be noted that in karst aquifers it represents a lumped parameter, which describes properties of an "equivalent porous media". In other words, the hydraulic response of all porosity types, including conduits and karst channels, is described with one parameter: an equivalent hydraulic conductivity (Goldscheider and Drew 2007).

4.2.2.3 Groundwater velocity

Because of widely varying hydraulic conductivity and effective porosity of karst carbonates, even within the same aquifer system, the groundwater velocity in karst can vary over many orders of magnitude. One should therefore be very careful when making a (surprisingly common) statement such as "groundwater velocity in karst is generally very high" (Goldscheider and Drew 2007). Although this may be true for turbulent flow taking place in karst conduits, a disproportionably larger volume of any karst aquifer "experiences" relatively low groundwater velocities (laminar flow) through small fissures and rock matrix.

It is interesting that, based on 281 dye tracing tests, the most frequent velocity (14% of all cases) in the classic Dinaric karst of Herzegovina, as reported by Milanovic (1979), is quite similar: between 864 and 1728 m/d. 25% of the results show groundwater velocity greater than 2655 m/d in West Virginia, and greater than 5184 m/d in Herzegovina.

Confined karst aquifers, which do not have major concentrated discharge points in forms of large springs, generally have much lower groundwater flow velocities. This is regardless of the predominant porosity type because the whole system is under pressure and the actual displacement of "old" aquifer water with the newly recharged one is rather slow. Groundwater flow velocity estimates using carbon fourteen isotope dating for the confined portion of the Floridan aquifer in central Florida (Hanshaw and Back 1974) showed that the average groundwater velocity based on 40 values is 6.9 m/y or 0.019 m/d.

4.2.2.4 Groundwater flow

Flow through fractures

Fracture aperture and thickness are two parameters used most often in various single-fracture flow equations, while spacing between the fractures and fracture orientation is used when calculating flow through a set of fractures. However, these actual physical characteristics are not easily and meaningfully translated into equations attempting to describe flow at a realistic field scale (Goldscheider and Drew 2007):

1) Fracture aperture is not constant and there are voids and very narrow or contact areas called asperities. Various experimental studies have shown that the actual flow in a fracture is channeled through narrow, conduit-like tortuous paths and cannot be simply represented by the flow between two parallel plates separated by the "mean" aperture (Cacas 1989);

2) Because of stress release, the aperture measure at outcrops or in accessible cave passages is not the same as an in-situ aperture. Aperture measured on drill cores and in borings is also not a true one – the drilling process commonly causes bedrock adjacent to fractures to break out thereby increasing the apparent widths of fracture openings as viewed on borehole-wall images (Williams et al. 2001);

3) Fractures have limited length and width, which can also vary between individual fractures in the same fracture set. Spacing between individual fractures in the same set can also vary. Since all these variations take place in the three-dimensional space, they cannot be directly observed, except through continuous coring or logging of multiple closely spaced boreholes, which is the main cost-limiting factor (Williams et al. 2001).

Flow through conduits and channels

Flow through conduits is generally described by the well-known Bernoulli equation for real viscous fluids. The total energy surface (E) of flow can only decrease from the upgradient cross section towards the downgradient cross section of the same flow tube (conduit) due to energy losses. On the other hand, the piezometric surface (H) can go "up" and "down" along the same flow tube depending on the cross sectional area. The total energy surface, which includes the flow velocity component ($\alpha v^2/2g$), can be directly measured only by the Pitot device whose installation is not feasible in most field conditions (Goldscheider and Drew 2007).

Monitoring wells and piezometers, on the other hand, only record the piezometric pressure (hydraulic head), which does not include the flow velocity component. It is therefore conceivable that two piezometers in or near the same karst conduit with rapid flow may not provide useful information for calculation of the real flow velocity and flow rate between them, and may even falsely indicate the opposite flow direction. There are additional complicating factors when attempting to calculate flow through natural karst conduits using the pipe approach: (1) flow through the same conduit may be both under the pressure and with the free surface; (2) since conduit walls are more or less irregular (“rough”), the related coefficient of roughness has to be estimated and inserted into the general flow equation; (3) conduit cross section may vary significantly over short distances; and (4) the flow may be both laminar and turbulent in the same conduit, depending on the flow velocity, cross-sectional area and wall roughness. The irregularities that cause turbulent flow are mathematically described through the Reynolds number and the friction factor.

4.2.3 Discharge of karst aquifer (output control)

Most of the largest springs in the world are karst springs (Ford and Williams 2007). They represent the termination of underground river systems and mark the point at which surface fluvial processes become dominant. The vertical position of the spring controls the elevation of the water table at the output of the aquifer, whereas the hydraulic conductivity and throughput discharge determine the slope of the water table upstream and its variation under different discharge conditions.

A distinguishing feature of karst aquifers is that most of the groundwater is discharged through a small number of large springs. In some aquifers, the entire discharge is through a single spring. In other, there is a distributary system to a small number of springs. One or a few of these carry the base-flow discharge and are called "underflow springs", while other springs flow only during periods of high discharge and are called "overflow springs" (Worthington 1991). The discharge from karst springs is a composite of all water moving through the aquifer. The spring (or springs), therefore, is an optimum location for measuring hydrographs, chemographs, and for monitoring the aquifer for contaminants.

4.3 Karst landform

Karst landscapes form in areas with carbonate bedrock subjected to slow dissolution processes (Fleury 2009). These processes typically result in the formation of visible surface and subsurface features, including sinkholes, caves, and springs, where the water is the main agent of landscape altercation (Palmer 2007). Subsequently, the basic understanding of the most common karst landforms will be discussed.

4.3.1 Sinkholes (Dolines)

Sinkholes, or dolines, are an extremely common type of karst landform, created by the subsidence of soils and rock at or near the land surface into empty space below (Fleury 2009). They are often located in areas where soluble rock is near the surface, either completely exposed or beneath a layer of topsoil. Sinkhole development can be triggered by any mechanism that increases the head differential between the artesian water in the limestone and the perched water in the surface soil (Beck 1986), resulting in depressions with a shape of bowls or funnels.

In order to form a sinkhole, three requirements are needed (Fleury 2009): (1) a drainage path for the surface water runoff to follow; (2) a zone of bedrock modified by solution located at or near the surface; and (3) a covering of soil or some other material making up the land surface.

With some exceptions, sinkholes are generally not large landforms. However, they are important to understand in the context of karst systems because they act as recharge routes for the aquifer below. The fact that surface water receives no natural filtering when entering a karst aquifer via sinkhole means that contaminants on the surface are easily carried into the groundwater (White 1988).

4.3.2 Caves

Caves are generally a natural opening in the earth that is large enough to be entered by a human (White 1988, Palmer 2007). Usually, cave systems are the result of a succession of active conduit networks that evolve through time (Klimchouk et al. 2000). It has been demonstrated that phreatic conduit systems may develop within a few thousand years if recharge is sufficient (Palmer 2000), especially if initial openings are wide enough (>0.1 mm). In many mountainous karst areas, those

conditions are fulfilled, and active conduits normally are located close to the valley bottoms. In mountain ranges, it can be assumed that uplift is more or less compensated for by the entrenchment of valleys, therefore new conduits have to form each time the valley floor is entrenched further, previous (higher-level) conduits become only temporarily active, and later are eventually permanently abandoned by the water. Most of the caves explored by cavers are part of those dry (fossil) systems. This simple model may be more complex if, for any reason, the base level was raised at any time in the past (Audra et al. 2004).

4.3.3 Springs

Springs are formed at the spots where karst waters emerge from the local underground drainage system. They can be found on the surface or in caves and are often used as sources of drinking water and as recreation areas (Fleury 2009). Their formation is a direct result of carbonate rock dissolution, creating large conduits and caves that can then channel groundwater up to the land surface. Springs can serve as hydrogeological trend indicators and are very stable in terms of water quality, temperature and flow, though even short-term variation in rainfall can be reflected by a spring's flow (Field 2002).

4.3.4 Poljes

Poljes - the largest karst hollows - are wide, closed depressions with flat floors, which are often adjacent to steep enclosing walls. They require extremely thick and geographically extensive carbonate bedrock to form at all. Poljes have their own internal drainage systems and often have complex hydrogeological characteristics, including shallows holes and disappearing streams (Field 2002).

4.3.5 Karst valleys

Karst valleys form when a developing underground drainage system diverts water away from the rivers feeding into the valley. They have all the properties of a stream valley except the stream itself, being more common in areas of flat, interbedded layers of limestone, sandstone and shale (White 1988).

4.3.6 Sinking streams

They are surface features that direct runoff into an underground channel, in other words, they are sinkholes that form in a stream bed, often with a large vertical shaft beneath (Ford and Williams 2007).

4.4 Human impacts on karst system

Karst environments are particularly fragile and vulnerable to damage compared with most other natural systems. The reason for this is the nature of the karst hydrological system. Efficient drainage of the surface down numerous widened joints, dolines, and sinkholes rapidly transmits surface pollution underground and readily evacuates soils stripped from the surface. Filtration of diffuse recharge is minimal because limestone soils are usually thin, while transmission of recharge is essentially unfiltered because subterranean conduits have large dimensions and rapid transmission provides minimal opportunity for die-off of pathogenic organisms (Ford and Williams 2007).

Thus, it is a fact that karst areas are highly vulnerable to overuse and misuse, having major subterranean components that require specialist knowledge to manage properly and, once damaged, can be extremely difficult to protect and restore. Because of this vulnerability, karst areas can be impacted in form of deforestation, agricultural activity, or rocky desertification, as well as subsidences induced by dewatering, constructions, or groundwater contaminations. Here, emphasis will be given to induced sinkholes and groundwater contamination, considering these impacts are more common in the study area of this thesis.

4.4.1 Groundwater contamination in karst aquifer

Karst aquifers are particularly vulnerable to contamination: due to thin soils, flow concentration in the epikarst (the uppermost, often intensively fractured and karstified layer of a carbonate aquifer), and point recharge via swallow holes, contaminants can easily reach the groundwater, where they may be transported rapidly in karst conduits over large distances. The residence times of contaminants are often short and processes of contaminant attenuation, therefore, often do not work effectively in karst systems. Karst aquifers, consequently, need special protection. However, protection zoning for karst is more complicated than for granular aquifers, because

karst systems are highly heterogeneous and anisotropic, the catchments may cover large areas and flow velocities may be as high as 500 m/h (Goldscheider and Drew 2007).

Many serious problems of human impacts on waters emphatically do exist, even if they are not obvious to the casual observer. Water contamination may be transmitted into karst by both allogenic and autogenic sources. In the autogenic context, contamination can arise from both dispersed and point sources. Dispersed-source contamination enters the epikarst before being transmitted to the phreatic zone, whereas point-source contamination normally bypass the epikarst, typically down doline drains, and is rapidly transmitted to the water table (Ford and Williams 2007).

Some cities built in carbonate rocks, especially in developing countries, have limited or no sewer systems. Consequently, considerable municipal and industrial waste has been and, in many cases, still is being discharged into karst without treatment, giving rise to many water quality problems. As a result, the presence of high nitrate concentrations are present in urban areas (indication of an inefficient management of domestic sanitation systems) in groundwater (Foster and Hirata 1987), exceeding all federal and state drinking water quality requirements. In agricultural areas, the most common is the contamination of pesticide and fertilizers, while in industrial zones, high concentrations of DNAPL (dense, non-aqueous phase liquids), LNAPL (light, non-aqueous phase liquids), and metals (chromium, nickel, cadmium and mercury) are more common (Ford and Williams 2007). All those elements can result in poor drinking water quality, loss of water supply, degraded surface water systems, high cleanup costs, high costs for alternative water supplies (specially in karst aquifers because of its inherent heterogeneities), and/or potential health problems.

4.4.2 Induced subsidences

After groundwater pollution, induced subsidences, a geotechnical problem, such as sinkholes and collapses, are the most prominent hazardous effect of human activity in karst regions. Agriculture, mining and quarrying, highways and railways, urban and industrial constructions all contribute. In 99% of reported cases or more events occur in an overburden of unconsolidated cover sands, silts or clays (Ford and Williams 2007).

These events can occur naturally (by dissolution of rock, or through the failure of a bedrock roof overlying a cave), or can be induced or accelerated by human activities, which are commonly characterized by catastrophic collapse (Newton 1976, LaMoreaux and Newton 1986, LaMoreaux 1997). The formation of both of these types of geotechnical issues generally occur over periods of geologic time, not within a human lifetime in carbonate formations. Therefore, it is important to emphasize that the differences between both natural and anthropogenic situations is the speed at which the collapse processes begin, which is accelerated in an anthropogenic situation (Albrecht 1996).

The induced geotechnical problems in these settings commonly form because of groundwater withdrawal, construction activities, or a combination of both (Newton 1987, Bell 1997). In the case of groundwater withdrawal in an urban aquifer, periods of drought are the most dangerous, corresponding increased demand for groundwater, leading to the formation of enlarged cones of depression (Oliveira 1997). Within these cones of depression, wells, springs, and streams can go dry or have their flows significantly reduced with the overall direction of groundwater flow being changed inducing geotechnical problems (Hobbs and Gunn 1998).

4.5 Isotopes and significance to karst hydrology

Karst groundwaters can be characterized by natural or anthropogenic tracers including isotopes, hydrochemical constituents, and artificial tracers, such as fluorescent dyes (Goldscheider and Drew 2007). Isotopic data elucidate the origin and age of karst waters and the rocks that enclose them, and show that mixing and carbonate reactivity are major variables. Hydrogen, carbon and oxygen are the dominant constituents in karst waters, karst bedrock, speleothems, travertine deposits, and in dissolved bicarbonate, which is normally the dominant anion in karst water. Fortunately, these elements all include stable isotopes that exhibit variations large enough to be routinely measured with mass spectrometers. In the case of this thesis, the stable isotopes hydrogen and oxygen were used for tracking the origin of water and its subsequent movement.

Physically, the stable isotopes are atoms that take the same position in the table of elements, but have a different number of neutrons and, therefore, mass. The most relevant isotopes for atmospheric and hydrologic sciences are ^{18}O for oxygen

(corresponding to the most abundant isotope ^{16}O), and ^{2}H (or Deuterium, D) for hydrogen (corresponding to the most abundant isotope ^{1}H) (Gat 1996, Mook 2001).

These isotopes, during evaporation and condensation phases, become enriched in one phase and depleted in the other. This separation of isotopes is named *isotopic fractionation* (Mook 2001), and quantifying these processes is possible by calculating the large variability of their isotopic ratios ($^{2}H/H$ and $^{18}O/^{16}O$).

Measurements of stable isotopes also require a common standard. For atmospheric applications, the usual standard is the Vienna Standard Mean Ocean Water (V-SMOW), published and distributed regularly by the International Atomic Energy Agency (IAEA). The delta (δ) notation is used to quantify stable isotope as relative ratios and the isotopes values are reported in per mil (‰) to make it easy to compare significant results.

Different results from the standard V-SMOW provide information about recharge and discharge processes; flow, mixing and interconnections between aquifers; evaporation; marine influence; and the sources and mechanism of pollution (Clark and Fritz 1997).

Craig (1961) observed that the $\delta\,^{18}O$ and $\delta\,^{2}H$ values of precipitation that have not been evaporated are linearly related by the equation $\delta^{2}H = 8\ \delta^{18}O + 10$. This equation, known as the Global Meteoric Water Line (GMWL), is based on precipitation data from locations around the globe, and has an $r^2 > 0.95$. This high correlation coefficient reflects the fact that the oxygen and hydrogen stable isotopes in water molecules are intimately associated. The slope and intercept of any Local Meteoric Water Line (LMWL), which is the line derived from precipitation collected from a single site or set of "local" sites, can be significantly different from the GMWL.

A GMWL reported by Rozansky (1993) related by the equation $\delta^{2}H = 8.17\delta^{18}O + 11.27$ is an enhancement to the meteoric water line proposed by Craig (1961) having much more data included, which can provide more accuracy in the meteoric water line.

REFERENCES

Albrecht KJ (1996) Evaluation of geological and geotechnical problems in karst land - Basis for geotechnical mapping. Sao Paulo. Master Graduate in Geology - University of Sao Paulo (USP)

Audra P, Mocochain L, Camus H, Gilli E, Clauzon G, Bigot JY (2004) The effect of the Messinian Deep Stage on karst development around the Mediterranean Sea. Examples from Southern France. Geodinamica Acta, 17, 27–38.

Auler A, Farrant AR (1996) A brief introduction to karst and caves in Brazil. Proc. Univ. Bristol Spelacol. Soc., 20 (3), 187-200.

Bakalowicz M (1992) Géochimie des eaux et flux de matières dissoutes. L'approche objective du rôle du climat dans la karstogénèse. (Water geochemistry and dissolved solid flux. The objective approach of climate part in the genesis of karst). Karst et évolutions climatiques. Hommage à Jean Nicod. Presses Universitaires de Bordeaux, Talence, pp 61–74.

Beck BF (1986) A generalized genetic framework for the development of sinkholes and karst in Florida, USA. Environmental geology, v. 8, nos. 1-2, p. 12.

Bell JW (1997) Las Vegas valley: Land subsidence and fissuring due to groundwater withdrawal. Nevada Bureau of Mines and Geology, Reno, NV. Impact of climate change and land use in the southwestern United State.

Cacas MC (1989) Développement d'un modèle tridimensionnel stochastique discret pour la simulation de l'écoulement et des transports de masse et de chaleur en milieu fracturé. Ph.D. thesis, Ecole des Mines de Paris, Fontainebleau, France.

Clark I, Fritz P (1997) Environmental Isotopes in Hydrogeology. New York, CRC Press. 328p.

Craig H (1961) Standard for reporting concentration of deuterium and oxygen-18 in natural waters. Science 133, 1702-1703.

Field MS (2002) A lexicon of cave and karst terminology with special reference to environmental karst hydrology. U.S. Environmental Protection Agency, Washington, DC.

Fleury S (2009) Land use policy and practice on karst terrains: Living on limestone. Springer. 187 p.

Ford DC, Williams PW (2007) Karst geomorphology and hydrology. 2nd edn. John Wiley & Sons, Chichester, U.K. 562 p.

Foster SSD, Hirata RCA (1987) Groundwater pollution risk evaluation: the methodology using available data. Lima: WHO/PAHO/HPE/CEPIS, 87 p.

Gat JR (1996) Oxygen and hydrogen isotopes in the hydrologic cycle. Annu. Rev. Earth Planet. Sci. 24, 225–262.Goldscheider N (2005) Karst groundwater vulnerability mapping: application of a new method in the Swabian Alb, Germany. Hydrogeology Journal, 13:555–564

Goldscheider N, Drew D (2007) Methods in Karst Hydrogeology. International Contributions to Hydrogeology, 26. London, Taylor & Francis, 264 p.

Halihan T, Sharp JMJr., Mace RE (1999) Interpreting flow using permeability at multiple scales. In Palmer AR, Palmer MV and Sasowsky ID (eds) Karst Modeling. Karst Waters Institute Special Publication no 5, Charlottesville, p 82-96.

Halihan T, Sharp JMJr., Mace RE (2000) Flow in the San Antonio segment of the Edwards Aquifer: Matrix, fractures, or conduits?: in C. M. Wicks and I. D. Sasowsky, eds., Groundwater flow and contaminant transport in carbonate aquifers: Balkema, Rotterdam, The Netherlands, p. 129–146.

Hanshaw BB, Back W (1974) Determination of regional hydraulic conductivity through use of 14 C dating of groundwater. Memoires, Tome X, 1. Communications. 10th Congress of the International Association of Hydrogeologists, Montpellier, France, 195–198.

Hobbs SL, Gunn J (1998) The hydrogeological effect of quarrying karstified limestone: options for protection and mitigation: Quarterly Journal of Engineering Geology, v. 31, p 147-157

Karamouz M, Ahmadi A, Akhbari M (2011) Groundwater Hydrology: Engineering, Planning, and Management. CRC Press. Taylor & Francis Group. 649 p.

Karman I (1994) Evolução e dinâmica atual do sistema cárstico do alto vale do rio Ribeira de Iguape, sudeste do Estado de São Paulo. Doctoral Thesis, University of São Paulo, 228 pp.

Király L (1975) Rapport sur l'état actuel des connaissances dans le domaine des caractères physique des roches karstique. In: Burger, A. and Dubertet, L. (eds). Hydrogeology of karstic terrains. Paris, International Association of Hydrogeologists, Series B, No. 3, p. 53-67.

Király L (2002) Karstification and groundwater flow. In: Gabrovšek, F. (ed.) Evolution of karst: from prekarst to cessation. ZRC Publishing, ZRC SAZU, pp. 155–190, Ljubljana.

Klimchouk AB, Ford DC, Palmer AN, Dreybrodt W. (Eds.) (2000) Speleogenesis, evolution of karst aquifers. Huntsville, Alabama, USA: National Speleological Society, Inc., 527 p.

LaMoreaux PE, Newton JG (1986) Catastrophic subsidence: an environmental hazard, Shelby County, Alabama: Environmental Geology Water Science, v. 8, no. 1/2, p 25-40.

LaMoreaux PE (1997) Legal aspects of karst and insurability, in Günay, Gültekïn, and Johnson, A.I., eds., Karst waters & environmental impacts: Proceedings of the 5thInternational Symposium and Field Seminar on Karst Waters and Environmental Impacts, Antalya, Turkey, A.A. Balkema, p 11-17

Maclay RW, Lamb LF (1988) Simulation of flow in the Edwards Aquifer, San Antonio Region, Texas, and Refinement of the Storage and Flow Concepts. U.S. Geological Survey Water-Supply Paper 2336-A, 48 p.

Milanovic P (1979) Hidrogeologija karsta i metode istraživanja [in Serbo-Croatian; Karst hydrogeology and methods of investigations]. HE Trebišnjica, Institut za korištenje i zaštitu voda na kršu, Trebinje, 302 p.

Mook WME (2001) Environmental Isotopes in the Hydrological Cycle. Principles and Applications. UNESCO/IAEA Series, http://www.naweb.iaea.org/napc/ih/volumes.asp.

Newton JG (1976) Induced sinkholes – A continuing problem along Alabama highways, in International Association of Hydrologic Sciences, Land Subsidence Symposium: Proceedings of the Second International Symposium on Land Subsidence held at Anaheim, California, IAHS-AISH Publication no. 121, p 453-463

Newton JG (1987) Development of sinkholes resulting from man's activities in the Eastern United States; U.S. Geological Survey Circular 968, 54 p

Oliveira LM (1997) The management of urban geological risks in karst areas. Undergraduate thesis. Pontifícia Universidade Católica do Paraná (PUC-PR). 46 p

Palmer AN (2000) Digital modeling of individual solution conduits. In Klimchouk A, Ford DC, Palmer AN, Dreybrodt W (Eds.), Speleogenesis: Evolution of Karst Aquifers (pp. 194–200). Huntsville, Alabama, USA: National Speleological Society.

Palmer AN (2007) Cave geology. Cave books, Dayton, OH., p. 288.

Rats MV (1967) Neodnorodnost Gornykh Porod i Ikh Fizicheskikh Svojstv. Nauka Moskva.

Rozanski K, Araguás-Araguás L, Gonfiantini R (1993) Isotopic patters in modern global precipitation, in *Climate Change in Continental Isotopic Records,* Geophys. Monogr. Ser., 78, ed. by P.K. Swart, et al, pp. 1-36, AGU, Washington, DC.

Smith DI, Atkinson TC (1976) The erosion of limestones. In: Ford TD, Cullingford CHD (eds) The science of speleology. Academic Press, London, pp 151–177.

Van Beynen PE (2011) Karst management. Springer Publishing, Dordrecht, 489 p.

White WB (1988) Geomorphlogy and hydrology of karst terrains. Oxford University Press, NY, 464 p.

White WB (2003) Conceptual models for karstic aquifers. Speleogenesis and Evolution of Karst Aquifers, 1 (1) January 2003, p.2.

Williams JH, Lane J W, Singha K, Haeni FP (2001) Application of advanced geophysical logging methods in the characterization of a fractured-sedimentary bedrock aquifer, Ventura County, California. U.S. Geological Survey Water-Resources Investigations Report 00-4083, 28 p.

Worthington SRH (1991) Karst hydrogeology of the Canadian Rocky Mountains. Ph.D. thesis, McMaster University, Hamilton, Ontario. 227 p.

CHAPTER 5: GEOLOGIC CONCEPTUAL MODEL OF THE MUNICIPALITY OF SETE LAGOAS (MG, BRAZIL) AND THE SURROUNDINGS

Paulo Galvão[1], Ricardo Hirata[2], Arnaldo Cordeiro[3], Daniela Barbati[4], Jorge Peñaranda[5]

Accepted in the Anais da Academia Brasileira de Ciências [Annals of the Brazilian Academy of Sciences]

Abstract

The study area is located in the state of Minas Gerais, Brazil, among the municipalities of Pedro Leopoldo, Matozinhos, and Sete Lagoas, with Velhas River as the eastern boundary. It is located in the São Francisco Craton, where carbonated argillo-arenaceous sediments are emplaced giving origin to the Bambuí Group, in the São Francisco Basin. Despite the geological knowledge previously developed, the region needs work on integration and detailing of such information. For this reason, the main objective was to contribute to the quality of the geologic cartography, the spatial distribution, and the structural framework geometry. Thus, geologic mapping, aerial photography interpretation, and evaluation of 270 lithologic well profiles were carried out. It was possible to establish a new geologic perspective of the region by obtaining the detailed geologic map of the municipality of Sete Lagoas, 14 geologic cross sections, and a geologic conceptual model. The study showed that the area is within a basin border, presenting a geometry conditioned by horst and graben system controlled by faulting. This structural feature displaced stratigraphic sequences positioning them side by side with lithologic sequences with different ages.

Keywords: Conceptual model, formations geometry, geology, stratigraphy

1. Introduction

The study area is located in the state of Minas Gerais, Brazil, among the municipalities of Pedro Leopoldo, Matozinhos, and Sete Lagoas, with Velhas River as the eastern boundary (Fig. 1). Geologically, this area is located in the São Francisco Craton, where carbonated argillo-arenaceous sediments are emplaced giving origin to the Bambuí Group, deposited in an epicontinental shelf in the São Francisco Basin. The geologic particularities provide important economic resources to the region, which have driven the economic development and population increase with the municipality of Sete Lagoas at the forefront. There is a considerable industrial, mineral, and metallurgical center in this region situated mainly along the main federal highway, which is a corridor of significant growth.

The previous studies about the Bambuí Group were carried out by Branco and Costa (1961), who proposed the first stratigraphic column of the region, later modified by Oliveira (1967), Schöll

(1973), Dardenne (1978) and, finally, by Ribeiro et al. (2003). In addition, other important studies related to structural (Magalhães 1989), geochronological (Babinski and Kaufman 2003), hydrogeological (Pessoa 1996, 2005), and geological evolution (Nobre-Lopes 1995, Uhlein et al. 2004, Tuller et al. 2009) were carried out. Despite the geologic knowledge being well developed, the area needs work on integration and detailing of the geologic information. Thus, the primary goal of this paper was to contribute to the quality of the geologic cartography, as well as the spatial arrangement, and the structural framework of the lithologies found in this region. Aerial photography, geologic mapping, and the evaluation of 270 lithological well profiles located in Sete Lagoas and in the adjacent municipalities were integrated with the available data to provide a new geologic perspective of the region. As a result, the update to the geologic map of the municipality of Sete Lagoas, 14 geologic cross sections, and a geologic conceptual model were created.

2. Site description

The study area (Fig. 1) overlies the São Francisco Craton (Almeida 1977), which is represented by crystalline rocks from the Paleoproterozoic age formed by the agglutination of different craton blocks from the Archean age. Extension events occurred between 900 and 600 Ma. (Condie 2002) allowing Neoproterozoic silicate-carbonate sediments from the Bambuí Group to be deposited.

Regionally, the Bambuí Group is about 300,000 km^2 (Almeida 1977), including mainly the states of Minas Gerais, Goiás, and Bahia. The basement being controlled by a faulting system causing the thickness of the sediments to be variable (Misi et al. 2007). According to seismic surveys conducted by Petrobras S.A., the central area of this group can have a thickness of 1,000 m, while in the municipality of Sete Lagoas it is estimated to 600 m thick on average (Pedrosa-Soares et al. 1994).

The sediments of the Bambuí Group were deposited in a low gradient stable epicontinental shelf in shallow water conditions, which explains a regional occurrence of the lithofacies. (Schobbenhaus 1984). Stratigraphically, there were three regressive sedimentary mega-cycles: (1) carbonated (Sete Lagoas Formation); (2) argillo-carbonated (Serra de Santa Helena and Lagoa do Jacaré formations); and (3) argillo-arenaceous (Serra da Saudade and Três Marias formations).

The Bambuí Group is represented by the following formations, from the base to the top: Carrancas (diamictites, sandstones, and rhythmites); Sete Lagoas (carbonate sequence); Serra de Santa Helena (siltstones, phyllites, slate, arkose, and marlstones), Lagoa do Jacaré (oolitic limestones); Serra da Saudade (siltstones, sands, and sandstones); and Três Marias (fluvial platform sandstones) (Tuller et al. 2009).

The basement is represented by gneissic rocks associated with granitoids and migmatite zones from the Belo Horizonte Complex. Overlying the Bambuí Group, are the unconsolidated sediments from Cenozoic surface coverage (Tuller et al. 2009). The Bambuí Group is represented by the following formations, associated with mega-cycles 1 and 2 (Fig. 1):

1) Sete Lagoas Formation (Dardenne 1978): overlies the Carrancas Formation in some areas, or may have direct contact with the basement. The ages range from 740±22 Ma. old, based on data from Pb-Pb analysis (Babinski et al. 2007), to 630 Ma., by C-O-Sr data (Caxito et al 2012), or 540 Ma., through paleontology investigations (Warren et al 2014). Three carbonate depositional systems are

recognized (Lima 1997): (1) internal ramp; (2) intermediary ramp; and (3) external ramp deposits; characterized by a shallowing upward cycle. This formation is divided and characterized by two members (Ribeiro et al. 2003): Pedro Leopoldo, at the base, composed of fine grained white limestones, dolomites, marlstones, and pelites; and Lagoa Santa, on the top, by medium grained black limestones;

2) Serra de Santa Helena Formation (Costa and Branco 1961): having an area greater than 7,000 km² and represented by three stratigraphic members (Grossi Sad et al. 1998): (1) lower, characterized by silt-clay rhythmites, generally carbonaceous, and dark shales (about 90 m thickness); (2) medium, composed of marble and shales (50 m thick); and (3) upper, consisting of shales, siltstones, slate cleavage, and cross bedding (around 140 m thick).

Regarding the structural geology, the main planar structures are faults, foliations and fractures, consisting of two types of faults (Danderfer Filho 1991, Tuller et al. 2009): normal and thrust, trending NNW-SSE. Kinematic indicators, such as stretching and mineral lineations, indicate tectonic transport from east to west, forming interstratal ramp thrust belts, accommodated in more argillous upper planes. The first generation of the structures is composed of normal synsedimentary faults. Based on structural surveys, the Bambuí Group is divided into four structural domains, according to the magnitude of the deformation (Tuller et al. 2009): (1) high intensity of deformation domain, where rocks from the Espinhaço Supergroup outcrop. The presence of mass transport commonly indicates movement from east to west; (2) intermediate domain, characterized by less intense deformation, more deformed to the east and less deformed to the west; (3) domain where the Bambuí Group rocks are presented less deformed to not deformed; and (4) domain less deformed at the far west portion of the area, affecting mainly the rocks from the Serra da Saudade Formation.

The study area is located only in the intermediate structural domain, extending from Velhas River to the far western border of the municipality of Sete Lagoas.

3. Methods

Three sets of data were integrated to evaluate the geologic setting of the region. These included geologic mapping, aerial photography interpretation, and lithologic well log analysis. These methods will be presented sequentially followed by the approach to data integration.

Geologic mapping of the entire municipality of Sete Lagoas was carried out in a scale of 1:25,000. The classification of the sedimentary rocks followed the definitions of Folk (1980) and the microscopic classification of the carbonate rocks followed the definitions of Folk (1959) and Dunham (1962). For the metamorphic and igneous rocks, the classification followed definitions of Winter (2001). All the data were recorded on paper topographic maps and converted to digital format. ArcGIS 10.1 was used throughout the project to construct the digital map. Later, integration of the field data and the sheet geologic maps Baldim (SE.23-Z-C-III), Sete Lagoas (SE.23-Z-C-II), Contagem (SE.23-Z-C-V), and Belo Horizonte (SE.23-Z-C-VI), scale 1:100,000, was performed. These maps were acquired from the CPRM database, available on: http://geobank.sa.cprm.gov.br/.

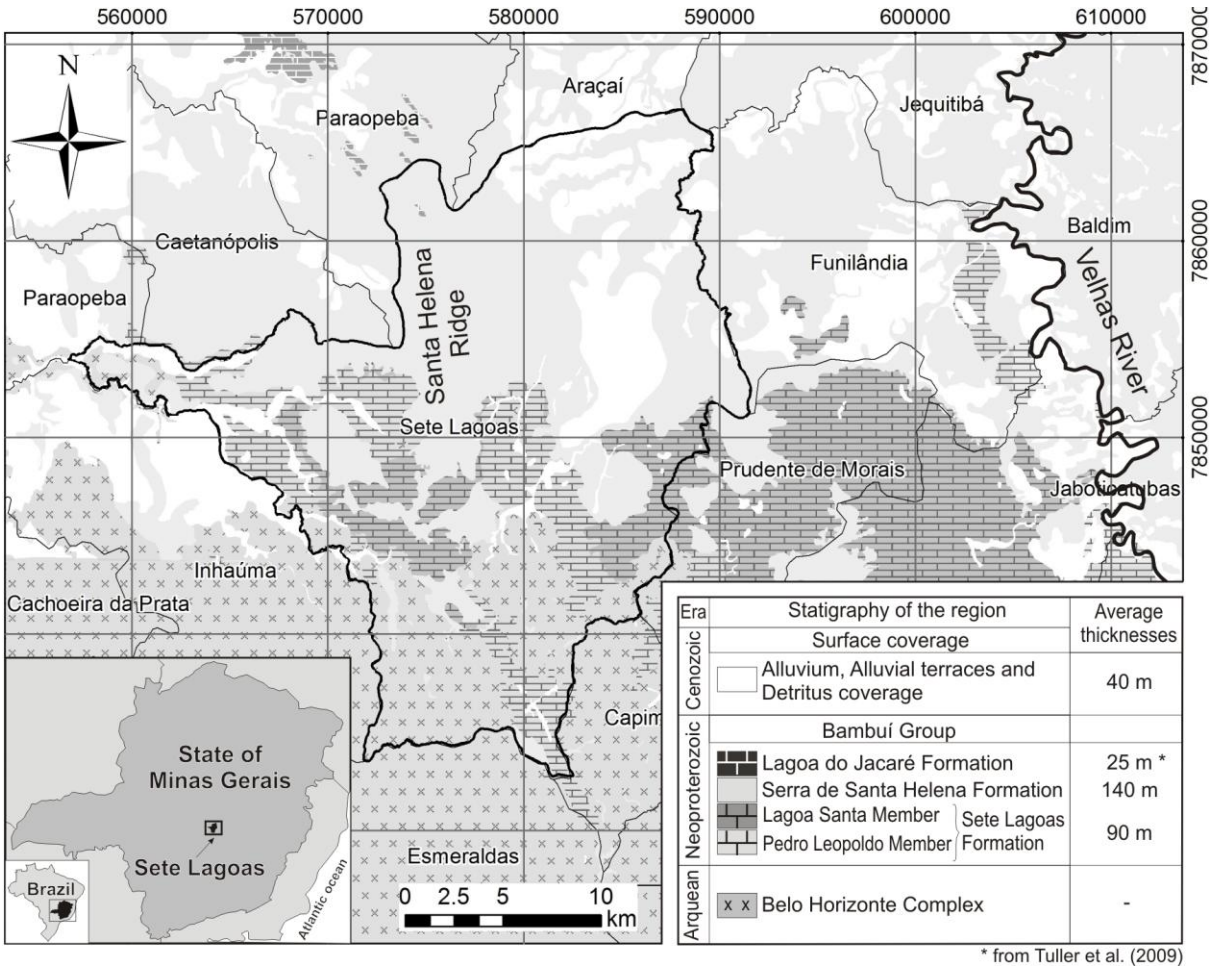

Fig. 1. Location map of the study area and the stratigraphic column showing the lithologies found in the study area limits and its respective average thicknesses (modified from Tuller et al. 2009). The municipality of Sete Lagoas is limited by the black continuous line.

Aerial photography interpretation (scale 1:40,000, dated 1977) and the SRTM image (Shuttle Radar Topography Mission), Sheet SE-23-Z-C, acquired from the EMBRAPA's website were evaluated to define the lithologic contacts (http://www.relevobr.cnpm.embrapa.br).

Information about lithologic well logs was taken from the SIAGAS database (http://siagasweb.cprm.gov.br). A serie of 218 lithologic well profiles were acquired, located in the municipalities of Baldim, Caetanópolis, Capim Branco, Cordisburgo, Esmeralda, Fortuna de Minas, Funilândia, Inhaúma, Inimutaba, Lagoa Santa, Maravilhas, Matozinhos, Papagaio, Paraobepa, Pedro Leopoldo, Prudente de Morais, São José da Lapa, and Sete Lagoas. In addition, 52 public well logs located in Sete Lagoas were analyzed, kindly provided by Water Supply and Sewage Service database (SAAE) [*SAAE -Serviço de Abastecimento de Água e Esgoto*]. Out of the 270 lithologic well profiles that were analyzed, the best and the most reliable were chosen.

In order to help understand the areas where data were sparse, and thus estimate the geologic contact depth, kriging interpolations of the data were carried out in Surfer 8 software.

The complete data sets were entered in a GIS database and georeferenced in ArcGIS 10.1 software. The coordinate system was Universal Transverse Mercator (UTM) projection, Zone 23, datum SAD 69, with units in meters.

Finally, 14 geologic cross sections were made (NW-SE and NE-SW), at a scale of 1:25,000, within the municipality of Sete Lagoas, and a scale of 1:100,000 in the surrounding areas. The topographic elevations were extracted from the SRTM image, using the Global Mapper 11 software.

4. Results and discussions

4.1. Geologic mapping

The lithologies found were the basement rocks from the Belo Horizonte Complex, the carbonate sequence from the Sete Lagoas Formation, the fine grained clastic rocks from the Serra de Santa Helena Formation, and the unconsolidated sediments from the Cenozoic surface coverage. Rocks from the Carrancas Formation (diamictites, sandstones, and rhythmites), stratigraphically below the Sete Lagoas Formation, were not identified and mapped within the study area, but were mapped over the southeast and northwest of the area by Ribeiro et al. (2003) and Tuller et al. (2009). In the case of the Lagoa do Jacaré Formation, these oolitic limestone rocks, with a mean thickness of 25 m, can be found in the far northwest portion of the area and it is more detailed by Tuller et al. (2009).

4.1.1. Belo Horizonte Complex

This igneous/metamorphic basement complex occurs in the SW and SE regions of the area (Fig. 6). It is characterized by a set of gneissic rocks and migmatite zones, with polymetamorphic features, corresponding to the São Francisco Craton (Ribeiro et al. 2003). The contacts between the different lithotypes are transitional, between gneiss, migmatites and/or granitoids. Stretched minerals are common, with presence of concordant shearing zones, layers and/or lengthened veins, many times boudinaged. The granitoids are light gray to whitish, with medium to coarse grained, sometimes with sparse porphyroblasts of tabular feldspars, xenoliths, or restites from partial fusion. Petrographically, they vary in composition with hornblende gneisses, biotite gneisses, or amphibole gneisses, whose protolytes would be granites and tonalites, subjected to a metamorphism of the amphibole facies, with hydrothermal alteration (Tuller et al. 2009). This complex was intensely affected by basic injections, resulting in a group of basic rock dikes (Ribeiro et al. 2003). In the south portion of Sete Lagoas, epigenic and igneous metamorphic/migmatite rocks with plutonic feature are common (Fig. 2), as well as intrusions of mafic rocks, filling the fracture planes. Schistosity and transposition foliation are also observed.

Fig. 2. Gneiss-migmatite rock outcrop (left, UTM: 570178/7843865), and mesoscopic migmatite feature (right, UTM: 570183/7843875).

4.1.2. Sete Lagoas Formation

This limestone occurs mainly in the SE region of the area. In the municipality of Sete Lagoas, it occurs in the central and western portions, and in the Santa Helena Ridge foothills (Fig. 6). The lower contact with the basement is abrupt, discordant, and tectonic, with faults. The upper contact with the Serra de Santa Helena Formation is also abrupt (Figs. 9 and 10).

The Sete Lagoas Formation is divided by two members: Pedro Leopoldo, at the base, composed of fine grained white limestones, dolomites, marlstones and pelites; and Lagoa Santa, on the top, composed of medium grained black limestones.

According to Vieira et al. (2007), there are six lithological facies, four in the Pedro Leopoldo Member and two in the Lagoa Santa Member: Facies 1, characterized by light gray to beige calcilutite, with intercalations of yellowish pelite and truncated wave-ripple stratification, and tidal plain sedimentation environment, with possible storm influence; Facies 2, with aragonite crystals, constituting tabular beds and/or layers of sea sedimentation in deep waters; Facies 3, constituted by dolomite rocks, which are disposed in overlaid benches with metric to sub-metric thickness; Facies 4, beige to light gray calcilutites, plane-parallel stratification, with rithmite terrigenous and carbonate sedimentation, suggesting calm to slightly agitated waters sedimentation; Facies 5, characterized by black calcarenites and calcisiltites, plane-parallel lamination, wave truncation, medium sized crossed stratifications; and Facies 6, represented by well preserved stromatolites, from a tidal flat environment.

In relation to the lithological facies mentioned above, 3 of the 4 facies in the Pedro Leopoldo Member were confirmed:

1) Facies 1: located in the Canaã quarry (near the Federal Road Police post, BR-040). It has a decametric thickness of approximately 40 meters, represented by micritic limestone with medium to dark gray recrystallized sparite grains. The occurrence of meter-scale recumbent bends is common, with recrystallization and intergrowth of calcite minerals parallel to the bedding, especially in joints;

2) Facies 2: located in the Ilcon quarry (South-East of the municipality of Sete Lagoas). It is characterized by regular and homogeneous intercalation of micritic stratums, with thicknesses of 15 -

20 cm, and an intercalation of marlstone levels with brown-pink color, with terrigenous grain sizes. Occurrence of euhedral millimetric pyrite grains is also observed, with well developed cubic form;

3) Facies 3: located in the Sambra, Paraíso, Capão do Meio quarries, and in the Capão do Inferno farm. Described as micritic rock, with occurrence of chlorite placoid minerals, and well-developed bedding planes. The presence of pseudomorph aragonite arborescentes, with reddish color, recovered with cream colored micrite are observed.

This Member presents important dissolution developed either in bedding planes (most frequent) and in sub-vertical fractures (less common), which are filled with terrigenous material (Fig. 3).

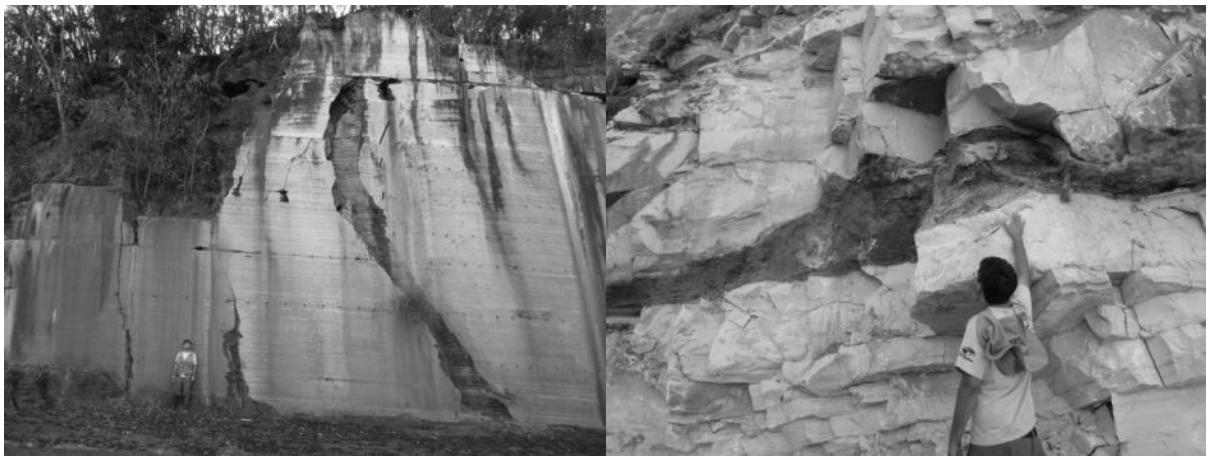

Fig. 3. Subvertical fractures (left, UTM: 565445/7851910) and bedding plane dissolution, most frequently observed, filling with terrigenous sediments (right, UTM: 563101/7853620).

In relation to the lithological facies seen in the Lagoa Santa Member:

1) Facies 5: rock with variable character, between gray micro-sparites and calcarenites, plane-parallel laminate;

2) Facies 6: occurrence of stromatolite layers, type *gyminosolens* (Marchese 1974) (Fig. 4).

This Member presents important dissolution resulting in caves and grottoes (Fig. 4).

Microscopically, the limestones from Pedro Leopoldo Member are composed of 85% micrite, 8% sparite, and 7% quartz, classified as micrite (Folk 1959) or mudstone (Dunham 1962). The limestones from Lagoa Santa Member are 55 % sparite, 30 % ooids, and 15 % micrite, classified as an oobiosparite (Folk 1959) or grainstone (Dunham 1962).

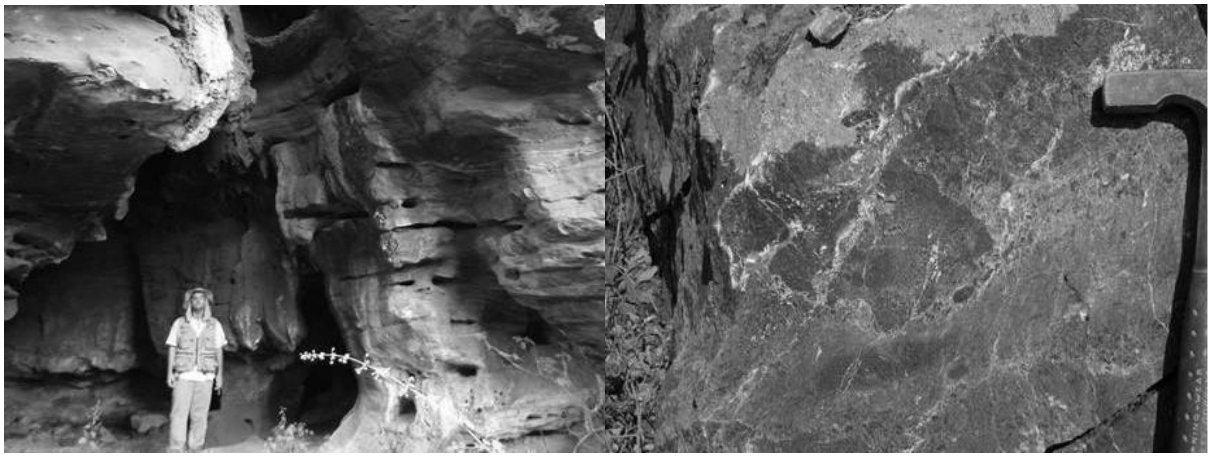

Fig. 4. Caves or grottoes in the Lagoa Santa Member (left; UTM: 571617/7850185), characterized by calcarenites rich in ooids (biosparites/grainstone, right, UTM: 571750/7847050).

4.1.3. Serra de Santa Helena Formation

This fine grained clastic formation occurs in the N, NE, NW regions (Fig. 6). It overlays the Sete Lagoas Formation with abrupt, tectonic, or occasionally, gradational contacts. The basement contacts are abrupt and discordant due to thrust faults apparent on the basin's border. The overlaying Lagoa do Jacaré and Serra da Saudade formations are characterized by transitional contacts and can be locally abrupt (Tuller et al. 2009) (Figs. 9 and 10). This formation presents schistosity type foliation, discordant and/or concordant with the bedding. This whole sequence is cut by abundant bended quartz-feldspar veins, usually filling fractures or relief zones, generated during extensional events (Tuller et al. 2009).

In Sete Lagoas, it was possible to see intercalated levels of slate rocks with well-developed cleavage planes in thin layers, presenting gray-greenish sericite. Locally, less developed cubic grains of pyrite may occur. At the base, slate, siltstone, and argillite are found, very friable. Vertical fractures filled with quartz veins with well-developed hexagonal forms (Fig. 5) and, locally, pegmatite veins, rich in feldspar and calcitite grains were also observed.

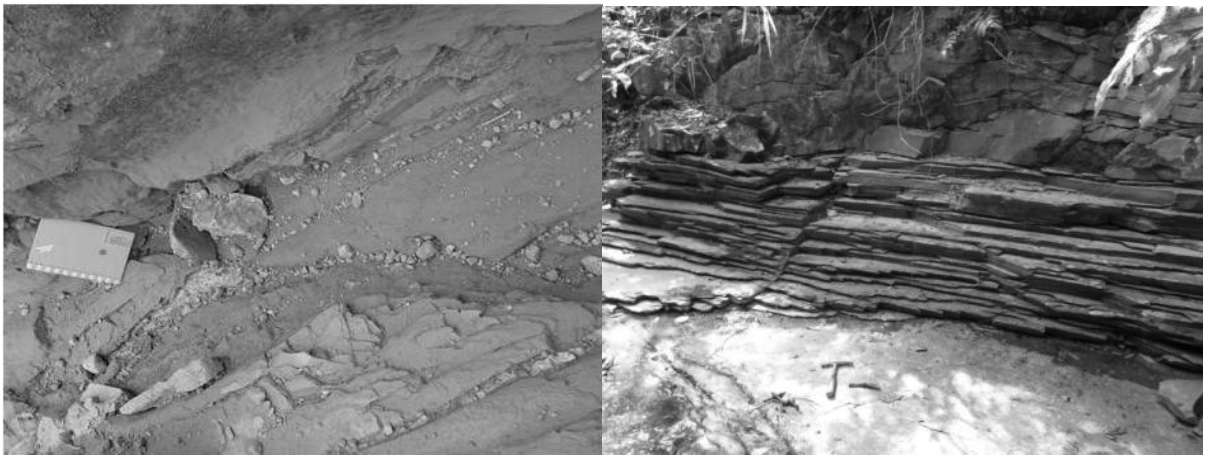

Fig. 4. Quartz veins in subvertical fracture systems in phyllites layers (top of the Santa Helena Ridge - left, UTM: 577708/7852972) and slate with a well-developed *rock cleavage* coincident to the bedding planes (right, UTM: 576695/7852000).

4.1.4. Cenozoic Surface Coverage

This unit (Fig. 6) is divided into (1) detritus coverage, (2) alluvial terraces, and (3) alluviums. The detritus coverage is composed by unconsolidated sediments with predominant red color, arenaceous-argillous with levels of gravel, which occur indistinctly on all units, but mainly on the rocks from the Serra de Santa Helena Formation. The alluvial terraces occur along the larger streams and rivers in the area, such as the Velhas River and its effluents. They are up to 5 m thick and mainly consist of argillo-arenaceous semi-consolidated sediments, with whitish to yellowish and reddish color. Finally, the alluviums occur along the meanders of the big watercourses. They are composed of fine to coarse grained sediments, with discontinuous levels of quartz pebbles, in general rounded and not well sorted, and siltstone and sandstone placoids.

In Sete Lagoas, the pedogenic features observed were: (1) nitosoil: argillo-arenaceous grains, brown-reddish color and “block” form. Its breaking plane presents a feature known as “cerosity”, a result from the concentration of argillous grains; (2) detritus-laterite: rich in mature quartz fragments and pebbles, cemented by a white-yellowish siltic-argillous matrix; (3) agrisol: well developed horizons,

with well selected clay grains (at the base), grading for arenaceous grains, also with well selected grains on the top; (4) latosoil: fine to coarse grains, with well cemented grains by the occurrence of aggregated oxides and clay, in addition to having red-yellowish color; (5) neosoil: low diagenetic degree, argillous matrix supporting the grains varying among sand, pebble and boulder; and (6) alluvial soil: constituted of alluvial argillo-arenaceous grains, carried by a fluvial body, and it may vary to argillo-silty.

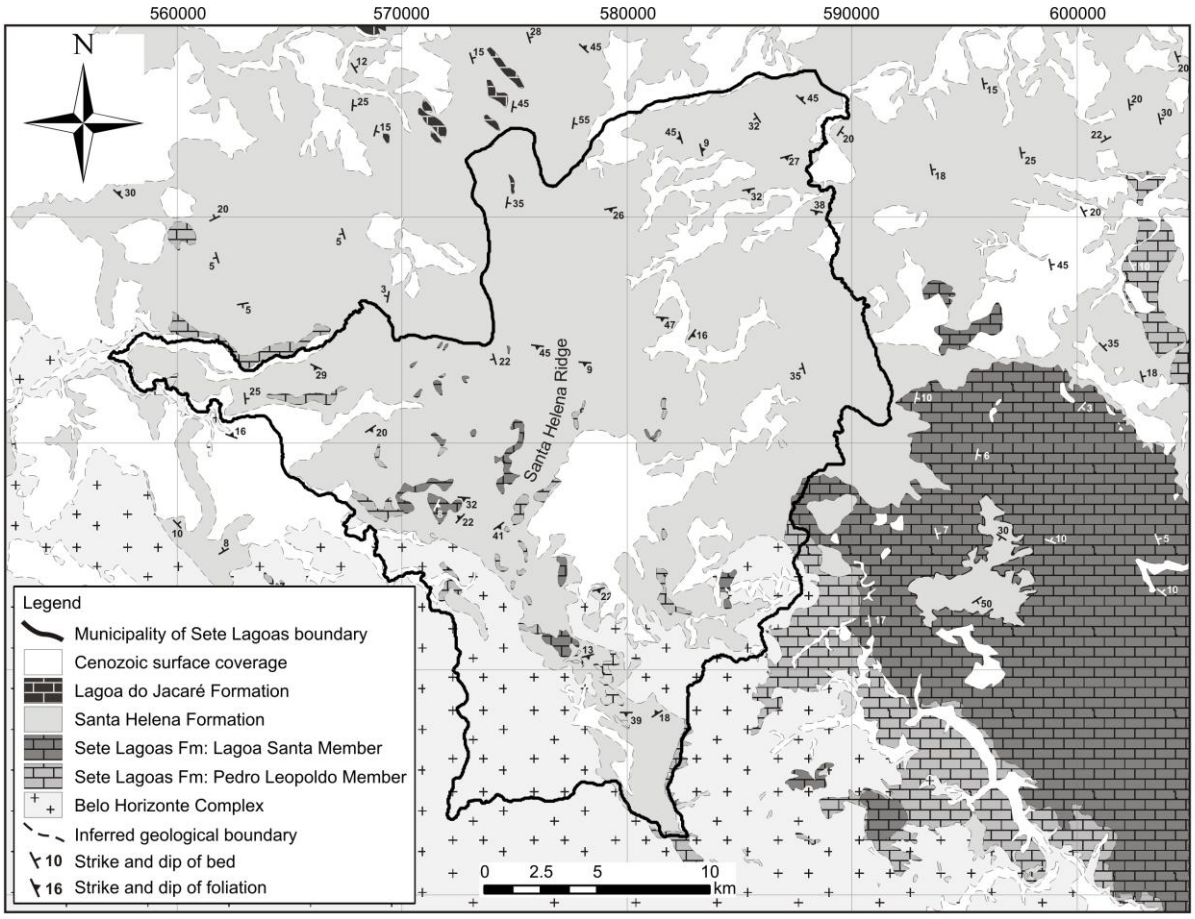

Fig. 6. Geologic map of the municipality of Sete Lagoas and the surroundings. The Belo Horizonte Complex (gneiss associated to granitoids) occurs in the SSW area. The Sete Lagoas Formation, divided by two members (Pedro Leopoldo: fine white limestones; and Lagoa Santa: medium grained black limestones) occurs mainly in the SE, W, and in the Santa Helena ridge foothills. The Serra de Santa Helena Formation (shales, siltstones, and slate) occurs in the NW, N, and NE regions, while the unconsolidated sediments from Cenozoic surface coverage occur along the large meanders and drainages. The structural information can be seen separately in the Fig. 11.

4.2. Structural geology

Included in the intermediate structural domain with low intensity of deformation (Tuller et al. 2009), within the municipality of Sete Lagoas, no lithostructural contacts with thrust features were seen, and only abrupt deposition contacts were noted. However, from the lithologic well profiles, abrupt changes of depth to the basement were observed. In addition, similar basement level changes were observed between its outcrops and the adjacent lithologic well profiles. From these data, it is suggested that faults displaced the lower stratigraphic sequences, placing them in contact with upper

blocks, which was observed in previous studies, in the eastern most portion of the area, out of the municipality Sete Lagoas.

The upper contact between Sete Lagoas and Serra de Santa Helena formations and Belo Horizonte Complex is abrupt, with a low angle. It is preferably developed in bedding rocks, associated with slate and phyllite from the Serra de Santa Helena Formation, and to the ductile-ruptile behavior phases of the limestone from Sete Lagoas Formation, locally represented by kink bands. In the case of Sete Lagoas Formation, the contact between Pedro Leopoldo (basal) and Lagoa Santa (upper) members is also abrupt, horizontal and well defined, which was confirmed in all quarry outcrops. Sigmoidal deformations were observed specifically in the Lagoa Santa Member, suggesting a stage where the formation was deformed in a ductile regimen (Fig. 7).

The main structures observed in the municipality of Sete Lagoas were fractures, folds, bedding planes, and foliations (Fig. 8). The only observed evidence of microfaulting was seen in the Serra de Santa Helena Formation, with displacement of a few millimeters, located on the top of the Santa Helena Ridge. For the Belo Horizonte Complex, sub-vertical fracture planes are common, with NNW/SSE direction, and main attitude N347/83.

In the case of the Sete Lagoas Formation, in the Pedro Leopoldo Member, the bedding planes presented a main orientation of N180/04 (27% of the 54 measured) and fold axis with main attitude N052/00 (Fig. 8). Projecting the data from the bedding planes oriented to the North direction, between N338/05 to N028/10, a subtle dip to N was seen, with trends to the NW. About the fracture planes, the average sub-vertical attitude was N092/67. In the Lagoa Santa Member, the bedding planes are well defined, and the most observed attitude was N060/24. Concerning the fold axes, the most frequent was N360/13. The structural evidences explain the presence of outcrops in the Lagoa Santa Member in lower topography and its occurrence in the center-west of Sete Lagoas. The Serra de Santa Helena Formation presents structural features with ductile-ruptile behavior, a consequence of the regional tectonic evolution, subdivided in: (1) bedding planes with attitude of N060/03 (15% of the 185 measured), in addition to the 6 measured related to the fold axis with main attitudes of N009/13; and (2) fracturing planes with subvertical character and filled in with quartz or pegmatite veins. The main attitude was N013/77 (13% of the 64 measured), following ESE-WSW orientation (Fig. 8).

Fig. 5. Sigmoidal deformations form outcrop in Lagoa Santa Member indicating mass transport (left, UTM: 571617/7850185) and contact between the Pedro Leopoldo Member (lower) and the Lagoa Santa Member (upper) (right, UTM: 570000/7847000).

4.3. Spatial distribution of the geologic formations

The basement outcrops in the SW portion of the study area with elevations between 750 and 950 m.a.s.l. and dips in the NE direction (Figs. 9, 10, and 11). The minimum surface contact is approximately 400 m.a.s.l., located in the north near the Velhas River. The overlying sediments from the Sete Lagoas and Serra de Santa Helena formations follow the dip of the basement.

According to the geologic cross sections, it was possible to propose, indirectly, a horst and graben system controlled by faulting, which indicated different basement depths over small lateral distances (e.g. 120 m offset in 1.4 km; 140 m in 2.5 km; or 200 m in 5 km). As an example, a lithologic well profile, located approximately 800 m from where the basement outcrops, shows a depth to basement of 80 m.

The Sete Lagoas and Serra de Santa Helena formations follow this horst and graben system, presenting thinner layers on the basin border in the SW region, and higher thickness in the NE (cross sections 1 to 14). In the case of the Sete Lagoas Formation, the limestones dip and become thicker to the northeast, being covered almost totally by the Serra de Santa Helena Formation, where these limestones arise mainly in the Santa Helena Ridge foothills and in the municipalities located to the southeast, near the Velhas River.

The Serra de Santa Helena Formation is situated immediately over the Sete Lagoas Formation, normally with abrupt contact. The contacts with basement are also abrupt, indicating that their sediments were deposited in area with little relief. This formation becomes thicker to the NE and contains bedding planes, which dip to the NE, and thinner on the basin borders and near the Velhas River. These formations can reach 160 m thickness, seen in the north of Sete Lagoas (cross section 3) and in the Santa Helena Ridge (estimated values).

The thickness of the Cenozoic surface coverage is low in comparison to the other geologic formations. The best representation was seen in the central part of Sete Lagoas (urbanized area) and in the western part of this municipality, with approximate values of 40 m in thickness (cross sections 3, 9, and 10).

In the urbanized area of Sete Lagoas, for the homonym formation, an antiform was interpreted (Fig. 11), with bedding planes oriented to the North (cross section 2) and surface contact around 500 m.a.s.l. (estimated, seen in section 4) and 580 m.a.s.l. (data from a stratigraphic drill hole made by SAAE, located on North of Sete Lagoas – seen in section 3 - near 40 km in the *x*-axis). The majority of the urbanized area is included in a graben area, filled with limestones and unconsolidated sediments (cross sections 3, 10, and 11; also see Fig. 11).

In the case of the Santa Helena Ridge, located near to the central part of Sete Lagoas, it was possible to deduce an upward displacement of the basement, indicated by a horst (cross sections 3, 10, and 11). This horst might have elevated the stratigraphic sequence, where the Sete Lagoas and Serra de Santa Helena formations have more elevated altitudes than other regions. The fact that this stratigraphic sequence is cut by fractures filled quartz veins, the ridge is more resistant to erosion.

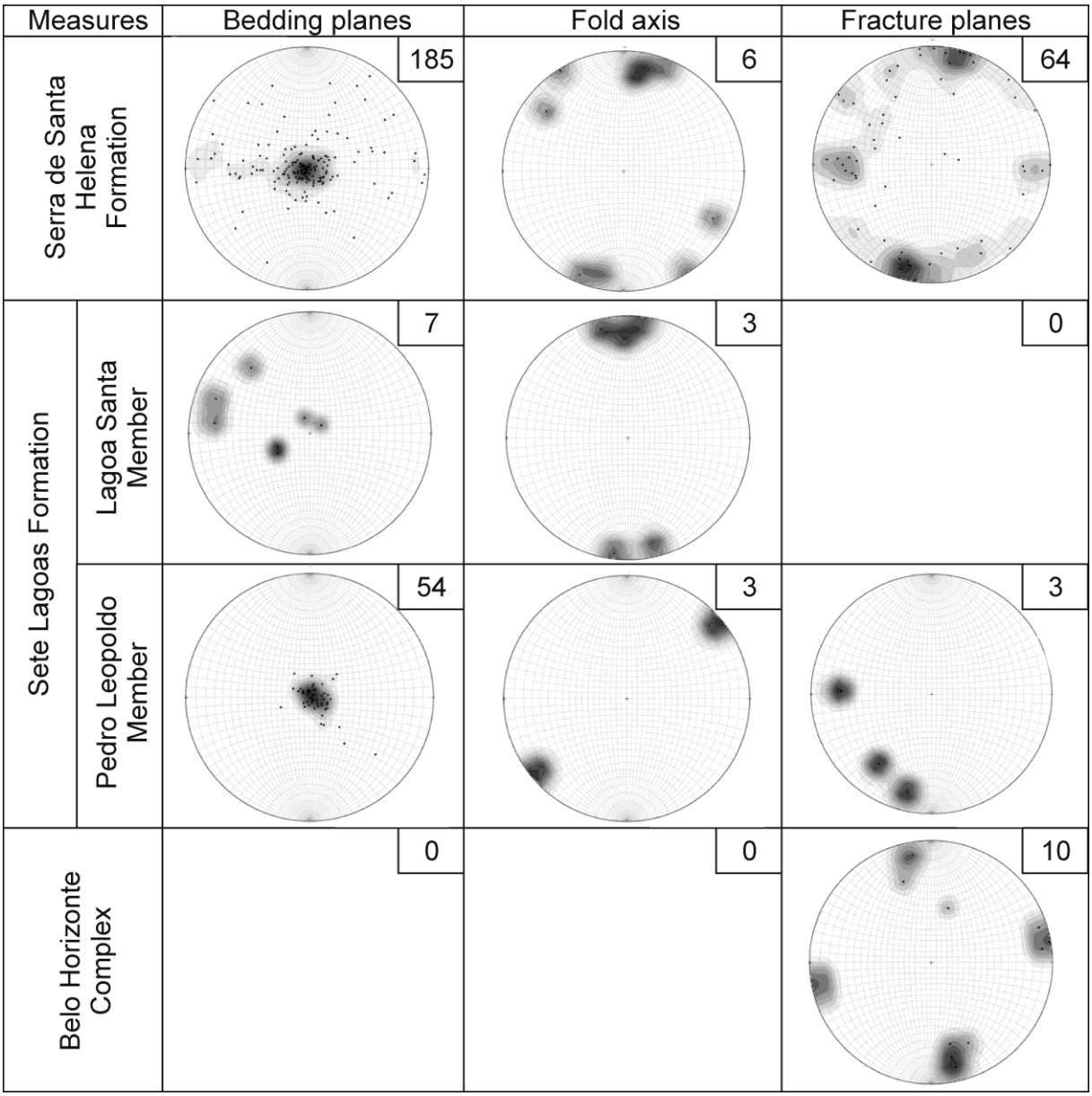

Fig. 8. Beddings, bend axes, and attitude planes measurements.

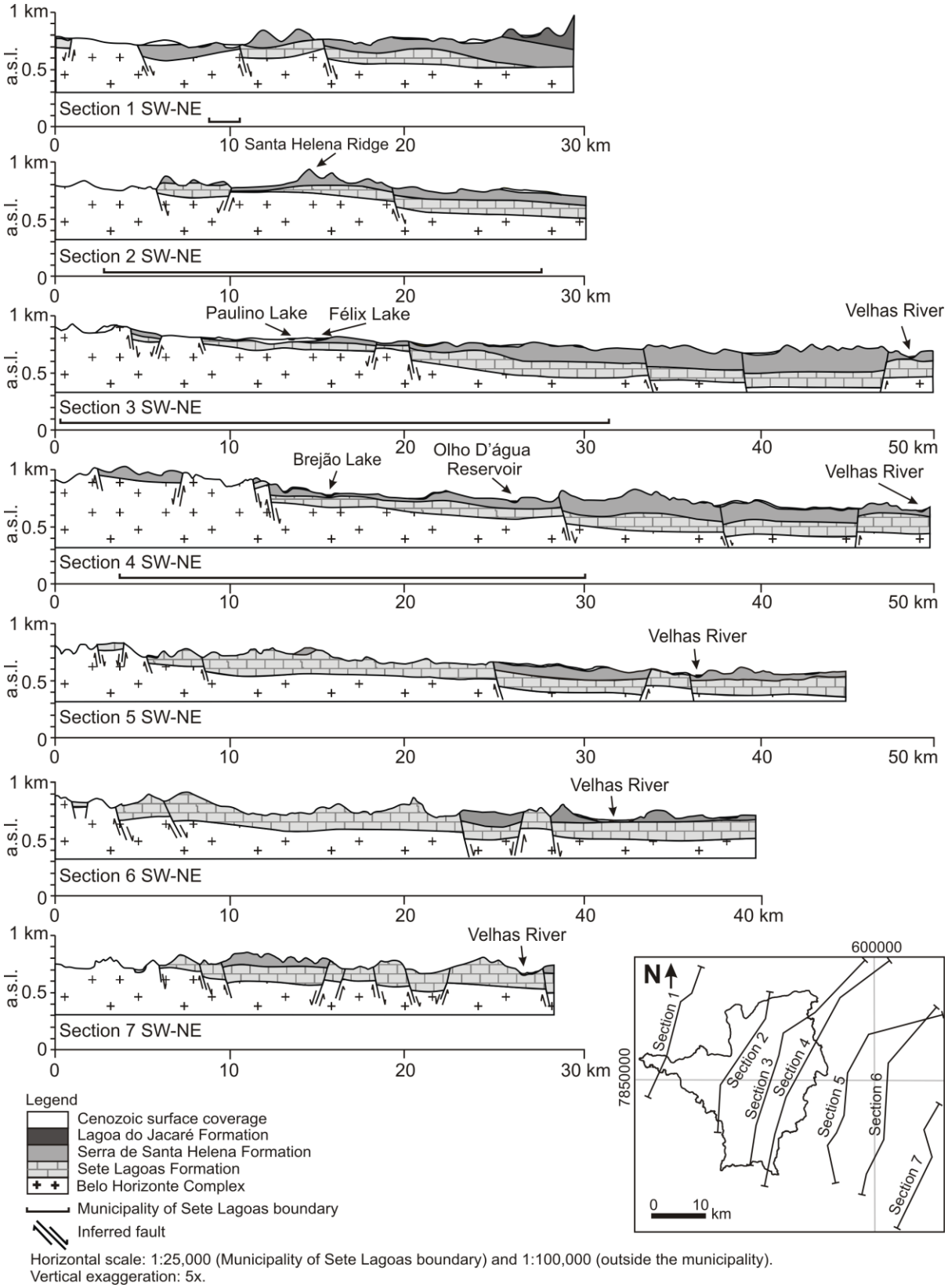

Fig. 9. Geologic cross sections SW-NE. The geological framework presents a typical geometry of basement border, which the Belo Horizonte Complex outcrops in the SW portion and dips in the NE direction.

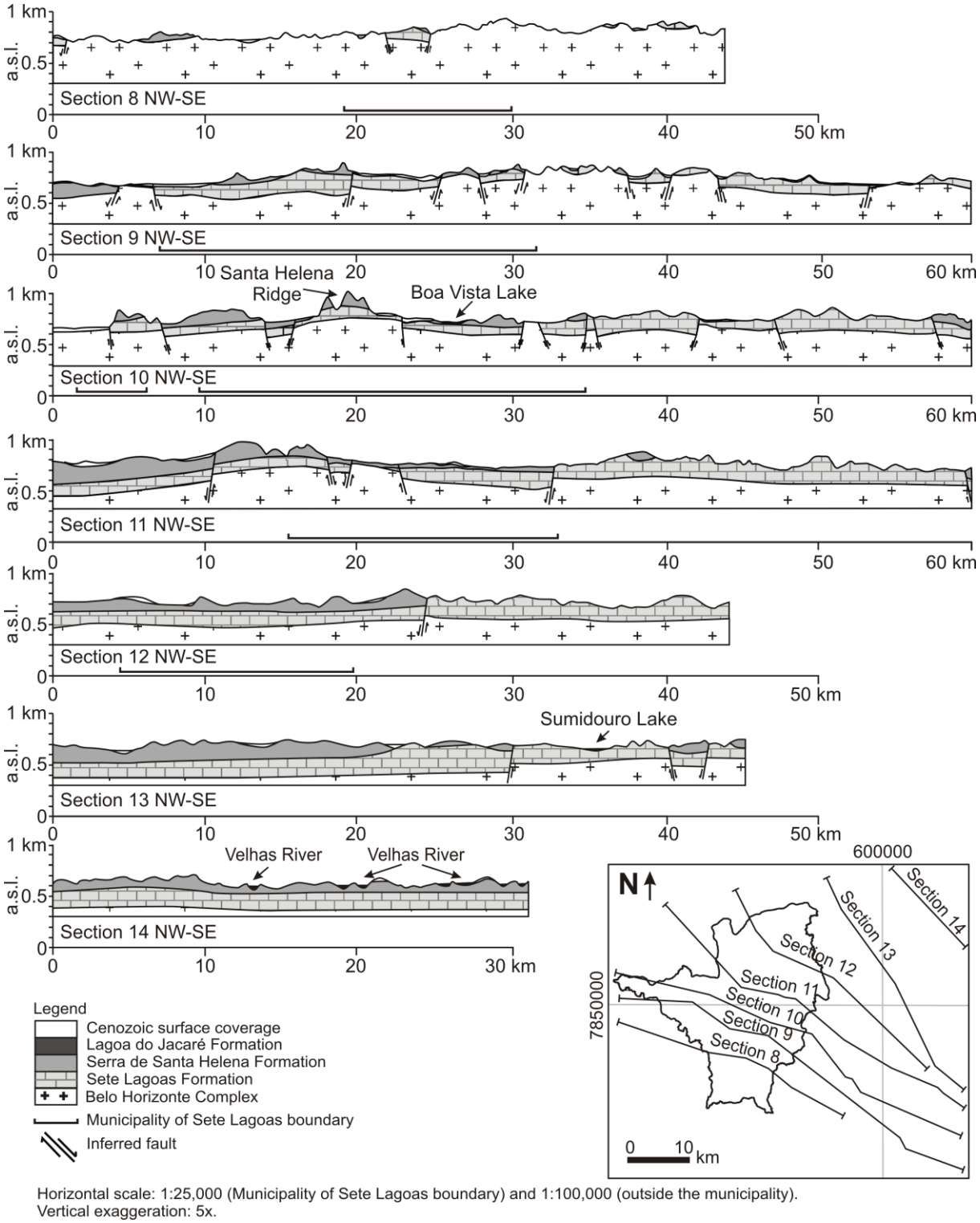

Fig. 10. Geologic cross sections NW-SE. The Sete Lagoas and Serra de Santa Helena formations follow the horst and graben system, presenting thinner layers on the basement border, in the SW region, and higher thickness in the NE direction.

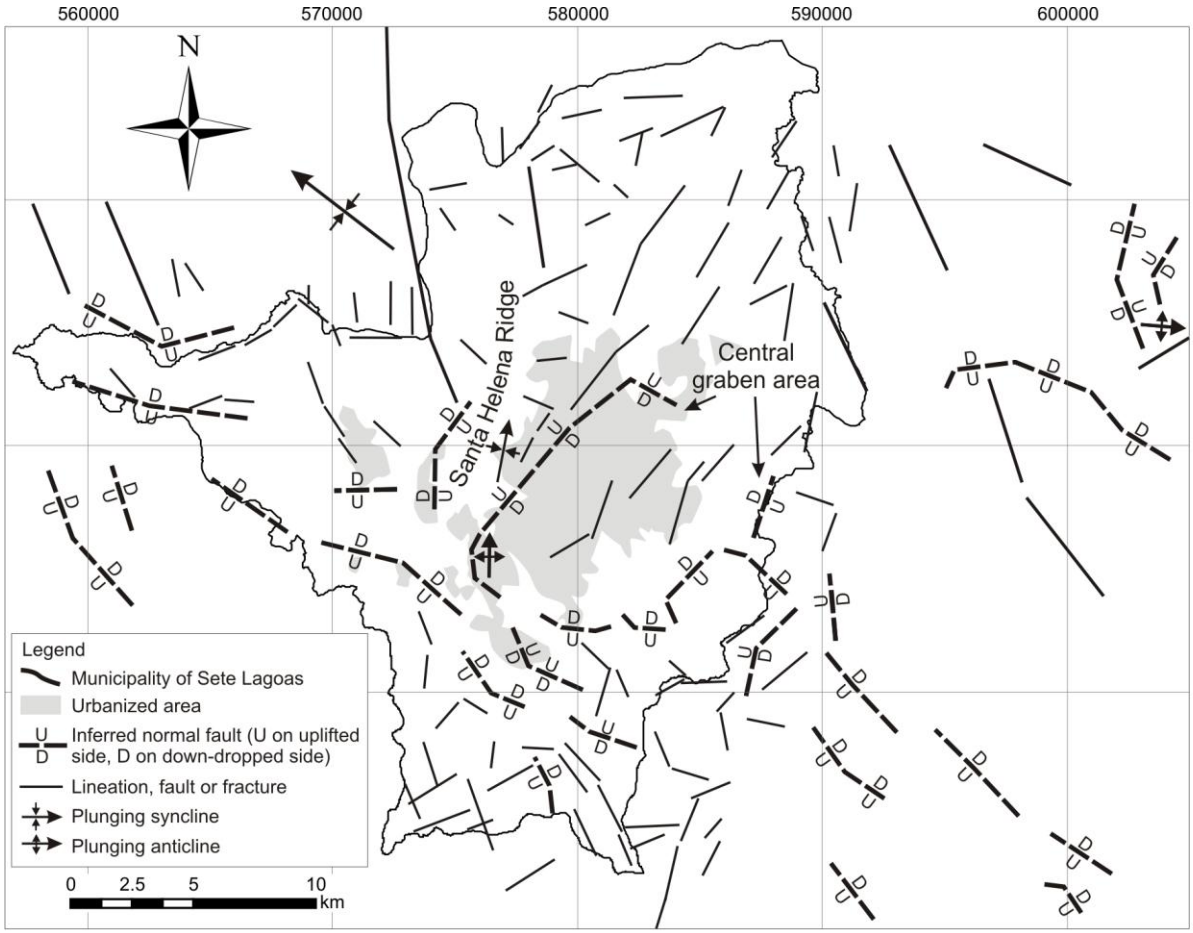

Fig. 11. Schematic map showing structural features. A graben area inferred by lithologic well profiles is located in the central portion of the municipality of Sete Lagoas, where the urbanized area is majority located within this graben area. Inferred normal faults also found using lithologic well profiles are located in the basement border, in South and Southwest of the map.

4.4. Geologic conceptual model

A geologic conceptual model of the municipality of Sete Lagoas and the surroundings (Fig. 12) and a schematic synthesis model about the geological evolution were proposed (Fig. 13).

From the extensional events between 900 and 600 Ma. (Condie 2002) in the São Francisco Craton, the São Francisco Basin was originated, depositing silicate-carbonate sediments of the Bambuí Group from the Neoproterozoic age, where the study area is included, directly on the border of this basin. These Neoproterozoic sediments were deposited on a stable epicontinental shelf with a low gradient, which had three regressive sedimentary mega-cycles (with argillo-carbonate origin), giving origin to the Sete Lagoas and Serra de Santa Helena formations, respectively.

Around 740±22 Ma. (Babinski et al 2007), 630 Ma. (Caxito et al. 2012), or 540 Ma. (Warren et al. 2014), the Sete Lagoas Formation, by carbonate depositional systems with intermediary internal and external ramps (Lima 1997), gave origin to the limestones of the Pedro Leopoldo Member, at the base, characterized by fine grained white limestones (in some cases, with dolomite and/or pelite level), and the Lagoa Santa Member, on the top, represented by medium grained black limestones.

Later, over the rocks from the Sete Lagoas Formation, a transgressive cycle (Ribeiro et al. 2003) characterized by sub-coastal sea and relatively deep and weak flow enabled the deposition of

pelite materials with plane-parallel stratums, crossed stratifications, and wave marks giving origin to the Serra de Santa Helena Formation. This formation might have achieved minimum thickness values as low as 160 m (confirmed in lithologic well profiles). At the end of this cycle, the deposition of silicate-carbonate sediments started giving origin to the Lagoa do Jacaré Formation, found in the far NNW part of the study area.

Due to the deformation of the Espinhaço Supergroup in the Brazilian age (~600 Ma.) (Trompette et al. 1993) and the proximity of this region (structural domain 1 - higher intensity of deformation) to the study area (structural domain 2 – intermediate deformation magnitude), the rocks from the Bambuí Group were intensely faulted and bended to the East, close to the stress coming from this deformation (Alkmim and Martins Neto 2001). In the west of the area, the structural features were less expressive and the sedimentary features were more preserved. These factors resulted in a horst and graben system, controlled by faulting, displacing the stratigraphic sequences, which enabled lithologic sequences of different ages side by side. Thus, the lower limestones of the Sete Lagoas Formation reached the surface in some areas.

Within the municipality of Sete Lagoas, it was observed that the limestones from the Sete Lagoas Formation, especially the Pedro Leopoldo Member, demonstrate important dissolution macro-features developed either in bedding planes (most frequent) and in subvertical fractures (less common). Some of these dissolution zones were filled with terrigenous material, suggesting a past meteoric water flow. In the case of the Lagoa Santa Member, the main dissolution features found were dry caves and grottoes, suggesting groundwater paleoconduits (e.g. Rei do Mato Cave). These evidences could suggest recent geomorphologic processes, such as a past meteoric water flow, or could have started at the time when groundwater flow paths started to develop, even if these limestones had not yet been exposed. As the timing of these processes is not precisely known, it is suggested a specific study to be conducted to better understand more about the origin of these processes.

Finally, the Cenozoic unconsolidated sediments deposited in the central portion of Sete Lagoas were a result of weathering and erosion of Santa Helena Ridge. These unconsolidated sediments also were deposited along the beds of the Velhas River and in areas of low relief.

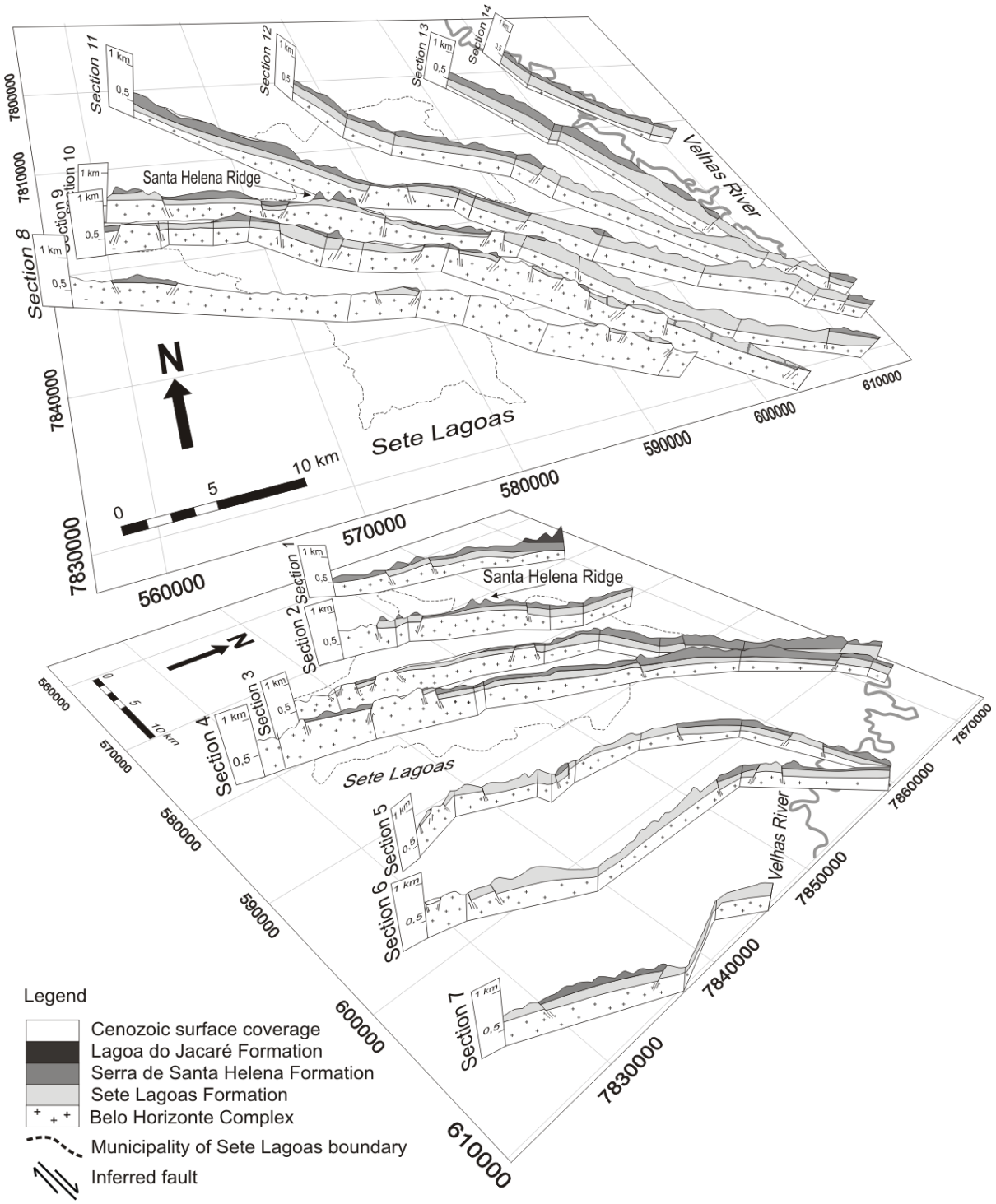

Fig. 12. Stratigraphic diagram blocks of the study area.

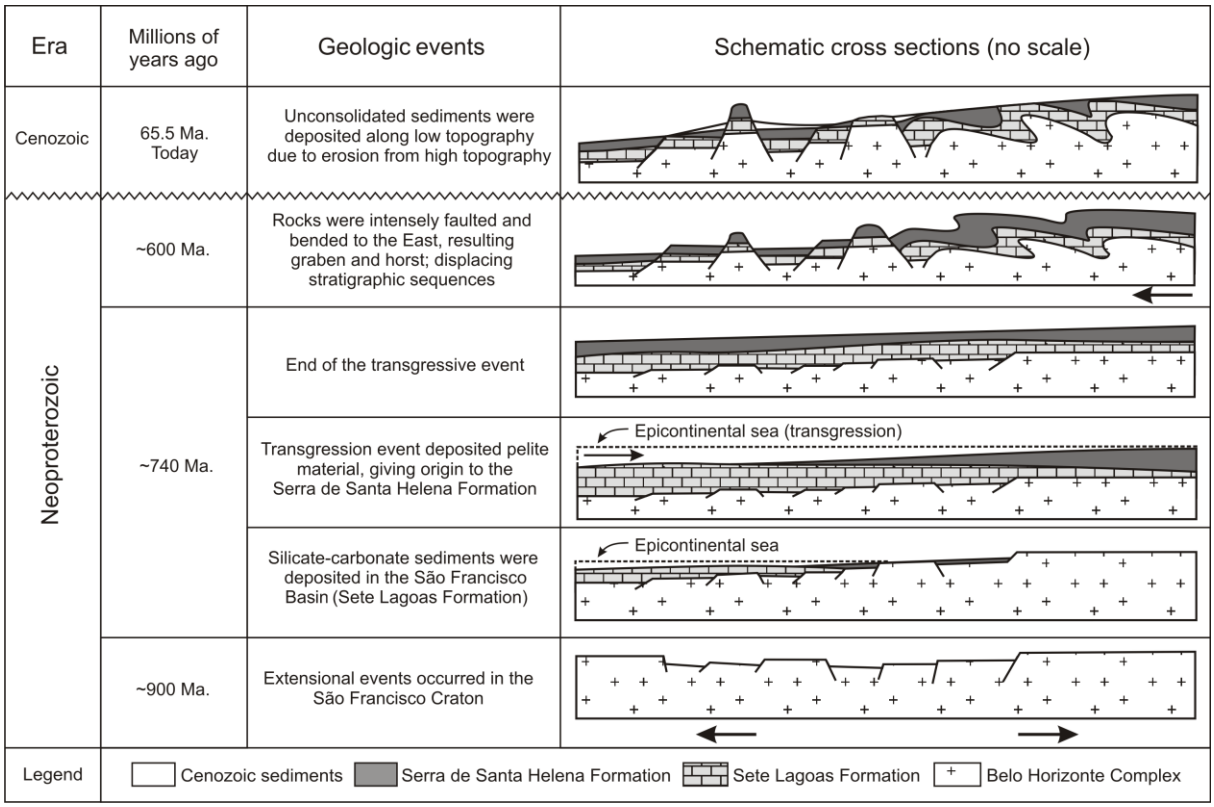

Fig. 13. Schematic synthesis about the geologic evolution of the study area, including schematic geologic cross sections and its respectively most important events.

5. Conclusion

The uses of data from geologic mapping combined with a good database of lithologic well profiles become an efficient set of tool to facilitate the spatial visualization and determine the geometry of the geologic formations in the subsurface and its side continuities. This fact also helped to identify possible blocks displaced indirectly by faults.

The study area is along basement border, a result of extensional events in the São Francisco Craton, where silicate-carbonate sediments from the Neoproterozoic age were emplaced giving origin to the Bambuí Group.

Due to the relative proximity of this area with the Serra do Espinhaço (situated to the east and which undergone intense deformation), the Bambuí Group presents a horst and graben system, controlled by faulting, displacing the stratigraphic sequences, which enables formations with different ages side by side.

In relation to the thickness of sedimentary layers, the NE portion of the area is estimated to approximately 400 m, near the Velhas River.

According to lithological well profiles, the limestones from the Sete Lagoas Formation present horizontal continuity, from the basement border to the Velhas River.

The Santa Helena Ridge was interpreted as a horst, which elevated the stratigraphic sequence, causing the Sete Lagoas and Serra de Santa Helena formations to have higher altitudes than in other regions. Considering that fracture filled quartz veins cut this stratigraphic sequence, the ridge became more resistant to erosion.

The urbanized area located in the municipality of Sete Lagoas is in a graben, where limestones from Sete Lagoas Formation and unconsolidated sediments from Cenozoic surface coverage having on average 90 m and 40 m in thickness, respectively.

Acknowledgements

To the companies Servmar Ambiental & Engenharia Ltda. and SAAE, and to FAPESP (process 2012/12846-9), for the financial support and the information release. A special thanks to Dr. Geane Carolina Cavalcante, for the contributions in the chapter about the structural geology, to Dr. Bernardo Tavares Freitas, for the contributions in the fieldwork, and to geologist Kyle Spears for the grammar revision and geologic advice.

References

Alkmim F, Martins-Neto M (2001) A bacia intracratônica do São Francisco: arcabouço estrutural e cenários evolutivos. In: Pinto, C.P.; Martins-Neto, M.A. (eds.). Bacia do São Francisco: geologia e recursos minerais. Belo Horizonte: Sociedade Brasileira de Geologia-MG, CBMM, COMIG, GEOSOL. p. 9-30.

Almeida F (1977) O Cráton do São Francisco. Revista Brasileira de Geociências. 7: 349-364.

Babinski M, Vieira C, Trindade R (2007) Direct dating of the Sete Lagoas cap carbonate (Bambuí Group, Brazil) and implications for the Neoproterozoic glacial events, Terra Nova 19 (6), 401-406.

Branco JJr, Costa M (1961) Roteiro da excursão Belo Horizonte – Brasília. In: Congresso Brasileiro de Geologia, 14, Brasília. Instituto de Pesquisas Radioativas, UFMG, Publicação 15, Belo Horizonte, 25 p.

Caxito F, Halverson G, Uhlein A, Stevenson R, Dias T, Uhlein G (2012) Marinoan glaciation in east central Brazil. Precambrian Research 200–203 (2012) 38–58.

Condie K (2002) The supercontinent cycle: are there two patterns of ciclicity? Journal of African Earth Sciences, 35: 179-183.

Dardenne MA (1978) Síntese sobre a estratigrafia do Grupo Bambuí no Brasil Central. In: Congresso Brasileiro de Geologia, 30. Recife. Anais Recife: Sociedade Brasileira de Geologia. v.2, p. 597-610.

Danderfer Filho A (1991) Cartografia geológica dos municípios Sete Lagoas, Funilândia, Lagoa Santa, Pedro Leopoldo, Vespasiano, Capim Branco, Matozinhos e Prudente de Morais – Capítulo 6 - Geologia Estrutural. Projeto Vida. MMe – CPRM.

Dunham RJ (1962) Classification of carbonate rocks according to depositional texture. In: W.E.HAM (ed): Classification of carbonate rocks. Am. Assoc. Petrol. Geol., Mem.1, Tulsa, Oklahoma, p. 108-121.

Embry A, Klovan J (1971) A Late Devonian reef tract on Northeastern Banks Island, NWT: Canadian Petroleum Geology Bulletin, v. 19, p. 730-781.

Folk RL (1959) Practical petrographic classification of limestones: American Association of Petroleum, Geologists Bulletin, v. 43, p. 1-38.

Folk RL (1980) Petrology of Sedimentary Rocks. Hemphill Publishing, Austin, TX, 184p.

Grossi-Sad J, Chiodi-Filho C, Chiodi D (1998) Panorama do setor de ardósias Estado de Minas Gerais, Brasil. Belo Horizonte: COMIG. CD- ROM.

Magalhães PM (1989) Análise estrutural qualitativa das rochas do Grupo Bambuí, na porção sudoeste da Bacia do São Francisco. Dissertação (Mestrado) – escola de Minas. Universidade Federal de Ouro Preto, Ouro Preto. 100 p.

Marchese AG (1974) Litoestratigráfia Y Petrología del Grupo Bambuí en los estados de Minas Gerais y Goiás, Brasil. Revista Brasileira Geociências, 3: 172-190.

Misi A, Kaufman Aj, Veizer J, Powis K, Azmy K, Boggianni P, Gaucher C, Teixeira J, Sanches A, Iyer S (2007) Chemostratigraphic Correlation of Neoproterozoic Successions in South America. Chem. Geol. 237: 161-185.

Nobre-Lopes J (1995) Faciologia e gênese dos carbonatos do Grupo Bambuí na região de Arcos, Estado de Minas Gerais. Dissertação (Mestrado em Geologia Sedimentar) - Instituto de Geociências. Universidade de São Paulo, SP. 166 p.

Oliveira M (1967) Contribuição à geologia da parte Sul da Bacia do São Francisco e áreas adjacentes. In: Coletânea de Relatórios de Exploração, 1. RJ: Petrobrás, n.3, p. 71-105.

Pedrosa-Soares A, Dardenne M, Hasui Y, Castro F, Carvalho M, Reis AC (1994) Mapa Geológico do estado de Minas Gerais e Nota Explicativa, Secretaria de Recursos Minerais, Hídricos e Energéticos, Companhia Mineradora de Minas Gerais (COMIG), mapas e texto, 97 p.

Pessoa P (1996) Caracterização Hidrogeológica da Região de Sete Lagoas - MG: Potencialidades e Riscos. Dissertação de Mestrado. Departamento de Geociências, Universidade de São Paulo. São Paulo.

Pessoa P (2005) Hidrogeologia dos aquíferos cársticos cobertos de Lagoa Santa, MG. Tese de Doutorado. Programa de pós-graduação em Saneamento, Meio Ambiente e Recursos Hídricos. Universidade Federal de Minas Gerais - UFMG. MG.

Ribeiro J, Tuller M, Danderfer Filho A (2003) Mapeamento geológico da região de Sete lagoas, Pedro Leopoldo, Matozinhos, Lagoa Santa, Vespasiano, Capim Branco, Prudente de Morais, Confins e Funilândia, Minas Gerais (1:50.000) – In: Projeto Vida. Belo Horizonte: CPRM. (CD-ROM).

Schobbenhaus C (1984) Geologia do Brasil. Departamento Nacional de Produção Mineral. p. 275, 276, 277.

Schöll W, Fogaça ACC (1979) Estratigrafia da Serra do espinhaço na região de Diamantina. In: Simpósio de Geologia de Minas Gerais, 1. Diamantina. Atas. Belo Horizonte: Sociedade Brasileira de Geologia/MG, 1980. p. 55-73.

Trompette R, Uhlein A, Selva ME, Karmann I (1993) O Cráton brasiliano do São Francisco - Uma revisão. Revista Brasileira de Geociências, v. 22, n. 4, p. 481-486.

Tuller M, Ribeiro J, Signorelli N, Féboli Wl, Pinho J (2009) Projeto Sete Lagoas - Abaeté, Estado de Minas Gerais (CPRM) Orgs.- Belo Horizonte: CPRM-BH. 160p. 06 mapas geológicos, escala 1:100.000 (Série Programa Geologia do Brasil) versão impressa e em meio digital, textos e mapas.

Uhlein A, Lima O, Fantinel L M, Baptista M (2004) Excursão 2. Estratigrafia e evolução geológica do Grupo Bambuí, Minas Gerais. In: Congresso Brasileiro de Geologia, 42, Araxá - MG.

Vieira L, Trindade R, Nogueira A, Ader M (2007) Identification of a Sturtian cap carbonate in the neoproterozoic Sete Lagoas carbonate platform, Bambuí Group, Brazil. Comptes Rendus, Géosciences, v.339, p. 240-258.

Warren L, Quaglio F, Riccomini C, Simões M, Poiré D, Strikis N, Anelli L, Strikis P (2014) The puzzle assembled: Ediacaran guide fossil Cloudina reveals an old proto-Gondwana seaway. Geology 42, 391–394.

Winter JD (2001) An Introduction to Igneous and Metamorphic Petrology. Prentice Hall Inc., Upper Saddle River, 697.

CHAPTER 6: EVALUATING KARST GEOTECHNICAL RISK IN THE URBANIZED AREA OF SETE LAGOAS, MINAS GERAIS, BRAZIL

Hydrogeology Journal
DOI 10.1007/s10040-015-1266-x

Evaluating karst geotechnical risk in the urbanized area of Sete Lagoas, Minas Gerais, Brazil

Paulo Galvão · Todd Halihan · Ricardo Hirata

Abstract An increase in groundwater consumption in the municipality of Sete Lagoas (Minas Gerais, Brazil) has induced subsidence and collapse in the last three decades. The area is associated with natural karst conditions. The primary objective of this research was to evaluate and identify the potential subsidence or collapse risk zones. Aerial photographs, lithologic well profiles, optical well logs, and geologic mapping were utilized to categorize risk factors influencing karst subsidence and collapse, which were then applied to an index system. The study showed that the majority of the urbanized area overlies mantled limestone from the Sete Lagoas Formation covered with unconsolidated sediments, contained within a graben, resulting in barrier boundaries for groundwater flow. This structure, together with natural karst processes, explains the location of solutionally enlarged bedding-plane conduits and high hydraulic conductivity in the limestone. Five risks zones in the municipality were identified (negligible, low, moderate, considerable, and high risks) related to geologic and hydrologic risk factors. The urbanized area is located largely in the high risk zone where the majority of the collapse features are located. Additional intensive groundwater extraction in that area will likely generate additional events.

Keywords Carbonate rocks · Karst · Subsidence · Collapse · Brazil

Received: 20 August 2014 / Accepted: 23 April 2015

Electronic supplementary material The online version of this article (doi:10.1007/s10040-015-1266-x) contains supplementary material, which is available to authorized users.

P. Galvão (✉) · R. Hirata
Institute of Geosciences,
University of São Paulo, Rua do Lago 562, São Paulo, SP 05508-080, Brazil
e-mail: hidropaulo@gmail.com
Tel.: 405.334.8879

T. Halihan
School of Geology,
Oklahoma State University, 105 Noble Research Center, Stillwater, OK 74078, USA

Published online: 19 May 2015

Introduction

Karst areas cover about 20 % of the Earth's land surface and are developed especially in carbonate rocks such as limestone and dolomite (Ford and Williams 2007). Knowledge of the properties of these karst rocks is increasingly important for effective management of groundwater reserves and for an understanding of the properties that influence a range of geotechnical issues. In many settings, the properties of a karst system are difficult to obtain due to the system's discrete structure and evolving history. The primary issue is that the groundwater storage and flow are conditioned by fracture patterns, conduit geometry and/or other discontinuities in the rocks that are often difficult to quantify in the subsurface.

Karst regions can have geotechnical problems such as subsidence and collapse. These can occur naturally (by dissolution of rock or through the failure of a bedrock roof overlying a cave) or can be induced or accelerated by human activities, which are commonly characterized by catastrophic collapse (Newton 1976; LaMoreaux and Newton 1986; LaMoreaux 1997). Both of these types of geotechnical issues generally develop over periods of geological time in carbonate formations, not within a human lifetime. Therefore, it is important to emphasize that the main difference between natural and anthropogenic situations is the speed at which the collapse processes begin, and this is accelerated in an anthropogenic situation (Albrecht 1996).

The induced geotechnical problems in these settings commonly form because of groundwater withdrawal, construction activities, or a combination of both (Newton 1987; Bell 1997). In the case of groundwater withdrawal in an urban aquifer, periods of drought are the most dangerous. These periods correspond with increased demand for groundwater, which often result in the formation of enlarged cones of depression (Oliveira 1997). Within these cones of depression, wells, springs and streams can go dry or have their flows significantly reduced, with the overall direction of groundwater flow being changed and geotechnical problems being induced (Hobbs and Gunn 1998). If human activities had not occurred, the geotechnical problems would not have occurred or, under natural conditions, would have occurred as subsidence, not rapid collapse. As an example, an estimated 4,000 sinkholes, areas of

subsidence or other related features were recorded in the state of Alabama (USA) between the years 1900 and 1976; only 50 (just over 1 %) of these were natural collapses (Newton 1976). In Missouri (USA), 97 catastrophic surface failures have been recorded for the period 1930s–1976, of which 46 were attributed to human activity (Williams and Vineyard 1976).

Collapsed sinkholes have been reported since the beginning of the 20th century in the Tournaisis area, in southern Belgium. Intensive pumping for domestic and industrial water supply, combined with the dewatering due to deep limestone quarries, resulted in the lowering of groundwater levels. This triggered the reactivation of paleokarstic systems resulting in sinkhole collapse (Kaufmann and Quinif 1999). Several other cities worldwide undergo subsidence and/or collapse attributed to groundwater withdrawal, construction activities, or a combination of both: Kanus, China (Fuller 1922); Kamloops, Canada (Buckham and Cockfield 1950); Memphis, Tennessee, USA (Terzaghi 1931); and West Driefontein, South Africa (Douglas 2013). Other regions that have possible collapse problems in urban areas can be seen in southern China, Southeast Asia, northern Australia, the Middle East, Central America, Caribbean, and South America (Day 2002).

In Brazil, the municipalities of Cajamar and Mairinque (São Paulo), Almirante Tamandaré and Colombo (Paraná), Teresina (Piaui), Lapão (Bahia), Lagoa Santa and Sete Lagoas (Minas Gerais), among others, are good examples of karst systems with urban development and corresponding subsidence and collapse problems. Specifically, in the case of Sete Lagoas, where this study was conducted, the first significant collapse was recorded in 1988 (Silva 1988), located in the central part of the urbanized area, which generated a 22-m diameter sinkhole and associated property damage. Other geotechnical problems of smaller magnitude are still being recorded in this municipality, illustrating an ongoing phenomenon.

Various methodologies are used to understand the mechanisms for collapse such as geologic methods evaluating geomorphic processes and geological structure via mapping or remote sensing (Newton 1976; Williams and Vineyard 1976); or hydrogeologic approaches analyzing properties from core samples, aquifer permeability, or transient evaluations of the potentiometric surface (Silva 1988; Kaufmann and Quinif 1999). Theoretical approaches have also been utilized such as numerical models to predict subsidence or collapse (Adamek and Jeran 1985; Dudley et al. 2009).

Risk assessment is applied to determine risks at all levels and locations (Karamouz et al. 2011). It includes a wide variety of disciplines and the perspectives of engineers, hydrogeologists, environmental scientists, chemists, geologists, geographers, and public administrators. One of the most common approaches to estimate high-risk and low-risk situations involves analyzing the different risk factors and their geographic distribution and assigning different degrees of importance (or weights), and then applying those to a calculated risk index (Karamouz et al. 2011). Depending of the thickness of the overlying strata and the lithology, active faults, groundwater withdrawal, human activities; or, in the case of karst areas, the degree of karstification, there will be several different risk factors to consider.

These index methods are widely used to estimate, for example, aquifer contamination vulnerabilities, which include the DRASTIC (Aller et al. 1987) and the GOD (Foster and Hirata 1988; Foster et al. 2013) methods for porous media and karst areas, and the EPIK method (Doerfliger et al. 1999), specifically for karst areas. Another use of index methods is to identify potential groundwater recharge zones; examples include the AHP method for porous media (Kaliraj et al. 2013) and the APLIS method for karst areas (Andreo et al. 2008; Farfán et al. 2009). In the case of geotechnical risk estimations, some index methods for non-karst areas are available (Wong 1998, Dai and Lee 2001), as well as those that specifically estimate risks in karst areas (Hu et al. 2001; Galve et al. 2009).

In the case of the Galve et al. (2009) study, multiple sinkhole susceptibility models in the Ebro Valley evaporite karst (NE Spain) were compared by applying different methods (nearest neighbor distance, sinkhole density, heuristic index system and probabilistic analysis) for each sinkhole type separately. The study revealed that the most reliable models are those derived from the nearest neighbor distance, the heuristic index system and the sinkhole density, which is conditioned by the degree of clustering of the sinkholes. Consequently, the karst areas in which sinkholes show a higher clustering are a priori more favorable for predicting new occurrences.

The Hu et al. (2001) study also used an index method to develop a regional risk assessment of karst collapse in Tangshan, China. The karst collapse problem, which has been increasing since 1978, usually originates from the loss of stability of an unmapped karst cave in a fragmented rock mass covered by Quaternary sediments, which is difficult to locate and assess. Hu et al. (2001) categorized different risk factors influencing karst collapse (such as prerequisite risk, intensity risk, triggering risk, economic risk, and mitigation risk) and gave different weights to them, resulting in the delineation of three zones in downtown Tangshan with different risk levels. These examples show that the index method for estimating geotechnical risks can give satisfactory results, facilitating stakeholder decision making in urban planning.

The primary goal of this research was to determine the distribution of areas with geotechnical karst risks in Sete Lagoas based on understanding of the underlying physical mechanisms of subsidence and collapse development, by integrating available data and acquiring additional low cost field data. Using data from geologic mapping (scale 1:25,000), aerial photography, lithologic well profiles, optical well logs, and previous investigations, a new geological perspective of the region, such as the structural framework of the subsurface lithologies, karst geometry, and the urban groundwater potentiometric surface, was developed. After defining the mechanisms that control the

location of subsidence and collapse features, an index method modifying the approach of Hu et al. (2001) was applied based on categorizing risk factors influencing karst collapse, giving different weights to them, and then delineating different risk levels for the region.

Site description

Sete Lagoas (Seven Lakes) is located in the state of Minas Gerais, Brazil, 70 km northwest of Belo Horizonte, the state capital (Fig. 1). This region has a population greater than 200,000, over an area of 538 km^2 (IBGE 2010). Urban development has been more intense in the northern and northeastern sectors, in comparison to the initial settlement (Fig. 1). There is considerable industrial activity located mainly along the main federal highway, which is a corridor of significant growth. The current water supply is entirely groundwater from the Sete Lagoas karst aquifer (Pessoa 1996), which is managed by the Water Supply and Sewage Service (Serviço de Abastecimento de Água e Esgoto, SAAE). Rapid urban growth has not always been guided by planning, especially in relation to environmental and geotechnical issues, registering 17 documented occurrences of subsidence or/and collapse since 1988 (Silva 1988; J. Peñaranda J, A. Cordeiro, Servmar Environmental & Eng., unpublished data, 2013; Fig. 1).

Geologically, the area is located in the São Francisco Craton, where carbonate argillo-arenaceous sediments are emplaced giving origin to the Bambuí Group (Branco and Costa 1961; Oliveira 1967; Schöll and Fogaça 1973; Dardene 1978; Schobbenhaus 1984; Ribeiro et al. 2003; Tuller et al. 2010). These are emplaced overlying the basement and are overlain by fluvial sediments.

The basement is represented by the Belo Horizonte Complex, which is generally characterized by a set of gneissic rocks and migmatite zones, with polymetamorphic features, belonging to the geotectonic unit corresponding to the São Francisco Craton (Ribeiro et al. 2003). Epigenic and igneous metamorphic/migmatite rocks with plutonic features mark this occurrence. Mafic intrusions may also occur, which preferentially fill in the fracture planes. The contacts between different lithotypes are generally transitional, mainly between gneiss, migmatites and/or granitoids. The granitoids are light gray to white, with granulation varying from gross to medium, sometimes with sparse porphyroblasts of tabular feldspars, xenoliths from other rocks or restites from partial fusion (Tuller et al. 2010). This complex was intensely affected by basic injections, provoking the appearance of a group of basic rock dikes (Ribeiro et al. 2003).

Overlying the basement, the Bambuí Group is represented by the lower Sete Lagoas Formation (Dardenne 1978) and the upper Serra de Santa Helena Formation (Branco and Costa 1961). The Sete Lagoas Formation is divided and characterized by two members (Ribeiro et al. 2003)—Pedro Leopoldo, at the base, composed of fine limestones, dolomites, marlstones and pelites; and Lagoa Santa, on the top, composed of medium-grained black limestones. In general, the lower contact of this formation with rocks from the Belo Horizonte Complex is abrupt, discordant and tectonic, with faults. The upper contact with the Serra de Santa Helena Formation is most commonly abrupt as well. The Serra de Santa Helena Formation is composed of slate, marble, siltstone and argillite. This formation overlies the Sete Lagoas Formation with abrupt, tectonic or occasionally gradational contacts. With the basement, the contacts are abrupt and discordant (angular discordance), tectonic and with thrust belt faults, easily seen on the basin border (Tuller et al. 2010). Three stratigraphic members (Grossi et al. 1998) constitute this formation: (1) lower, represented by silt-clay rhythmites, generally carbonaceous, and dark shales; (2) middle, represented by marble and shales; and (3) upper, constituted by shales, siltstones, slate cleavage, and cross bedding.

The Bambuí Group is covered by Cenozoic surface cover, which is divided into (1) detritus coverage, (2) alluvial terraces, and (3) alluvium (Ribeiro et al. 2003). The detritus coverage is composed of unconsolidated sediments with a predominant red color, sands to silts with varying levels of gravel, which occur indistinctly on all units, but mainly over the Serra de Santa Helena Formation. The alluvial terraces occur along drainages of the area. They are mainly constituted of semi-consolidated sand to silt material, with whitish to yellowish and reddish color. Finally, the alluvium occurs along the meanders of the large watercourses. They are composed of fine to coarse sand, with discontinuous amounts of quartz pebbles, siltstone and sandstone (Tuller et al. 2010).

Geomorphologically, the area is in a karst setting, which facilitates the presence of lakes (located mainly in the central area), caves, sinkholes, and closed drainage basins (Pessoa 1996; Fig. 1). Areas that have denser drainage are related to the Santa Helena Ridge foothills in the center, basement outcrops in the south, and metasediments in the north.

Methods

Four sets of data were integrated to understand the mechanism and origin of subsidence and collapse events and develop the karst-geotechnical-risk estimation for these types of events. These included geologic mapping, aerial photography interpretation, lithologic well log analysis, potentiometric surface mapping, and optical well log analysis. After that, a karst-geotechnical-risk assessment was made delineating risk levels. These methods will be presented sequentially followed by the approach to data integration.

Geologic mapping of Sete Lagoas was carried out on a scale of 1:25,000. The classification of the sedimentary rocks followed the definitions of Folk (1980) and the microscopic classification of the carbonate rocks followed the definitions of Folk (1959) and Dunham (1962). For the metamorphic and igneous rocks, the classification

DOI 10.1007/s10040-015-1266-x

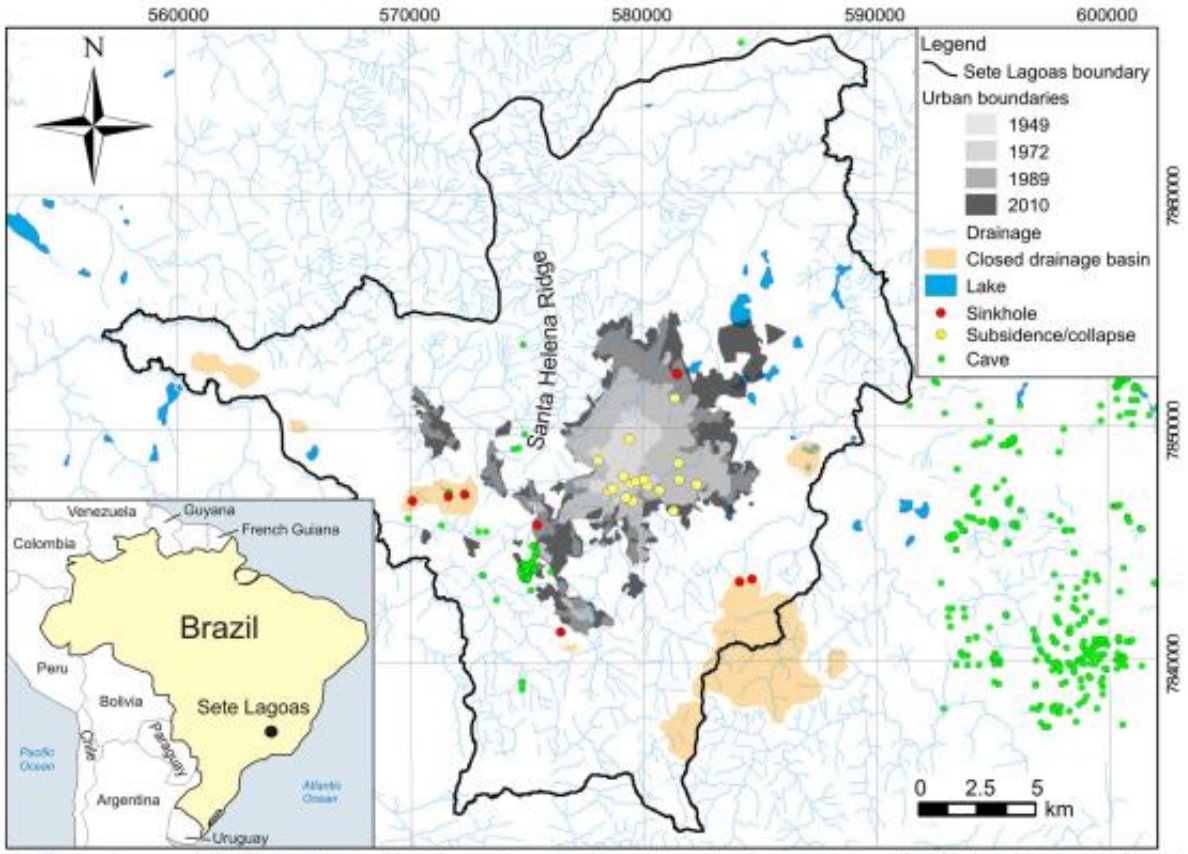

Fig. 1 Location map in UTM coordinates of Sete Lagoas showing the evolution of urban growth (years *1949*, *1972*, *1989*, and *2010*), the karst feature locations (*caves*, *sinkholes*, and *closed drainage basins*), the location of the subsidence/collapse events, and the drainage pattern (from georeferenced images, including aerial photography and Landsat imagery)

followed the definitions of Winter (2001). Aerial photography interpretation (scale 1:40,000, dated 1977) and an SRTM image (Shuttle Radar Topography Mission), Sheet SE-23-Z-C, acquired from the Embrapa's website were evaluated to define lithological contacts (Embrapa 2006). Information about the location of karst features (caves, sinkholes, and closed drainage basins) was acquired from the CECAV's website, as a GIS file (CECAV 2009).

All the data were recorded on paper topographic maps and converted to digital format. ArcGIS 10.1 was used throughout the project to construct the digital maps. A four-step process was used to convert the map data to digital form: (1) automation: a scanned image of the original field map was vectorized, edited, and processed into arc, polygon, and point formats; (2) projection: digital files were transformed from digitizer coordinates to real-world coordinates and converted to a cartographic projection; (3) tables: tables were created to hold label information for polygons, arcs, and points; and (4) symbology: symbols were added for each different layer to indicate different information on the map plots.

A series of 270 lithologic well logs, divided onto 218 lithologic well profiles located in the municipalities surrounding Sete Lagoas, were acquired from the SIAG AS's website (SIAGAS 2006), and 52 public wells logs located in Sete Lagoas were analyzed. The profiles contain information about depth, lithology, thickness of the karst features, and the original groundwater elevation. The public supply wells located in Sete Lagoas were used to collect potentiometric data during 2012, to build the potentiometric map.

Thirty optical well logs were collected to evaluate the karst well features in the urbanized area. The R-Cam 1000 Camera (Laval Underground Surveys) was used in the study. In addition to the standard downhole view, it offered a 360 ° side-view perspective, and was capable of capturing a comprehensive survey of water wells. The imaging was used to obtain information on lithologic contacts, water-table elevation, and karst features. The camera had a maximum depth of 300 m and was connected to a receiver with a monitor that enabled real time imaging.

The purpose of the karst-geotechnical-risk evaluation was to divide the study area into subareas of different risk levels. Using an index method similar to Hu et al. (2001), a risk assessment model was made, categorizing risk

factors influencing karst collapse. Two categories of risk factors were included in the model—geologic risk factors and hydrologic risk factors. Each one was further divided into risk values with different weights (Fig. 2), converting it into two risk factor raster maps. It should be noted that the determination of risk values is not easy in such a complex setting as a karst area. The reason is that there are so many factors affecting these areas that complete structural data cannot be collected. The weights were determined by comparing the relative importance of each factor, checking the location of pre-existing sinkholes, and the karst geometry. Karst geometry can be affected by some level of subjectivity, but existing research supports using this for a guide (Hu et al. 2001, Galve et al. 2009).

The geologic risk factors were based on the lithologies found in the region and their relative geologic relationships. Surface limestone outcrops and limestone covered only by unconsolidated sediments corresponded to the largest weight, a risk value of 5. To determine the limits of these areas, lithologic well profiles and optical well logs were used to generate geologic cross sections. Areas with limestones covered by competent rocks were divided by two categories: (1) areas with relative proximity to the high risk category (around 500 m laterally), having a risk value of 3, based on geotechnical occurrences located in these regions; and (2) outside these 500 m limits having a risk value of 1, based on the lateral continuity of the limestones where, depending on the size and depth of the conduit and the thickness of the layers above, some collapse may occur. In the case of the igneous/metamorphic basement outcrops, a risk value of 0 (zero) was assigned, as no limestone karstification processes occur in these rocks (Fig. 2).

The hydrologic risk elements were based on groundwater use. Groundwater extraction in the area is sufficient to generate a zone of influence (ZOI; US Environmental Protection Agency 1994) characterized by a regional cone of depression in the potentiometric surface. Factors such as withdrawal rate, well locations, and dimensions of the ZOI, as well as the elevations where bedding plane conduits became unsaturated, were evaluated. Within this ZOI, risk areas were assigned corresponding to the magnitude of drawdown. Thus, areas within the ZOI and <720 m (the lowest groundwater elevations, in m.a.s.l.) corresponded to the largest weight, a risk value of 5. Between 720 and 740 m, the risk value adopted was 3. Between 741 and 760 m, the correspondent value was 2, while for >760 m, the value was 1. In areas outside the

Karst Geotechnical Risk Evaluation Matrix

Hydrologic Risk Factor	Groundwater elevation (m.a.s.l)	Value	Geologic Risk Factor: Lithologic Basement	Limestone covered by competent rocks >500 m	Limestone covered by competent rocks <500 m	Limestone (outcrops or mantled)
Outside zone of influence	Not applicable	0	0	1	3	5
Inside zone of influence	>760	1	0	2	4	6
	741-760	2	0	3	5	7
	720-740	3	0	4	6	8
	<720	5	0	6	8	10

Karst Geotechnical Risk Value	Level	Recommendations
8-10	High	Decrease overall pumping rates; prohibit drilling new wells; priority to public wells; switching to surface water supply, where possible.
5-7	Considerable	Maintain pumping rates; prohibit drilling new wells.
3-4	Moderate	Allow well drilling with an evaluation of relative locations and karst features.
1-2	Low	Allow well drilling; increase pumping rates; and monitor for problems.
0	Negligible	Allow well drilling and increase pumping rates.

Fig. 2 Karst-geotechnical-risk-evaluation matrix showing the risk factor values and the overall risk levels, and their respective recommendations. On the geologic risk factors, areas with limestone covered by competent rocks were divided in two sub-categories: 500 m from higher risk zones, or outside these 500 m limits

Hydrogeology Journal DOI 10.1007/s10040-015-1266-x

ZOI, the risk value was 0 (zero), corresponding to no significant hydrologic risk factor (Fig. 2).

Next, summing up and overlaying the geologic and hydrologic raster risk factor maps, a karst-geotechnical-risk map was obtained for the area. The karst-geotechnical-risk values ranged from zero to ten, where values 8–10 were considered as "high risk", 5–7 "considerable risk", 3–4 "moderate risk", 1–2 "low risk", and 0 as "negligible risk" (Fig. 2).

The complete data sets were entered in a GIS database and georeferenced in ArcGIS 10.1 software. The coordinate system was Universal Transverse Mercator (UTM) projection, zone 23, datum SAD 69, with units in meters. The model of karst risk evaluation was also digitized in the GIS environment.

Results

The results are composed of geologic mapping, lithologic well log, potentiometric mapping, and optical well log analysis, followed by the mapped site geologic and hydrologic setting, and karst risk evaluation.

Geology

The Belo Horizonte igneous/metamorphic basement complex occurs in the SSW portion occupying around 25 % of the area (Fig. 3) and it is characterized by epigenic and igneous metamorphic/migmatite rocks with plutonic features, and intrusions of mafic rocks, filling the fracture planes.

The Sete Lagoas Formation occurs mainly in the SE, central and west areas, and in the Santa Helena Ridge foothills, occupying around 5 % of the area at the surface (Fig. 3). The Pedro Leopoldo Member presents important macro-features of dissolution developed more commonly in the solutionally enhanced bedding planes and, locally, in sub-vertical fractures (Fig. 4). This dissolution in bedding planes has been observed in all quarry outcrops and confirmed by optical well logs, indicating that there is a continuity of such features. Locally, some of these cavities are filled with terrigenous material. Three of the four lithological facies observed by Vieira et al. (2007) were confirmed in the area (facies 1, 2, and 3)—facies 1 (thickness of approximately 40 m): this is a micritic limestone with medium to dark gray sparitic grains due to recrystallization where the occurrence of meter-scale recumbent bends is common, with recrystallization and intergrowth of calcite minerals parallel to the bedding, especially in joints; facies 2: regular and homogeneous intercalation of micritic stratums, with thickness of 15–20 cm, evidenced by the beddings systems, and also an intercalation of marlstone levels with brown-pink color, with terrigenous grain levels; facies 3: micritic rock, with occurrence of chlorite placoid minerals, with well-developed solutionally enlarged bedding planes; and facies 4: calcilutites, plane-parallel stratification, with rhythmite terrigenous and carbonate sedimentation. In the Lagoa Santa Member, the main dissolution features are the vadose grottoes and caves (e.g. Rei do Mato cave), indicating groundwater paleoconduits. In relation to the sedimentary facies, the descriptions are—facies 5: rock with variable character, between gray micro-sparites and calcarenites, plane-parallel laminate; and facies 6: occurrence of stromatolite levels of the type "gyminosolens". The limestones from Pedro Leopoldo Member are composed of 85 % micrite, 8 % sparite and 7 % quartz, classified as micrite (Folk 1959) or mudstone (Dunham 1962). The limestones from Lagoa Santa Member are 55 % sparite, 30 % ooids, and 15 % micrite, classified as an oobiosparite (Folk 1959) or grainstone (Dunham 1962).

The rocks from Serra de Santa Helena Formation occur in the NW, N, and NE, occupying around 55 % of the study area (Fig. 3). The formation was mapped; at the top of the formation, levels of slate rocks with well-developed cleavage planes are found, and at the base, slate, marble, siltstone and argillite are found, as well as vertical fractures filled with quartz veins with well-developed hexagonal forms.

The unconsolidated sediments from the Cenozoic surface coverage occur indistinctly on all units (15 % of the area, Fig. 3), but mainly over the Serra de Santa Helena Formation, along the meanders of the large watercourses and in the central portion of the municipality, especially where the urbanized area is located.

Lithostructural contacts and spatial distribution

Due to the difficulty in observing the member contact in the optical well logs, and the lack of data in the lithologic well logs about the depth of the contact between the Pedro Leopoldo and Lagoa Santa members of the Sete Lagoas Formation, it was not possible to separate these members in the geologic cross sections (Figs. 5 and 6). Thus, the cross sections only indicate the contacts between the formations and the basement, the overlying sediments, and the inferred faults.

The basement outcrops in the SW part of the area with elevations between 750 and 950 m.a.s.l. Located in the NE portion of the area, it dips in the NE direction (Fig. 5, cross sections 1–4) and the minimum surface contact is approximately 400 m.a.s.l. Following the dip of this basement, there are sediments from Sete Lagoas Formation and Serra de Santa Helena Formation. The litho contacts between these two formations is abrupt. In the case of Sete Lagoas Formation, the contact between Pedro Leopoldo (basal) and Lagoa Santa (upper) members is also abrupt, horizontal and well defined, which was confirmed in all quarry outcrops.

Based on the developed cross sections, it was possible to propose indirectly a horst and graben system controlled by faulting (Fig. 5). This interpretation was based on data from the lithologic well profiles and their spatial locations, which indicated different basement depths over small lateral distances (e.g. 120 m offset in 1.4 km distance; 140 m in 2.5 km; or 200 m in 5 km). It was also possible to deduce a horst in the central portion of the municipality

DOI 10.1007/s10040-015-1266-x

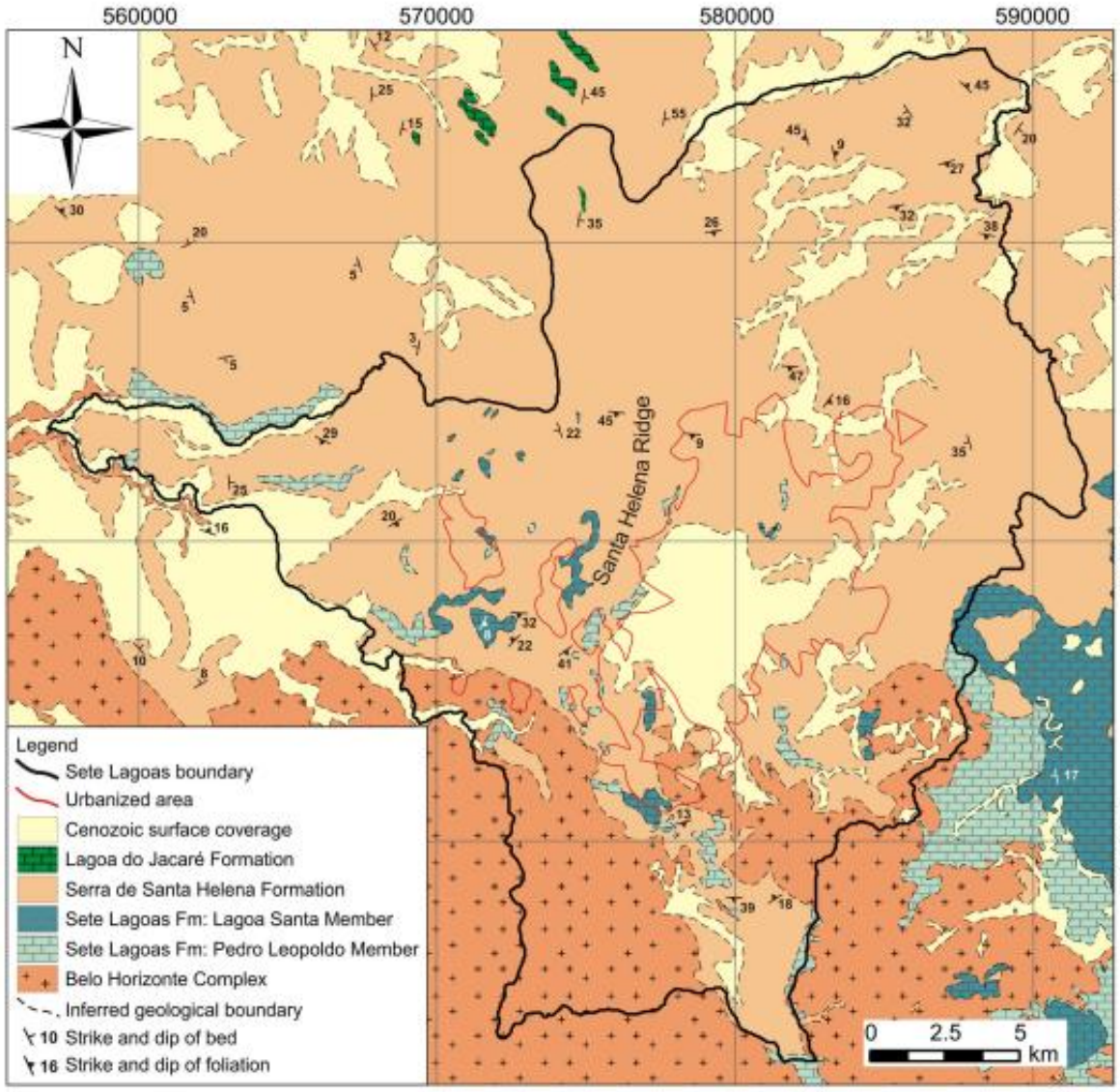

Fig. 3 Geologic map of the study area. The *Belo Horizonte Complex* (igneous/metamorphic) occurs in the *SSW* area. *The Sete Lagoas Formation*, divided into two members (*Pedro Leopoldo*: fine limestones; and *Lagoa Santa*: medium black limestones) occurs mainly in the *SE*, *W*, and in the *Santa Helena Ridge* area. The *Serra de Santa Helena Formation* (shales, siltstones, marble, and slate) occurs in the *NW*, *N*, and *NE* regions, while the Cenozoic unconsolidated sediments occur along the large fluvial meanders and drainages

(close to the urbanized area), in the Santa Helena Ridge (Fig. 5, cross section 3), indicating an upward displacement of the basement.

The Sete Lagoas Formation and Serra de Santa Helena Formation follow this horst and graben system. They have thinner layers on the basement border (southwest portion) and higher thickness in the northeast (cross sections 1 and 2). In the case of the Sete Lagoas Formation, the limestones dip and become thicker to the northeast, being covered almost totally by the Serra de Santa Helena Formation, where these limestones from the Sete Lagoas Formation arise mainly in the Santa Helena Ridge foothills. As the Sete Lagoas Formation and Serra de Santa Helena Formation become thicker, their associated bedding planes dip to the northeast. These formations can reach 160 m thickness, seen in the north region of the municipality (cross section 1) and in the Santa Helena Ridge (cross section 3).

In the majority of the urbanized area, limestones from Sete Lagoas Formation and unconsolidated sediments from the Cenozoic surface coverage are deposited within the graben area. The deposits are 90 and 40 m thick on average, respectively (see central graben area on Fig. 5).

Hydrogeology Journal DOI 10.1007/s10040-015-1266-x

Fig. 4 **a** The Pedro Leopoldo Member of the Sete Lagoas Formation, with bedding plane dissolution filled with terrigenous sediments, suggesting a past meteoric water flow that followed the bedding planes. This feature has been observed in all quarry outcrops, indicating that there is a continuity of such bedding plane dissolution. **b** Lagoa Santa Member of the Sete Lagoas Formation, with cave development, indicating groundwater paleoconduits and a higher degree of dissolution compared to the Pedro Leopoldo Member, which can be explained by the medium-grained composition of the Lagoa Santa Member, confirmed by thin section analysis

Locations of the subsidence/collapse events and hydrogeological correlations

All of the subsidence or collapse events have occurred in the urbanized area, within limestone from Sete Lagoas Formation and Cenozoic unconsolidated sediments contained within the central graben area, and in a zone of influence (ZOI) caused by considerable groundwater extraction (Fig. 6).

According to the detailed cross sections, as evidenced primarily from optical logs and geologic mapping, two continuous bedding planes that have undergone dissolution were confirmed and identified in this region (Fig. 6): (1) a shallower and thicker continuous dissolution zone with solutionally enlarged bedding planes that are 1–8 m thick, near the contact with unconsolidated sediments; and (2) 10–20 m below, a thinner continuous dissolution zone with solutionally enlarged bedding planes ranging from 20 cm to 1 m thick.

The shallowest one, in some areas, is entirely in the unsaturated zone (Fig. 6, see the supply well PT-01 indications and the downhole view photo on the cross sections A–A′ and B–B′) or very close to this zone due to groundwater extraction. These locations correlate with some subsidence/collapse areas, with highest concentration of wells with an intermediate and high pumping rate (500–2,000 m^3/day and greater than 2,000 m^3/day, respectively) and with the dissolution in bedding planes evidenced by optical well logs (see map on Fig. 6).

Based on this evidence, well log profiles located close to the collapse events in the urbanized area were chosen to evaluate the drawdown evolution through decades and determine if there is a correlation—see Table S1 in the electronic supplementary material (ESM). Due to absence of data about water-table measurements at the drilling time or data about the year of drilling, some supply wells were not included on the list. The first well (PT-01), drilled in the 1940s, had a mean drawdown of 48 m after seven decades, while PT-11, drilled in the 1960s, had 30 m of drawdown after five decades. Wells from the 1970s and 1980s also have considerable drawdowns, between 10 and 38 m. Wells drilled in the 1990s such as PT-07 (12 m drawdown) and PT-16 (about 7 m drawdown), had smaller values of drawdown, probably influenced by previous pumping wells. These data showed that during several decades, since the first supply well drilled in 1942 until present, some areas had significant decreases in the water table, around 40 m lower due to pumping.

Groundwater extraction caused a considerable ZOI located in the central portion of the urbanized area. Within this zone, in some areas, the shallowest enlarged bedding plane is entirely in the unsaturated zone (see cross sections, Fig. 6). All the major geotechnical events are located within the ZOI limits (see black dashed line on the map in Fig. 6). Thus, considering the drawdown history, location of the ZOI, the similar geology setting, date of first significant geotechnical event recorded in 1988 (Silva 1988), and these event locations, a correlation between the emergence of subsidence/collapse and groundwater exploitation is justified. It is also possible to conclude, based on the depth of the shallow conduit, that this conduit was in the saturated zone prior to development.

Regarding the locations of the geotechnical events, points 1–3, 5–10 and 12–16 (black dots, Fig. 6) are located within the same hydrogeological situation—limestone with two enlarged bedding planes covered by only unconsolidated sediments, close to wells with intermediate and high groundwater extraction rates (500–2,000 m^3/day and greater than 2,000 m^3/day, respectively), and within the ZOI. These features can explain the clustered sinkholes in this area. As stated in the previous, the shallowest conduit close to some wells can be completely dry or almost dry in some areas; in these

DOI 10.1007/s10040-015-1266-x

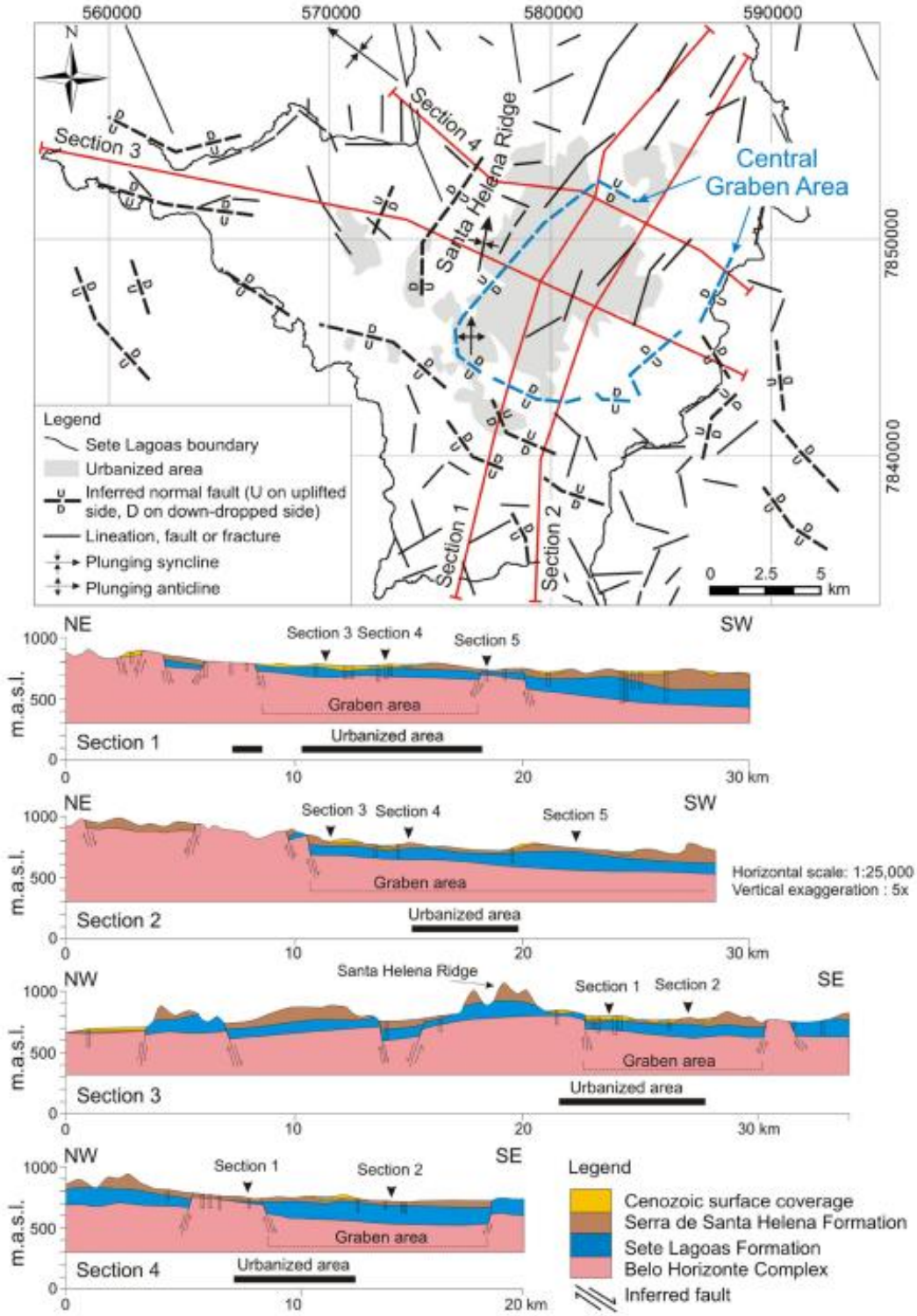

Fig. 5 Geologic cross sections and schematic map showing structural features. The Sete Lagoas Formation and Serra de Santa Helena Formation dip are thicker in the NE direction. The majority of the urbanized area is contained in a graben, which contain limestones from Sete Lagoas Formation and unconsolidated sediments from Cenozoic surface coverage

Hydrogeology Journal DOI 10.1007/s10040-015-1266-x

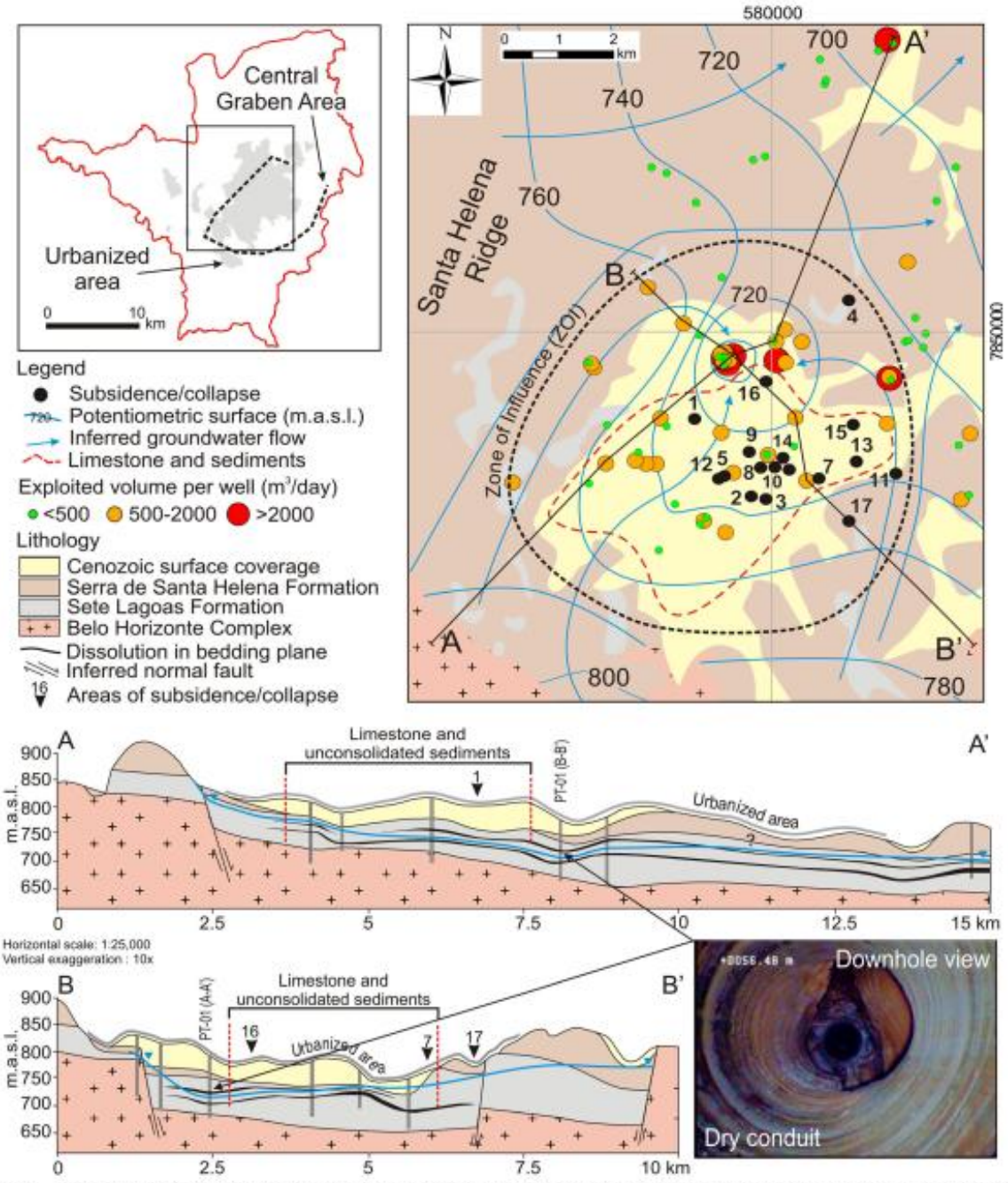

Fig. 6 Map of the subsidence/collapse locations, potentiometric surface, and detailed cross sections of the central urbanized area. The map indicates the relation between extraction rate per well and the 17 collapse areas (*black dots*, listed according to the historical occurrences). The *red dashed line* indicates that, within this limit, only limestone covered by unconsolidated sediments occurs. The potentiometric surface lines (measured in 2012) shows a relationship between the 17 collapse areas and the zone of influence (ZOI) localized in the central area caused by the high pumping rate in wells. The *geologic cross sections* (*A–A'* and *B−B'*), displayed *below the map*, indicate the relation between karst conduits (both vadose and phreatic), the water table and its cone of depression and litho contacts. Note that in the well *PT-01*, the shallowest conduit is entirely in the unsaturated zone

areas, only unconsolidated overlying materials have significant risk for collapse events, which is already happening.

The remainder of the collapse events (4, 11, and 17) are located in regions more distant from wells with high flow rates; these collapse events are also outside of the area with only limestone and unconsolidated sediments, but adjacent to them and still located within the ZOI (Fig. 6). Thus, the relative proximity to the limestone and unconsolidated sediments outcrops (around 500 m laterally) with a thin competent rock layer from Serra de Santa Helena Formation (e.g. point 17, cross section B–B', Fig. 6), and located within the ZOI, can explain that these particular events could be also related to groundwater extractions, thereby making it possible to consider that areas 500 m beyond the limestone and unconsolidated sediment outcrops, and/or within the ZOI, are still at risk of collapse.

Karst-geotechnical-risk evaluation

The sum of the geologic risk factor and hydrologic risk factor maps (Figs. 2 and 7) defined the karst-geotechnical-risk map (Fig. 8). The high risk zone (red area) is characterized by only limestone outcrops or limestones covered by unconsolidated sediments within the ZOI with the lowest drawdown. The majority of geotechnical events (82 %, see yellow dots on Fig. 8) occurred in this zone. The considerable risk zone (orange area) occurs in regions with unconsolidated sediments or limestone outcrops outside of the zone of influence and/or with rocks from Serra de Santa Helena Formation between those within the ZOI. Some natural sinkholes (blue dots) and induced collapse features (events 4, 11 and 17) are located in that area. The moderate risk zone (yellow area) is represented by areas 500 m beyond the limestones outcrops outside of the ZOI and areas with thin competent rocks from the Serra de Santa Helena Formation within the ZOI. This area should be considered as a caution zone. The low risk zone (green area) is represented by rock layers from the Serra de Santa Helena Formation covering the limestones. Finally, the negligible risk zone (white area) is where the basement outcrops or has other lithology except limestone covering the basement. This is an area with negligible possibility for subsidence or collapse.

Discussion

The study provided significant insight into the distribution of karst conduits in the municipality, as well as generating a significantly improved understanding of the risk of collapse due to both geologic and hydrologic causes. This discussion will provide an interpretation of the karst development and an evaluation of the tools used for the karst-geotechnical-risk assessment.

The results showed that areas with natural sinkholes and caves/grottos are related to the Sete Lagoas Formation outcrops, especially the upper Lagoa Santa Member. These limestones reached the surface during structural uplift and came in contact with meteoric waters, resulting in a dissolution process that is most strongly affecting the bedding planes of these rocks, and, in lower magnitude, the sub-vertical fracture planes, forming karst conduits. The medium-grained Lagoa Santa Member had a higher degree of dissolution compared to the fine-grained lower

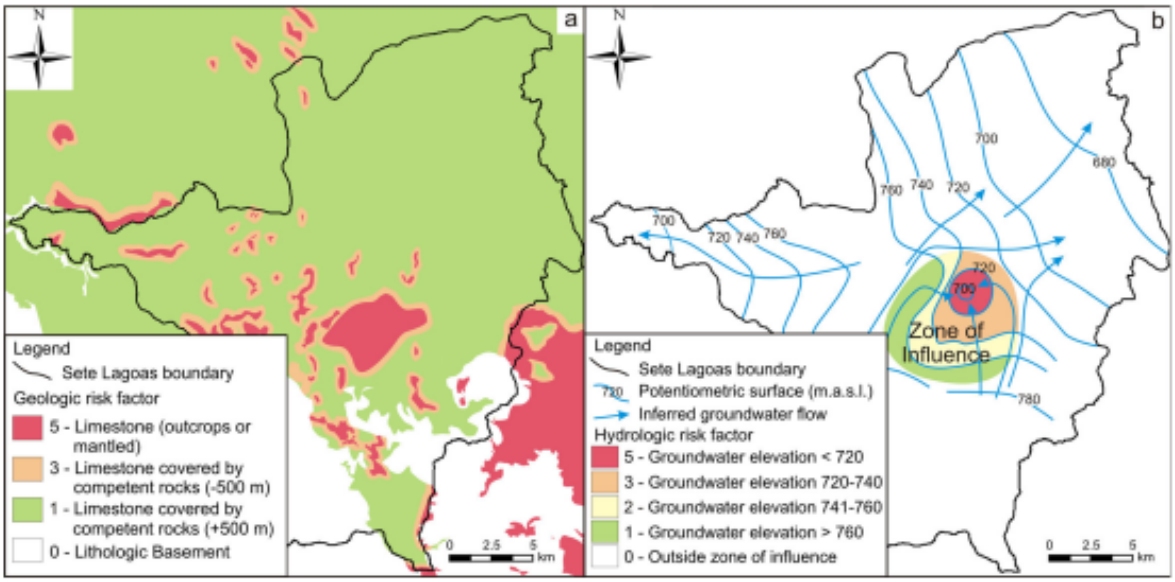

Fig. 7 **a** Geologic risk factor map and **b** hydrology risk factor map, showing the risk values for each elements based on geology or hydrology relationships. These two maps were computed and summed up to obtain the karst-geotechnical-risk map in Fig. 8

DOI 10.1007/s10040-015-1266-x

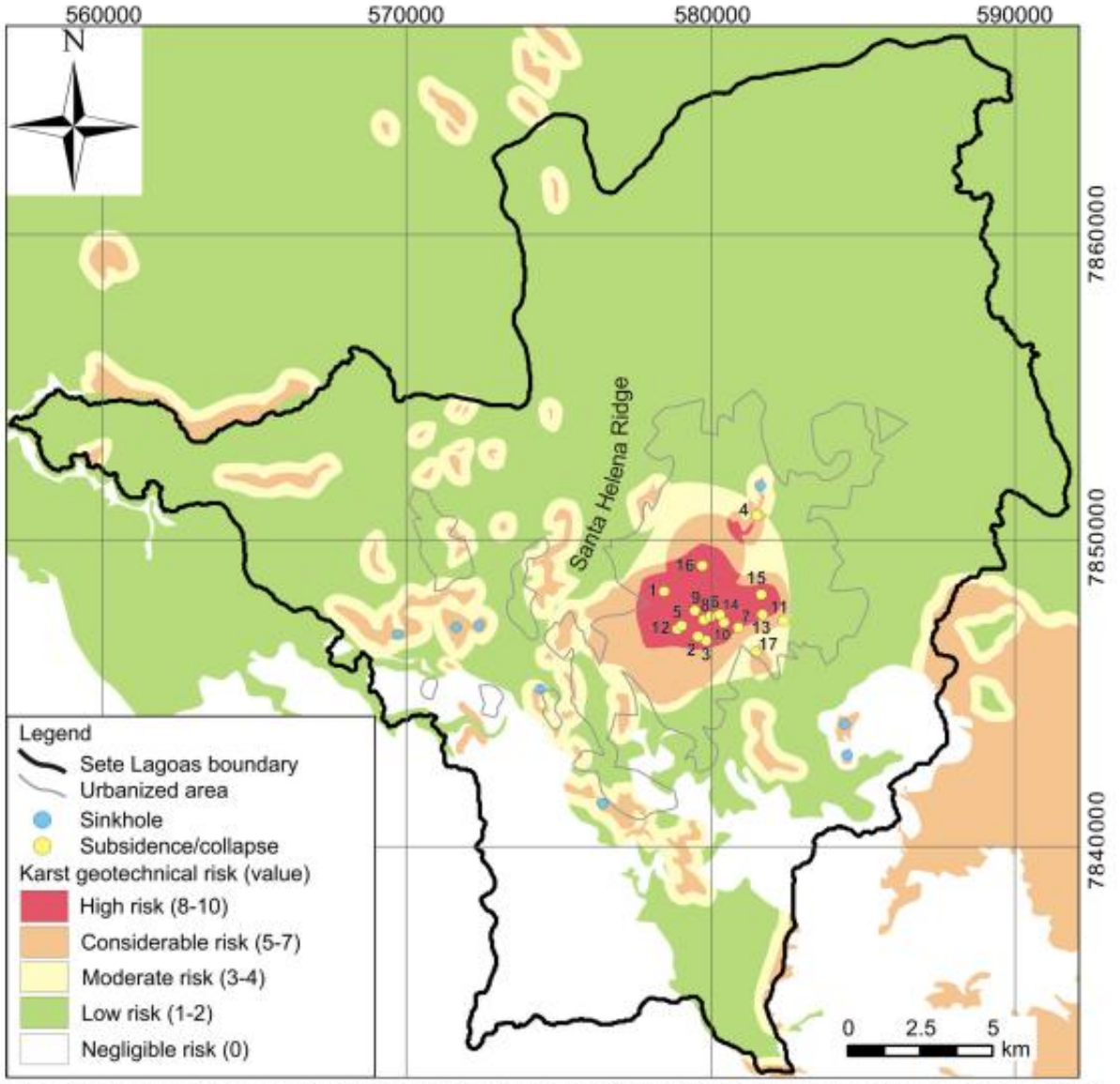

Fig. 8 Karst-geotechnical-risk map showing the mapped risk zones, sinkholes and induced collapse locations. In the urbanized area, largely located in the *high*, *considerable*, and *moderate risk* zones, and where the majority of the collapse features are located, additional intensive groundwater extraction will likely generate additional events

Pedro Leopoldo Member. Others sinkhole areas are related to zones where the Sete Lagoas Formation is covered by only Cenozoic unconsolidated sediments, with the karst conduits in the subsurface (see red dashed line limits in the map and cross sections on Fig. 6). Due to intensive groundwater extraction in this mantled karst area, subsidence can occur causing depressions on the land surface. Depending on the size and depth of the conduit and the thickness of the layers above, these depressions can collapse, which in some situations may grow to over 20 m diameter, as happened in the municipality in 1988 (Silva 1988; Fig. S1 of the ESM).

The bounding faults of some areas bring the limestones in lateral contact with the basement creating barrier boundaries for the groundwater system (central graben area, Figs. 5 and 6). In the urbanized area, these boundaries together with natural karst processes explain the location of two solutionally enlarged bedding planes and, consequently, a karst geotechnical risk. Thus, the combination of unconsolidated sediments overlying limestones or simple exposed limestone outcrops with two solutionally enlarged bedding planes provided a geologic framework for geotechnical issues. The subsequent extraction of groundwater resulting in a considerable zone of influence explains the emergence

DOI 10.1007/s10040-015-1266-x

of the cluster of induced subsidence or collapse events in this urbanized area. As the bedding planes became exposed in the vadose zone, some areas of the zone collapsed and resulted in either a sinkhole, or caused soil piping in the overlying sediments to generate a subsidence area or collapse in the overlying sediments.

The objective of this report is not to present a geomechanical model for sinkhole formation in the study area, but an evaluation of geotechnical risks. The authors believe that possible processes of collapse formation are related to the combination of (1) limestone dissolution; (2) the location, especially adjacent to the surface or in the subsurface; (3) the type of overlying cover rocks; and (4) the groundwater extraction during several decades of pumping. The tertiary porosity, composed of the two primary bedding planes and some dissolved sub-vertical fractures, can be modeled based on saturation, with an increased risk occurring with significant decreases in water table. In the unsaturated enlarged bedding plane zones or close to it, a gradual subsidence of the land surface could develop a bowl-shaped depression. In the case of sub-vertical fractures or areas adjacent to big cavities, collapse sinkholes could be considered a more common mechanism, in which the overlying cover material can no longer support its own weight, causing soil piping in the overlying sediments (Fig. S1 of the ESM). The relative importance of soil piping effects, compared to carbonate collapse, is not yet clear, as both mechanisms seem to be active at different times in this system. However, it is important to say that these processes normally are accelerated in an anthropogenic situation, induced by water-table decline. Geotechnical modeling of the estimated increase in risk due to generating unsaturated conditions would allow a better understanding of risks for the area.

This study illustrates some recommendations for the sustainable use of the underground resources in karst settings (Fig. 2). In the case of areas with high geotechnical risk (red area), completely within the urbanized area, and where the majority of the population is living, recommendations include reducing groundwater use based on potentiometric surface elevation, prohibition to drilling new wells, prioritizing public wells to supply, and switching to surface-water supply where possible. The main objective is to preserve groundwater resources to reduce the localized drawdown, which creates vadose conduits. Supply wells could be relocated to more protected areas, outside of that zone, to avoid future subsidence or collapse. Areas with considerable risk should maintain the pumping rate, prohibiting the drilling of new wells, and only substituting pre-existing public and private wells. These two risk areas should be monitored for possible new geotechnical events. In the areas of moderate risk for collapse, new wells (both public and private) are allowed to be drilled; however, a careful evaluation of relative locations for pumping is necessary. A geomorphologic analysis in the surroundings is suggested in order to find possible karst features such as dolines or sinkholes that may indicate possible considerable karstification in the subsurface. In the low risk area, increase in the pumping rate and drilling of new wells, both public and private, are allowed.

This inexpensive integrated analysis produced satisfactory results in karst aquifers with conduits strongly developed in bedding layers in an urban setting. It took advantage of information already available such as lithologic well logs, to help understand the geologic structure, and data from optical well logs collected in public supply wells. The disadvantages for this approach include the difficulty in observing geologic contacts between formations or members and problems observing fractures or conduits using optical well logs when the water is turbid, caused by particles (rust, dirt, minerals) in suspension. Additional geophysical data may allow the municipality to confirm some interpretations in the geologic cross sections and maps.

For the index system approach, due to lack of information about construction activities, these data were not included in the estimation. In future studies, including construction activities could improve the assessment in some parts of the urbanized area. Additionally, as water supply management evolves with a changing potentiometric surface, observations can be made regarding the evolution of risk for the municipality. This karst-geotechnical-risk map is not static, as it is linked to the extraction of groundwater. If the groundwater extraction increases, the dimension of the areas with greatest risks will increase, while conversely, improved management can lower the risks.

Conclusion

The results indicate that optical logging and hydrogeologic mapping are useful tools to develop an understanding of the distribution of subsidence and collapse risks in a karst area, and they have become an efficient set of tools to facilitate the spatial visualization, including the location/depth of the conduits, and to determine the geometry of the geologic formations.

The urbanized area of Sete Lagoas is primarily located in a graben, filled with a deposit of limestones from the Sete Lagoas Formation and Cenozoic unconsolidated sediments. This setting results in barrier boundaries for groundwater, which together with natural karst processes explains the location of two main solutionally enlarged bedding planes and a large groundwater storage capacity in this medium of tertiary porosity. The setting also explains why the groundwater-dependent urbanized area developed in this location.

The karst geotechnical problems are related to both geologic factors (unconsolidated sediments deposited over the limestones) as well as hydrologic factors related to decreases in the water table in areas with solution features creating vadose conduits, which were formerly phreatic. Areas with unconsolidated sediments over the limestone with the absence of interlying lithologies of the Serra de Santa Helena Formation, near high flow-rate production

DOI 10.1007/s10040-015-1266-x

wells, are the most susceptible areas to having subsidence and collapse.

In the urbanized area, largely located in this high risk zone and where the majority of the karst geotechnical features are located, additional intensive groundwater extraction will likely generate additional events. Limiting further collapse could be aided by limiting high flow-rate wells to prevent the solutionally enlarged bedding planes from becoming unsaturated.

Acknowledgements This work was funded by Servmar Environmental & Engineering and by São Paulo Research Foundation (FAPESP) [Fundação de Amparo à Pesquisa do Estado de São Paulo (FAPESP)] (process 2012/12846-9). Special thanks go to Kaitlyn Beard and Kyle Spears for their discussion and editing assistance. We would also like to thank three anonymous reviewers for their thoughtful and thorough reviews of the original manuscript.

References

Adamek J, Jeran PW (1985) Precalculation of subsidence over longwall panels in the northern Appalachian coal region. BuMines IC 9042:34–56

Albrecht KJ (1996) Evaluation of geological and geotechnical problems in karst land: basis for geotechnical mapping. MSc Thesis, University of Sao Paulo (USP), Sao Paulo, Brazil

Aller L, Bennett T, Lehr J, Petty R, Hackett G (1987) DRASTIC: a standardized system for evaluating ground water pollution potential using hydrogeologic settings. EPA-600/2-87-035, National Water Well Association, Dublin, OH; EPA, Ada, OK

Andreo B, Vías JM, Durán JJ, Jiménez P, López Geta JA, Carrasco F (2008) Methodology for groundwater recharge assessment in carbonate aquifers: application to pilot sites in southern Spain. Hydrogeol J 16:911–925

Bell JW (1997) Las Vegas Valley: land subsidence and fissuring due to groundwater withdrawal. In: Impact of climate change and land use in the southwestern United States. Nevada Bureau of Mines and Geology, Reno, NV

Branco Jr, Costa MT (1961) Belo Horizonte-Brasilia roadmap tour. In: Brazilian Congress of Geology, Brasilia. Publ. 15, Radioactive Research Institute, Belo Horizonte, Brazil, 25 pp

Buckham AF, Cockfield WE (1950) Gullies formed by sinking of the ground (British Columbia). Am J Sci 248(2):137–141

CECAV (2009) Centro Nacional de Pesquisa e Conservação de Cavernas [National Center for Research and Conservation of Caves]. Available http://www.icmbio.gov.br/cecav/downloads. Accessed on March 2014

Dai FC, Lee CF (2001) Terrain based mapping of landslide susceptibility using a geographical information system: a case study. Can Geotech J 38(5):911–923

Dardenne MA (1978) Synthesis on the stratigraphy of Bambuí Group in central Brazil. In: 30th Brazilian Congress of Geology, vol 2, Recife, Nov. 1978, Brazilian Soc. Geol., Recife, Brazil , pp 597–610

Day M (2002) The role of valley systems in the evolution of tropical karst areas. In: Gabrovšek F (ed) Evolution of karst: from prekarst to cessation. Inštitut za Raziskovanje Krasa, ZRC SAZU, Postojna/Ljubljana, Slovenia, pp 235–241

Doerfliger N, Jeannin PY, Zwahlen F (1999) Water vulnerability assessment in karst environments: a new method of defining protection areas using a multi-attribute approach and GIS tools (EPIK method). Environ Geol 39(2):165–176

Douglas I (2013) Cities: an environmental history. Environmental history and global change series, Tauris, London, 369 pp

Dudley JW, van der Linden AJ, Mah KG (2009) Predicting accelerating subsidence above the highly compacting Luconia carbonate reservoirs, offshore Sarawak Malaysia. SPE Reserv Eval Eng 12:104–115

Dunham RJ (1962) Classification of carbonate rocks according to depositional texture. In: Ham WE (ed) Classification of carbonate rocks. Mem. 1, AAPG, Tulsa, OK, pp 108–121

Embrapa (2006) Empresa Brasileira de Pesquisa Agropecuária [Brazilian Agricultural Research Corporation]. Available: http://www.relevobr.cnpm.embrapa.br/download/mg/mg.htm. Accessed March 2013

Farfán H, Corvea JL, de Bustamante I (2009) Sensitivity analysis of APLIS method to compute spatial variability of karst aquifers recharge at the National Park of Viñales (Cuba). Adv Res Karst Media Environ Earth Sci 2010:19–24

Folk RL (1959) Practical petrographic classification of limestones. Am Assoc Pet Geol Bull 43:1–38

Folk RL (1980) Petrology of sedimentary rocks. Hemphill, Austin, TX, 184 pp

Ford DC, Williams PW (2007) Karst geomorphology and hydrology, 2nd edn. Wiley, Chichester, NY, 562 pp

Foster SSD, Hirata RCA (1988) Groundwater pollution risk evaluation: the methodology using available data. CEPIS/PAHO/WHO, Lima, Peru

Foster SSD, Hirata R, Andreo B (2013) The aquifer pollution vulnerability concept: aid or impediment in promoting groundwater protection? Hydrogeol J 21(7):737–750

Fuller ML (1922) Some unusual erosion features in the loess of China. Geog Rev 12:570–584

Galve JP, Castañeda C, Gutiérrez F, Herrera G (2009) Assessing sinkhole activity in the Ebro Valley mantled evaporite karst using advanced DInSAR. Geomorphology 229:30–44

Grossi Sad JH, Chiodi Filho C, Chiodi DK (1998) Overview of slates at Minas Gerais State, Brazil. COMIG, Belo Horizonte, Brazil, CD-ROM

Hobbs SL, Gunn J (1998) The hydrogeological effect of quarrying karstified limestone: options for protection and mitigation. Q J Eng Geol 31:147–157

Hu RL, Yeung MR, Lee CF, Xiang JX (2001) Regional risk assessment of karst collapse in Tangshan. Chin Environ Geol 40:1377–1389

IBGE (2010) Instituto Brasileiro de Geografia e Estatística [Brazilian Institute of Geography and Statistics] Basic Municipal Information. Available: http://www.cidades.ibge.gov.br/xtras/home.php. Accessed on March 2014

Kaliraj S, Chandrasekar N, Magesh NS (2013) Identification of potential groundwater recharge zones in Vaigai upper basin, Tamil Nadu, using GIS-based analytical hierarchical process (AHP) technique. Arab J Geosci. doi:10.1007/s12517-013-0849-x

Karamouz M, Ahmadi A, Akhbari M (2011) Groundwater hydrology: engineering, planning, and management. CRC Press, Boca Raton, FL, 649 pp

Kaufmann O, Quinif Y (1999) Cover-collapse sinkholes in the "Tournaisis" area, southern Belgium. Eng Geol 52(1–2):15–22

LaMoreaux PE (1997) Legal aspects of karst and insurability. In: Günay G, JohnsonAI (eds) Karst waters & environmental impacts. Proceedings of the 5th Int. Symp. and Field Seminar on Karst Waters and Environmental Impacts, Antalya, Turkey, September 1995, Balkema, Dordrecht, The Netherlands, pp 11–17

LaMoreaux PE, Newton JG (1986) Catastrophic subsidence: an environmental hazard, Shelby County. Alabama. Environ Geol Water Sci 8(1/2):25–40

Newton JG (1976) Induced sinkholes: a continuing problem along Alabama highways. Proceedings of the 2nd Int. Symp. on Land Subsidence, Anaheim, CA, IAHS Publ no. 121, IAHS, Wallingford, UK, pp 453–463

Newton JG (1987) Development of sinkholes resulting from man's activities in the eastern United States; US Geol Surv Circ 968, 54 pp

Oliveira LM (1997) A gestão de riscos geológicos urbanos em áreas de carste [The management of urban geological risks in karst areas]. BSc Thesis, Pontifícia Universidade Católica do Paraná, Curitiba, Brazil, 46 pp

Oliveira MAM (1967) Contribuição à geologia da parte Sul da Bacia do São Francisco e áreas adjacentes [Contribution to the geology of the southern part of the São Francisco Basin and adjacent areas]. In: Collection of exploration reports, no. 3, Petrobras, Rio de Janeiro, pp 71–105

Pessoa P (1996) Hydrogeological characterization of the region of Sete Lagoas, MG: potentials and risks. MSc Thesis, University of São Paulo, São Paulo, Brazil

Ribeiro JH, Tuller MP, Danderfer Filho A (2003) Mapeamento geológico da região de Sete lagoas, Pedro Leopoldo, Matozinhos, Lagoa Santa, Vespasiano, Capim Branco, Prudente de Morais, Confins e Funilândia, Minas Gerais (escala 1:50.000) [Geological mapping of the region of Sete Lagoas, Pedro Leopoldo, Matozinhos, Lagoa Santa, Vespasiano, Capim Branco, Prudente de Morais, Confins and Funilândia, Minas Gerais State, Brazil (scale 1:50,000), 2nd edn]. CPRM, Belo Horizonte, Brazil, 54 pp

Schobbenhaus C (1984) Geology of Brazil. National Department of Mineral Production, Brasilia, pp 275–277

Schöll WU, Fogaça ACC (1973) Stratigraphy of the Espinhaço in the Diamantina region. In: Symposium on Geology of Minas Gerais State, Brazil. Bulletin 1, Brazilian Geology Society, Belo Horizonte, pp 55–73

SIAGAS (2006) Sistema de informações de águas subterrâneas [System of groundwater information]. Available at: http://siagasweb.cprm.gov.br/layout/. Accessed August 2013

Silva AB (1988) Abatimento de solo na Cidade de Sete Lagoas, Minas Gerais, Brasil [Soil subsidence in the city of Sete Lagoas, Minas Gerais State, Brazil]. Rev Água Subterrânea 12:57–66

Terzaghi K (1931) Earth slips and subsidences from underground erosion. Eng News-Rec 107(3):90–92

Tuller MP, Ribeiro JH, Signorelli N, Féboli WL, Pinho JMM (2010) Projeto Sete Logoas-Abaeté, Estado de Minas Gerais, Brasil [Sete Lagoas-Abaeté Project, Minas Gerais State, Brazil]. 6 geological maps, scale 1:100,000, Geology Program of Brazil, Belo Horizonte, Brazil, 160 pp

US Environmental Protection Agency (1994) Handbook: ground water and wellhead protection. EPA/625/R-94/001, US EPA, Washington, DC

Vieira LC, Trindade RIF, Nogueira ACR, Ader M (2007) Identification of a Sturtian cap carbonate in the neoproterozoic Sete Lagoas carbonate platform, Bambuí Group, Brazil. C R Geosci 339:240–258

Williams JH, Vineyard JD (1976) Geologic indicators of catastrophic collapse in karst terrain in Missouri. Natl Acad Sci Trans Res Rec 612(pt. 1):31–37

Winter JD (2001) An introduction to igneous and metamorphic petrology. Prentice Hall, Upper Saddle River, NJ, 697 pp

Wong CKL (1998) The new priority classification systems for slopes and retaining walls. GEO report no. 68. Geotechnical Engineering Office, The Government of the Hong Kong Special Administrative Region, Hong Kong, 117 pp

Hydrogeology Journal DOI 10.1007/s10040-015-1266-x

Electronic supplementary material – Hydrogeology Journal

Evaluating karst geotechnical risk in an urbanized area in Sete Lagoas, Minas Gerais, Brazil

Paulo Galvão[1], Todd Halihan[2], Ricardo Hirata[1]

1. University of São Paulo, Institute of Geosciences, Rua do Lago 562, São Paulo, SP 05508-080, BRA
hidropaulo@gmail.com
2. Oklahoma State University, School of Geology, 105 Noble Research Center, Stillwater, OK 74078, USA

Corresponding Author: Paulo Galvão, Phone: +5511986677505, Email: hidropaulo@gmail.com

Table S1 Supply wells drawdown evolution by decade. All these wells are located close to subsidence/collapse events in the urbanized area

Well ID	Year drilled	Depth to water post drilling (m)	Depth to water 2012 (m)	Drawdown (m)
PT-01	1942	14	62.30	48
PT-11	1968	26	58.06	32
PT-05	1970	24	62.14	38
PT-08	1974	28.7	63.97	35.3
PT-48	1976	20	36.82	17
PT-15	1981	21	54.40	33
PT-04	1982	51	60.89	10
PT-09	1982	36	62.50	27
PT-13	1984	44.7	68.50	23.8
PT-14	1985	38	60.47	22
PT-28	1986	32.9	48.43	15.5
PT-19	1987	5.35	16.90	11.55
PT-16	1990	41	47.86	7
PT-07	1990	49	61.17	12
PT-39	1991	1.5	1.76	0.3

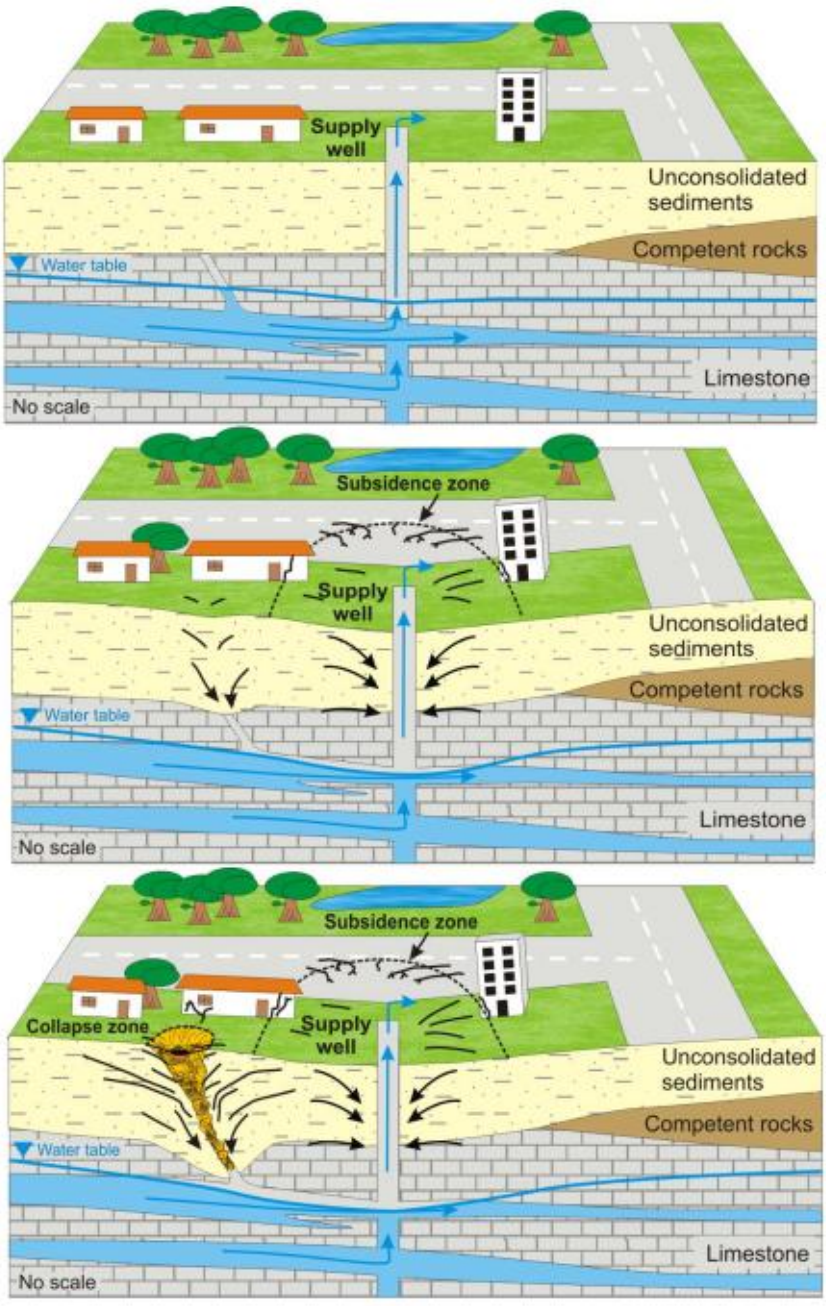

Figure S1 Schematic figure showing the processes of subsidence and collapse in Sete Lagoas caused by the falling water table, induced by over extraction of groundwater. The majority of the geotechnical events are related to zones where the limestones from Sete Lagoas Formation are covered by Cenozoic unconsolidated sediments, with the two enlarged bedding planes in the subsurface (adapted from Murck et al. 1995 – see References in the main article)

CHAPTER 7: THE KARST PERMEABILITY SCALE EFFECT OF SETE LAGOAS, MG, BRAZIL

Paulo Galvão[1], Todd Halihan[2], Ricardo Hirata[1]

Submitted in the Journal of Hydrology

Abstract

Collecting and interpreting permeability data in karst systems is considered complicated due to three distinct properties of these systems. First, the permeability distribution of high permeability features may be as one-dimensional features that are difficult to detect with wells, or may be so high in the wells that the upper measurement limit is encountered during aquifer testing. Secondly, turbulent flow may make the application of continuum hydraulic principles difficult. Finally, permeability commonly has a scale effect in which permeability in these systems increases with the scale of measurement. The aquifer for Sete Lagoas, Brazil, is used to evaluate a permeability combination model methodology to test the permeability structure across a range of spatial scales in order to develop a quantitative model of permeable features that is consistent across all scales of measurement, from matrix properties to regional-scale flow. The aquifer in this study has some wells that do not have measurable drawdown during pumping due to high permeability. Permeability data indicated an increase in permeability from the small- to the well-scale and a decrease from the well- to regional-scale. This is due to the localized development of karst bedding plane dissolution in one structurally controlled region of an aquifer with low matrix permeability. The results show that, based on measurement technique, the permeability data vary over many orders of magnitude, while the physical size of permeable features of the aquifer are consistent across the scales of data collection with less than an order of magnitude variation. The aquifer geometry of these hydraulically active features provides a quantitative understanding of the scale effects of permeability measurements.

Keywords: karst, permeability, transmissivity, hydraulic conductivity, scale effect, Brazil.

1. Introduction

Formation bulk permeability depends on the shape, amount, and interconnectivity of void spaces, or permeability structure. This is often quantified with testing in the form of hydraulic conductivity or transmissivity values, which incorporate fluid properties and aquifer dimensions into the measurements. Grain size analyses, permeameters, aquifer tests and groundwater models are most commonly used to obtain permeability estimates from small- to regional-scales. However, the permeability values can vary within a wide range over orders of magnitude, depending on the geological formation. While flow properties are determined in rock bodies as hydraulic conductivity,

transmissivity, or permeability, permeability data are the fundamental property of the rock body and most easily converted to the physical dimensions of pores, fractures, or conduits. This work will assume that fractures are two dimensional features and conduits are conceptually one dimensional flow features.

Karstic carbonate rocks are one of the most heterogeneous and anisotropic of all formations found in nature, because the permeability structure of these formations are created by fluid flow generating a hierarchal rock structure of flow features that facilitates circulation in the downgradient direction (Mangin, 1975). Consequently, karst hydraulic parameters are not an independent, inherited static attribute of the rock, but rather are dynamic over geological time (Huntoon, 1985). Another consideration is that this structure can adjust as the flow regime responds to changing hydraulic boundary conditions. Thus, the hierarchy of permeability pathways and their organization within the formation are dictated by the hydrodynamic characteristics of the flow system operating within the recent geological past and, to a variable degree, the characteristics of older flow systems (Ewers, 1982).

The difficulties in the estimation of karst permeability are amplified by flow that may be non-Darcian, which leads to the cautious use of continuum estimations that assume Darcian flow. Depending on the dissolution feature size, causing locally high permeability, some standard aquifer tests may obtain no measurable drawdown as the test reaches the upper measurement limit, making calculations of transmissivity and hydraulic conductivity values only a lower bound estimate (Halihan et al., 1999). These factors resulting in uncertainties in making permeability estimates are a key factor to understand groundwater flow and solute transport in the subsurface (Quinlan and Ewers, 1985; Rehfeldt et al., 1989).

These formations and their heterogeneity can lead to well-known permeability scale effects (Ratz, 1967; Király, 1975; Maclay and Land, 1988; Hovorka et al., 1995; Halihan et al., 1999). Scale effects are generally defined as continual increases in permeability magnitude from small- to regional-scale estimates (Király, 1975; Schulze-Makuch et al., 1999). In the Király (1975) study, made in Mesozoic fractured and karstic limestone aquifers located in the Jura Mountains, Switzerland, it was hypothesized that the increase from small- to the well-scale was caused by fractures, and that the largest permeabilities on the regional-scale were caused by karstic conduits. Halihan et al. (2000) tested if the Király (1975) hypothesis has an underlying physical basis using a permeability database for the Cretaceous carbonates from the San Antonio segment of the Edwards aquifer and found that the Király hypothesis was applicable for that aquifer, with nine orders of magnitude variability in permeability. In another study, Clauser (1992), analyzing a compilation of different type of crystalline rocks, noted that the permeability can increase three orders of magnitude from small- to well-scale, but from well- to regional-scale, the increase would not continue, but the Halihan et al. (2000) model indicated that if larger fractures were present, the permeability would continue to increase with scale. Many of these approaches compiled permeability data at a range of scales, but few provide a physical basis for the values to allow increased predictability and scalability.

One approach to quantify the physical basis of the scale effect is via permeability combination models (PCM), providing estimates of the averaged permeability generated by a mixture of different permeable features in an aquifer, or the numerical effect of small-scale features on the well- or

regional-scale data (Halihan et al., 1998; 1999; 2000). These models are steady-scale geometric models that estimate the effects of different heterogeneities on formation permeability structure, assuming measurements on different scales are all valid estimates for the scale the data were collected. These models are modifications of equations for layered aquifers (Leonards, 1962; Fetter, 1994).

To predict formation values at the well-scale in a karstic formation, standard aquifer tests (slug tests, time-drawdown tests and step-drawdown tests) and the standard analytical equations (e.g. Theis, 1935; Cooper and Jacob, 1946), assuming Darcian flow, often provide reasonable fits to the data (Kresic, 2013). These estimates should be used with caution, due to anisotropic or potential non-Darcian conditions. Additionally, these estimates may not be valid on a regional-scale, due to scale dependency. In case of regions with limited pumping test data, but having specific capacity test data, an alternative method to estimate permeability from these data utilizes empirical relationships between transmissivity and specific capacity (Razack and Huntley, 1991; Mace 1997). In cases with no measurable drawdown occurring in a well, due to high permeability, a lower bound estimate can be obtained using a Thiem (1906) method (Halihan et al., 2000).

On the regional-scale, groundwater models can be used to obtain permeability estimates (Scanlon et al., 2001; 2003), but other analytical approaches are available as well. One of these other techniques is using a regional capture zone analysis, defined as the area of an aquifer in which all the water will be removed by a pumping well or wells within a certain time period (Todd, 1980; Grubb, 1993). In some cases, equations can be superimposed to calculate the capture zone of multiple well systems (Javandel and Tsang, 1986).

In this research, an evaluation of multi-scale permeability structure, estimating values of permeability at the small-, well-, and regional-scale (along with hydraulic conductivity and transmissivity) was conducted. These data were compared against observations of the physical size of permeable features, as well as calculations of the hydraulic dimension of fractures (hydraulic apertures) and conduits (hydraulic diameters). Combining different methodologies, a quantitative hydrogeologic conceptual model was developed, consistent across all scales of measurement. The aquifer studied was the Sete Lagoas karst aquifer (Pessoa, 1996), located within the limits of the municipality of Sete Lagoas, Minas Gerais, Brazil. This aquifer has common complications for karst systems with meter scale pores and some pumping tests that obtain no measurable drawdown. Quantifying these parameters through different scales is important because of the increasing demands on the aquifer, which require users to have a quantitative understanding of how the aquifer functions, so that it can be properly utilized and protected. For this, the PCM approach was utilized, comparing small-scale permeability data calculated by a permeameter with well-scale parameters calculated by standard pumping tests and an estimated regional-scale value, via capture zone analysis of a multiple pumping well system. These calculations were made to test possible correlations between different ranges of scale and quantify variations in the permeability scale effect. The hypothesis is that while values of permeability vary over many orders of magnitude, the hydraulic dimensions of flow features controlling permeability measurements would remain a consistent physically quantifiable dataset for the aquifer.

2. Site description

The aquifer studied was the Sete Lagoas karst aquifer (Pessoa, 1996), located in the municipality of Sete Lagoas, Minas Gerais, Brazil, 70 km northwest of Belo Horizonte, the state capital (Fig. 1). This municipality has a population greater than 200,000 over an area of 538 km^2 (IBGE, 2010). The greatest population density is located in the older urbanized areas of the city. The current water supply is almost entirely groundwater from the aquifer sourced from private and public wells. The public supply wells are managed by the Water Supply and Sewage Service (SAAE) [*SAAE - Serviço de Abastecimento de Água e Esgoto*]. The highest pumping rates are located in areas with the greatest population density (Fig. 1).

Geologically, the area is located in the São Francisco Craton, where carbonate argillo-arenaceous sediments are emplaced giving origin to the Bambuí Group (Branco and Costa, 1961; Oliveira, 1967; Schöll and Fogaça, 1973; Dardene, 1978; Schobbenhaus, 1984; Ribeiro et al., 2003; Tuller et al., 2010; Galvão et al., in press). The hydrostratigraphic relationships for the Sete Lagoas karst aquifer and spatial distribution are given in Pessoa (1996) and Galvão et al. (2015). The aquifer, which is approximately 75 meters thick, consists of Neoproterozoic limestones, composed of two members: the Pedro Leopoldo Member (at the base) and the Lagoa Santa Member (on the top), in which the primary porosity and matrix permeability can be considered low (Moore, 1989) and the secondary porosity is mostly filled by the precipitation of calcite (Tonietto, 2010). The majority of groundwater migrates through dissolution features characterized as tertiary porosity.

According to Galvão et al. (2015), results from geologic mapping and optical well logging suggest that the urbanized area of Sete Lagoas (Fig. 1) is primarily located in a graben, filled with limestones from Sete Lagoas Formation, overlying Cenozoic unconsolidated sediments, and occasionally covered by competent rocks from the Serra de Santa Helena Formation (slate, marble, siltstone and argillite). This setting results in fault bounded barrier boundaries for groundwater, which together with natural karst processes, explains the location of two dominant solutionally enlarged bedding planes in the Sete Lagoas formation with high permeability and significant storage capacity: 1) a shallower and thicker continuous dissolution zone with conduits that are 1-8 m thick, near the contact with the overlying unconsolidated sediments; and 2) 10-20 m below, a thinner continuous dissolution zone with conduits that are 20 cm to 1 m thick. These limestones dip and become thicker (reaching about 160 m thickness) and are completely covered by rocks from the Serra de Santa Helena Formation to the northeast. The two bedding plane conduits become thinner to the northeast.

The hydrogeologic conceptual model for the aquifer in the urbanized area includes both non-karstic and karstic bedding plane apertures based on optical well logs and outcrop field observations (Fig 2). This conceptual model is based on previous work conducted for a karst risk assessment (Galvão et al., 2015). The terms "non-karstic bedding planes" for zones without karstification, and "solutionally enlarged bedding planes" for dissolution zones will be used here.

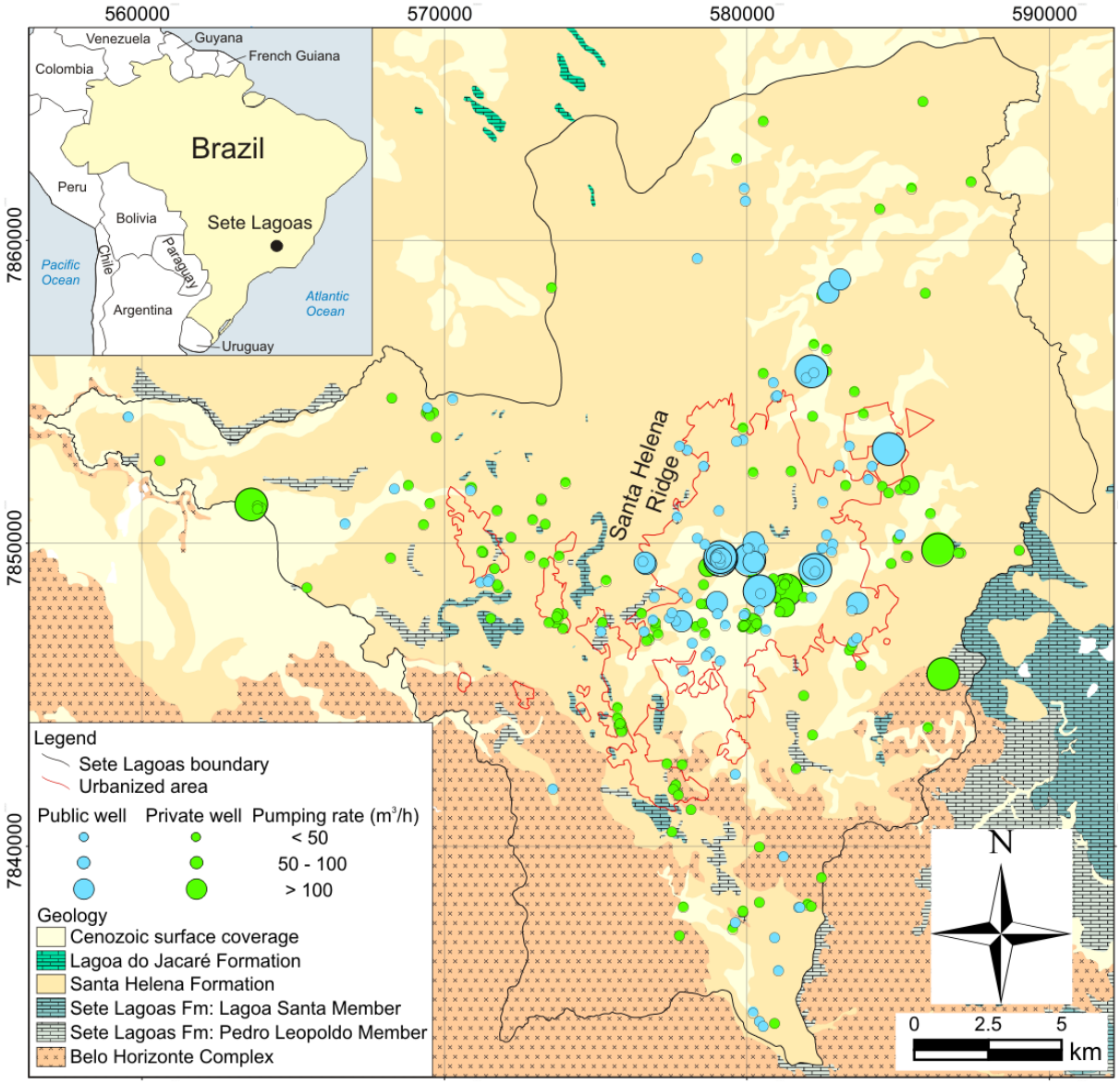

Fig. 1. Location map in UTM coordinates of Sete Lagoas showing the municipal boundary and urbanized area, the well locations (private and public) and the geology of the study area. The highest pumping rates are located in the areas with the greatest population density.

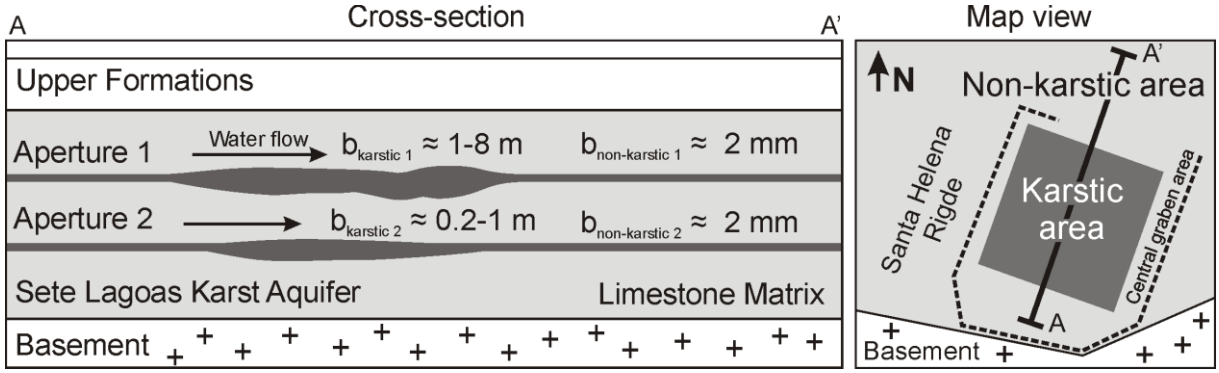

Fig. 2. Schematic of the hydrogeologic conceptual model of Sete Lagoas showing the non-karstic and the central solutionally enlarged bedding planes, based on optical well logs and field observations. The cross-sectional view (left) illustrates the relative location of the bedding planes and the map view (right) illustrates the karst zone in the central graben area, located in the central urbanized area seen in the Fig. 1. The conceptual hydraulic apertures of 1 mm in nonkarstified locations and 5 mm in karstified locations is based on the inversion of field permeability data.

3. Methods

The evaluation of scale effects in this research first involved building a database of permeability measurements from small- to regional-scales for the aquifer. Small-scale permeabilities were measured by means of a hand-held air permeameter. Well-scale evaluation utilized aquifer tests and a relationship derived between specific capacity and transmissivity. A regional-scale estimate utilized potentiometric surface measurements and a capture zone analysis.

Once the multi-scale database of permeability was available, empirical calculations were utilized to invert the database values to determine what size hydraulic features (i.e. pore diameter, fracture hydraulic aperture, or conduit hydraulic diameters) would be required to obtain measured field values of formation permeabilities. These inverted hydraulic values were utilized in a forward modeling PCM approach similar to Halihan et al. (1999) to test the stability of hydraulic features across the scales of data. These methods will be presented sequentially from the bulk permeability database to the inverted estimate of the size of hydraulic features, and finally the PCM forward modeling.

For this paper, the name of each order of magnitude for scale was based on Király (1975). These dimensions included: 1) small-scale from 10^{-2} to 10^{0} m, utilizing a rock matrix permeameter analysis; 2) well-scale between 10^{0} and 10^{2} m, by pumping test drawdown radius of influence; and 3) regional-scale from 10^{2} to 10^{4} m, according to the size of the capture zone analysis of the multiple pumping well system.

3.1. Permeability database

For this work, small-scale measurements utilize hand samples and thin sections of aquifer matrix. This measurement scale is occasionally divided by authors into a hand-scale and a micro-scale, but they are combined here to represent measurements of carbonate matrix pore properties. Well-scale data commonly are derived from aquifer tests. In this case, wells that have reached their testing measurement limit by not being able to draw down the water table are included in the analysis. Finally, while many authors utilize groundwater model data for regional estimates (Thorkildsen and McElhaney, 1992; Halihan et al., 2000; Scanlon et al., 2001; 2003), this work utilizes an analytical capture zone solution.

3.1.1. Small-scale: matrix data, optical microscopy analysis and permeability measurements

Field observations and optical microscopy using thin section for the two members of the Neoproteozoic limestone rocks from the Sete Lagoas karst aquifer were made in order to describe the features of the matrix, such as rock mineralogy, grain size and micro-fractures. To measure the permeabilities in the matrix of these members, a TinyPerm II portable hand-held air permeameter, manufactured by New England Research (NER), was utilized.

Permeability measurements were performed on dry hand samples of limestones sourced from the two members of the Sete Lagoas formation. The measurements were collected across dry, fresh and planar rock surface free of dust and without any weathering effects. Measurements (24 total) were taken to determine the mean small-scale permeability, k_{sm}, in darcys. These measurements were

converted to square meters, and then estimates of the small-scale hydraulic conductivity, K_{sm}, and transmissivity, T_{sm}, of the entire aquifer thickness were calculated. The advantage of this non-destructive method is the rapid and reproducible results (Fossen et al., 2011).

3.1.2. Well-scale: aquifer test data and empirical relationship analysis

Seven long duration (48 hours) transient pumping tests were conducted to measure the well-scale transmissivity, T_w [L^2/t], using the Theis (1935) method. Pumping rates ranged from 47 to 194 m^3/h. For the case of a zero drawdown well test in well PT-01, the Thiem equation (Thiem, 1906) was used for analysis by assuming 0.01 m (1 cm) of drawdown in the pumping well. This well and the observation wells at distances of 25 m and 51 m were located in the central portion of the urbanized area. This test involved pumping PT-01 at a constant rate, Q_w [L^3/t], of 130 m^3/h (see Table S1 in the electronic supplementary material (ESM) for more information about pumping wells, well coordinates, and respective pumping rates and observation wells).

Twenty-seven time-drawdown or step-drawdown tests to estimate specific capacity, S_C [L^2/t], were made utilizing the SAAE's supply wells. In mathematical terms, S_C is defined as the pumping rate in the well, Q_w [L^3/t], divided by the observed decline in hydraulic head in the well, Δh_w [L], from an aquifer test. In the case of the step-drawdown tests, every discharge value was divided by its respective drawdown, Δh_w, observed in each step, and then the mean S_C was calculated. These results were analyzed by an empirical relationship derived for this karst aquifer by fitting a power law function between measured specific capacity and transmissivity, based on the Razack and Huntley (1991) and Mace (1997) methods. The goal was to estimate the most representative well-scale transmissivity, and then estimate the well-scale hydraulic conductivity, K_w [L/t], both in non-karstic and solutionally enlarged bedding planes, to estimate the well-scale permeability. Information about the physical thickness of bedding planes, b_w [L], were taken via optical well logging and outcrop field observations (Galvão et al., 2015).

A transmissivity map was constructed from the data to observe the variability at the regional scale from well scale data (Fig. 4). For this, T_w values were utilized assuming the long duration pumping test data were more accurate data than the empirical values from specific capacity data. It was assumed that the values that were found in the observation wells for their respective pumping wells were located in the same hydrogeologic setting (Table S1 in the electronic supplementary material (ESM)).

3.1.3. Regional-scale: potentiometric data and capture zone analysis

To develop a potentiometric map for regional-scale permeability evaluation, measurements of the water table were taken only in SAAE's supply wells in the Sete Lagoas karst aquifer. The well casing elevation data were acquired using a SRTM image (Shuttle Radar Topography Mission). According to Demétrio et al. (2006), the accuracy in the use of this data is less than 5 m, which makes the data a viable and economical source.

A capture zone analysis for the central high pumping rate well area was performed and an assessment of the accuracy of the analytical results was estimated. For this, some assumptions were made, such as pumping wells in a confined aquifer with a uniform flow, under steady-state conditions.

From the potentiometric map, a capture zone area was determined, based on estimated flow lines in the potentiometric surface. Based on this geometry, analytical equations derived for confined aquifers by Todd (1980) and Grubb (1993) delineating the edge of the capture zone were used to estimate the regional-scale transmissivity, T_r [L^2/t]:

$$T_{r,x} = -\frac{Q_r}{2\pi X_L i} \quad (1)$$

$$T_{r,y} = \pm\frac{Q_r}{2Y_L i} \quad (2)$$

where $T_{r,x}$ and $T_{r,y}$ [L^2/t] are the regional transmissivities in their respective directions, Q_r [L^3/t] is the overall pumping rate or regional discharge rate, X_L [L] is the distance from the pumping well to the downgradient edge of the capture zone (stagnation point), Y_L [L] is the half width of the maximum capture zone, and i [dimensionless] is the hydraulic gradient.

The regional discharge rate, Q_r, was estimated by summing the pumping rate data values from public supply wells (data provided by SAAE and Servmar Environmental & Engineering) and private wells (data acquired from the SIAGAS's database - SIAGAS, 2006) extracting groundwater within the capture zone. The next step was to estimate the transmissivity, T_r, based on the best fit-empirical capture zone in comparison to the potentiometric capture zone, using the equation that describes the empirical edge of the capture zone for a confined aquifer:

$$x = \frac{-y}{\tan\left[\frac{2\pi T_w i y}{Q_r}\right]} \quad (3)$$

where x [L] is the distance parallel to the regional hydraulic gradient and y [L] is the distance perpendicular to the regional hydraulic gradient (Todd, 1980; Grubb, 1993). A sensitivity analysis was conducted to evaluate the variability possible in this approach.

The final T_r was considered the average of both analytical values calculated, while the regional-scale hydraulic conductivity, K_r [L/t], was calculated by dividing these transmissivity values by the total thickness, b_{total} [L] (estimated at 75 m), and then converted the values to permeability in square meters.

Finally, all these permeability data sets were entered in a GIS database and georeferenced in the ArcGIS 10.1 software. The coordinate system was Universal Transverse Mercator (UTM) projection, Zone 23, datum SAD 69, with units in meters. Data from optical well logs and analytical calculation results were considered to estimate the physical sizes of the dissolution zones, b_r [L]. These values allowed a comparison between observed physical apertures and inverted hydraulic apertures for the various data.

3.2. Permeability component data

In order to test the stability of permeability feature sizes across various scales of measurement, permeability data were inverted to determine the physical size of hydraulic features that would be capable of producing the various permeability values. This included calculating the hydraulic size of fracture apertures and conduit diameters, both under assumed laminar and turbulent flow conditions.

3.2.1. Sub-horizontal fracture hydraulic apertures

The conversion between permeability values and the size of a sub-horizontal fracture was calculated using the cubic law (Lamb 1932) allowing a relationship between the intrinsic permeability of a fracture, k_f, [L^2] and a fracture hydraulic aperture, b_f [L]:

$$k_f = \frac{{b_f}^2}{12} \tag{4}$$

This relationship allows the conversion between measured permeability values and physical feature size. It is only an approximation in that it does not accommodate for fracture plane roughness and variability in fracture geometry.

The hydraulic fracture aperture was calculated from transmissivity or conductivity data from aquifer tests using the hydraulic aperture of a single low-angle fracture equation (Halihan et al. 1999), b_f [L]:

$$b_f = \left[\left(\frac{12v\cos(\theta)}{g}\right)(T_w - K_{sm}b_{total})\right]^{1/3} \tag{5}$$

where υ is the kinematic viscosity of the water [L^2/t], T_w is the well-scale transmissivity [L^2/t] calculated by pumping test, K_{sm} is the small-scale hydraulic conductivity of the matrix [L/t], b_{total} is the total thickness of aquifer [L], g is gravitational constant [L/t^2], and θ is the angle between the fracture and the horizontal plane, which is zero if the fracture is horizontal.

3.2.2. Hydraulic conduit diameters

The hydraulic conductivity of a conduit, K_c [L/t], can be related to a conduit hydraulic diameter assuming both laminar and turbulent flow (Halihan et al. 1998). These hydraulic conductivity equations can also be converted to permeability, but to illustrate the turbulent case, hydraulic conductivity is simpler to illustrate. The laminar hydraulic conductivity, $K_{c,lam}$ [L/t]:

$$K_{c,lam} \cong \frac{g{d_c}^2}{32v} \tag{6}$$

For turbulent hydraulic conductivity $K_{c,turb}$ [L/t]:

$$K_{c,turb} \cong 4.706\frac{g^{\frac{4}{7}}}{v^{\frac{1}{7}}}\left(\frac{d_c}{2}\right)^{\frac{5}{7}} \tag{7}$$

To estimate the hydraulic conduit diameter, d_c [L], from aquifer tests, the single horizontal conduit equation was utilized (Halihan et al. 1999), assuming the hydraulic conductivity of the matrix is much less than the hydraulic conductivity of the conduit, K_c:

$$K \cong \frac{K_c d_c}{b_{total}} \Rightarrow d_c \cong \frac{K b_{total}}{K_c} \Rightarrow d_c \cong \frac{T_w}{K_c} \tag{8}$$

Substituting d_c in the equation (6), to estimate the laminar hydraulic conduit diameter, $d_{c,lam}$ [L]:

$$d_{c,lam} \cong \left(32T_w\frac{v}{g}\right)^{\frac{1}{3}} \tag{9}$$

Substituting d_c in the equation (7), to estimate the turbulent hydraulic conduit diameter, $d_{c,turb}$ [L]:

$$d_{c,turb} \cong \left(\frac{T_w\frac{v^{\frac{1}{7}}}{g^{\frac{4}{7}}}0.349}{}\right)^{\frac{7}{12}} \tag{10}$$

The use of these equations allows permeability data from the range of scales to be inverted into a hydraulic feature size. These estimates should be smaller than the physical size of the features estimated from optical logging or outcrop evaluation, as they are hydraulic dimensions, not physical ones. This set of equations allowed inversion of the permeability database and the same concept can be used to generate forward models for evaluation of permeability scale effects.

3.3. Permeability combination models

For the permeability combination forward model approach (PCM) to evaluate the scale effects in the karst aquifer, the analytical models developed for small- to regional-scale were combined and compared. These models are steady state and modifications of equations for layered aquifers. In addition, others assumptions were used to simplify the models, such as: 1) the hydraulic conductivity of the matrix is much less than the hydraulic conductivity of the fracture/conduit (this can be evaluated by utilizing the permeability database); and 2) according to Galvão et al. (2015), the solutionally enlarged bedding planes are continuous permeable features controlling the hydraulic system, where sub-vertical fractures do not have significant influence on permeability structure across the scales of measurement.

For the inverted hydraulic dimensions, the equations used to estimate the values for each scale were: equation (4) at the small-scale; equations (5), (9) and (10) at the well-scale for both laminar and turbulent flow; and the respective equations (4), (9), and (10) were assumed to estimate the hydraulic dimensions at the regional-scale.

4. Results

The results will be presented sequentially from the bulk permeability measurements, to the inverted estimate of the size of hydraulic features, and finally the PCM results.

4.1. Sete Lagoas permeability database

The permeability database for Sete Lagoas illustrates that permeability values do not always increase with scale. A figure illustrating the Sete Lagoas permeability scale effect, compared against the Király (1975), Clauser (1992) and Halihan et al. (2000) studies, as well as with igneous rock, limestone, karst, and gravel permeabilities (Heath, 1983) was generated to illustrate the effect in comparison to other carbonate aquifers (Fig. 6).

4.1.1. Small-scale analysis and measurements

Optical microscopy analysis indicates the Neoproteozoic limestones from the Pedro Leopoldo Member (at the base) and the Lagoa Santa Member (on the top) are low permeability competent bedrock, with the secondary porosity (i.e. micro-fractures) generally filled by calcite. The rocks from Pedro Leopoldo Member are composed of 85% micrite, 8% sparite and 7% quartz, classified as micrite (Folk, 1959) or mudstone (Dunham, 1962), while the rocks from Lagoa Santa Member are 55%

sparite, 30% ooids, and 15% micrite, classified as an oobiosparite (Folk, 1959) or grainstone (Dunham, 1962). These low porosity limestone features are in accordance with Moore (1989) and Tonietto (2010).

Hand sample TinyPerm measurements indicate no significant differences in permeability between the Pedro Leopoldo and Lagoa Santa members. The matrix permeabilities in the Sete Lagoas Formation, combining both members, range from 1.9 x 10^{-16} to 4.2 x 10^{-15} m^2. This results in hydraulic conductivity values, K_{sm}, between 1.6 x 10^{-4} and 3.5 x 10^{-3} m/d (1.9 x 10^{-9} to 4.1 x 10^{-8} m/s). The matrix transmissivities, T_{sm}, based on the mean total thickness of aquifer, b_{total} = 75 m, are between 1.2 x 10^{-2} and 2.6 x 10^{-1} m^2/d (1.4 x 10^{-7} to 3.1 x 10^{-6} m^2/s) (Table S2 of the ESM). These measurements are in accordance with values for limestone in other settings (Freeze and Cherry, 1979), where permeability values of the matrix for limestone are approximately 10^{-13} to 10^{-16} m^2 and the hydraulic conductivities are between 10^{-6} and 10^{-9} m/s. The results are on the lower end of the range, but the values are consistent for limestone with secondary calcite precipitation.

4.1.2. Well-scale: aquifer test data and empirical relationship analysis

The seven long duration transient pumping tests that were conducted in wells with karst bedding planes indicated a range of well-scale transmissivities (T_w) from 90 m^2/d, in the northeast region, to around 3600 m^2/d, close to the Santa Helena Ridge foothills. Wells tested in the central urbanized area also showed high T_w values, above 1500 m^2/d, while wells located in the northeast region, generally, indicated low values, below 500 m^2/d (Table S1 of the ESM). The well-scale hydraulic conductivity values found (K_w) are in accordance with the T_w results, showing high values in the central area and low numbers in the northeast region (Table 1).

In a particular pumping test, conducted in the PT-01, central area, no drawdown was observed. For this zero drawdown well, the Thiem equation was used to estimate a transmissivity value (Table S1 of the ESM). Using a pumping rate of 130 m^3/h from the test, and assuming a drawdown of 0.01 m (1 cm), and the respective distances of 25 and 51 m of the piezometers PT-02 and PT-03 from the pumping well PT-01, the result showed a transmissivity of 6 x 10^4 m^2/d (6 x 10^{-1} m^2/s). This would results, based on an aquifer thickness of 75 m, in a local hydraulic conductivity of 700 m/d (8 x 10^{-3} m/s), and a permeability of 8 x 10^{-10} m^2. The uncertainty in these calculations may limit them as permeability data, but ignoring them adds bias. These data represent the highest well permeabilities in the aquifer and are 5 orders of magnitude above the highest small-scale measurements.

The results of the specific capacity test analysis indicated results similar to previous research (Razack and Huntley, 1991; Mace, 1997). A plot of the logarithms of transmissivity and specific capacity values for the Sete Lagoas karst aquifer appears linear in log-log space (Fig. 3). The best-fit line to these data was:

$$T_w = 330(S_c)^{0.21}$$

where T_w and S_c are in m^2/d. The coefficient of determination, R^2, was 0.55.

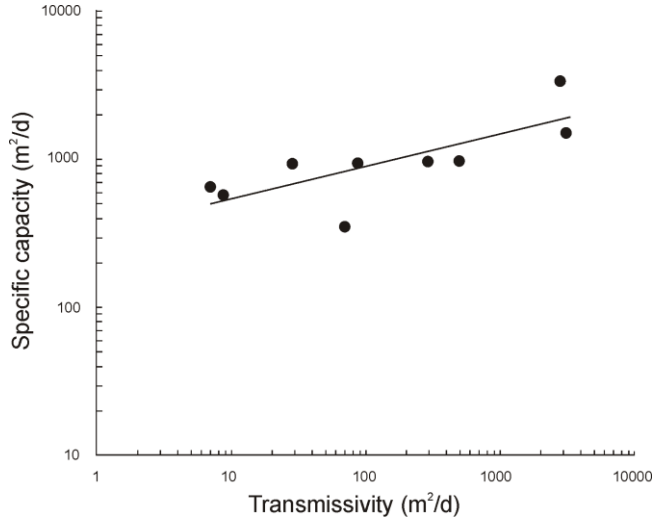

Fig. 3. Relationship between specific capacity and transmissivity values for the Sete Lagoas karst aquifer, showing the best-fit line.

To evaluate if this empirical equation was reliable, a T_w recalculation was made and compared to the T_w values obtained in the seven pumping tests (Table S1 of the ESM). This comparison showed reasonable results, generally of the same order of magnitude, which was expected due to some inherent uncertainties of this method (Razack and Huntley, 1991; Mace, 1997).

Utilizing the best T_w data over the various portions of the aquifer (Table 1 and Table S2 of the ESM), a transmissivity map was made (Fig. 4). The highest well-scale transmissivities, T_w = 1,500 - 3,600 m^2/d (1.7 x 10^{-2} - 4.1 x 10^{-2} m^2/s) and the zero drawdown well test (located in the area of the solutionally enlarged bedding plane) are concentrated in the central area, within the graben area and close to the Santa Helena Ridge foothills. A decrease in these values occurs in the northeast direction, T_w = 90 - 250 m^2/d (1.1 x 10^{-3} - 2.9 x 10^{-3} m^2/s) (Fig. 4). These values coincide with the optically observed fracture apertures of the solutionally enlarged bedding planes described by Galvão et al. (2015), where the thicker apertures are located in the central graben area and close to the Santa Helena Ridge foothills.

These data suggest a direct relationship between karstified fracture apertures and high well transmissivities. In the case of K_w, dividing both results from the central and the north portions by the respective thickness of the aquifer, the hydraulic conductivity values range from 1 to 36 m/d (1.2 x 10^{-5} - 4.2 x 10^{-4} m/s) (Table 1 and Table S2 of the ESM). This would result in well-scale permeability, k_w, values of 1.2 x 10^{-12} and 4.2 x 10^{-11} m^2, respectively. These results represent an increase of 2 to 4 orders of magnitude above the highest small-scale permeability values.

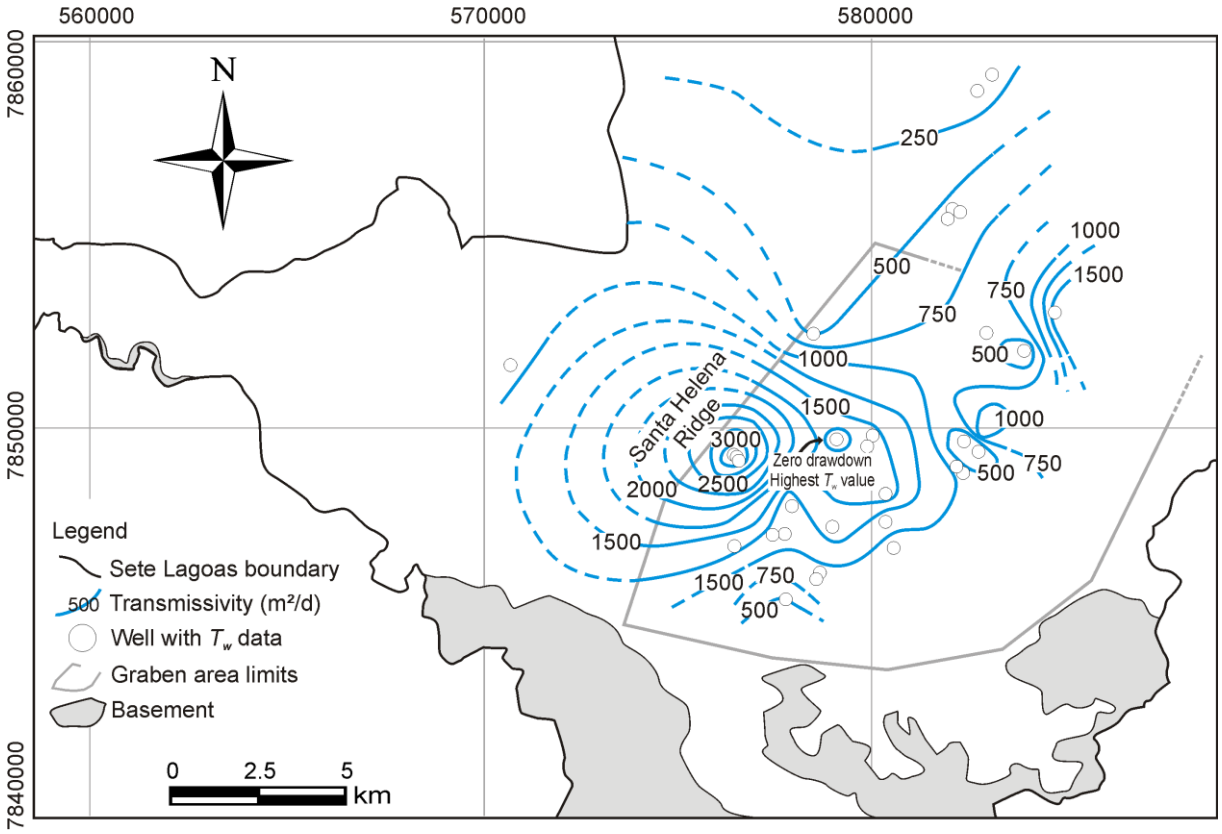

Fig. 4. Well-scale transmissivity map showing the variation of transmissivity, which the highest values are concentrated in the central area, close to the Santa Helena Ridge foothills, and in the eastern portion of the city. The majority of these high values are located within a central graben area, including the "zero drawdown well" controlled by the solutionally enlarged bedding planes. The dashed lines indicate uncertainties. The graben area boundary was based on the delineation of Galvão et al. (2015).

4.1.3. Regional-scale: potentiometric data and capture zone analysis

To estimate the regional-scale permeability, a capture zone method in a multiple well system was applied. According to the potentiometric data and approximate flow lines (Fig. 5), the Santa Helena Ridge is a watershed boundary, where the eastern portion of the map has the groundwater flowing to the northeast, while the western portion has the groundwater flowing to the northwest. In the central area, there is a flow convergence, generated by a considerable cone of depression, explained by the high pumping rate in the central wells. In this specific area, a capture zone was recognized (Fig. 5a).

Utilizing equations (1) and (2), with a stagnation point (X_L) = - 2,000 m; half width of capture zone (Y_L) =± 4,000 m; regional pumping rate (Q_r) = 75,000 m^3/d; and hydraulic gradient (i) = 0.008 (Fig. 5a, b), the analytical regional-scale transmissivities, T_r [L^2/t], were estimated:

$$T_{r,x} = -\frac{75{,}000}{2 * 3.1416 * (-2{,}000) * 0.008} \cong 750\ \mathrm{m^2/d}\ (8.7 \times 10^{-3}\ \mathrm{m^2/s})$$

$$T_{r,y} = \pm\frac{75{,}000}{2 * 4{,}000 * 0.008} \cong 1{,}170\ \mathrm{m^2/d}\ (1.3 \times 10^{-2}\ \mathrm{m^2/s})$$

With transmissivities between 750 and 1,170 m^2/d, this would results in an analytical regional-scale hydraulic conductivities from 10 to 16 m/d (1.2 x 10^{-4} - 1.8 x 10^{-4} m/s) and regional-scale

permeabilities of 1.2 x 10^{-11} - 1.8 x 10^{-11} m^2. This represents a three order of magnitude increase over the small-scale measurements, but a decrease relative to many of the well-scale data.

To evaluate the possible variability using this analytical methodology, a sensitivity analysis was conducted adjusting T_w values within this capture zone, found in the Fig. 4 (T_w = 700 - 1,000; 3,000 m^2/d) to assess the relative accuracy (Fig. 5c). The best-fit empirical capture zone was found with a transmissivity = 900 m^2/d (1.1 x 10^{-2} m^2/s - see black continuous and dashed lines on Fig. 5c), which would result in a hydraulic conductivity of 12 m/d (1.4 x 10^{-4} m/s) and permeability of 1.4 x 10^{-11} m^2. The calculation of the best-fit empirical capture zone can be seen below:

Part A: half width of the capture zone, X_L [L]:

$$Y_L = \pm\frac{75{,}000}{2 * 900 * 0.008} \pm 5{,}210 \text{ m}$$

Part B: distance to the stagnation point, X_L [L]:

$$X_L = -\frac{75{,}000}{2 * 3.1416 * 900 * 0.008} \cong -1{,}660 \text{ m}$$

Part C: shape of the curve describing the capture zone, x [L]. The following values are for one-half of the capture zone, which is symmetrical about the x-axis:

$$x = \frac{-y}{\tan\left[\frac{2 * 3.1416 * 900 * 0.008y}{75{,}000}\right]} = -y/\tan\left(0.000603y\right)$$

In the case of a possible lower estimate of pumping rate value from private wells that perhaps were not included in the analysis (no data or not being registered) and, thus, not added to the final Q_r value used in the calculations above, a sensitivity analysis also tested the effects of pumping rate (Fig. 5d). The transmissivity was fixed at 900 m^2/d (best-fit) adjusting only the pumping rate. The result showed that, using Q_r = 100,000 m^3/d, the value of X_L had no significant change, while Y_L had a small change. Now, using Q_r = 50,000 and 150,000 m^3/d, there was a significant change, both in $X_{L\ and}$ Y_L. However, if some private wells data have not been included, the majority are residential wells, with lower pumping rates, which is not significant in the total sum of Q_r. The public wells located within the captured zone that were included in the analysis represent the highest pumping rates and have the greatest impact on the discharge value used in the equations.

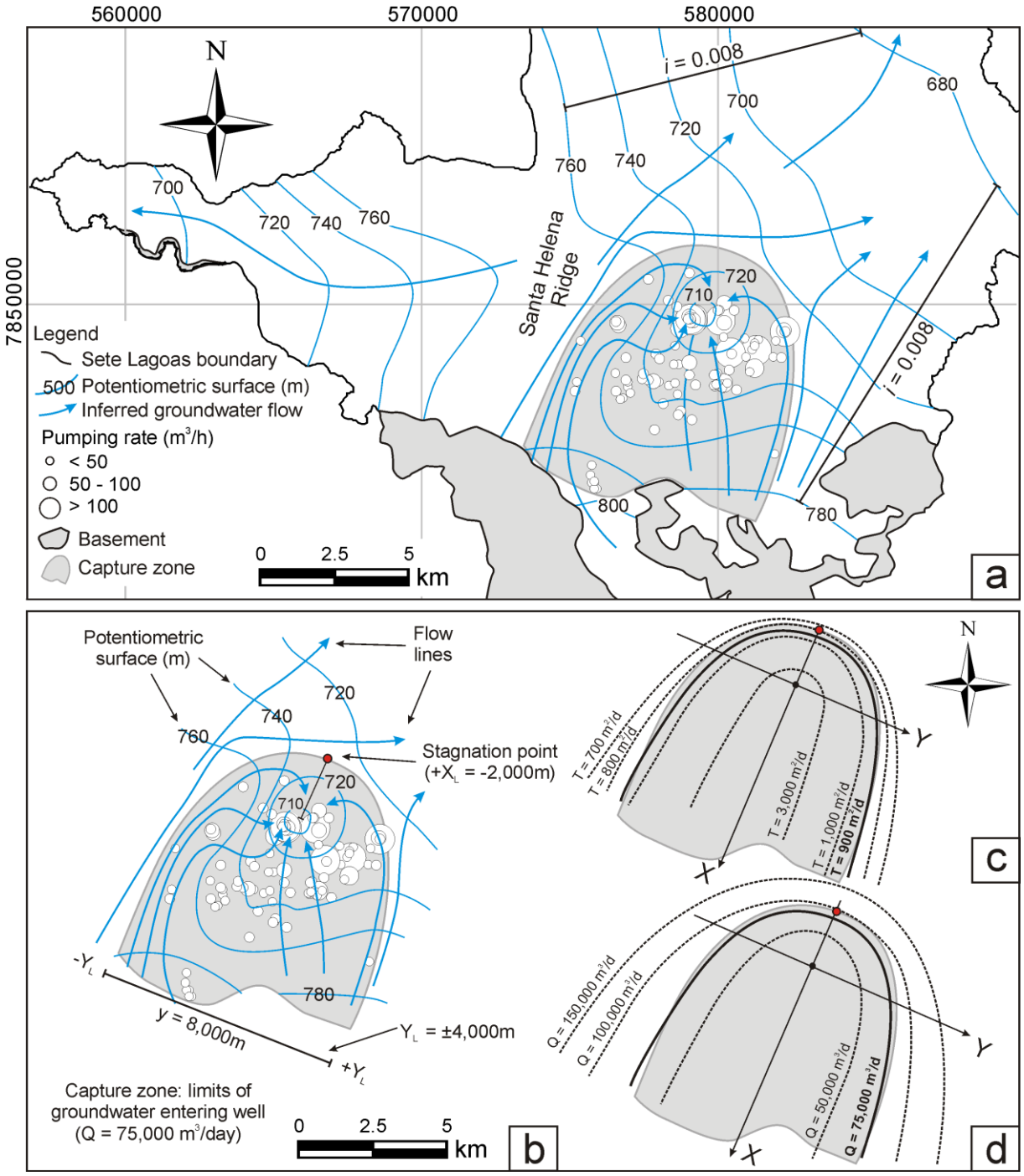

Fig. 5. Regional-scale permeability evaluation of Sete Lagoas. (a) Potentiometric surface map, flow lines, and capture zone. (b) Description of the capture zone model shape, its parameters and respective variables. (c) Comparison between the best-fit empirical capture zone curves (black continuous and dashed lines) and the potentiometric surface capture zone (grey area) assuming variations in the regional-scale transmissivity. (d) Sensitivity analysis using different discharge values for a regional-scale transmissivity = 900 m^2/d. Note that the *x*-axis has been aligned with the regional groundwater flow direction.

4.2. Permeability feature sizes from inversion

4.2.1. Small-scale: matrix data and feature sizes

According to permeameter and microscopy analysis for these types of lithologies, the permeability of the matrix is between 10^{-16} and 10^{-15} m^2, classified as low permeability competent

bedrock, with the secondary porosity generally filled by calcite. The hydraulic fracture aperture, b_{sm}, required to generate this level of permeability would be considered between 10^{-8} and 10^{-7} m (or 0.01 and 0.1 μm). These values are in accordance with values for limestone pore diameters of the matrix, ϕ_{sm}, around 0.1 μm (Zinszer and Pellerin 2007).

4.1.2. Well-scale permeable feature sizes

Using empirical hydraulic equations for estimating sub-horizontal fracture apertures, the results analyzed for each well showed that the hydraulic fracture aperture, b_f, has a range of 1 - 4 mm. For the estimated hydraulic conduit diameter, assuming laminar flow, $d_{c,lam}$, the result is between 2 - 5 mm, while assuming turbulent flow, the hydraulic conduit diameter, $d_{c,turb}$, ranges from 2 to 13 mm (Table 1). The mechanical apertures seen in the optical well logs showed local values between 0.2 m and 8 m, which illustrates a large difference between hydraulic and physical feature size, with hydraulic sizes being orders of magnitude smaller. These empirical hydraulic values are a combination of both the flow from the upper and lower bedding planes, as the values of T_w used in the equations (5), (9) and (10) were from pumping tests simultaneously extracting water from the two bedding planes.

4.1.3. Regional-scale: overall bedding planes and karst aquifer thicknesses

Using values of T_r found via regional capture zone method to estimate the values of regional hydraulic fracture aperture, laminar and turbulent conduit in that range, the respective equations (4), (9), and (10) were assumed. The combined results ranged between 2 to 6 mm (fracture aperture: 2 - 3 mm, laminar flow conduit: 3 - 4 mm, and turbulent flow conduit: 5 - 6 mm), slightly lower than the well-scale hydraulic size.

4.3. Permeability combination model

Combining different approaches for different scales, according to the basic model of two bedding planes (Fig. 2), it was possible to accommodate appropriately the small-, well-, and regional-scales of measurement and compare the values against a conceptual model of hydraulic features. These forward models were used to test whether the hydraulic feature sizes of the inverse conceptual model could be extended across the scale of measurements for a single quantitative conceptual model for the aquifer. For the Sete Lagoas permeability combination model, the only significant permeable features were the two solutionally enlarged bedding planes in the aquifer. The model assumes that the measured permeabilities at the various scales are valid estimates of permeability at each scale.

At the small-scale, the mean permeability of the matrix is very low (from 10^{-16} to 10^{-15} m^2) (Fig. 6), because the matrix is composed of a Neoproterozoic fine-grained (Pedro Leopoldo Member, at the base) and a medium-grained (Lagoa Santa Member, on the top) limestone, with the secondary porosity (micro-fractures) generally filled by calcite. Relative to the bedding plane features, these values can be approximated on time scales for pumping or regional flow estimates as zero. For the simple conceptual model across the scales, a value of 10^{-15} m^2 was assumed to represent the matrix permeability.

In the case of well-scale permeability features, an increase of between four and six orders of magnitude in comparison to the matrix (10^{-12} - 10^{-10} m^2) is noted (Fig. 6), due to the solutionally enlarged bedding planes. Regarding the zero drawdown wells, the result showed permeability around 10^{-9} m^2. The inversion indicates that these can be simulated as a single hydraulic fracture that is 1 - 2 mm in size in the non-karstified bedding plane regions (values from fracture apertures) and 2 - 13 mm in size in the karstified region depending (values from laminar, 2 - 5 mm, and turbulent conduit diameters, 2 - 13 mm) on whether the model allowed for turbulent flow (Table 1). For the simple conceptual model for the system, a non-karstic fracture with a 1 mm aperture and a karstic fracture with a 5 mm aperture were assumed. At the well-scale in a 75 meter thick aquifer, these fractures yield permeabilities of 10^{-12} m^2 in non-karstic areas and 10^{-10} m^2 in karstic areas.

At the regional-scale, the values of permeability have a slightly smaller value in comparison to the largest well-scale values. The regional-scale permeability was approximately 10^{-11} m^2 (Fig. 6). The inverted permeability sizes were 2 - 6 mm though, consistent with the non-karstic and karstified bedding plane estimate at the well-scale. For the simple conceptual model of the system at the regional-scale, the regional value of permeability was 10^{-11} m^2 for the area encompassed by the capture zone analysis. This estimate can be reached by assuming a 2 mm fracture existing over the regional-scale, or by constructing the regional permeability from the well-scale permeabilities. Using the two well-scale permeabilities from the simple model of 1 and 5 mm fractures, the karstic zone in the center of the pumping area can be modeled as a layered aquifer averaging the flow with the result being similar to the larger value. When the lower value is utilized near the southwest portion of the aquifer, this would be flow across the layers, resulting in a value similar to the lower value. With reasonable approximations for karstic and non-karstic zones, this again results in a regional permeability of 10^{-11} m^2.

Table 1. Values of sub-horizontal fracture aperture, hydraulic conduit diameter in laminar and turbulent flow and its respective *K* and *T* values. Zero drawdown pumping test not included.

	Measurement				
	Well-scale Transmissivity adopted (m^2/d)	Well-scale Hydraulic conductivity (m/d)	Estimated fracture aperture (m)	Estimated conduit diameter assuming laminar flow (m)	Estimated conduit diameter assuming turbulant flow (m)
	Method / Equations				
Well ID	Most representative	$K = T_w/b_m$	$b_f = [(12u.\cos(\theta)/g).(T_w - K_m.b_m)]^{1/3}$	$d_{c,lam} = (32.T_w.u/g)^{1/3}$	$d_{c,turb} = (T_w.u^{1/7}/g^{4/7}0.349)^{7/12}$
PT-12	1550	19	2.8	3.9	7.7
PT-13	1550	19	2.8	3.9	7.7
PT-18	1620	20	2.8	3.9	7.9
PT-19	980	12	2.4	3.3	5.9
PT-21	980	12	2.4	3.3	5.9
PT-22	330	3.7	1.7	2.3	3.1
PT-24	1590	18	2.8	3.9	7.8
PT-25	330	3.7	1.7	2.3	3.1
PT-28	1100	18	2.5	3.5	6.3
PT-29	3190	32	3.6	4.9	12
PT-30	3590	36	3.7	5.1	13
PT-36	1320	17	2.7	3.7	7.0
PT-39	940	16	2.4	3.3	5.7
PT-40	940	16	2.4	3.3	5.7
PT-41	980	16	2.4	3.3	5.9
PT-45	440	7.3	1.8	2.6	3.7
PT-46	1020	26	2.4	3.4	6.0
PT-47	1210	30	2.6	3.6	6.6
PT-48	1490	25	2.8	3.8	7.5
PT-51	930	16	2.4	3.3	5.7
PT-52	1025	17	2.4	3.4	6.0
PT-57	450	7.5	1.9	2.6	3.7
PT-63	580	8.3	2.0	2.8	4.3
PT-64	580	8.3	2.0	2.8	4.3
PT-66	650	9.3	2.1	2.9	4.6
PT-73	545	5.5	2.0	2.7	4.2
PT-74	1820	18	3.0	4.1	8.4
PT-77	840	8.4	2.3	3.2	5.4
PT-92	130	1.0	1.2	1.7	1.8
PT-93	90	0.69	1.1	1.5	1.5
PT-99	855	21	2.3	3.2	5.4
PT-105	3190	32	3.6	4.9	12

Hydraulic conductivity of the matrix (K_m) = 10^{-8} m/s

$\cos(\theta)$ = 1 or θ = 0 degrees, horizontal fracture

Kinematic viscosity (u) = 10^{-6} m^2/s

Gravitational constant (g) = 9.81 m/s^2

Assuming $K_{matrix} << K_{conduit}$

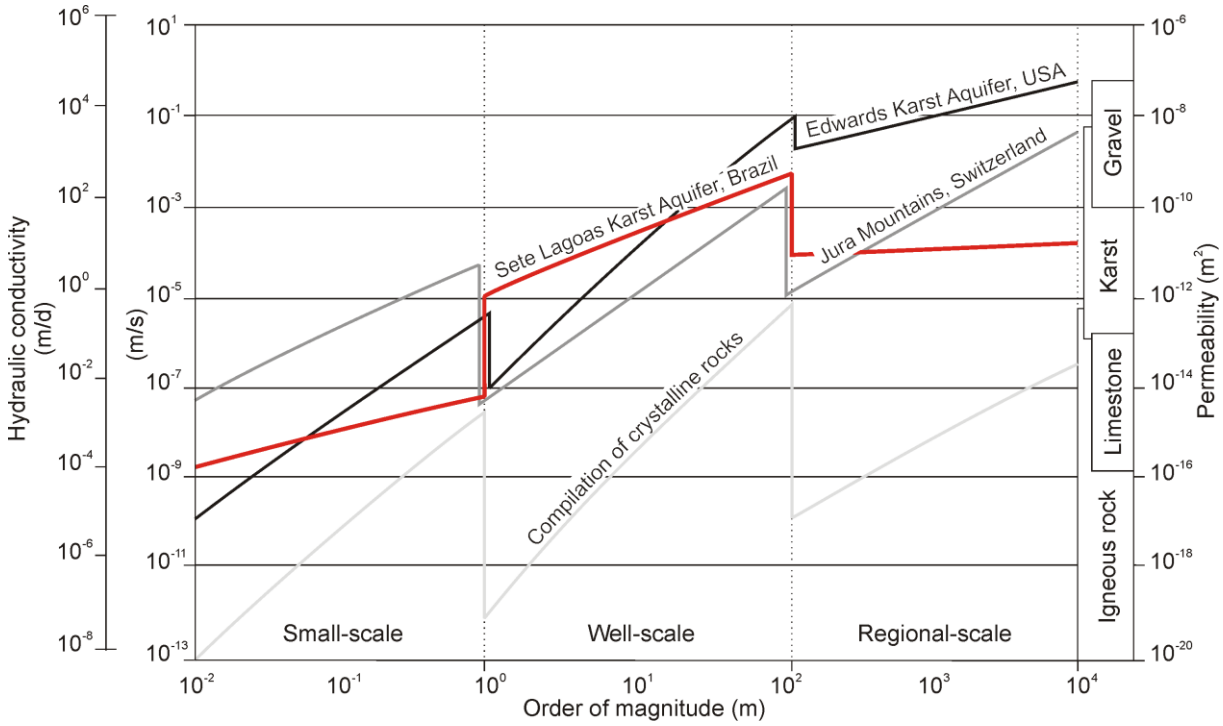

Fig. 6. Permeability scale effects in the Sete Lagoas karst aquifer (red line) in comparison with other carbonate scale effect studies and with permeability ranges for various lithologies (Heath 1983). The scale effect of the study area presents an increase of hydraulic conductivities from small- to well-scale and a decrease of these values from well- to regional-scale, having similar behavior with the compilation of crystalline rocks scale effects (Clauser 1992 - grey line). In the case of Edwards aquifer scale effect line (Cretaceous limestones and dolomites from San Antonio segment, Halihan et al. 2000 - black line) and the Jura Mountains scale effect line (Mesozoic fractured and karstic limestone aquifers, Király 1975 - dashed grey line) significant increases in permeabilities across scales are observed.

5. Discussion

A schematic scale effect conceptual model block diagram for Sete Lagoas karst aquifer was made (Fig. 7) to show how a simple model of hydraulic feature size affects each scale, considering permeabilities measured and the inverted hydraulic feature size. The changes in permeability (*k*) or associated hydraulic values (*K*, and *T*), the respective size permeable features from small- to well-scale, and a decrease of these values in some areas from well- to regional-scale were quantitatively observed for the aquifer, both through the inversion of field measurements and the forward modeling of a simple conceptual model with a single fracture of both karstic and non-karstic settings.

The porosity and permeability, as well as the aperture of the fractures in the matrix are very low. Thus, the hydraulic conductivity of the matrix is much lower than the hydraulic conductivity of the bedding planes intercepted at the well-scale. Increases between four and six orders of magnitude in the parameters from small- to well-scale were observed. However, from well- to regional-scale, the increase did not continue, having a small decrease in the values (Figs. 6 and 7). The same behavior in the empirical size permeable features was observed, where values of hydraulic aperture of 0.01 - 0.1 μm (small-scale) are increasing to 2 - 13 mm (well-scale) and decreasing to 2 - 6 mm (regional-scale). These inverted hydraulic sizes are significantly smaller than outcrop fracture or conduit sizes consistent with previous investigations based on connectivity and fracture variability.

These quantitative relationships between feature size and hydraulic properties showed that, unlike other karst areas have increases in permeability in scale effects from small- to regional-scale, such as Edwards Aquifer located in the United States (Halihan et al., 2000) and Juras Mountain in Switzerland (Király, 1975), this behavior does not happen in Sete Lagoas karst aquifer in Brazil (Fig. 6). The relationships are in accordance with Clauser (1992) results, where permeabilities increase from small- to well-scale, but from well- to regional-scale they do not continue. The difference is that the effects that Clauser (1992) observed happened in crystalline rock (Fig. 6). According to Király (1975) and Halihan et al. (2000), increase from small- to the well-scale are caused by fractures being incorporated into the well-scale measurements of permeability, and the largest permeabilities on the regional-scale were caused by karstic conduits being incorporated. This increase can obtain nine orders of magnitude variability (Halihan et al., 2000) (see Edwards aquifer scale effect line on Fig. 6). This can be interpreted that the scale effect and dependency in karst aquifers is more related to fracture and conduit connectivity.

In the study area, based on the geologic mapping and optical well logs data (Galvão et al., 2015), the sub-horizontal solutionally enlarged bedding planes have the primary role in providing aquifer transmissivity. All the wells are intercepting sub-horizontal bedding plane discontinuities, extracting groundwater from the Neoproterozoic Sete Lagoas karst aquifer dominantly from the main two continuous bedding planes, which are more solutionally enlarged in the central area and less karstic to the northeast (Figs. 2 and 7). Thus, in the case of a low matrix permeability in a karst aquifer in which is governed by bedding planes and low sub-vertical fractures, the chance to have a considerable increase in the scale effect from well- to regional-scale is considered low. Both in well- and regional-scale, in this case, the largest permeabilities occur due to the same karstic solutionally enlarged bedding planes. This interpretation is in accordance with Singhal and Gupta (2010), where carbonate rocks of Paleozoic and Mesozoic ages, which are well cemented and recrystallized, often have water flow primarily through conduits and fractures. The physical reality is that the flow through these planar features may be best modeled as conduits instead of fractures, but the quantitative variability does not alter the result.

At the well-scale, there is variation between low and high values of transmissivity and hydraulic conductivity. The central area, located within a graben area and with more karstification, has the greatest permeabilities values, including the zero drawdown well pumping test. These solutionally enlarged bedding planes are the most important structural features in the Neoproterozoic limestones from the Sete Lagoas karst aquifer, providing pathways for groundwater flow and great storage capacity. In the northeast portion of the area, smaller values of transmissivity are more common, suggesting less karstic bedding planes (confirmed by lithologic well logs, by Galvão et al., 2015). The depth of these limestones and its lithologic contacts could explain these different degrees of karstification. According to Ford and Williams (2007), transmissivity values, and consequently hydraulic conductivity and permeability, can be expected to vary according to vertical position in karst rock. In most cases, it will be highest in the most weathered zone of limestone near the surface (epikarst) and usually diminishes exponentially with depth.

Regarding the zero drawdown aquifer test, located in the central urbanized area, some researchers believe that these tests are unusable or useless, while others affirming that permeability

may be at some "practical infinity" or simple testing limit for aquifer testing methodologies (Rovey, 1994; Halihan et al., 2000). The limitation of aquifer tests to predict permeabilities was examined using the Thiem equation, for steady-state flow in a confined aquifer, estimating the highest local permeabilities values caused by the solutionally enlarged bedding planes.

At the regional-scale, a capture zone with dimensions of 8 km by 8.5 km (68 km^2), caused by the high pumping rate in wells estimated in 75,000 m^3/d (Fig. 5) was present. The permeability at the regional-scale has a little decrease of these values compared to well-scale (Fig. 6), which means that, at the regional-scale, the groundwater is also governed by the same karstic conduits observed at the well-scale, but the value is decreased by incorporating non-karstic areas in the regionally averaged value. If a groundwater model was generated at the regional-scale with grid dimensions below a kilometer, it would be expected that higher permeabilities than generated using the capture zone analysis may be required to simulate the system with lower adjacent values to represent non-karstic areas. This would modify the permeability scale effect database to indicate a leveling off of values between well- and regional-scales instead of a decrease in permeability.

The implications of this analysis are that an increase of measurement scale does not always imply an increase of permeability in these settings, because it will depend of the type of lithology and the connectivity of high permeability features. In the case of the study area, the scale effect had a reduction of the permeability values, due to the localized development of karst bedding plane dissolution in one structurally controlled region of the aquifer. Another implication is that measurements can be applied at different scales if the connectivity and structure is well understood to develop a robust quantitative model of the hydraulic structure of the aquifer. One limitation is that transport should not be calculated at a given scale using continuum approximations, as they will underestimate transport times by averaging low permeabilities with high permeability values. A second limitation is the need to consider whether turbulent effects are important for estimating permeability or the hydraulic size of a feature supplying flow.

Compared to other regions of the world, a single quantitative model of permeability scale effects can be elucidated from this and other associated studies. Aquifers are composed of a range of hydraulically connected permeable features. As these systems are sampled, the features sizes and connections vary depending on the choice of measurement method. Determining a strong evidence-based conceptual model of what features control permeability allows us to make prediction about quantitative values of permeability expected at various scales. Matrix permeability is often small in these systems, but should not be assumed to be neglected. A number of young carbonate systems have significant permeability in the matrix of the system. Well-scale permeability is expected to vary significantly in most cases as fracture aperture distribution may be strongly variable as in the Edwards aquifer of Texas (Halihan, 2000), or the aperture of single horizontal fractures can also be highly variable as they are sampled spatially (this study; Muldoon et al., 2001). On a regional-scale, understanding of potentially connected conduits is important for many karst aquifers, but this study illustrates that conduit permeability may not be a strong regional effect if large conduits are not well connected on the scale of measurement. For this aquifer, a smaller grid size regional model would likely observe some high permeability grid blocks in the central aquifer, but these values would be well supported by the conceptual model built from aquifer testing and optical logging of the system.

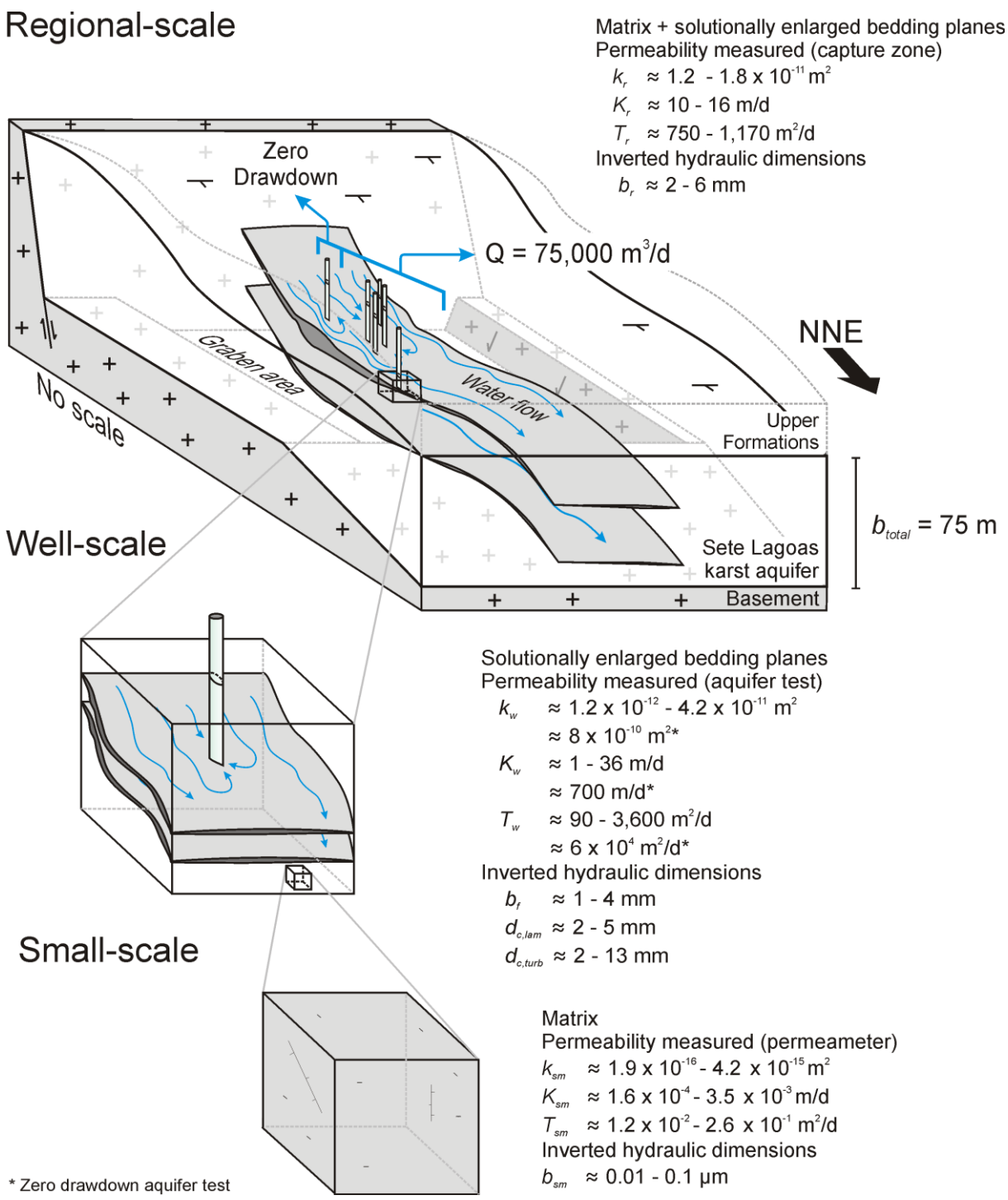

Fig. 7. Schematic scale effect conceptual model for Sete Lagoas. In a Neoproterozoic karst aquifer governed by solutionally enlarged bedding planes, with negligible permeability of the matrix, the chance to have a considerable increase in the scale effect from the well- to the regional-scale is low.

6. Conclusion

Unlike other karst areas that have increases in permeability from small- to regional-scale, such as Edwards Aquifer located in the United States (Halihan et al., 2000) and Juras Mountain in Switzerland (Király, 1975), this behavior does not happen in Sete Lagoas karst aquifer, in Brazil. In this area, an increase of about four to six orders of magnitude in the permeabilities from small- to well-scale is common, but from well- to regional-scale, the value decreases.

At the well-scale, the highest permeability wells are concentrated in the central area and close to the Santa Helena Ridge foothills, within the graben area, and in the East portion of the study area, with decreases occurring to northeast direction. These data coincide with the thickness of the karst bedding planes, suggesting a direct relationship between solutionally enlarged bedding planes thickness and formation permeability. However, the Sete Lagoas karst aquifer has some zones of high karstification, which the standard aquifer test used is an insufficient method for estimation, evidenced by zero drawdown, illustrating the limits of aquifer tests. These zones are located specifically in the central portion of the urbanized area. Non-Darcian flow likely occurs in these wells. At the regional-scale, in the central portion of the study area, there is a potentiometric flow convergence, setup by a cone of depression and high pumping rate in wells, being recognized as a capture zone.

The results indicate that multi-scale evaluation using different approaches is useful to develop a quantitative hydrogeological conceptual model in karst aquifers, consistent across scales of measurement, from small- to regional-scale flow. These methodologies used obtained results suggesting that in Neoproterozoic karst aquifers with negligible permeability of the matrix, governed by bedding planes discontinuities, would not have increases in permeability from well- to regional-scale, unless a zone of more significant karstification occurred on that scale.

Acknowledgments

This work was funded by Servmar Environmental & Engineering and by São Paulo Research Foundation (FAPESP) [*Fundação de Amparo à Pesquisa do Estado de São Paulo*] (process 2012/12846-9). Special thanks go to Prof. Dr. Renato Paes de Almeida for providing the TinyPerm II portable hand-held air permeameter.

Appendix: Notation

b_f hydraulic aperture of a single low-angle fracture [L];
b_{total} total thickness of aquifer [L];
b_w well-scale bedding plane aperture [L];
b_r regional-scale aperture [L];
d_c hydraulic conduit diameter [L];
$d_{c,lam}$ laminar hydraulic conduit diameter [L];
$d_{c,turb}$ turbulent hydraulic conduit diameter [L];
g gravitational constant [L/t^2]: 9.81 m/s^2;
i hydraulic gradient [dimensionless];
k_f intrinsic permeability of a fracture [L^2];
k_{sm} small-scale permeability [L^2];
k_w well-scale permeability [L^2];
k_r regional-scale permeability [L^2];
K_c conduit hydraulic conductivity [L/t];
$K_{c,lam}$ laminar hydraulic conductivity of the conduit [L/t];
$K_{c,turb}$ turbulent hydraulic conductivity of the conduit [L/t];
K_{sm} small-scale hydraulic conductivity of the matrix [L/t];
K_w well-scale hydraulic conductivity [L/t];

K_r regional-scale hydraulic conductivity [L/t];
Q_w pumping rate in the well [L^3/t];
Q_r regional multiple well pumping rate [L^3/t];
R^2 coefficient of determination [dimensionless];
S_c specific capacity [L^2/t];
T transmissivity [L^2/t];
T_{sm} small-scale transmissivity [L^2/t];
T_w well-scale transmissivity [L^2/t];
T_r regional-scale transmissivity [L^2/t];
x distance parallel to the regional hydraulic gradient (*i*) [L];
X_L distance from pumping well to the downgradient edge of the capture zone (stagnation point) [L];
y distance perpendicular to the regional hydraulic gradient (*i*) [L];
Y_L half width of the maximum capture zone [L];
Δh_w hydraulic head in the well [L].
π pi = 3.1416;
θ angle between fracture and horizontal;
v kinematic viscosity of the water [L^2/t]: 10^{-6} m^2/s;
ϕ_{sm} porosity of matrix [µL].

References

Branco Jr., Costa MT (1961) Belo Horizonte-Brasilia roadmap tour. In: Brazilian Congress of Geology, Brasilia. Radioactive Research Institute, Federal University of Minas Gerais (UFMG), Publication 15, Belo Horizonte, p 25.

Clauser C (1992) Permeability of crystalline rocks. EOS, Transactions America Geophysical Union, 73 (21): 233-238.

Cooper HHJr, Jacob CE (1946) A generalized graphical method for evaluating formation constants and summarizing well field history. Transactions of the American Geophysical Union. v. 27, pp.526-534.

Dardenne MA (1978) Synthesis on the stratigraphy of Bambuí Group in Central Brazil. In: Brazilian Congress of Geology, 30, Recife. Annals Recife: Brazilian Society of Geology, 1978 v.2, p.597-610.

Demétrio JGA, Correia LC, Saraiva AL (2006) Using SRTM images to developing potentiometric maps. In: Brazilian Groundwater Congress. Abstracts. Curitiba, ABAS, 176p.

Dunham RJ (1962) Classification of carbonate rocks according to depositional texture. In: W.E.HAM (ed): Classification of carbonate rocks. Am. Assoc. Petrol. Geol., Mem.1, Tulsa, Oklahoma, p. 108-121.

Ewers RO (1982) An analysis of solution cavern development in the dimensions of length and breadth: McMaster University (Hamilton, Ontario, Canada), Ph.D. dissertation, 398 p.

Fetter CW (1994) Applied Hydrogeology. New York: Macmillan, 691 p.

Folk RL (1959) Practical petrographic classification of limestones: American Association of Petroleum, Geologists Bulletin, v. 43, p 1-38.

Ford DC, Williams PW (2007) Karst geomorphology and hydrology. 2nd edn. John Wiley & Sons, Chichester, U.K. 562 p

Fossen H, Schultz RA, Tobari A (2011) Conditions and implications for compaction band formation in the Navajo Sandstone, Utah. Journal of Structural Geology, 33, 1477-1490.

Freeze AR, Cherry JA (1979) Groundwater: Englewood Cliffs, New Jersey, Prentice-Hall, 604 p.

Galvão P, Halihan T, Hirata R (2015) Evaluating karst geotechnical risk in the urbanized area of Sete Lagoas, Minas Gerais, Brazil. Hydrogeology Journal (online). DOI: 10.1007/s10040-015-1266-x

Grubb S (1993) Analytical model for estimation of steady-state capture zones of pumping wells in confined and unconfined aquifers. Ground Water, vol. 31, no. 1, p. 27-32.

Halihan T, Wicks CM, Engeln JF (1998) Physical response of a karst drainage basin to flood pulses: example of the Devil's Icebox cave system (Missouri, USA). Journal of Hydrology, 204: 24-36.

Halihan T, Sharp JMJr, Mace RE (1999) Interpreting flow using permeability at multiple scales. In Palmer AR, Palmer MV and Sasowsky ID (eds) Karst Modeling. Karst Waters Institute Special Publication no 5, Charlottesville, p 82-96.

Halihan T, Sharp JMJr, Mace RE (2000) Flow in the San Antonio segment of the Edwards Aquifer: Matrix, fractures, or conduits?: in C. M. Wicks and I. D. Sasowsky, eds., Groundwater flow and contaminant transport in carbonate aquifers: Balkema, Rotterdam, The Netherlands, p. 129–146.

Heath RC (1983) Basic ground-water hydrology, U.S. Geological Survey Water-Supply Paper 2220, 86p.

Hovorka SD, Mace RE, Collins EW (1995) Regional distribution of permeability in the Edwards Aquifer. Draft contract report to the Edwards Underground Water District under contract no. 93-17-FO, Bureau of Economic Geology, The University of Texas at Austin. 77 pp.

Huntoon PW (1985) Gradient controlled caves, Trapper-Medicine Lodge area, Bighorn Basin, Wyomig: Ground Water, v. 23, p. 443-448.

IBGE - Brazilian Institute of Geography and Statistics, 2010. Basic Municipal Information. Avaliable: http://www.ibge.gov.br/cidadesat/topwindow.htm?1 Accessed on March 2014.

Javandel IC, Tsang CF (1986) Capture zone types curves: A tool for aquifer cleanup. Ground Water. v. 24, no. 5, pp. 616-625.

Király L (1975) Rapport sur l'état actuel des connaissances dans le domaine des caractères physique des roches karstique. In: Burger, A. and Dubertet, L. (eds). Hydrogeology of karstic terrains. Paris, International Association of Hydrogeologists, Series B, No. 3, p. 53-67.

Kresic N (2013) Water in karst. Management, vulnerability and restoration. McGraw-Hill, New York, 708 p.

Lamb H (1932) Hydrodynamics, 6th edition. New York: Dover, 738 p.

Leonards GA (1962) Foundation Engineering. New York: McGraw-Hill, 1136 p.

Mace RE (1997) Determination of transmissivity from specific capacity tests in a karst aquifer, Edwards Group, south-central Texas. Ground Water. v.35 pp 735-742.

Maclay RW, Lamb LF (1988) Simulation of flow in the Edwards Aquifer, San Antonio Region, Texas, and Refinement of the Storage and Flow Concepts. U.S. Geological Survey Water-Supply Paper 2336-A, 48 p.

Mangin A (1975) Contribution a l'étude hydrodynamique des aquifères karstiques. Thèse, Institut des Sciences de la Terre de l'Université de Dijon.

Moore CH (1989) Carbonate diagenesis and porosity. Development in sedimentology 46. Amsterdam: Elsevier, 338 p.

Muldoon MA, Simo JA, Bradbury KR (2001) Correlation of hydraulic conductivity with stratigraphy in a fractured-dolomite aquifer, northeastern Wisconsin, USA. Hydrogeology Journal 9, no. 6: 570-583.

Oliveira LM (1997) The management of urban geological risks in karst areas. Undergraduate thesis. Pontifícia Universidade Católica do Paraná (PUC-PR). 46 p

Pessoa P (1996) Hydrogeological characterization of the region of Sete Lagoas - MG: Potentials and Risks. Master Thesis. Department of Geosciences, University of São Paulo. São Paulo.

Quinlan JF, Ewers RO (1985) Groundwater flow in limestone terrenes: strategy, rationale, and procedures for reliable, efficient monitoring of groundwater quality in karst areas. National Symposium and Exposition on Aquifer Restoration and Ground Water Well Assoc. pp. 197-234.

Rats MV (1967) Neodnorodnost Gornykh Porod i Ikh Fizicheskikh Svojstv. Nauka Moskva.

Razack M, Huntley D (1991) Assessing transmissivity from specific capacity in a large and heterogeneous alluvial aquifer. Ground Water. v. 24, pp. 519-524.

Rehfeldt KR, Hufschmied P, Gelhar LW, Schaefer ME (1989) Measuring hydraulic conductivity with the borehole flowmeter. Palo Alto, California, Electric Power Research Institute, Research Report EPRI EN-6511, Project 2485-5, 209 p.

Ribeiro JH, Tuller MP, Danderfer Filho A (2003) Geological mapping of the region of Sete Lagoas, Pedro Leopoldo, Matozinhos, Lagoa Santa, Vespasiano, Capim Branco, Prudente de Morais, Confins and Funilândia, Minas Gerais State, Brazil (scale 1:50,000). 2nd edn. Belo Horizonte. 54 p

Rovey CW II (1994) Assessing flow system in carbonate aquifers using scale effects in hydraulic conductivity. Environmental Geology, 24: 244-253.

Scanlon BR, Mace RE, Smith B, Hovorka S, Dutton AR, Reedy R (2001) Groundwater availability of the Barton Springs segment of the Edwards aquifer, Texas: Numerical simulations through 2050 prepared for Lower Colorado River Authority under contract number UTA99-0, Austin, Texas.

Scanlon BR, Mace RE, Barrett ME, Smith B (2003) Can we stimulate regional groundwater flow in a karst system using equivalent porous media models? Case study, Barton Springs Edwards aquifer, USA, Journal of Hydrology, v. 276, p. 137–158.

Schobbenhaus C (1984) Geology of Brazil. National Department of Mineral Production, p 275-277.

Schöll WU, Fogaça ACC (1973) Stratigraphy of the Espinhaço in the Diamantina region. In: Symposium on Geology of Minas Gerais State, Brazil, 1. Acts. Belo Horizonte: Brazilian Geology Society p 55-73 [Bulletin. 1].

Schulze-Makuch D, Carlson D, Cherkauer D, Malik P (1999) Scale dependency of hydraulic conductivity in heterogeneous media. Groundwater 37 (6), 904–919.

SIAGAS (2006) Sistema de Informações de Águas Subterrâneas [System of Groundwater Information]. Available: http://siagasweb.cprm.gov.br/layout/. Accessed on August 2013

Singhal BBS, Gupta RP (2010) Applied Hydrogeology of Fractured Rocks. 2nd ed. Springer, XIX, 408 p.

Theis CV (1935) The relation between the lowering of the piezometric surface and the rate and duration of discharge of a well using groundwater storage. Transactions of the American Geophysical Union. v. 16, pp.519-524.

Thiem G (1906) Hydrologische Methoden; Gebhardt, Leipzig.

Thorkildsen D, McElhaney PD (1992) Model refinement and application for the Edwards (Balcones fault zone) aquifer in the San Antonio region, Texas: Austin, Texas, Texas Water Development Board, Report 340, 33p.

Todd DK (1980) Groundwater Hydrology. John Wiley and Sons, NY. 535 pp.

Tonietto SN (2010) Diagenesis and hydrothermal rocks in Proterozoic carbonates: Bambuí and Vazante Groups, São Francisco Basin. Master Thesis. Institute of Geosciences, University of Brasília. Federal District.

Tuller MP, Ribeiro JH, Signorelli N, Féboli WL, Pinho JMM (2010) Sete Lagoas - Abaeté Project, Minas Gerais State, Brazil. 6 geological maps, scale 1:100,000 (Geology Program of Brazil), 160p.

Worthington SRH (1999) A comprehensive strategy for understanding flow in carbonate aquifers, in Palmer, A.N., Palmer, M.V., and Sasowsky, I.D., eds., Karst modeling: Leesburg, Va., Karst Waters Institute Special Publication 5, p. 30–37.

Zinszer B, Pellerin F (2007) A Geoscientist's Guide to Petrophysics. IFP Publications. 363 pp.

Electronic supplementary material

Table S1. Values of pumping rate, aquifer thickness, specific capacity, transmissivity, empirical transmissivity, hydraulic conductivity, and values adopted used in the transmissivity map. Bolded wells were the pumping wells used in the long duration transient pumping tests and their respective observation wells (**PT-01**: PT-02 and 03; **PT-13**: PT-12; **PT-19**: PT-21; **PT-22**: PT-25; **PT-40**: PT-39 and 41; **PT-64**: PT-63 and 66; **PT-105**: PT-29 and 30). In the case of pumping wells with two observation wells, an average value from both observation wells was adopted.

Well ID	UTM (E)	UTM (N)	Pumping rate (m^3/h)	Aquifer thickness (m)	Specific capacity (Sc = m^2/d)	Transmissivity observation well (m^2/d)	Transmissivity pumping well (m^2/d)	Transmissivity (m^2/d) by $T=330(Sc)^{0.21}$	Transmissivity adopted (m^2/d)	Hydraulic conductivity (m/d)
PT-01	579268	7848716	130	80	-	-	6×10^4 *	-	6×10^4 *	700 *
PT-02	579246	7848691	-	80	-	-	6×10^4 *	-	6×10^4 *	700 *
PT-03	579216	7848676	-	80	-	-	6×10^4 *	-	6×10^4 *	700 *
PT-12	580113	7849030	-	80	-	1550	-	-	1550	19
PT-13	580332	7849256	96	80	3090	-	1550	1784	1550	19
PT-18	580559	7847547	-	80	1955		-	1620	1620	20
PT-19	582376	7848299	130	80	-	-	980	-	980	12
PT-21	582403	7848241	-	80	-	980	-	-	980	12
PT-22	582655	7849049	92	90	69	-	330	803	330	4
PT-24	582969	7849173	-	90	1771	-	-	1587	1590	18
PT-25	582940	7848896	-	90	430	330	-	1179	330	4
PT-28	578001	7847528	-	60	306	-	-	1098	1100	18
PT-29	576698	7848632	-	100	-	3190	-	-	3190	32
PT-30	576712	7848588	-	100	2731	3590	-	1738	3590	36
PT-36	576691	7846287	-	80	731		-	1318	1320	17
PT-39	578827	7845533	-	60	88	940	-	845	940	16
PT-40	578873	7845671	61	60	28	-	960	664	940	16
PT-41	578699	7845444	-	60	287	980	-	1083	980	16
PT-45	577956	7845008	-	60	4	-	-	442	440	7
PT-46	577926	7846636	-	40	216	-	-	1020	1020	26
PT-47	577745	7846644	-	40	486	-	-	1210	1210	30
PT-48	579120	7846837	-	60	1302	-	-	1488	1490	25
PT-51	580745	7846316	-	60	138	-	-	929	930	16
PT-52	580513	7846988	-	60	222	-	-	1026	1025	17
PT-57	578596	7851764	-	60	4	-	-	449	450	8
PT-63	582178	7854596	-	70	205	580	-	1009	580	8
PT-64	582351	7854808	194	70	-	-	615	-	615	9
PT-66	582454	7854749	-	70	168	650	-	968	650	9
PT-73	584150	7851271	-	100	11	-	-	546	545	5
PT-74	584809	7851679	-	100	3429	-	-	1823	1820	18
PT-77	583165	7851755	-	100	85	-	-	840	840	8
PT-92	583144	7858729	-	130	130	-	-	-	130	1
PT-93	582764	7858339	-	130	90	-	-	-	90	1
PT-99	570843	7851762	-	40	93	-	-	855	855	21
PT-105	576698	7848588	47	100	3190	-	3390	-	3390	34

* = using Thiem (1906) method.

Bolded wells were the pumping wells.

Table S2. Values of hand sample permeability measured by hand-held air permeameter, and values of hydraulic conductivity and transmissivity.

Sample	Description	Darcy	k (m^2)	K (m/d)	T (m^2/d)
		6.63E-04	6.55E-16	5.55E-04	4.16E-02
13-SL-46		7.63E-04	7.53E-16	6.38E-04	4.79E-02
		3.58E-04	3.53E-16	2.99E-04	2.24E-02
		1.16E-03	1.15E-15	9.73E-04	7.29E-02
13-SL-25	Lagoa Santa Member. Compact limestone, less micro-fractures filled by calcite	9.55E-04	9.43E-16	7.99E-04	5.99E-02
		1.10E-03	1.08E-15	9.19E-04	6.90E-02
		2.93E-03	2.90E-15	2.45E-03	1.84E-01
13-HV-18		2.85E-03	2.82E-15	2.39E-03	1.79E-01
		4.12E-04	4.06E-16	3.44E-04	2.58E-02
		2.41E-03	2.38E-15	2.02E-03	1.51E-01
13-SL-16		2.85E-03	2.82E-15	2.39E-03	1.79E-01
		1.87E-03	1.85E-15	1.57E-03	1.18E-01
		2.70E-04	2.67E-16	2.26E-04	1.70E-02
13-FN-09		6.27E-04	6.19E-16	5.25E-04	3.93E-02
		1.23E-03	1.21E-15	1.03E-03	7.72E-02
		9.55E-04	9.43E-16	7.99E-04	5.99E-02
13-FN-02a	Pedro Leopoldo Member. Compact limestone with well developed bedding planes	4.23E-03	4.17E-15	3.54E-03	2.65E-01
		3.19E-03	3.15E-15	2.67E-03	2.00E-01
		2.78E-04	2.74E-16	2.32E-04	1.74E-02
13-IN-19		2.35E-04	2.32E-16	1.96E-04	1.47E-02
		2.63E-04	2.59E-16	2.20E-04	1.65E-02
		1.41E-03	1.40E-15	1.18E-03	8.88E-02
13-IN-14		1.98E-04	1.96E-16	1.66E-04	1.25E-02
		8.78E-04	8.67E-16	7.35E-04	5.51E-02

CHAPTER 8: STABLE ISOTOPES AND GEOCHEMICAL STUDIES TO EVALUATE FLOWPATHS AND RECHARGE AREAS IN AN URBAN KARST AQUIFER OF SETE LAGOAS, MG, BRAZIL

Paulo Galvão[1], Ricardo Hirata[1], Todd Halihan[2]

To be submitted in the Anais da Academia Brasileira de Ciências [Annals of the Brazilian Academy of Sciences]

Abstract

The study area is the city of Sete Lagoas, located in the state of Minas Gerais, Brazil, which is currently supplied by groundwater from karst aquifers. Identifying the various sources and areas of recharge in this karst area, its flowpaths, and surface-ground water interaction is important for proper water resource management, avoiding eventual contaminations and other future problems. The main goal is to determine, by stable isotopes ^{18}O and ^{2}H and major ions measurements, the identification of hydrogeologic processes, surface-ground water connections, possible recharge zones and its flowpaths. The majority of the groundwater samples were collected in this urban karst aquifer, while the superficial waters were collected in seven main lakes. The stable isotopes results indicated that the origin of groundwaters is directly from precipitation, having a limited period of recharge. In the central urbanized area, where the karst aquifer is in contact with Cenozoic unconsolidated sediments, it could have punctual superficial water infiltration. The major ions presented the highest values at the same region, where the most karstic area from the Sete Lagoas Formation is located. These data could suggest higher water reservoir indicating more mineralization, which are in concordance with the geologic information.

Keywords: Stable isotopes, geochemistry, hydrogeology, groundwater, Brazil.

1. Introduction

A better understanding of hydrological processes and the hydrochemical evolution is very important for regional water resources development and management in karst region, where a unique and complex flow system exists because of special rock-water reactions (Han et al. 2014). Due to groundwater storage and flowpath in karst aquifers are extremely heterogeneous, it is often difficult to describe and quantify the flow characteristics with traditional methods. These features also reflect in the type of recharge, where are often characterized by high vertical permeabilities due to vertical conduits and sinkholes allowing rapid recharge of the groundwater (Ford and Williams 1989, Hess et al. 1989) as well as, in some cases, are also connected to surface-water interaction making groundwater highly susceptible to contamination (Ryan and Meiman 1996).

Generally, a karst aquifer is a result of a karstification by chemical, and sometimes, mechanical actions of water in lands composed by soluble rocks such as limestone, dolomite, or gypsum bedrocks, in which the flowpath of the groundwater is closely related to the degree of the karst development (Palmer 1991). This development is characterized by the dominance of chemical weathering in the surface and subsurface. When the acidic water, as result of rainwater passing through the atmosphere, or in the ground/soil picking up carbon dioxide (CO_2), starts to break down the surface of soluble bedrock near its cracks, or bedding planes (Ford and Williams 1989). As time goes on, these fractures will become wider, and eventually, a drainage system of some sort may start to form underneath.

These processes can result in many different groundwater transmission and storage conditions. Some display strictly in single porosity, either as matrix only (common in young reefal and eolian limestones), or as fissure only (e.g. incipient karst in marble). Large volumes of most karst aquifers will display at least dual porosity, exhibiting matrix plus fissure, matrix plus conduit or fissure plus conduit, or can have a true triple porosity (matrix-fissure-conduit) recognized in some portions of most large explored caves (Ford 1999).

There are different categories for karst recharge areas. If the karst area recharges itself, it is called autogenic recharge. Allogenic recharge occurs when the adjacent non-karst areas recharge the karst aquifer. The presence of sinkholes gives a distinct recharge feature, which can be separated into point (shaft and conduit dominated), and diffuse (matrix, meso-pore, and macro-pore dominated) infiltration and recharge. These areas are the major flowpath for contaminants (Goldsheider and Drew 2007, Karamouz et al. 2011).

Identifying the various sources and areas of recharge in karst systems, its flowpaths, and the surface-ground water interaction is important for proper water resource management. Many researchers have focused to understand these mechanisms using different tools, such as hydrogeochemistry, geomorphologic structure, hydrologic dynamics of karst flow, as well as estimating the mean rate and spatial distribution of the recharge areas (Andreo et al. 2008, Farfán et al. 2009, Liu et al. 2009, Li et al. 2010, Zhao et al. 2010). Other techniques including dye tracers, salts, smoke and gaseous tracers and stable isotopes are also used (Käss et al. 1998, Ginsberg and Palmer 2002, Karamouz et al. 2011).

Among these, the stable isotopes of ^{18}O and ^{2}H have been used in numerous hydrogeologic investigations combining with geochemistry data. Some examples can be cited: storm hydrograph separation (Kennedy et al. 1986, Buttle 1994, Harris et al. 1995, Machavaram et al. 2006), surface-ground water interactions (Fontes 1980, McKenna et al. 1992, Coplen and Kendall 2000, O'Driscoll et al. 2005, Lee and Kim 2007), or geochemical variations and origins of dryland and salinity (Winston and Criss 2003, Cartwright et al. 2004). This method also has been successful in identifying the contribution of surface water to groundwater in karst environment (Katz 1995, Meyers et al. 1993, Plummer et al. 1998).

While the use of stable isotopes in hydrogeology started in the 50s, with the pioneering works of Urey et al. and Epstein and Mayeda (*in* Clark and Fritz 1997), in Brazil, the first hydrogeological studies using this method started in the late 60s and early 70s in the northeast, southeast and Amazon regions (Silveira and Silva Junior 2002). However, due to karst areas in Brazil are not so

extensive in comparison to other regions in the world, such as USA, Europe and Asia, the use of this technique to identify the various sources and areas of recharge in karst aquifers is still incipient.

In regards to this paper, the primary goal was to determine, by ^{18}O and ^{2}H isotopes and major ions measurements, the hydrogeologic flow processes in Sete Lagoas' aquifers, in order to understand possible origin and mechanisms of groundwater recharge and its flowpaths. In this city, the current water supplies is almost entirely groundwater from the karst aquifer (Pessoa 1996) and this understanding is important to promote aquifer protection against problems related to intensive exploitation and water contamination. The majority of the water samples were collected from lakes and groundwater wells, between August 2011 and June 2013 for stable isotopic and geochemistry analyzes.

2. Site description

The study area is the city of Sete Lagoas, located in the state of Minas Gerais, Brazil, 70 km northwest of Belo Horizonte, the state capital (Fig. 1). This city has a population greater than 200,000, over an area of 538 km^2 (IBGE 2010). The greatest population density is located in the central, west-central and north-central areas of the city, corresponding to the older areas of occupation. There is a considerable industrial, mineral and metallurgical center located mainly along the main federal highway, which is a corridor of significant growth. The current water supply is almost entirely groundwater from the Sete Lagoas karst aquifer (Pessoa 1996), pumping by private and public wells, which in the case of the last one, is managed by the Water Supply and Sewage Service (SAAE) [*SAAE - Serviço de Abastecimento de Água e Esgoto*].

Geologically, the area is located in the São Francisco Craton, where carbonate argillo-arenaceous sediments are emplaced giving origin to the Bambuí Group (Branco and Costa 1961, Oliveira 1967, Schöll and Fogaça 1973, Dardene 1978, Schobbenhaus 1984, Ribeiro et al. 2003, Tuller et al. 2010, Galvão et al. in press). The hydrostratigraphic relationships for the Sete Lagoas karst aquifer and spatial distribution are given in Pessoa (1996) and Galvão et al. (2015).

The Sete Lagoas karst aquifer consists of Neoproterozoic limestones, in which the primary porosity and matrix permeability can be considered very low (Moore 1989) and the second porosity (micro-fractures) is mostly filled by calcite (Tonietto 2010, Galvão et al. 2015). Thus, the majority of the fluids migrate through dissolution features characterized as tertiary porosity, in conduits. According to Galvão et al. (2015), results from geologic mapping and optical well logging suggest that the urbanized area of Sete Lagoas is primarily located in a graben, filled with limestones from the Sete Lagoas Formation, Cenozoic unconsolidated sediments, and occasional competent rocks from the Serra de Santa Helena Formation (slate, marble, siltstone and argillite). This setting results in barrier boundaries for groundwater, which together with natural karst processes, explains the location of two main solutionally enlarged bedding planes with large groundwater storage capacity: (1) a shallower and thicker continuous dissolution zone with conduits that are 1-8 m thick, near the contact with unconsolidated sediments; and (2) 10-20 m below, a thinner continuous dissolution zone with conduits that are 20 cm to 1 m thick. These limestones dip and become thicker and completely covered by

rocks from the Serra de Santa Helena Formation to the northeast, reaching about 160 m thickness, where the two bedding plane conduits become thinner to the northeast (Galvão et al. 2015).

Geomorphologically, the area is in a karst setting, which provides the presence of lakes, located mainly in the central area, some caves, close drainage basin, and sinkholes located in a limestone outcrops context (Pessoa 1996) (Fig. 1). Areas that have denser drainage are related to the Santa Helena Ridge foothills in the center, basement outcrops in the south, and metasediments in the north. The elevation of the area ranges from around 750 to 1000 m, declining from southwest to northeast, where the highest elevations are located in the Santa Helena Ridge.

Regarding the climate, the mean total monthly precipitation is 106 mm, while the total annual is 1271.8 mm. The rainy season occurs from October to March, with total rainfall of 1132 mm, corresponding to 89% of annual precipitation. The period with less precipitation occurs from April to September, with 139 mm. The average annual temperature is 20.9 ºC, which July has the lowest monthly mean value (17.5 °C), and February the highest one (22.9 °C). The annual variation is around 5 °C. According to Pessoa (1996), the water balance of Sete Lagoas is divided, monthly, in: 1) water excess from January to March; 2) water deficit from April to September; and 3) water replacement between October and December, period of groundwater recharging.

3. Methods

To obtain information about groundwater and superficial water to better understand the above described hydrogeological setting and its interconnections, 30 supply wells, and 7 lakes sampling surveys were conducted during August 2011 and August 2013, collecting data of in-situ physicochemical parameters and carrying out chemical analyses of major ions and stable isotopes. These methods will be presented sequentially followed by the approach to data integration.

3.1 Stable isotopes

Groundwater samples were taken during August 2011 and November 2012 in 30 SAAE's public wells (Table 1 and Fig. 1) used to supply Sete Lagoas (25 samples from Sete Lagoas karst aquifer and 5 samples from the basement). In the case of the karst aquifer, according to Galvão et al. (2015), the wells located in the central area are pumping waters from the two main solutionally enlarged bedding planes, corresponding to the majority of the wells analyzed. These samples were taken after removing several well volumes of water, using pumps installed in these wells. This was done to purge the aquifer of stagnant water and to acquire fresh aquifer samples for analysis. After sampling, were measured physicochemical parameters (pH, temperature - T, electrical conductivity - EC, and oxidation-reduction potential - ORP) using the HI 9828 portable multiparameter meter.

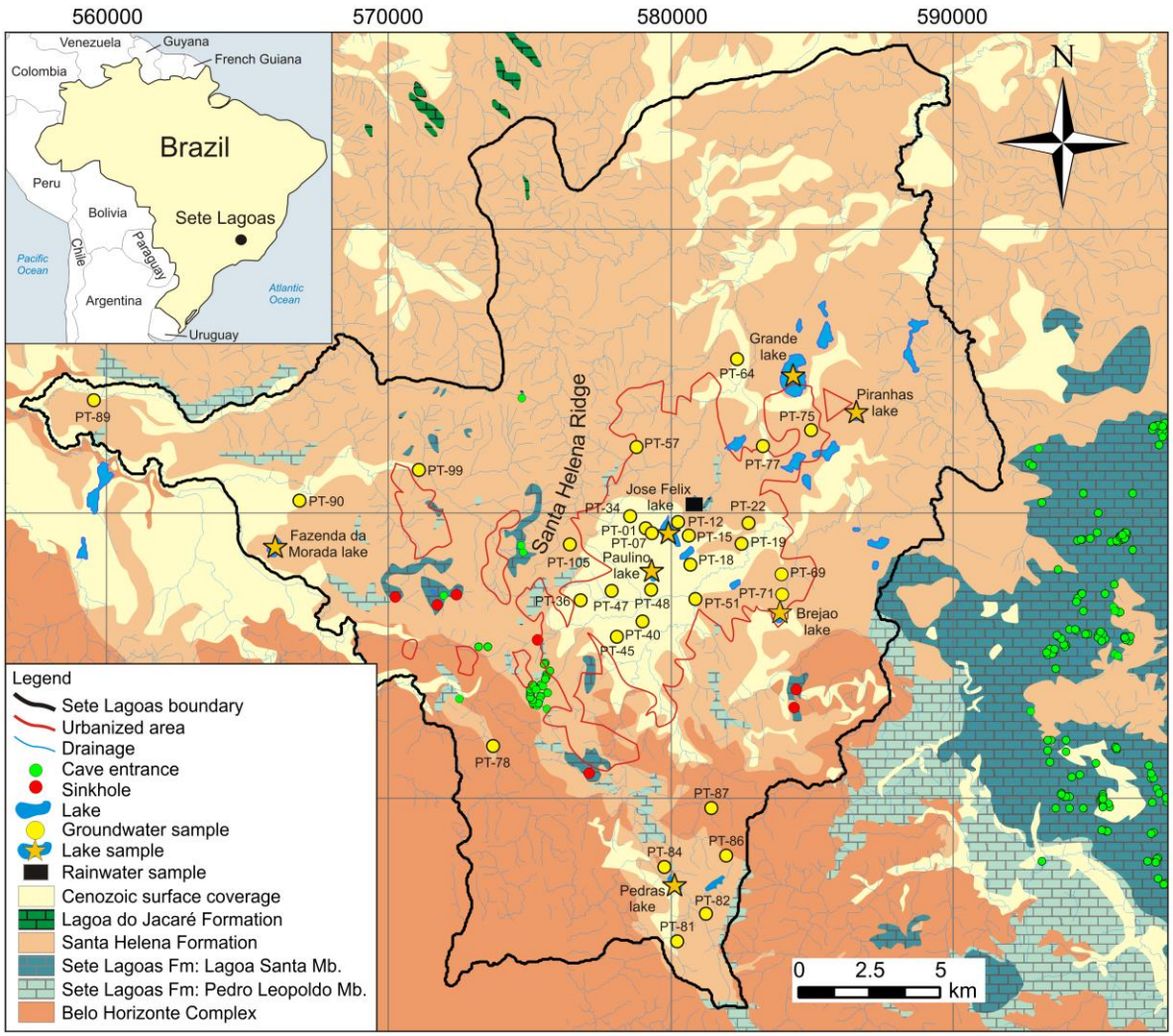

Fig. 1. Location map, in UTM coordinates, of Sete Lagoas showing the geology, the drainage pattern (interpreted from georeferenced images, including aerial photography and Landsat imagery), and karst features location (caves and sinkholes) (modified from Galvão et al. 2015). The figure also shows the location of sampling points, such as groundwater in supply wells (yellow dots), rainwater collector (central black rectangle, next to José Felix lake), and surface water in seven lakes (orange star).

The surface water samples were collected only in June 2013, in seven lakes: Brejão, Grande, José Felix, Paulino, Pedras, Piranhas, and Fazenda da Morada (Table 1 and Fig. 1). For this, samples were taken in the center of each lake using a peristaltic pump (brand Geopump). This method followed the low flow principle, avoiding sediment from the lake's substrate (Puls and Barcelona 1996).

Eleven cumulative monthly rain isotope samples were also collected representing a hydrological year, from April 2012 to April 2013 (no samples in July 2012 due to lack of rain). For this, a polypropylene bottle (10 L) with an also polypropylene funnel connected in that bottle were used and placed in a cooler to keep the temperature and prevent sunlight penetration. A silicone hose with 6 m long was also attached on the bottle to balance the pressure and prevent exchanges with atmospheric air. This method followed the GNIP (Global Network of Isotopes in Precipitation) instruction, where evaporation and loss of lighter isotopes are negligible (IAEA/WMO 2004).

The main concern with these samples was to avoid the post-sampling fractionation. For this, pre-cleaned polypropylene vials (30 ml) were used. These vials were completely filled with samples, avoiding air bubbles inside and stored in coolers maintaining the temperature. All samples were

analyzed for ^{18}O and ^{2}H at the Groundwater Research Center (CEPAS) [*CEPAS - Centro de Pesquisas de Águas Subterrâneas*], Institute of Geosciences, University of São Paulo. The samples were run on PICARRO L2130i, processed by Laboratory Information Management System (LIMS) for Lasers software, and were normalized to internal laboratory water standards that were previously calibrated relative to the Vienna Standard Mean Ocean Water (VSMOW). The results were expressed as $\delta^{18}O$ and $\delta^{2}H$, where δ_{sample} (‰) = ((R_{sample} /$R_{standard}$) − 1) × 1000, where R is D/H, $^{18}O/^{16}O$. The analytical precisions were ±0.09‰ for $\delta^{18}O$ and ±0.9‰ for $\delta^{2}H$.

After all these analysis, all the samples were compared with the latest Global Meteoric Water Line (GMWL) reported by Rozanski et al. (1993). This meteoric water line is linearly related by the equation $\delta^{2}H = 8.17\ \delta^{18}O + 11.27$, and it is an enhancement to the first meteoric water line proposed by Craig (1961), related by the equation $\delta^{2}H = 8\ \delta^{18}O + 10$. This high correlation coefficient reflects the fact that the oxygen and hydrogen stable isotopes in water molecules are intimately associated.

3.2 Geochemistry analysis

The same supply wells used to collect groundwater samples for isotopic analysis were also used for geochemistry analysis (Table 2). Samples for major cations (Na^{+}, K^{+}, Ca^{2+}, Mg^{2+}), major anions (HCO^{-}_{3}, CO^{-2}_{3}, SO^{2-}_{4}, Cl^{-}, NO^{-}_{3}), total dissolved solids (TDS), and total water hardness (WH) were collected in pre-cleaned 1 L plastic polyethylene bottles, and then, stored in coolers at 4°C, according to the Brazilian Sampling and Water Preservation Guide (CETESB 1998). For some analyses, samples were filtered through a 0.45 µm filter, while for major cations were acidified with nitric acid to a pH of less than 2. All these samples were analyzed at the Analytical Solution Company's laboratory, in São Paulo.

After that, all the measurements were checked for accuracy by calculating the mass balance, and then the water types were classified using the Piper's diagram of water (Piper 1944) using the AquaChem 4.0 software (Fig. 6). In order to help understand the spatial concentrations of each parameter, kriging interpolations of the data were carried out using the Surfer 8 software to drawn isopleth maps.

Finally, all the data sets were entered in a GIS database and georeferenced in the ArcGIS 10.1 software. The coordinate system was Universal Transverse Mercator (UTM) projection, Zone 23, datum SAD 69, with units in meters.

4. Results

The results will be presented sequentially from the stable isotope analysis for rainwater, superficial water and groundwater, and finally the geochemistry results, for groundwater.

4.1 Stable isotopes

The groundwater stable isotopic composition was little variable, not reflecting significant difference signatures through one year. The $\delta^{18}O$ values varied from -5.26 to -7.31‰, with a mean of -

6.45‰, while δ^2H values varied from -37.6 to -47.0‰, with a mean of -42.5‰. The deuterium excess values ranged from 6.78 to 11.48‰, with a mean of 9.08‰ (Table 1). The mean isotopic compositions of the groundwater fell in the GMWL, with mostly samples on or near the GMWL, while others plotted fairly tightly in the lower right, where the best-fit linear regression line had a slope of 4.80 and an interception of -11.53. Both waters from Sete Lagoas karst aquifer and basement are mostly located at the same region on the graphic, clustered, with no discernible spatial trend (Fig. 2).

The $\delta^{18}O$ and δ^2H values from the seven lakes collected were well variable (Table 1). When $\delta^{18}O$ is plotted against δ^2H (Fig. 2), the mean isotopic compositions of the lake water fell well to the right of the global meteoric water line along a best-fit linear regression line with a slope of 5.13 and an interception of -9.04. Even both groundwater and lake water had some similarities in their linear regressions, with slopes values around 5 and negative interceptions around 10, the distribution of $\delta^{18}O$ and δ^2H values through the meteoric water line were not similar, where the groundwaters presented more negative values.

The $\delta^{18}O$ values of rainfall varied from 2.93 to -5.62‰, mostly being negative. Rainwater δ^2H values varied from 25.8 to -36.5‰. Deuterium excess values ranged from 2.36 to 13.82‰ with a mean of 11.72‰. The result shows that mostly rainwater samples fell along the GMWL (Fig. 2), where some deviations of highest rainwater values can be attributed to atmospheric-evaporative effects during the sampling. Due to this effects, probably caused by a problem in the rain collector in some isolated months, as well as an insufficient data of rain to build a consistent local meteoric water line (only 11 samples, because in July there was no rain enough for sampling), the samples was just compared with the GMWL together with the groundwater and lake samples.

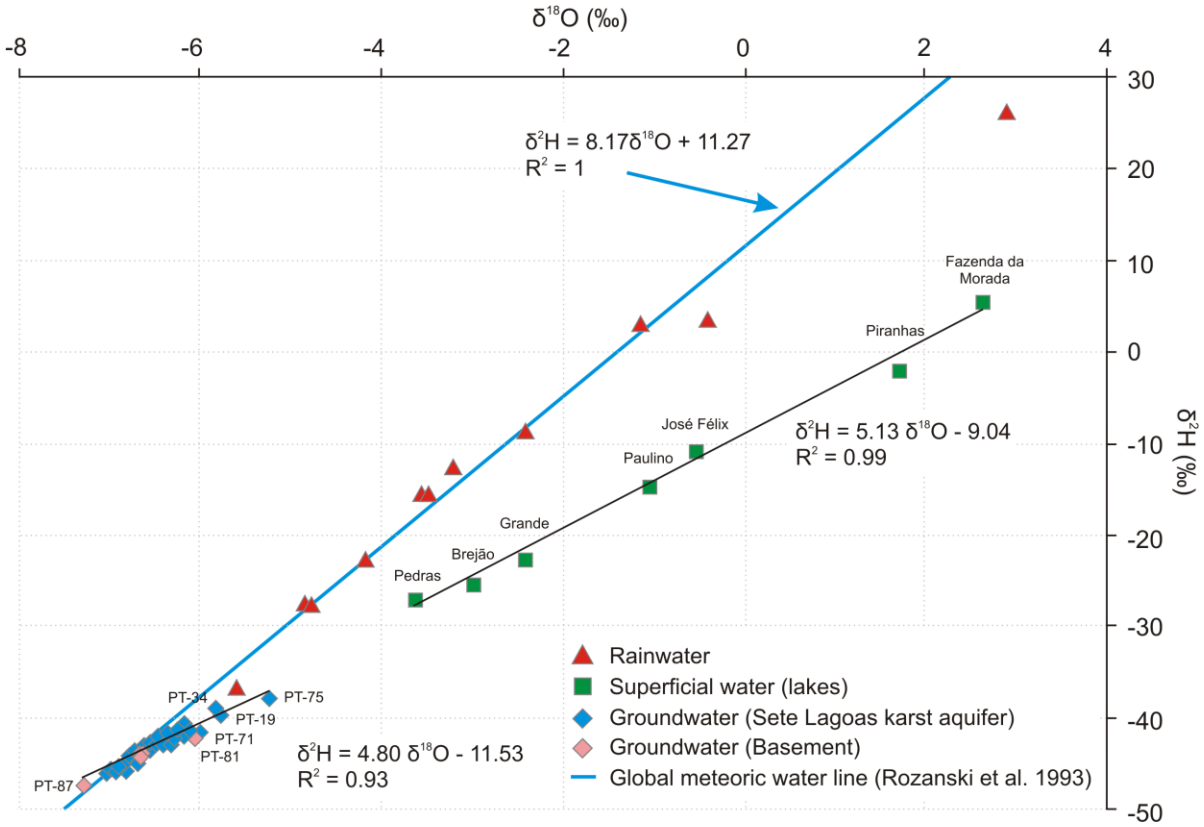

Fig. 2. Plot of mean δ^2H versus $\delta^{18}O$ for groundwaters from Sete Lagoas karst aquifer and basement, local rainwater, and lake waters in comparison to the global meteoric water line (Rozanski et al. 1993).

Table 1. Stable isotopic data groundwater and lake water from Sete Lagoas.

	Sampling ID	Date (mm/yy)	$\delta^{18}O$ (‰)	$\delta^{2}H$ (‰)	*d-excess (‰)*	Origin
Groundwater samples	PT-01	04/12	-6.37	-42.4	8.56	SLKA
	PT-07	04/12	-6.42	-42.5	8.86	SLKA
	PT-12	10/12	-6.24	-41.4	8.52	SLKA
	PT-15	03/12	-6.18	-41.1	8.34	SLKA
	PT-18	11/11	-6.18	-40.9	8.54	SLKA
	PT-19	03/12	-5.80	-39.1	7.3	SLKA
	PT-22	01/12	-6.17	-40.4	8.96	SLKA
	PT-34	03/12	-5.85	-38.8	8	SLKA
	PT-36	11/11	-6.51	-42.1	9.98	SLKA
	PT-40	12/11	-6.60	-42.7	10.1	SLKA
	PT-45	02/12	-6.57	-42.8	9.76	SLKA
	PT-47	04/12	-6.71	-44.3	9.38	SLKA
	PT-48	03/12	-6.21	-41.8	7.88	SLKA
	PT-51	01/12	-6.51	-42.3	9.78	SLKA
	PT-57	10/11	-6.91	-45.1	10.18	SLKA
	PT-64	12/11	-6.64	-43.9	9.22	SLKA
	PT-69	03/12	-6.33	-42.2	8.44	SLKA
	PT-71	03/12	-6.84	-45.4	9.32	SLKA
	PT-75	03/12	-5.26	-37.6	4.48	SLKA
	PT-77	12/11	-6.01	-41.3	6.78	SLKA
	PT-78	09/11	-6.73	-43.4	10.44	Basement
	PT-81	11/11	-6.06	-41.7	6.78	Basement
	PT-82	08/11	-7.06	-45.6	10.88	SLKA
	PT-84	01/12	-7.02	-45.4	10.76	SLKA
	PT-86	01/12	-6.72	-43.5	10.26	Basement
	PT-87	10/11	-7.31	-47.0	11.48	Basement
	PT-89	09/11	-6.36	-41.2	9.68	Basement
	PT-90	09/11	-6.31	-41.5	8.98	SLKA
	PT-99	11/11	-6.83	-44.3	10.34	SLKA
	PT-105	11/12	-6.77	-43.7	10.46	SLKA
	Average	**-**	**-6.45**	**-42.5**	**9.08**	**-**
Lake samples	Grande	06/13	-2.44	-22.4	-2.88	Natural
	José Félix	06/13	-0.55	-10.8	-6.4	Natural
	Paulino	06/13	-1.07	-14.4	-5.84	Natural
	Pedras	06/13	-3.64	-26.9	2.22	Natural
	Fazenda da Morada	06/13	2.62	5.6	-15.36	Artificial
	Brejão	06/13	-3	-25	-1	Natural
	Piranhas	06/13	1.71	-2.1	-15.78	Natural
	Average	**-**	**-0.91**	**-13.71**	**-6.43**	**-**
Rainwater samples	-	Mar/12	-4.2	-22.4	11.2	Rain
	-	Apr/12	-3.24	-12.1	13.82	Rain
	-	May/12	-3.58	-15	13.64	Rain
	-	Jun/12	-2.43	-8.3	11.14	Rain
	-	Jul/12	-	-	-	Rain
	-	Aug/12	-0.44	4	7.52	Rain
	-	Sep/12	-3.6	-15	13.8	Rain
	-	Oct/12	2.93	25.8	2.36	Rain
	-	Nov/12	-4.89	-27.4	11.72	Rain
	-	Dec/12	-1.2	3.9	13.5	Rain
	-	Jan/13	-4.87	-27.2	11.76	Rain
	-	Fev/13	-5.62	-36.5	8.46	Rain
	Average	**-**	**-2.83**	**-11.84**	**10.81**	**-**

SLKA: Sete Lagoas Karst Aquifer

4.2 Geochemistry

The physical parameters and chemical compositions of waters in Sete Lagoas are given in the Table 2. The values of pH ranged from 6.1 to 8.1 with a mean value of 7.1, and EC ranged from 69 to 590 µS/cm, with a mean value of 322 µS/cm. The T ranged between 21.8 and 25.5ºC and mean value of 23.2 ºC, while ORP from 74 to 329 mV, with a mean value of 134 mV. While pH and EC had the highest values in the central portion, within the graben area, data for T and ORP did not present the same pattern (Fig. 3).

Regarding the major ions, Na^+ and Ca^{2+} together accounted for 75–99% of total cations (except in some wells located around the basement - PT-78, 81, 86, 87, and 89, between 43–66%, and in the Santa Helena Ridge foothills - PT-105, around 26%). HCO^-_3 was the most abundant anion in the waters, while SO^{2-}_4 was the second most abundant one. On the other hand, the anion CO^{-2}_3 almost did not occur (only observed in the PT-69). All these highest values, as well as the high values in the rest of the cations and anions are essentially located in the central portion of the area, within the graben area in the Sete Lagoas karst aquifer (Figs. 4 and 5). The spatial distribution of major ion concentrations is consistent, coinciding with the pH and EC, TDS and WH concentrations (Fig. 3).

According to Custodio and Llamas (2001), the classification of hardness as $CaCO_3$, in mg/L, is: < 50 (soft), 50-100 (moderately hard), 100-200 (hard), and > 200 (very hard). 56% of the water hardness results presented values between 100 and 200 mg/L classified as hard waters, 26% between 50 and 100 mg/L, classified as moderately waters, and 13% with a content below 50 mg/L. The supply well PT-51 exceeded 200 mg/L classified as very hard, while PT-105 did not presented hardness (Fig. 3).

According to the Piper's diagram (Fig. 6), the majority of the sampled waters, 50%, were classified as of Ca^{2+}–HCO^-_3 type, fitting with those classified by Pessoa (1996). The second most common water type was Ca^{2+}–Na^+–HCO^-_3, about 23% of the samples, while 10% of the waters were classified as of Ca^{2+}–Na^+–HCO^-_3 type, and 7% as of Ca^{2+}–Mg^{2+}–Na^+–HCO^-_3 type (Appelo and Postma 2005). The rest of the sampled water, 10%, were classified as of Na^+–Ca^{2+}–Mg^{2+}–HCO^-_3, Mg^{2+}–Na^+–HCO^-_3, and Mg^{2+}–HCO^-_3, being noted in individual sampled wells (Fig. 6). In some cases, waters near the basement outcrops or located in had more pronounced Mg^{2+} and Na^++ K in their compositions. In the case of waters relatively far from the basement, generally, were more enriched in Ca^{2+} and Na^+, associated to limestones from the Sete Lagoas Formation. However, the presence of bicarbonate ions (HCO^-_3) in all cases is predominant. Waters from the basement (PT-78, 81, 86, 87 and 89) had enrichment of Mg^{2+}, as well as close to the Santa Helena Ridge (PT-105). Some samples with nitrate (PT-12, 18, 19, 22) indicated different behavior, being not clustered with the rest of the samples, which means that this water probably had some alteration on their natural compositions.

Table 2. Sampling sites of the study area and average values of the chemical analyses.

Well ID	Date	Aquifer	pH	CE	T	OD	ORP	Na^+	K^+	Ca^{2+}	Mg^{2+}	Cl^-	HCO^-_3	CO^{-2}_3	SO^{2-}_4	NO^-_3	F^-	SiO_2	TDS	Alkalinity	Total water hardness	Water type
	(mm/yy)			(µS/cm)	(°C)	(mg/L)	(mV)	(mg/L)												(mg $CaCO_3$/L)		
PT-01	04/12	SLKA	6.7	458	24.7	2.3	107	4.35	0.30	39.37	3.56	0.02	103.1	0.0	0.015	10.34	0.052	24.39	178	168.9	112.94	Ca^{2+} - HCO^-_3
PT-07	04/12	SLKA	6.7	444	24.6	2.1	98	4.31	0.27	36.65	2.87	0.02	93.2	0.0	0.015	9.56	0.07	10.07	222	152.8	103.34	Ca^{2+} - HCO^-_3
PT-12	10/12	SLKA	8.1	590	23.0	2.8	76	17.12	0.63	23.51	2.21	13.82	149.2	0.0	0.015	37.5	0.002	15.88	337	244.6	95.54	Ca^{2+} - Na^+ - HCO^-_3
PT-15	03/12	SLKA	7.4	546	24.3	0.0	91	7.89	0.86	61.64	3.39	14	170.2	0.0	5.12	17.55	0.002	8.94	165	141.5	167.87	Ca^{2+} - HCO^-_3
PT-18	11/11	SLKA	6.5	489	25.6	0.2	147	21.65	1.49	51.29	3.96	14.62	144.5	0.0	3.7	3.41	0.21	43.5	0	198.2	144.39	Ca^{2+} - Na^+ - HCO^-_3
PT-19	03/12	SLKA	7.5	473	23.9	0.0	74	9.67	1.22	49.07	3.87	12	139.8	0.0	5.67	7.54	0.002	6.25	390	229.2	138.47	Ca^{2+} - HCO^-_3
PT-22	01/12	SLKA	7.1	449	23.8	2.8	148	24.23	3.04	62.81	0.13	15	178.2	0.0	6.2	17.00	0.05	9.79	250	229.3	117.90	Ca^{2+} - Na^+ - HCO^-_3
PT-34	03/12	SLKA	6.9	180	25.5	1.2	93	1.07	0.05	23.91	3.31	0.02	48.6	0.0	4.96	2.18	0.002	32.70	105	79.7	73.33	Ca^{2+} - Mg^{2+} - HCO^-_3
PT-36	11/11	SLKA	6.5	372	24.1	2.3	157	1.59	0.38	59.16	2.71	9.00	191.5	0.0	5.78	2.00	0.090	2.21	236	158.2	158.88	Ca^{2+} - HCO^-_3
PT-40	12/11	SLKA	6.7	316	23.1	1.7	129	1.41	0.37	114.45	23.97	0.02	105.2	0.0	6.73	0.05	0.002	36.86	200	166.2	138.42	Ca^{2+} - Mg^{2+} - HCO^-_3
PT-45	02/12	SLKA	-	-	-	-	-	1.85	0.99	23.73	3.10	0.02	68.8	0.0	11.30	0.69	0.097	10.00	124	114.6	74.04	Ca^{2+} - HCO^-_3
PT-47	04/12	SLKA	6.7	315	24.6	4.7	109	0.13	0.05	29.29	3.73	0.02	75.6	0.0	0.02	2.87	0.058	9.61	143	124.1	88.50	Ca^{2+} - Mg^{2+} - HCO^-_3
PT-48	03/12	SLKA	8.0	438	24.1	0.1	102	5.45	0.35	46.98	4.43	0.02	112.9	0.0	9.16	17.00	0.100	13.46	201	185.1	135.53	Ca^{2+}- HCO^-_3
PT-51	01/12	SLKA	8.0	492	23.8	5.0	161	9.44	2.17	91.63	5.24	13.00	291.1	0.0	0.02	5.50	0.080	18.40	280	441.1	245.07	Ca^{2+}- HCO^-_3
PT-57	10/11	SLKA	7.5	328	25.0	3.5	85	4.07	1.11	37.48	7.69	0.02	141.6	0.0	5.13	0.65	0.090	0.19	212	231.2	125.27	Ca^{2+} - Mg^{2+} - HCO^-_3
PT-64	12/11	SLKA	6.6	235	24.1	3.4	127	2.91	0.53	35.08	3.37	0.02	75.4	0.0	0.02	0.05	0.061	30.81	220	123.6	101.47	Ca^{2+} - HCO^-_3
PT-69	03/12	SLKA	-	-	-	-	-	1.70	0.29	45.02	3.69	0.02	194.5	6.0	11.32	3.72	0.002	7.57	178	169.4	127.63	Ca^{2+} - HCO^-_3
PT-71	03/12	SLKA	7.3	271	24.0	3.6	132	0.50	0.05	42.73	3.20	7.50	142.8	0.0	4.54	0.37	0.002	4.30	175	234.1	119.87	Ca^{2+} - HCO^-_3
PT-75	03/12	SLKA	7.9	252	23.9	2.3	88	0.80	0.05	27.19	1.40	6.00	85.1	0.0	6.00	0.05	0.070	6.23	137	139.5	73.65	Ca^{2+} - HCO^-_3
PT-77	12/11	SLKA	7.0	205	25.3	3.1	124	0.13	0.05	28.05	3.27	0.02	73.6	0.0	0.02	0.05	0.002	13.68	106	120.3	83.49	Ca^{2+} - HCO^-_3
PT-78	09/11	Basement	6.3	178	24.9	1.2	153	7.62	0.57	12.04	6.63	1.07	54.5	0.0	0.75	1.52	0.061	52.56	123	89.4	57.38	Ca^{2+} - Mg^{2+} - Na^+ - HCO^-_3
PT-81	11/11	Basement	6.3	69	23.3	2.8	112	2.80	0.41	5.35	3.20	0.02	48.5	0.0	4.71	0.05	0.002	0.01	74	94.1	26.53	Ca^{2+} - Mg^{2+} - HCO^-_3
PT-82	08/11	SLKA	7.8	168	21.8	3.7	329	2.26	0.71	28.58	4.05	0.02	54.5	0.0	1.13	0.05	0.002	10.67	148	89.4	88.05	Ca^{2+} - Mg^{2+} - HCO^-_3
PT-84	01/12	SLKA	6.7	245	22.9	3.8	147	0.73	0.05	49.61	0.13	0.02	83.3	0.0	0.02	0.70	0.002	12.55	154	136.6	147.42	Ca^{2+}- HCO^-_3
PT-86	01/12	Basement	6.1	355	23.7	3.4	148	6.66	1.56	5.52	2.44	0.02	34.4	0.0	0.02	0.05	0.100	5.63	108	56.1	3.86	Na^+ - Ca^{2+} - Mg^{2+} - HCO^-_3
PT-87	10/11	Basement	6.9	112	25.5	4.2	85	4.20	0.88	2.35	4.45	0.02	43.9	0.0	0.02	0.05	0.044	50.55	177	71.9	26.97	Mg^{2+} - Na^+ - HCO^-_3
PT-89	09/11	Basement	7.3	114	24.8	11.0	284	7.99	2.39	9.30	4.04	0.02	42.4	0.0	0.02	0.05	0.165	53.70	200	69.1	39.87	Ca^{2+} - Mg^{2+} - Na^+ - HCO^-_3
PT-90	09/11	SLKA	7.0	278	24.0	2.1	174	1.02	0.05	41.98	7.76	0.02	100.0	0.0	0.02	0.05	0.036	18.67	148	163.9	136.78	Ca^{2+} - Mg^{2+} - HCO^-_3
PT-99	11/11	SLKA	7.7	354	22.9	2.7	125	1.79	0.37	45.97	4.14	0.02	194.0	0.0	5.19	1.30	0.090	3.60	230	210.2	131.83	Ca^{2+} - HCO^-_3
PT-105	11/12	SLKA	7.0	290	23.1	3.3	134	1.83	0.55	49.89	2.47	0.02	97.4	0.0	4.14	0.05	0.002	33.90	158	158.2	0.00	Mg^{2+} - HCO^-_3
Average	-	-	7.1	322	24.1	2.8	134	5.24	0.73	39.32	4.28	3.55	111.3	0.2	3.39	4.73	0.052	18.22	179	160	102.81	-

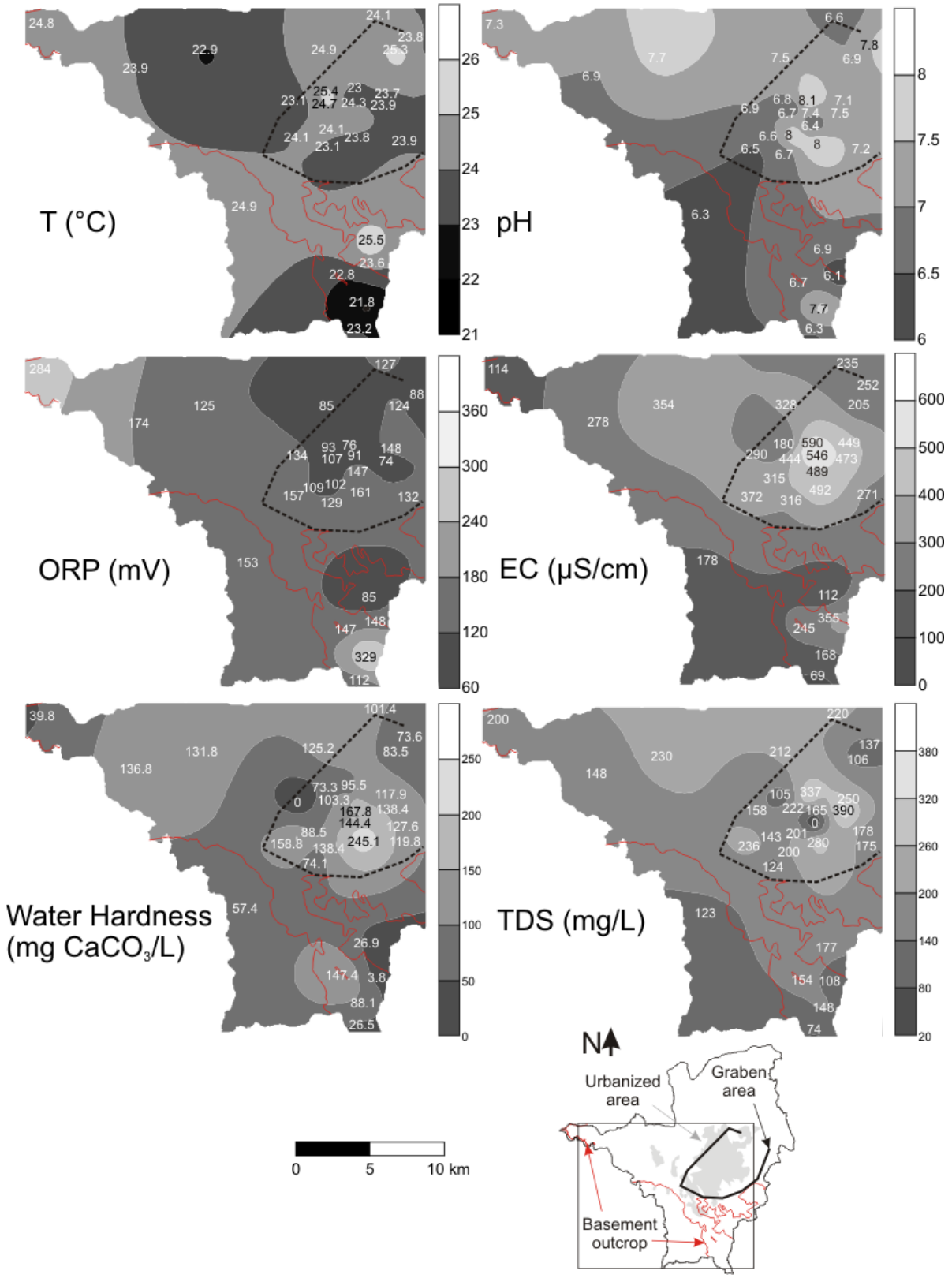

Fig. 3. Isopleths of T, pH, ORP, EC, TDS and WH. The lower-right sketch map shows the zoom in limits and the location of urbanized area, basement outcrops, and the central graben area.

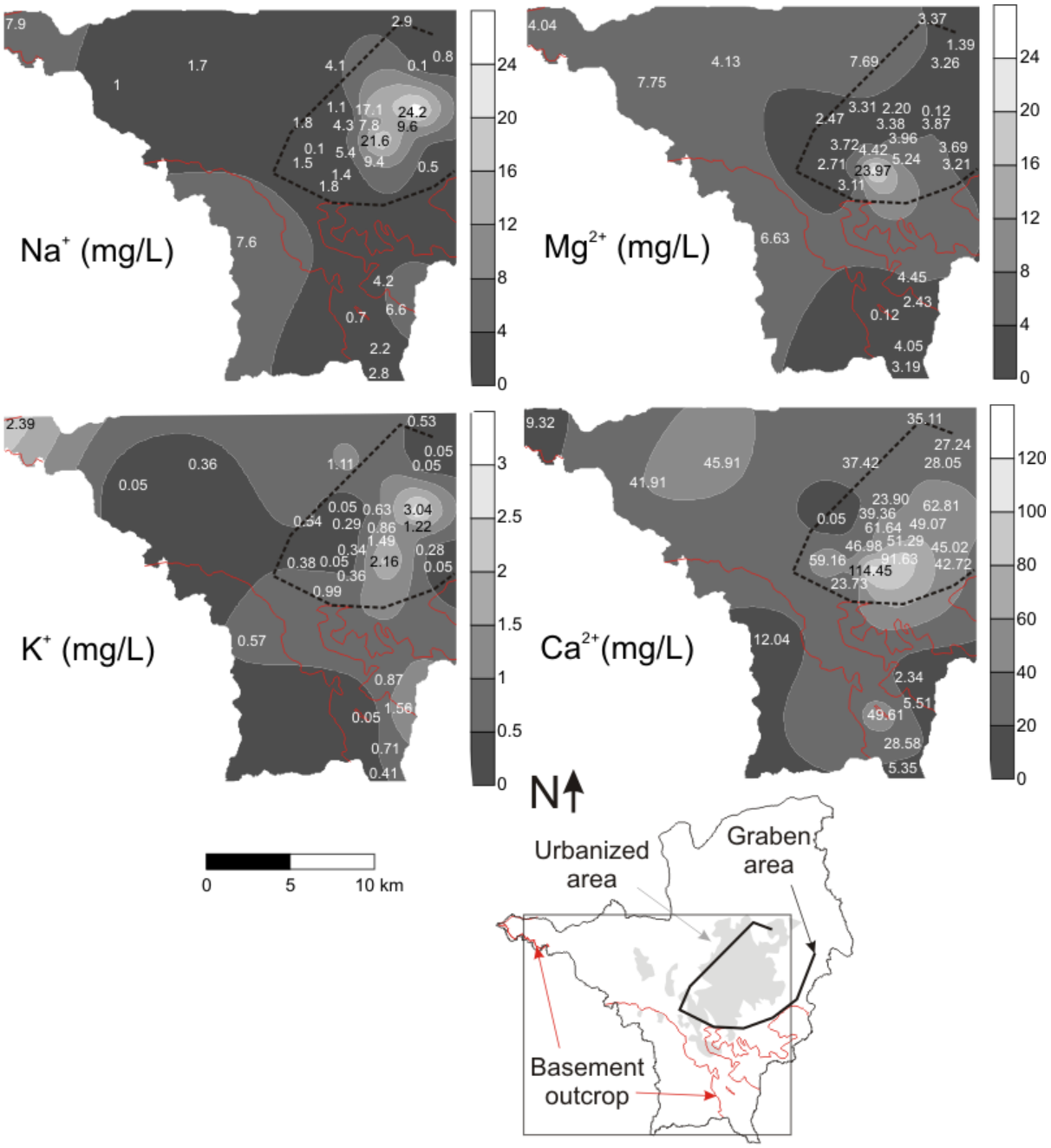

Fig. 4. Isopleths of Na^+, K^+, Ca^{2+}, and Mg^{2+} cation concentrations in mg/L. It can be noted that the highest cation concentration values are located within the graben area.

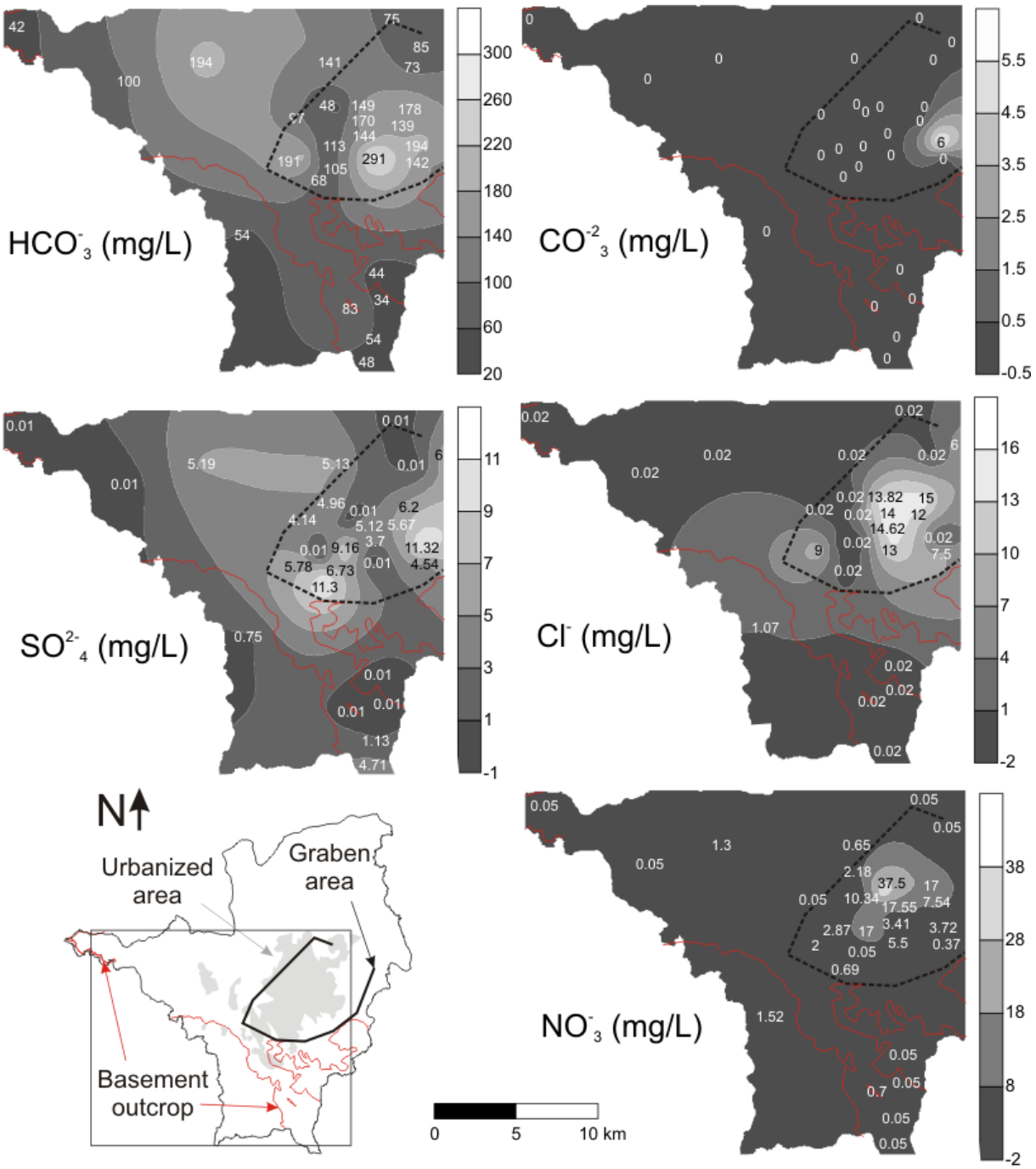

Fig. 5. Isopleths of HCO^{-}_{3}, CO^{-2}_{3}, SO^{2-}_{4}, Cl^{-}, and NO^{-}_{3} anion concentrations in mg/L. The highest anion concentration values are also located within the graben area.

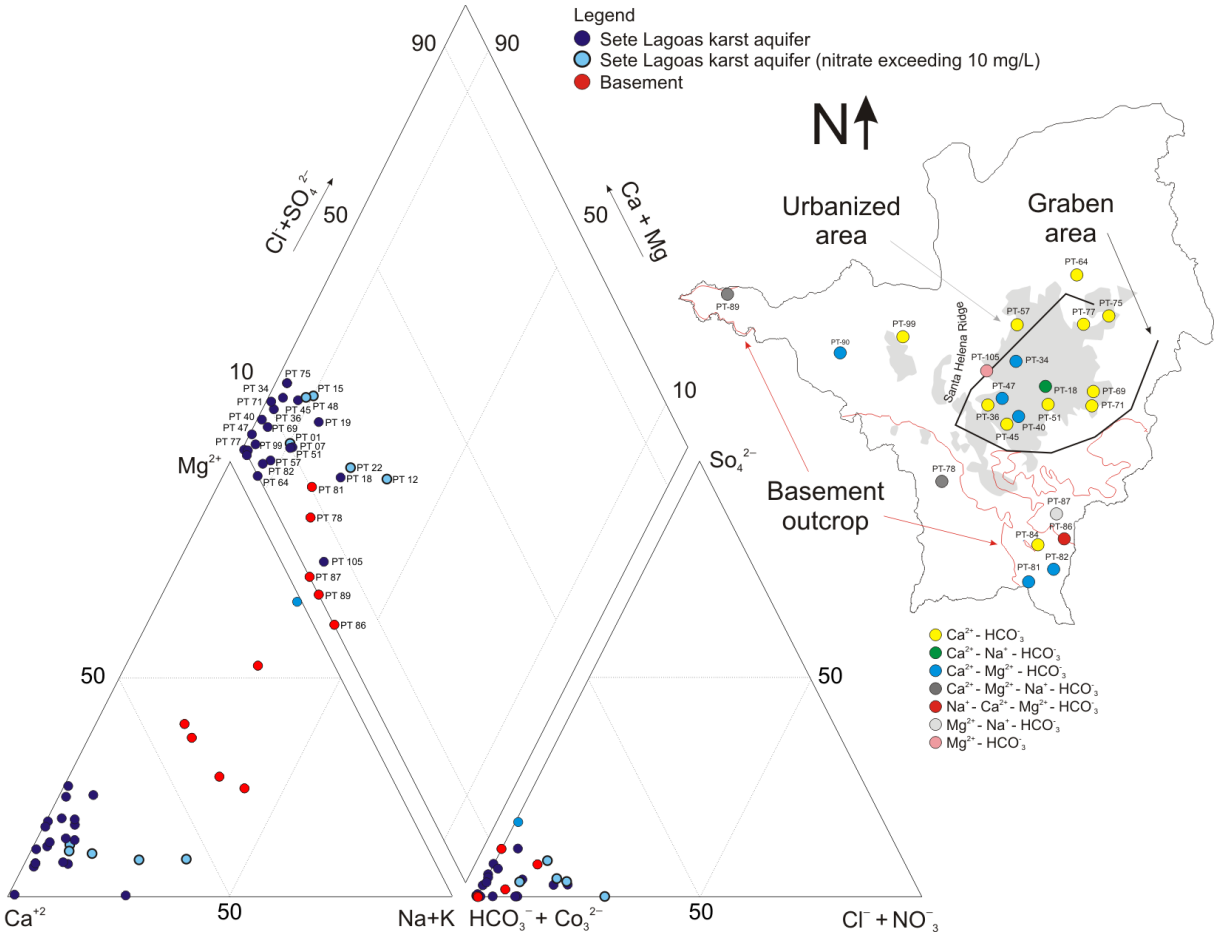

Fig. 6. Piper's diagram of the major ion composition of waters collected in Sete Lagoas. On the map (right), it is possible to see the location of each one type of water. Waters near the basement outcrops or located in had more pronounced Mg^{2+} and Na^{+}+ K on their compositions. In the case of waters relatively far from the basement, they are more enriched in Ca^{2+} and Na^{+}, associated to limestones from the Sete Lagoas Formation. The presence of bicarbonate ions (HCO^{-}_{3}) in all cases is predominant. Waters in the basement (PT-78, 81, 86, 87 and 89) had a little enrichment of Mg^{2+}, as well as close to the Santa Helena Ridge (PT-105). Some samples exceeding 10 mg/L can indicate different behavior, being not clustered with the rest of the samples, probably having any alteration on their natural composition.

5. Discussion

The discussion will be presented sequentially from the stable isotope and geochemistry interpretations, to the water evolution and sources of recharge, presenting a schematic conceptual model of Sete Lagoas.

5.1 Stable isotopes

The lake waters from Sete Lagoas have the highest values of $\delta^{2}H$ and $\delta^{18}O$, falling well below the global meteoric water line, forming an evaporation line, an indication that these waters are exposed to a high degree of evaporation (Fig. 2). It is important to relativize that these lake waters were collected during the dry season, in June, where the evaporation rate is high, reflecting the location of these points in the graphic.

The groundwater samples, both from karst aquifer and basement, which were collected during dry and rainy seasons, have mostly samples clustered, with the majority of them on or near the GMWL, indicating recharging directly from precipitation. Other samples were plotted fairly tightly in the lower left, which give an appearance of evaporation. Regarding the clustering of groundwater samples, it could suggest a limited period of recharge, according to Clark and Fritz (2007), where the rainy season in Sete Lagoas occurs from October to March, corresponding to 89% of annual precipitation (Fig. 2), having October, November and December as being the recharging period, according to the water balance proposed by Pessoa (1996).

In the case of groundwater samples plotted in the lower left, this situation could suggest that, in some situations, groundwater locally could receive superficial water contributions. Some pumping wells, which the groundwater samples were collected, are located next to some lakes, e.g. PT-71 (Brejão Lake), PT-75, 77 (Grande Lake and Piranhas Lake). Other wells also have evidences of little evaporation and are located or close to some lakes (José Felix Lake and Paulino Lake) or close to drainages and in the Cenozoic unconsolidated sediments. The groundwaters in Sete Lagoas are stored in two main solutionally enlarged bedding planes, where in the central portion of the area are covered by these unconsolidated sediments (Galvão et al. 2015). In this region, groundwater could have punctual superficial water contributions (from lakes or small drainage, Fig. 1), reflecting in the plotting of some dots in the lower left of the GMWL, forming this evaporation pattern.

Thus, the overall evidences could suggest that the groundwaters in Sete Lagoas: (1) are recharged directly from precipitation; (2) have a limited period of recharge during the recharging season, from October to December; and (3) in the central portion, where the karst aquifer is in contact with Cenozoic unconsolidated sediments, could have superficial water infiltration.

5.2 Geochemistry

The major ions presented the highest values at the same region, where the most karst area from the Sete Lagoas Formation is located, within the graben area, coinciding with the pH, EC, TDS and WH values, which present the same concentration behavior (Figs. 3 to 5). These data could suggest a large water reservoir indicating more mineralization, which are in concordance with the geologic information commented by Galvão et al. (2015). This area is primarily located in a graben, filled with a deposit of limestones resulting in barrier boundaries for groundwater, which together with natural karst processes explain the location of two main solutionally enlarged bedding planes with large groundwater storage capacity.

The water hardness, which refers to the ability of water to form encrustations, prevent the sudsing of soap, is due the presence of calcium and magnesium cations, forming insoluble compounds. Hard water contributes to inefficient and costly operation of water-using appliances. Pipes can become clogged with encrustations that reduces water flow and ultimately requires pipe replacement. This can pose serious problems in industrial settings, as well as in domestic purposes, when hardness is above 100 mg/L. The highest values were found in the central urbanized area, which the population living in this area can have problems related of encrustations. Indeed, according to fieldwork investigations and interviews with local residents, these problems are common.

The presence of a high value of Mg^{2+} ion in the central area (23.97 mg/L) compared to the remaining areas could indicate localized dolomite occurrences or dolomitic limestones, enriching some water compositions. These ions also could indicate water residence time because of its low dissolution kinetic (Mudry 1987, Plagnes 1997, Batiot et al. 2003). Commonly, the more severe the low flow conditions, the more mobilized becomes the water, with increased residence time (Fig. 4).

Nitrate (as NO^-_3) occurs in almost all natural water, except when contamination is present, when they seldom exceed 20 mg/L (Hounslow 1995). However, 10 mg/L or greater may be regarded as a probable indication of contamination (e.g. from fertilizer, municipal wastewaters, septic systems, etc.). In the central portion of the urbanized area, values over 10 mg/L (PT-01: 10.34 mg/L; PT-15: 17.55 mg/L; PT-17: 17.00 m/L) and even greater than 20 mg/L (PT-12: 37.5 mg/L) were found. According to Foster and Hirata (1987), inefficient management of domestic sewage in-situ sanitation systems is the main source of nitrate in urbanized areas, particularly in developing countries. The NO^-_3 is also an indication of recent contamination related to construction problems in wells or a lack of aquifer protection (Alaburda and Nishihara 1998). As construction problems on these wells with high nitrate values were not observed during fieldworks, and the concentrations are located only in the central portion of the urban area (Fig. 5), it could be interpreted as a local contamination by superficial infiltration probably by domestic sewage or septic tank, which can be considered as an evidence of local connections between surface waters and groundwaters, corroborating with the isotopic data.

Regarding the higher Ca^{2+} concentrations in the central area, is probably due to the reaction of calcite with carbon dioxide (CO_2) derived from respiration or oxidation of organic matter. In this region, is common the presence of Cenozoic unconsolidated sediments right above the limestones (may reach up to 40 m thick - Galvão et al. 2015, in press), which could provide carbon dioxide reacting with water that infiltrates through these sediments to form carbonic acid (H_2CO_3). This acid provides protons (H^+), which can associate with the carbonate ion (CO^{2-}_3) from calcite ($CaCO_3$) to form bicarbonate (HCO^-_3), and then take place dissolution and precipitation. It can be seen in the Fig. 6 that the concentrations of HCO^-_3 are much higher and located in the whole area, while the CO^{2-}_3 values is only seen in one sampling well, being zero in the rest of the area, indicating the last stage of the reaction of the dissolution of calcite. Other evidences are the concentrations of these ions as function of pH. The pH values are between > 6.3 and < 10, where within this interval HCO^-_3 is the most predominant species than CO^{2-}_3 (Fig. 5).

Waters tend to precipitate calcite or dolomite when it is oversaturated and tend to dissolve them if it is undersaturated. The Saturation Index (SI) is perhaps the most widely used method to determine the amount of calcite that will be precipitated or dissolved. The results show that almost all groundwaters are undersaturated in dolomite and calcite (Fig. 7). The fact that the waters are undersaturated in dolomite and calcite indicates that both elements can dissolve in this system, which means that the two main solutionally enlarged bedding planes that the groundwaters are stored and are being pumped are still undergoing processes of karstification.

So, a question can be asked: is this a natural phenomenon or is this event a result of pumping through decades? Analyzing the Fig. 8, where there is a comparison between SI and pumping rate, no relationship was noted, such as high pumping rates and low values of SI, suggesting a natural phenomenon that took place well before the origin of the city and the anthropogenic well pumping.

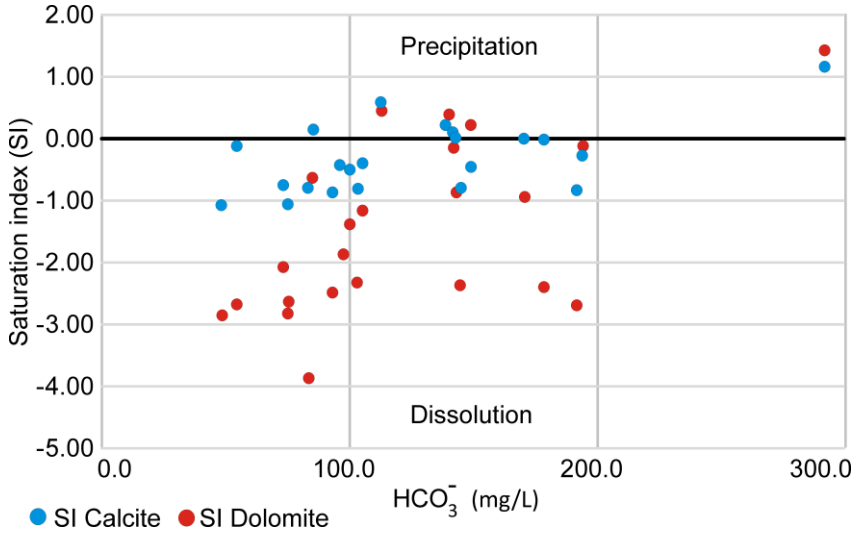

Fig.7. Saturation Index (SI) of calcite and of dolomite versus HCO^-_3 of all collected samples. Almost all groundwaters are undersaturated in dolomite and calcite. This fact indicates that both elements are dissolving in this system, which the two main solutionally enlarged bedding planes are still undergoing processes of karstification.

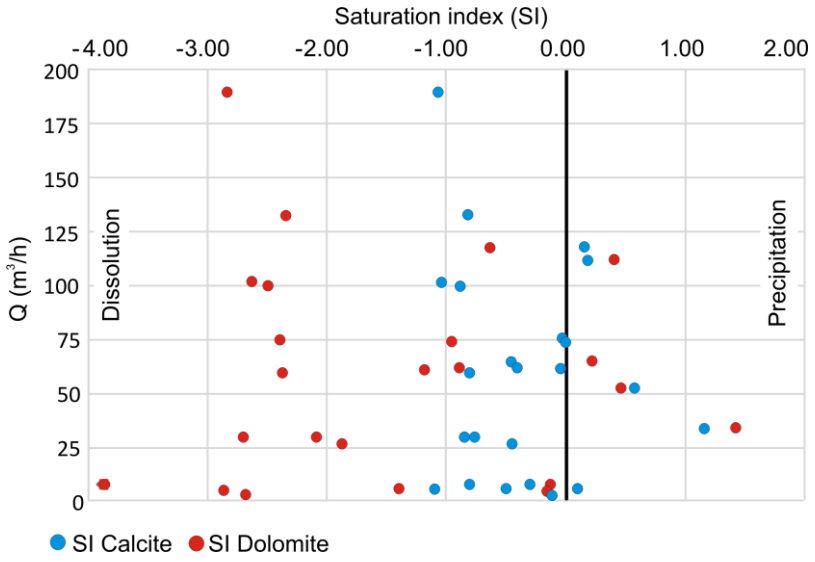

Fig. 8. Saturation Index (SI) of calcite and of dolomite versus pumping rates. No relationship between those parameters was seen, such as high pumping rates and low values of SI, suggesting a natural phenomenon that took place well before the origin of the city and the well pumping.

5.3 Water evolution and sources of recharge

A schematic water evolution conceptual model of Sete Lagoas was proposed (Fig. 9). Generally, the Sete Lagoas karst aquifer consists of Neoproterozoic limestones that has the primary porosity and matrix permeability very low and the second porosity (micro-fractures) mostly filled by calcite (Galvão et al. 2015). Thus, the majority of fluids migrate through dissolution features characterized as tertiary porosity developed in bedding planes (most frequent) and sometimes in subvertical fractures (less common), not receiving much contribution from the matrix (Galvão et al. 2015). In the case of the basement, waters fluid through subvertical fractures.

In areas where the limestone outcrops, where some sinkholes and caves are located (Figs. 1 and 9), can be considered as direct recharge zones (or autogenic recharge), receiving rainfall waters by runoff. In some cases, these waters infiltrate through unconsolidated sediments and in the basement outcrops until reach the water table in the karst aquifer, being classified as allogenic recharge. The autogenic waters infiltrate in the sinkholes and caves located mostly in the south and southeast (Fig. 1), with higher elevations and flowing mainly in the two solutionally enlarged bedding planes, to the NNE direction, according the potentiometric surface map and its flow directions (Fig. 9). Some waters could pass through dolomitic rocks being enriched of magnesium, with increased residence time, which could indicate a dissolution zone storing waters for more period of time in that particular area.

Regarding the basement, when it outcrops, there is an autogenic basement recharge, with waters infiltrating in subvertical fractures. In some areas, where this basement is covered by other formations, there is an allogenic basement recharge, with waters passing through overlaying lithologies until reach the basement water table (Fig. 9). Waters from the basement (PT-78, 81, 86, 87 and 89), as well as close to the Santa Helena Ridge (PT-105) are more enriched in Mg^{2+}. They can mix with waters more enriched in Ca^{2+} and Na^{+}, associated with limestones from the Sete Lagoas Formation, and dilute, influencing in their final composition types, seen in some samples located in the south (PT-81, 82), west (PT-90), and close to Santa Helena Ridge (PT-34, 47).

In the central area, waters can also have some mixing with allogenic recharge from unconsolidated sediments that can reach the two main conduits. Occurrences of nitrate and isotopic evaporations evidence this type of local infiltration and superficial-ground water interconnections, such as local drainage and lakes. In the central urbanized area, the presence of the highest values of major ions indicates more mineralization in the groundwater, suggesting large groundwater storage capacity. According to Galvão et al. (in review), this region has the highest transmissivity values in Sete Lagoas, considered other evidence of karstification.

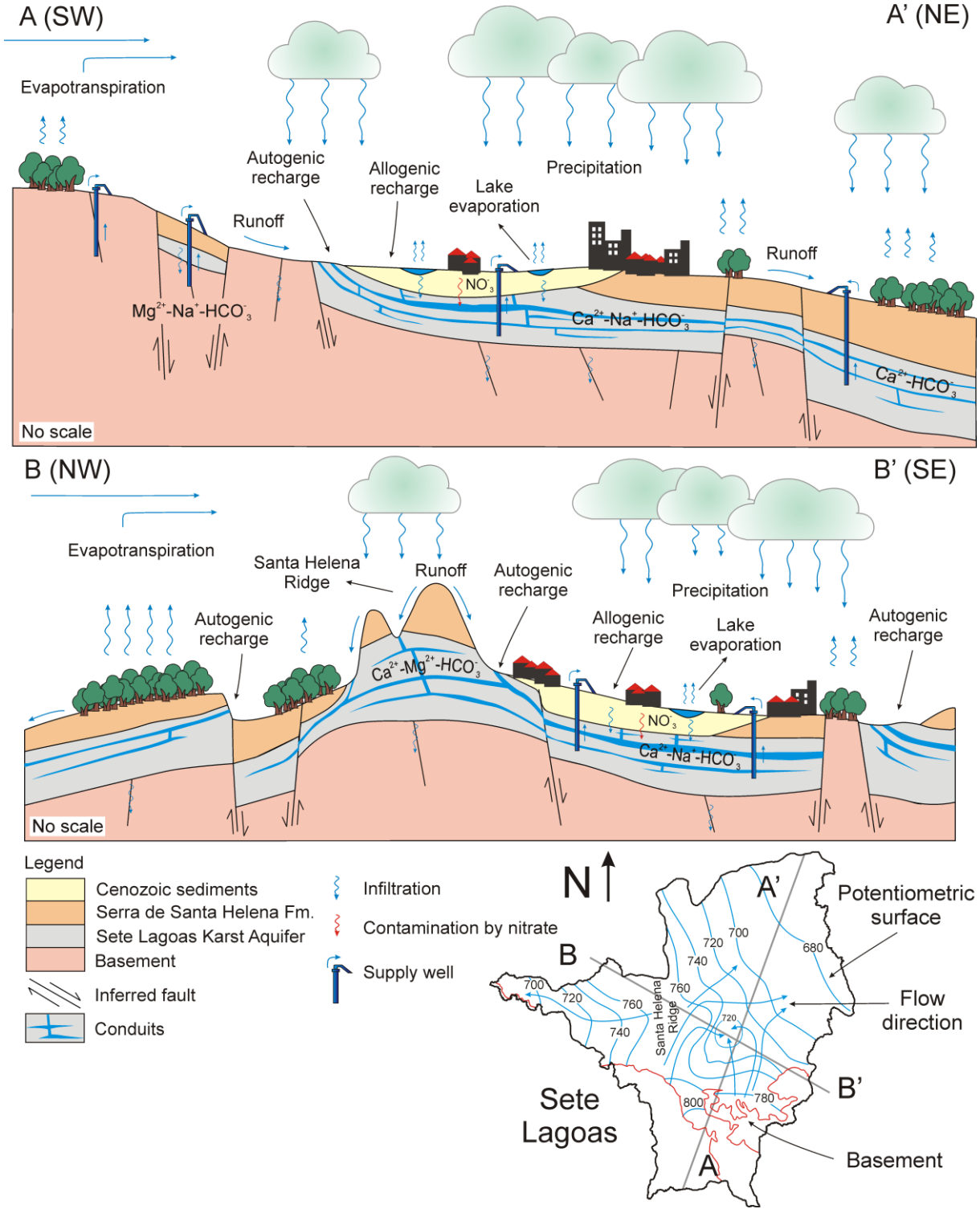

Fig. 9. A schematic water evolution conceptual model of Sete Lagoas, based on Galvão et al. (in press). Autogenic recharge zones occurring when limestones outcrop, receiving rainfall waters by runoff. When the karst aquifer receives waters from unconsolidated sediments or from basement, there is an allogenic recharge. Some waters could pass through dolomitic rocks being enriched of magnesium, with increased residence time. The majority of fluids migrate through dissolution features characterized as tertiary porosity developed in bedding planes (most frequent) and sometimes in sub-vertical fractures (less common). In the case of basement, waters fluid through subvertical fractures.

6. Conclusion

Groundwaters in Sete Lagoas are the result of direct recharge from precipitation, during a limited period from October to December. The recharging zones are mainly the sinkholes and caves entrances, as well as in areas where the limestones are covered by Cenozoic unconsolidated sediments. The majority of the fluids migrate through tertiary porosity, characterized by solutionally enlarged bedding planes and less common by sub-vertical enlarged fractures.

The isotopic data in the lakes reflect evaporation processes, which combining with some groundwater samples also with evaporation evidences, indicate some interconnections. Nitrate occurences can be interpreted as an evidence of local connections between surface waters and groundwaters, corroborating with these isotopic data. Groundwaters from the basement, with the same isotopic signature in comparison to water from the karst aquifer also have the same origin, by precipitation.

The majority of these groundwaters are classified as of Ca^{2+}–HCO^{-}_{3} type, associated to limestones from the Sete Lagoas Formation. Waters in the basement and close to the Santa Helena Ridge are enriched of Mg^{2+}. These different types of water can mix with waters more enriched in Ca^{2+} and Na^{+}, diluting, resulting in other composition types. These mixing waters also indicate interconnections between karst aquifer and basement waters.

The central urbanized area, where the Cenozoic unconsolidated sediments cover the limestones, as well as in areas with sinkholes and cave entrances are located, are considered the major flowpaths for contaminants in Sete Lagoas. However, for the sinkhole and cave entrances regions, it is recommended directed studies to confirm this consideration. The occurrences of nitrate in the central area exceeding 20 mg/L indicate that the stakeholders must protect these areas.

Acknowledgments

This work was funded by Servmar Environmental & Engineering and by São Paulo Research Foundation (FAPESP) [*Fundação de Amparo à Pesquisa do Estado de São Paulo*] (process 2012/12846-9). A special thanks to Groundwater Research Center (CEPAS) [*CEPAS - Centro de Pesquisas de Águas Subterrâneas*] for the isotopic analysis and to Rafael Terada for the discussion and assistance.

References

Alaburda JE, Nishihara L (1998) Presence of nitrogen compounds in well water. Journal of Public Health [*Revista de Saúde Pública*], 32(2):160-165.

Andreo B, Vías J, M, Durán JJ, Jiménez P, López Geta JA, Carrasco F (2008) Methodology for groundwater recharge assessment in carbonate aquifers: application to pilot sites in southern Spain. Hydrogeology Journal 16: 911-925.

Appelo CAJ, Postma D (2005) Geochemistry, groundwater and pollution (2nd ed.): Leiden, The Netherlands, A.A. Balkema, 649 p.

Batiot Emblanch C, Blavoux B (2003) Carbone organique total et magnésium: deux traceurs complémentaires du temps de séjour dans l'aquifere karstique. Académie des sciences, éditions scientifiques Elsevier: 205-214.

Branco Jr, Costa MT (1961) Belo Horizonte-Brasilia roadmap tour. In: Brazilian Congress of Geology, Brasilia. Radioactive Research Institute, Federal University of Minas Gerais (UFMG), Publication 15, Belo Horizonte, p 25

Buttle JM (1994) Isotope hydrograph separations and rapid delivery of pre-event water from drainage basins. Progress in Physical Geography 18 (1), 16–41.

Cartwright I, Weaver TR, Fulton S, Nichol C, Reid M, Cheng X (2004) Hydrogeochemical and isotopic constraints on the origins of dryland and salinity, Murray Basin, Victoria, Australia. Applied Geochemistry 19 (8), 123-1254.

CETESB (1998) Sampling and Water Samples Preservation Guide. São Paulo, 150 p.

Clark I, Fritz P (1997) Environmental Isotopes in Hydrogeology. New York, CRC Press. 328p.

Coplen TB, Kendall C (2000) Stable hydrogen and oxygen isotope rations for selected sites of the U.S. Geological Survey's NASQAN and Benchmark Surface-Water Networks: I.S. Geological Survey Open-File Report 00-160. 103 p.

Craig H (1961) Standard for reporting concentration of deuterium and oxygen-18 in natural waters. Science 133, 1702–1703.

Custodio E, Llamas MR (2001) Hidrologia subterrânea. Tomo I e II, Ediciones Omega, S.A, Barcelona. 2350p.

Dardene MA (1978) Synthesis on the stratigraphy of Bambuí Group in Central Brazil. In: Brazilian Congress of Geology, 30, Recife. Annals Recife: Brazilian Society of Geology, 1978 v.2, p.597-610

Farfán H, Corvea JL, de Bustamante I (2009) Sensitivity analysis of APLIS method to compute spatial variability of karst aquifers recharge at the national Park of Viñales (Cuba). Advances in Research in Karst Media Environmental Earth Sciences 2010, pp 19-24.

Fontes JC (1980) Environmental isotopes in groundwater hydrology, *in* Fritz P and Fones JC, eds., Handbook of environmental isotopes geochemistry, Volume 1: New York, Elsevier, p. 75-140.

Ford DC (1999) Perspectives in karst hydrogeology and cavers genesis. In Palmer AR, Palmer MV and Sasowsky ID (eds) Karst Modeling. Karst Waters Institute Special Publication no 5, Charlottesville, p 17-29.

Ford DC and Williams PW (1989) Karst geomorphology and hydrology: Boston, Unwin Hyman, 601 p.

Foster SSD, Hirata RCA (1987). Groundwater pollution risk evaluation: the methodology using available data. Lima: WHO/PAHO/HPE/CEPIS, 87 p.

Galvão P, Halihan T, Hirata R. (2015) Evaluating karst geotechnical risk in the urbanized area of Sete Lagoas, Minas Gerais, Brazil. Hydrogeology Journal (online). DOI: 10.1007/s10040-015-1266-x

Ginsberg M, Palmer AN (2002) Delineation of source-water protection areas in karst aquifers of the Ridge and Valley and Appalachian Plateaus physiographic provinces: rules of thumb for estimating the capture zones of springs and wells. Unpublished report EPA 816-R-02-015, 51p. US Environmental ProtectionAgency, Office of Water; Available from: http://www.epa.gov/safewater.

Goldsheider N, Drew D (2007) Methods in karst hydrology. Taylor & Francis Group, London, U.K. 264 p.

Han Z, Tang C, Wu P, Zhang R, Zhang C (2014) Using stable isotopes and major ions to identify hydrological processes and geochemical characteristics in a typical karstic basin, Guizhou, southwest China. Isotopes in Environmental and Health Studies. Vol. 50, No. 1, 62–73

Harris DM, McDonnell JJ, Rodhe A (1995) Hydrograph separation using continuous open system isotope mixing. Water Resources Research 31 (1), 157–171.

Hess JW, Wells SG, Quinlan JF, White WB (1989) Hydrogeology of the south-central Kentucky karst, *in* White WB and White EL, eds., Karst hydrology concepts the Mammoth Cave area: New York, Van Nostrand Reinhold, p. 15.63.

Hounslow AW (1995) Water Quality Data: Analysis and Interpretation, CRC Lewis Publishers, Boca Raton, FL, pp. 86-87.

IAEA/WHO. (2004) Global Network of Isotopes in Precipitation. The GNIP Database. Available at: http://isohis.iaea.org.

IBGE - Brazilian Institute of Geography and Statistics (2010). Basic Municipal Information. Avaliable: http://www.ibge.gov.br/cidadesat/topwindow.htm?1 Accessed on March 2014.

Karamouz M, Ahmadi A, Akhbari M (2011) Groundwater Hydrology Engineering, planning, and management. CRC Press Tylor and Francis Group Boca Raton London New York, pp. 31-35, 578.

Käss W, Behrens H, Himmelsbach T, Hötzl H (1998) Tracing technique in geohydrology. Rotterdam: Balkema.

Katz BG, Lee TM, Plummer LM, Busenberg E (1995) Chemical evolution of groundwater near a sinkhole lake, northern Florida; 1, Flow patterns, age of groundwater, and influence of lake water leakage: Water Resources Research, v. 31, no. 6, p. 1549-1564.

Kennedy VC, Kendall C, Zellweger GW, Wyerman TA, Avanzino RJ (1986) Determination of the components of stormflow using water chemistry and environmental Isotopes, Mattole River Basin, California. Journal of Hydrology 84 (1-2), 107–140.

Lee KS, Kim Y (2007) Determining the seasonality of groundwater recharge using water isotopes: a case study from the upper North Han River basin, Korea. Environmental Geology 52 (5), 853–859.

Li SL, Liu CQ, Li J, Lang YC, Ding H, Li L (2010) Geochemistry of dissolved inorganic carbon and carbonate weathering in a small typical karstic catchment of Southwest China: isotopic and chemical constraints. Chem Geol. 2010;277:301–309.

Liu L, Shu L, Chen X, Oromo T (2009) The hydrologic function and behavior of the Houzhai underground river basin, Guizhou Province, southwestern China. Hydrogeol J.;18:509–518.

Machavaram MV, Whittemore DO, Conrad ME, Miller NL (2006) Precipitation induced stream flow: an event based chemical and isotopic study of a small stream in the Great Plains region of the USA. Journal of Hydrology 330 (3-4), 470–480.

McKenna SA, Ingraham, NL, Jacobson RL, Cochran GF (1992) A stable isotope study of bank storage mechanisms in the Truckee river basin. Journal of Hydrology 134 (1-4), 203–219.

Meyers JG, Swart PK, Meyers JL (1993) Geochemical evidence for groundwater behavior in an unconfined aquifer, south Florida: Journal of Hydrology, v. 148, p. 249-272, DOI: 10.1329/1999W900352.

Moore CH (1989) Carbonate diagenesis and porosity. Development in sedimentology 46. Amsterdam: Elsevier, 338 p.

Mudry J (1987) Apport du traçage physico-chimique naturel à la connaissance hydrocinematique des aquifères carbonates. Mémoire n4 Univ. Besançon, 382p.

O'Driscoll MA, DeWalle DR, McGuire KJ, Gburek WJ (2005) Seasonal O-18 variations and groundwater recharge for three landscape types in central Pennsylvania, USA. Journal of Hydrology 303 (1-4), 108–124.

Oliveira MAM (1967) Contribution to the geology of the southern part of the São Francisco Basin and adjacent areas. In: Collection of Reports Exploration, Rio de Janeiro 1: Petrobras, n.3, p 71-105

Palmer AN (1991) Origin and morphology of limestone caves, Geological Society of America Bulletin, v. 103, p 1-21.

Pessoa P (1996) Hydrogeological characterization of the region of Sete Lagoas - MG: Potentials and Risks. Master Thesis. Department of Geosciences, University of São Paulo. São Paulo.

Piper AM (1944) A graphical procedure in the geochemical interpretation of water-analysis. Transactions American Geophysical union. v. 25, p. 914-928

Plagnes V (1997) Le transport de matière dans les aquifères karstiques. 6th conf on limeston hydrology and fissured media, La Chaux de Fond, Suisse, 14-18/08/97:179-183

Plummer LN, Busenberg E, McConnell JB, Drenkard S, Schlosser P, Michel RL (1998) Flow of river water into a karstic limestone aquifer. Tracing the young fraction in groundwater mixtures in the upper Floridan aquifer near Valdosta, Georgia: Applied Geochemistry, v. 13, no.8, p. 995-1015, DOI: 10.1016/S0883-2927(98)00031-6.

Puls RW, Barcelona MJ (1996) Low flow (minimal drawndown) groundwater sampling procedures. United States Environmental Protection Agency, Office of Research and Development, Office of Solid Waste and Emergency Response, EPA/540/S-95/504, April, 12p.

Ribeiro JH, Tuller MP, Danderfer Filho A (2003) Geological mapping of the region of Sete Lagoas, Pedro Leopoldo, Matozinhos, Lagoa Santa, Vespasiano, Capim Branco, Prudente de Morais, Confins and Funilândia, Minas Gerais State, Brazil (scale 1:50,000). 2nd edn. Belo Horizonte. 54 p

Rozanski K, Araguás-Araguás L, Gonfiantini R (1993) Isotopic patters in modern global precipitation, in *Climate Change in Continental Isotopic Records,* Geophys. Monogr. Ser., 78, ed. by P.K. Swart, et al, pp. 1-36, AGU, Washington, DC.

Ryan M and Meiman J (1996) An examination of short-term variation in water quality at the karst spring in Kentucky: Ground Water, v. 34, no 1, p. 23-30, DOI: 10.1111/j.1745-6584.1996.tb01861.x

Schobbenhaus C (1984) Geology of Brazil. National Department of Mineral Production, p 275-277

Schöll WU, Fogaça ACC (1973) Stratigraphy of the Espinhaço in the Diamantina region. In: Symposium on Geology of Minas Gerais State, Brazil, 1. Acts. Belo Horizonte: Brazilian Geology Society p 55-73 [Bulletin. 1]

Silveira CS, Silva Junior GC (2002) The use of environmental isotopes in hydrogeological studies in Brazil: a critical review. Yearbook of the Institute of Geosciences - UFRJ. Vol. 25.

Tonietto SN (2010) Diagenesis and hydrothermal rocks in Proterozoic carbonates: Bambuí and Vazante Groups, São Francisco Basin. Master Thesis. Institute of Geosciences, University of Brasília. Federal District.

Tuller MP, Ribeiro JH, Signorelli N, Féboli WL, Pinho JMM (2010) Sete Lagoas - Abaeté Project, Minas Gerais State, Brazil. 6 geological maps, scale 1:100,000 (Geology Program of Brazil), 160p

Winston WE, Criss RE (2003) Oxygen isotope and geochemical variations in the Missouri River. Environmental Geology 43 (5), 546–556.

Zhao M, Zeng C, Liu Z, Wang S (2010) Effect of different land use/land cover on karst hydrogeochemistry: a paired catchment study of Chenqi and Dengzhanhe, Puding, Guizhou, SW China. J. Hydrol.; 388:121–130

CHAPTER 9: CONCLUSIONS

This section provides the overall conclusions of the most relevant results about the karst hydrogeological system of Sete Lagoas. For easy comprehensions, these conclusions are separated by subtopics, according to their importance.

9.1 Geological features of Sete Lagoas and surroundings

The city of Sete Lagoas and surroundings are along basement border, a result of extensional events in the São Francisco Craton, where silicate-carbonate sediments from the Neoproterozoic age were emplaced giving origin to the Bambuí Group. Due to the relative proximity of the study area with the Serra do Espinhaço (the Serra do Espinhaço is situated to the east of the study area and had undergone intense deformation), the Bambuí Group presents a horst and graben system, controlled by faulting, displacing the stratigraphic sequences, which enables formations with different ages side by side. In the west of the area, the structural features were less expressive and the sedimentary features were more preserved.

Lithologies from the Belo Horizonte Complex basement, the Sete Lagoas Formation, the Serra de Santa Helena Formation, and Cenozoic unconsolidated sediments occur in the area. The Sete Lagoas and the Serra de Santa Helena formations follow the horst and graben system, presenting thinner layers on the basin border in the SW region, and higher thickness in the NE area. The limestones from the Sete Lagoas Formation dip and become thicker to the northeast, being covered almost totally by competent rocks from the Serra de Santa Helena Formation (slate, marble, siltstone, and argillite). These limestones arise mainly in the Santa Helena Ridge foothills and in the municipalities located to the southeast of the city of Sete Lagoas, near the Velhas River. The Serra de Santa Helena Formation is immediately over the Sete Lagoas Formation, with abrupt contact. The contacts with basement are also abrupt, with sediments deposited in area with little relief. This formation also dips and becomes thicker to the NE and thinner on the basin borders and near the Velhas River. The thickness of the sedimentary basin layers, in the NE portion of Sete Lagoas, is estimated in 400 m, near this river. The limestones from the Sete Lagoas Formation present horizontal continuity, from the basement border to the Velhas River.

Within the city of Sete Lagoas, limestones from the Sete Lagoas Formation had undergone dissolution process that most strongly affected the bedding planes of these rocks, and, in lower magnitude, the sub-vertical fracture planes, forming karst conduits. Some of these dissolution zones were filled with terrigenous material. The medium-grained Lagoa Santa Member had a higher degree of dissolution (e.g. dry caves and grottoes) compared to the fine-grained lower Pedro Leopoldo Member (e.g. solutionally enlarged bedding planes). These evidences suggest geomorphological processes, such as a past meteoric water flow, or have started at the time when groundwater flowpaths started to develop, even if these limestones had not yet been exposed. As the timing of these processes is not precisely known, it is recommended specific studies to be conducted for a better understanding about the origin of these processes.

The Santa Helena Ridge, in the central portion of the city, was interpreted as a horst, which elevated the stratigraphic sequence, causing the Sete Lagoas and the Serra de Santa Helena formations to have higher altitudes than in other regions. Considering that fracture filled quartz veins cut this stratigraphic sequence, the ridge became more resistant to erosion. The Cenozoic unconsolidated sediments deposited in the central portion of Sete Lagoas were a result of weathering and erosion of Santa Helena Ridge rocks.

9.2 Hydrogeological features of the city of Sete Lagoas

The Sete Lagoas karst aquifer, which is approximately 75 meters thick on average, consists of Neoproterozoic limestones, composed of two members: the Pedro Leopoldo Member (at the base) and the Lagoa Santa Member (on the top), in which the primary porosity and matrix permeability can be considered very low and the secondary porosity is mostly filled by the precipitation of calcite. The majority of groundwater migrates through dissolution features characterized as tertiary porosity.

The urbanized area of Sete Lagoas is primarily located in an inferred graben, filled with limestones from the Sete Lagoas Formation, with Cenozoic unconsolidated sediments, and occasionally covered by competent rocks from the Serra de Santa Helena Formation. This setting results in fault bounded barrier boundaries for groundwater, which together with natural karst processes, explains the location of two dominant solutionally enlarged bedding planes with high permeability and

significant water storage capacity in the limestones: (1) a shallower and thicker continuous dissolution zone with conduits that are 1-8 m thick, near the contact with the overlying unconsolidated sediments; and (2) 10-20 m below, a thinner continuous dissolution zone with conduits that are 20 cm to 1 m thick. These two bedding plane conduits become thinner to the northeast.

Regarding the permeabilities of the karst aquifer, the solutionally enlarged bedding planes have the primary role in providing aquifer transmissivity. Unlike other karst areas that have increases in permeability in scale effects from small- to regional-scale, this behavior does not happen in the Sete Lagoas karst aquifer. An increase of about four to six orders of magnitude in the permeabilities from small- to well-scale is common, but from well- to regional-scale, the values decrease, due to the localized development of karst bedding plane dissolution in one structurally controlled region of the aquifer.

In small-scale, the mean permeability of the matrix is very low, because it is composed of a Neoproterozoic fine-grained (Pedro Leopoldo Member, at the base) and a medium-grained (Lagoa Santa Member, on the top) limestone that undergone recrystallization, with the secondary porosity (micro-fractures) generally filled by calcite. Relative to the bedding plane features, these values can be approximated on time scales for pumping or regional flow estimates as zero.

At the well-scale, the highest permeability features and groundwater storage are concentrated in the central urbanized area and close to the Santa Helena Ridge foothills, within the graben area, and in the East portion of the study area, with decreases occurring to northeast direction. These data coincide with the thickness of the karst bedding planes, suggesting a direct relationship between solutionally enlarged bedding planes and karst permeabilities. However, the Sete Lagoas karst aquifer has some permeability characterized by zones of high karstification and storage, which the standard well aquifer test is an insufficient method for estimation, evidenced by zero drawdown, illustrating the limits of aquifer tests. Non-Darcian flow likely occurs in these wells.

At the regional-scale, the permeability have a slightly smaller value in comparison to the largest well-scale numbers, indicating that conduit permeability may not be a strong regional effect if large conduits are not well connected on the scale of measurement. Both in well- and regional-scale, the largest permeabilities occur due to the same karstic conduits, but at the regional-scale, the permeability

values of matrix are more incorporated in the overall regional scale resulting in smaller values. Thus, in a low matrix permeability karst aquifer in which is governed by bedding planes and low sub-vertical fractures, the chance to have a considerable increase in the scale effect from well- to regional-scale is considered low.

9.3 Groundwater evolution and source of recharges

The groundwaters in Sete Lagoas are results of direct recharge from precipitation, during a limited period from October to December. The recharging zones are mainly the sinkholes and caves entrances, as well as in areas where the limestones are covered by Cenozoic unconsolidated sediments. The majority of the fluids migrate through the solutionally enlarged bedding planes and less common by sub-vertical enlarged fractures. The majority of these groundwaters are classified as of Ca^{2+}–HCO^{-}_{3} type, associated to limestones from the Sete Lagoas Formation. Waters in the basement and close to the Santa Helena Ridge are enriched of Mg^{2+}. These different types of water can mix with waters more enriched in Ca^{2+} and Na^{+}, diluting, resulting in other composition types. These mixing waters also indicate interconnections between waters from the karst aquifer and the basement.

In the central urbanized area, where the karst aquifer is in contact with Cenozoic unconsolidated sediments, and is more karstified, could have punctual superficial water infiltration. Isotopic results evidencing evaporation signatures in both lake water and groundwater samples, as well as nitrate in groundwater (in that last case, indication of recent contamination by domestic sewage or septic tank), corroborating this conclusion. Even in this region, high values of major ions indicating water mineralization and, hence, higher groundwater storage capacity, which is in concordance with the location of the highest transmissivity values and the most karstic dissolution zones.

9.4 Urban groundwater extraction and karst geotechnical risks

In the urbanized area, the combination of unconsolidated sediments overlying limestones or simple exposed limestone outcrops with two solutionally enlarged bedding planes in subsurface provided a geologic framework for geotechnical issues. In that region, there is a cone of depression (dimensions of 8 km by 8.5 km = 68 km^2)

caused by high pumping rates in wells, estimated in 75,000 m^3/d. During several decades, since the first supply well drilled in 1942 until present, some areas had significant decreases in the water table, around 40 m lower due to pumping. In some points, the shallowest conduit is entirely in the unsaturated zone. Depending on the size and depth of the conduit and the thickness of the layers above, subsidence can occur causing depressions on the land surface or, in extreme situations, collapse. This combination between geologic framework and high groundwater extraction explains the emergence of the cluster of induced subsidence or collapse.

In this area, largely located in the highest geotechnical risk zone, and where the majority of the population is living, recommendations include reducing groundwater use based on potentiometric surface elevation, prohibition to drilling new wells, prioritizing public wells to supply, and switching to surface water supply where possible. The main objective is to preserve groundwater resources to reduce the localized drawdown, which creates vadose conduits. Supply wells could be relocated to more protected areas, outside of that zone, avoiding future collapses.

9.5 General recommendations

This doctoral thesis, from a hydraulic, geotechnical, and geochemical point of view, clarified important issues in regional scale, with punctual characterization in local scale. The multidisciplinary methodologies integrating geological, hydrogeological, geochemical, and isotopes studies that were used to understand the water circulation in karst terrain, obtained satisfactory results, giving alternative responses for a better use of water. However, specific questions remain without answers, being interesting, in scientific terms and of water management, more clarified. Researches focusing on water flow system at the two main sollutionally enlarged bedding planes located in the urbanized area, where the majority of the population lives, are strongly recommended. Possible interconnections between these conduits, calculating the hydraulic parameters independently, determining the apparent age of the waters separately, and estimating the preferential groundwater flowpaths should be evaluated. These studies could contribute in the improvement of the hydrogeological conceptual model in more detail, giving clarifications in terms of groundwater flowpaths and its storages, contamination vulnerabilities, among others, improving the groundwater management.